



National Library  
of Canada

Bibliothèque nationale  
du Canada

Canadian Theses Service

Service des thèses canadiennes

Ottawa, Canada  
K1A 0N4

## NOTICE

The quality of this microform is heavily dependent upon the quality of the original thesis submitted for microfilming. Every effort has been made to ensure the highest quality of reproduction possible.

If pages are missing, contact the university which granted the degree.

Some pages may have indistinct print especially if the original pages were typed with a poor typewriter ribbon or if the university sent us an inferior photocopy.

Reproduction in full or in part of this microform is governed by the Canadian Copyright Act, R.S.C. 1970, c. C-30, and subsequent amendments.

## AVIS

La qualité de cette microforme dépend grandement de la qualité de la thèse soumise au microfilmage. Nous avons tout fait pour assurer une qualité supérieure de reproduction.

S'il manque des pages, veuillez communiquer avec l'université qui a conféré le grade.

La qualité d'impression de certaines pages peut laisser à désirer, surtout si les pages originales ont été dactylographiées à l'aide d'un ruban usé ou si l'université nous a fait parvenir une photocopie de qualité inférieure.

La reproduction, même partielle, de cette microforme est soumise à la Loi canadienne sur le droit d'auteur, SRC 1970, c. C-30, et ses amendements subséquents.

THE UNIVERSITY OF ALBERTA

DIRECT SAMPLE INSERTION SYSTEM FOR THE INDUCTIVELY COUPLED  
PLASMA (DSI-ICP)

by

WING TAT CHAN

A THESIS

SUBMITTED TO THE FACULTY OF GRADUATE STUDIES AND RESEARCH IN  
PARTIAL FULFILMENT OF THE REQUIREMENTS FOR THE DEGREE OF  
DOCTOR OF PHILOSOPHY

DEPARTMENT OF CHEMISTRY

EDMONTON, ALBERTA

SPRING 1989



National Library  
of Canada

Bibliothèque nationale  
du Canada

Canadian Theses Service    Service des thèses canadiennes

Ottawa, Canada  
K1A 0N4

The author has granted an irrevocable non-exclusive licence allowing the National Library of Canada to reproduce, loan, distribute or sell copies of his/her thesis by any means and in any form or format, making this thesis available to interested persons.

The author retains ownership of the copyright in his/her thesis. Neither the thesis nor substantial extracts from it may be printed or otherwise reproduced without his/her permission.

L'auteur a accordé une licence irrévocable et non exclusive permettant à la Bibliothèque nationale du Canada de reproduire, prêter, distribuer ou vendre des copies de sa thèse de quelque manière et sous quelque forme que ce soit pour mettre des exemplaires de cette thèse à la disposition des personnes intéressées.

L'auteur conserve la propriété du droit d'auteur qui protège sa thèse. Ni la thèse ni des extraits substantiels de celle-ci ne doivent être imprimés ou autrement reproduits sans son autorisation.

ISBN C 9515-52876-1

Canada

THE UNIVERSITY OF ALBERTA

RELEASE FORM

NAME OF AUTHOR: CHAN, WING TAT

TITLE OF THESIS: DIRECT SAMPLE INSERTION SYSTEM FOR THE  
INDUCTIVELY COUPLED PLASMA (DSI-ICP)

DEGREE FOR WHICH THESIS WAS PRESENTED: Ph.D.

YEAR THIS DEGREE GRANTED: 1989

Permission is hereby granted to THE UNIVERSITY OF ALBERTA LIBRARY to reproduce single copies of this thesis and to lend or sell such copies for private, scholarly or scientific research purposes only.

The author reserves other publication rights, and neither the thesis nor extensive extracts from it may be printed or otherwise reproduced without the author's written permission.

.....*W. Chan*.....  
(Student's signature)

Permanent Address:

2706 Tsui Shek House,  
Ping Shek Estate,  
Kowloon, Hong Kong

Date: *April 21, 1989*  
.....



THE UNIVERSITY OF ALBERTA

FACULTY OF GRADUATE STUDIES AND RESEARCH

The undersigned certify that they have read, and recommend to the Faculty of Graduate Studies and Research for acceptance, a thesis entitled DIRECT SAMPLE INSERTION SYSTEM FOR THE INDUCTIVELY COUPLED PLASMA (DSI-ICP) submitted by WING TAT CHAN in partial fulfilment of the requirements for the degree of DOCTOR OF PHILOSOPHY.

*G. Horlick*  
.....  
G. Horlick, Supervisor

*N.J. Dovichi*  
.....  
N.J. Dovichi

*L.G. Hepler*  
.....  
L.G. Hepler

*D.J. Harrison*  
.....  
D.J. Harrison

*M.J. Dudas*  
.....  
M.J. Dudas

*R.E. Sturgeon*  
.....  
R.E. Sturgeon, External Examiner

Date: *April 21, 1989*

To my parents

## Abstract

Direct sample insertion for the inductively coupled plasma (DSI-ICP) is a sample introduction technique that can handle both solid and liquid samples. This technique involves placing small quantities of liquids and/or solids in a sample cup and inserting the cup into the plasma directly. Sample introduction efficiency is 100 %, which is superior to that of any other method.

The emission signal for a discrete sample is transient and peak-like in shape. The emission temporal behavior of the signal was digitized in real time with custom software and electronics. Fast digitization enables subtle changes in the emission temporal behavior of the signal to be studied. These changes are sensitive to the method of sample treatment, i.e., the dry/ash processes and chemical modification of the sample matrix.

Quantitative analysis was performed by integrating the digitized signal, i.e., peak area was used. Standard addition, matrix matching and matrix modification with NaF have been used for the analysis of standard reference materials of botanical matrices. Semi-quantitative analysis of the samples using graphite-based standards has also been investigated.

Thermal properties of the sample cup assembly have been examined. Maximum sample cup temperature was estimated to be 2000 K. A model of the temperature rise for the assembly was

verified with experimental data. Suggestions for improved design of the assembly, i.e., faster temperature rise and higher cup temperature, based on this model were proposed.

A microcomputer-based DSI system has been developed. The DSI device was driven by a computer-controlled stepper motor. Thus the sample insertion sequence was automated. Custom software and faster electronics enable simultaneous data acquisition for up to six channels. A robot arm was used for sample cup transfer between the DSI device and the sample cup organizer. Therefore the system can be fully automated.

A solution sample introduction system for an atmospheric pressure chemical ionization/triple-quadruple mass spectrometer (APCI/MS/MS) was also developed. The system consisted of a heated inlet tube coupled with either a spray chamber/pneumatic nebulizer or an ultrasonic nebulizer. The performance of the system is presented in Appendix A.

## **Acknowledgement**

I would like to thank my research director Dr. Gary Horlick for his guidance, support, and patience throughout this work.

I have learnt a lot from Mr. Youbin Shao, our post-doctoral fellow from China, on both technical know-how and the way of life. He is a good friend and a teacher to me.

It is fun to have discussion with members of the group, especially Kuniyuki Kitagawa of Nagoya University and Joseph Lam. I must thank them for sharing their research experience with me.

Staffs in electronic shop, glass shop, and machine shop are helpful and skillful. Thanks for all the excellent jobs.

I would also like to thank the Department of Chemistry for providing excellent research environment and financial support.

## TABLE OF CONTENT

CHAPTER	PAGE
1. SOLID SAMPLE INTRODUCTION FOR THE INDUCTIVELY COUPLED PLASMA	
1.1 Introduction .....	1
1.2 Powder injection .....	3
1.3 Slurry nebulization .....	8
1.4 Electrothermal vaporization .....	10
1.5 Electroerosion .....	13
1.6 Laser ablation .....	18
1.7 Direct sample insertion .....	21
1.8 Conclusion .....	27
REFERENCES .....	29
2. INSTRUMENTATION FOR A DSI-ICP SYSTEM	
2.1 Introduction .....	34
2.2 The ICP spectrometer .....	37
2.3 The direct sample insertion device .....	37
2.3.1 The DSI-ICP torch .....	38
2.3.2 The drive .....	38
2.3.3 The sample cup assembly .....	42
2.4 Samples .....	46
2.4.1 Solution samples .....	46
2.4.2 Powdered samples .....	47
2.4.3 Sample cup organizer .....	47
2.5 Robot arm .....	48
2.5.1 The position parameters of the robot arm.....	48

2.5.2 The end effector .....	53
2.6 Readout electronics .....	55
2.7 Computer hardware and software .....	59
2.7.1 ADC operation .....	59
2.7.2 Software .....	61
2.7.2.1 parameter files .....	62
i. All parameters.....	62
ii. Stepper motor parameters.....	64
iii. Sample parameters.....	66
2.7.2.2 Software for the analysis process .....	66
i. The BASIC main program.....	67
ii. Assembly subroutines.....	68
2.7.2.3 Data processing .....	69
2.8 Conclusion .....	72
REFERENCES .....	73

3. THERMAL PROPERTIES OF THE SAMPLE CUP ASSEMBLY FOR A DSI-ICP SYSTEM	
3.1 Introduction .....	75
3.2 Temperature of a sample cup .....	75
3.3 Input power to the sample cup .....	83
3.4 Temperature rise rate of a sample cup .....	88
3.5 Theoretical calculation of the temperature of a sample cup as a function of insertion time.....	94
3.6 Distribution of the input power among different processes.....	96
3.7 Conclusion .....	101
REFERENCES .....	107

<b>4. CHARACTERIZATION OF DSI-ICP-AES</b>	
4.1 Introduction .....	109
4.2 <i>In situ</i> sample treatment (drying and ashing) ....	110
4.3 Desolvation of samples ( <i>in situ</i> and external) .....	116
4.3.1 Samples with desolvation but without ashing.....	118
4.3.2 Samples with desolvation and ashing .....	123
4.3.3 Conclusion .....	130
4.4. Detection limits .....	131
REFERENCES .....	136
<b>5. ANALYSIS OF POWDERED BOTANICAL SAMPLES</b>	
5.1 Introduction .....	138
5.2 Experimental .....	142
5.3 Matrix matching method .....	143
5.3.1 Experimental .....	144
5.3.2 Results and discussion .....	145
5.3.3 Conclusion .....	157
5.4. Standard addition method .....	159
5.4.1 Experimental .....	160
5.4.2 Results and discussion .....	161
5.4.3 Limitations and assumptions of the standard addition method.....	165
5.4.4 Correction for the variation of sample weight.....	167
5.4.5 Conclusion .....	171
5.5 Matrix modification with NaF .....	173
5.5.1 Experimental .....	174



5.5.2 Determination of the amount of NaF required.....	175
5.5.3 Results and discussion .....	184
5.5.4 Comparison of the sensitivities of standard solutions and those of standard addition analysis.....	190
5.5.5 Conclusion .....	201
5.6 Semi-quantitative survey .....	202
5.6.1 Experimental .....	202
5.6.2 Results and discussion .....	203
5.7 Conclusion .....	204
REFERENCES .....	211
6. CONCLUDING REMARKS AND FUTURE EXPERIMENTS.....	213
6.1 A fully automated DSI system .....	214
6.2 Ohmic heating of the sample cup .....	215
6.3 Consumable sample cup and the capillary sampler.....	215
6.4 Photodiode array spectrometer .....	220
6.5 Sample throughput .....	221
REFERENCES .....	222
APPENDIX A. SAMPLE INTRODUCTION SYSTEMS FOR A TRIPLE- QUADRUPOLE MASS SPECTROMETER	
A.1 Introduction .....	223
A.2 Experimental .....	224
A.2.1 The mass spectrometer .....	224
A.2.2 The sample introduction system .....	225
A.3 Qualitative analysis .....	231
A.4 Quantitative analysis .....	243

A.5 Conclusion .....	258
REFERENCES .....	260
APPENDIX B. PROGRAM LISTING .....	262
PROGRAM DA.MAIN .....	263
PROGRAM PARATE .....	267
PROGRAM TRAINING .....	270
PROGRAM FILE BLENDER .....	277
PROGRAM DA.POSITION .....	283
PROGRAM DP 2.0 .....	284
PROGRAM ADP .....	290
SUBROUTINE DAI13 .....	296
SUBROUTINE TIMER1 .....	297
SUBROUTINE TIMER2 .....	297
SUBROUTINE CTRL.IOB.CHAR .....	298

## LIST OF TABLES

TABLE	PAGE
3-1. Vapor pressures of cobalt, iron, and titanium .....	77
3-2. Appearance temperatures and appearance times of candidate elements undergoing graphite-furnace atomization .....	90
4-1. Absolute and relative detection limits for Cd, Zn, Cu, Pb, and Fe .....	132
5-1. Comparison of the signals for Pb from pine needles, standard solution, and standard addition analysis .....	141
5-2. The pre-amplifier gain of the AI13 for the eight elements of the SRMS .....	145
5-3. Standard addition results for Orchard Leaves .....	165
5-4. Standard addition results for Pine Needles .....	165
5-5. A hypothetical set of samples .....	168
5-6. Successive approximation for the hypothetical standard addition results .....	170
5-7. Successive approximation for the hypothetical standard addition results .....	172
5-8. Standard addition results for Orchard Leaves with NaF matrix modifier added .....	184
5-9. Calibration curves for semi-quantitative analysis ....	208
5-10. Semi-quantitative analysis of Pine Needles .....	209
5-11. Semi-quantitative analysis of Orchard Leaves .....	209
5-12. Semi-quantitative analysis of Tomato Leaves .....	210
5-13. Semi-quantitative analysis of Spinach .....	210
A-1. Operating parameters for the TAGA 6000e .....	227
A-2. List of the candidate amino acids and their molecular weights .....	242
B-1. Apple II Plus configuration for the DSI system .....	262

## LIST OF FIGURES

FIGURE	PAGE
1-1. A Typical DSI torch configuration .....	22
1-2. Three dimensional view of the DSI device of Shao and Horlick .....	25
2-1. Experimental set-up of the direct sample insertion (DSI) system .....	35
2-2. The modified ICP torch for the DSI device (left) and a typical Fassel type torch (right) .....	39
2-3. Dimensions of the DSI torch in mm .....	40
2-4. The sample cup assembly .....	43
2-5. Dimensions of the sample cup and the cup holder. A dc arc electrode is also shown for comparison. ....	44
2-6. The sample cup organizer .....	49
2-7. (a) Schematic diagram of the robot arm RM101 at home position. (b) Diagram showing the angles of the forearm and upper arm to the horizon at home position .....	51
2-8. The robot station and the ARL34000 spectrometer (Dimensions in cm). The height of the station is 71 cm .....	52
2-9. The end effector for the robot RM101 .....	54
2-10. Temporal behavior of the emitting signal for 10 $\mu$ L of 100 ppm multi-element standard solution. The pre-amplifier gain for the analytes are: Pb, $10^6$ ; Mn, $10^6$ ; Ni, $10^7$ ; Cu, $10^6$ ; Fe, $10^6$ ; Cd, $10^5$ V/A. ....	56
2-11. Readout electronics of the DSI system. The OAs are Analog Devices AD515 FET-input electrometer op amp; R= 1 or 10 MW; C= 220 pf .....	58
2-12. Calibration curves of Fe, Cu, and Ni standard solutions. The intensities are peak heights normalized to the full scale of the AI13 with pre-amplifier gain of $10^7$ V/A. ....	63
2-13. Calibration curve of Fe standard solution. Intensity is peak area instead of peak height .....	65

2-14. Off-peak background correction for the peak area of a DSI time profile .....	71
3-1. Dimensions (cm) of the graphite sample cup assembly .....	85
3-2. Graphite sample cup temperature rise curve. The solid line is a curve-fit of the experimental results .....	93
3-3. The theoretical graphite sample cup temperature rise curve. (a) first 3 seconds of the curve. (b) first 10 seconds of the curve .....	97
3-4. Distribution of the input power to a graphite sample cup among different processes as a function of temperature of the sample cup .....	99
3-5. Distribution of the input power to a graphite sample cup among different processes as a function of insertion time .....	100
3-6. Hypothetical sample cup temperature rise curve with no conductive heat loss .....	102
3-7. Hypothetical sample cup temperature rise curve with no radiative heat transfer .....	103
4-1. Signal for Cu from 10 mg of Pine Needles as a function of ashing height. Ashing time is 120 s .....	113
4-2. Signal for Cu from 10 mg of Pine Needles with concentrated nitric acid as a function of ashing height. Ashing time is 120 s .....	114
4-3. Signal for Pb from 10 mg of Pine Needles with concentrated nitric acid as a function of ashing height. Ashing time is 120 s .....	115
4-4. The effect of concentrated nitric acid on the signals for Cu and Pb in 10 mg of Pine Needles. The samples are dried at 35 mm b/c for 30 s then ashed at 18 mm b/c .....	117
4-5. Emission intensity-time profiles for atomization of 10 $\mu$ l of 100 ppm of Pb and Fe in nitrate and chloride forms. The samples were dried <i>in situ</i> at 35 mm b/c for 30 s before full insertion. No ashing cycle was used .....	119
4-6. Emission intensity-time profiles for atomization of 10 $\mu$ l of 100 ppm of Pb and Fe in nitrate and chloride forms. The samples were dried externally,	

then heated at 35 mm blc for 30 s before full insertion. No ashing cycle was used ..... 122

4-7. Emission intensity-time profiles for atomization of 10  $\mu$ l of 100 ppm of Cu in nitrate form. All samples were heated at 35 mm blc for 30 s. The time profiles on the left hand side are for samples without ashing cycle. The time profiles on the right hand side are for samples with 60 s ashing at 18 mm blc ..... 124

4-8. Emission intensity-time profiles for atomization of 10  $\mu$ l of 100 ppm of Fe in nitrate form. All samples were heated at 35 mm blc for 30 s. The time profiles on the left hand side are for samples without ashing cycle. The time profiles on the right hand side are for samples with 60 s ashing at 18 mm blc ..... 126

4-9. Emission intensity-time profiles for atomization of 10  $\mu$ l of 100 ppm of Pb in nitrate form. All samples were heated at 35 mm blc for 30 s. The time profiles on the left hand side are for samples without ashing cycle. The time profiles on the right hand side are for samples with 60 s ashing at 18 mm blc ..... 127

4-10. Emission intensity-time profiles for atomization of 10  $\mu$ l of 100 ppm of Ni in chloride form. All samples were heated at 35 mm blc for 30 s. The time profiles on the left hand side are for samples without ashing cycle. The time profiles on the right hand side are for samples with 60 s ashing at 18 mm blc ..... 129

4-11. Emission intensity-time profiles for Pb and Fe at concentrations close to detection limits. The time profiles of their blanks are shown on the bottom for comparison ..... 133

4-12. Emission intensity-time profiles for Zn and Cd at concentrations close to detection limits. The time profiles of their blanks are shown on the bottom for comparison ..... 135

5-1. Signals for Pb from 10  $\mu$ L of 10 ppm standard solution, 10 mg of Pine Needles (Pb content is 10.8 ppm), and standard addition of the standard solution to Pine Needles ..... 139

5-2. Calibration curves for Pb standard addition and standard addition analysis of Pine Needles. The curve for standard addition analysis is corrected to pass through origin, so that the slopes of the curves can be compared .....	140
5-3. Calibration curves for (a) Pb, (b) Cd, (c) Cu, (d) Fe, (e) Al, (f) As, (g) Zn, and (h) Mn from standard reference materials of botanical matrix .....	146
5-4. Signal for (a) Pb, (b) Cu, (c) Fe, (d) Al, (e) Zn, and (f) Mn from standard reference materials of botanical matrices .....	151
5-5. Calibration curve for (a) Zn and (b) Mn. Intensity is peak height (anodic current of the PMT) .....	158
5-6. Calibration curves for the standard addition analysis of (a) Pb, (b) Cu, and (c) Fe in Orchard Leaves .....	162
5-7. Signals for B from 5 mg of Orchard Leaves with increasing amount of NaF added (top row) and signal for the corresponding NaF solutions (bottom row). The concentrations of NaF solutions are given on the top of each column .....	176
5-8. Calibration curve for B in NaF solution .....	177
5-9. Signals for Cu from 5 mg of Orchard Leaves with various amounts of NaF added .....	178
5-10. Signals for Pb from 5 mg of Orchard Leaves with various amounts of NaF added .....	179
5-11. Relationship between analyte intensities from 5 mg of Orchard Leaves to the volume of 0.8 M of NaF solution for (a) B, (b) Cu, (c) Fe, (d) Cr, and (e) Pb .....	181
5-12. Calibration curves for the standard addition analysis of (a) B, (b) Cu, (c) Pb, (d) Fe, and (e) Cr in Orchard Leaves with NaF matrix modifier .....	185
5-13. Calibration curve for B standard solution with NaF added. The volume of the standard solution is 10 $\mu$ L and that of the 0.8 M NaF solution is 40 $\mu$ L .....	191
5-14. Calibration curves for standard solutions with and without NaF, and the standard addition	

analysis of Orchard Leaves with NaF. (a) Cu, (b) B, (c) Pb, (d) Fe, and (e) Cr .....	192
5-15. Signal for 10 $\mu$ L of (a) Cu, (b) B, (c) Pb, (d) Fe, and (e) Cr standard solutions with NaF added (top row) and without NaF added (bottom row). The concentration of the standard solution is shown on the top of each column .....	196
5-16. Calibration curves for (a) Mo, (b) V, (c) S, and (d) P from SPEX G standards. Note that the sensitivities are low and slopes for the log-log plots are much less than one for the nonvolatile elements (Mo and V) and for elements with emission lines in the vacuum UV region (S and P) .....	205
5-17. Calibration curves for (a) Al, (b) Cr, (c) Cu, and (d) Zn from SPEX G standards .....	206
6-1. A modified ICP torch and the capillary sampler .....	217
6-2. Temporal behavior of the signal for two consecutive runs of (a) Ca from calcium carbonate and (b) Zn in GSD-1, with the capillary sampler .....	218
6-3. Temporal behavior of the signal for Ni in (a) GSD-2 (5.5 ppm) and (b) GSD-1 (76 ppm). Background intensity changes with (i) capillary sampler inserted into the the ICP torch, (ii) Ar injector gas turned on, (iii) Ar injector gas turned off and the capillary sampler withdrawn from the torch, and (iv) Ar injector gas turned off and the capillary sampler remained inserted into the torch .....	219
A-1. Schematic diagram of the APCI source of the TAGA 6000e .....	226
A-2. Heated tube for sample aerosol desolvation .....	229
A-3. Temperature distribution in the APCI source with the heated inlet tube .....	230
A-4. The ultrasonic nebulizer assembly .....	232
A-5. Background spectrum of the APCI .....	234
A-6. Mass spectra for ethanol, pyridine, and toluene. The background spectrum is included for comparison .....	235



A-7. Mass spectrum for 0.001 M of aqueous glucose solution with the nebulizer/spray chamber/heated tube as the sample introduction system .....	237
A-8. Mass spectrum of coffee. The peak at m/z 195 is from caffeine .....	239
A-9. CAD spectra obtained experimentally for m/z 195 from coffee (above) and CAD spectrum for caffeine stored in the spectrum library (below) .....	240
A-10. Mass spectrum (above) and daughter spectrum for tyrosine .....	241
A-11. Mass spectrum for the same tyrosine solution in Figure A-10. Higher ion energy was used .....	244
A-12. Mass spectrum for a mixture of four amino acids: glycine (M=75), histidine (M=155), tryptophan (M=204), and tyrosine (M=181) .....	245
A-13. CAD spectra for glycine, histidine, tryptophan, and tyrosine in a mixture of the amino acids .....	246
A-14. CAD spectrum for valine and norvaline .....	247
A-15. CAD spectra for leucine, isoleucine, and norleucine .....	248
A-16. Calibration curves for histidine; top curve for ion of m/z=155, bottom curve for ion of m/z=156. Samples are introduced with pneumatic nebulizer .....	250
A-17. Calibration curves for histidine with both quadrupoles Q1 and Q3 operating simultaneously. Samples are introduced with pneumatic nebulizer .....	251
A-18. Calibration curve for histidine; the intensity is the sum of that of ions m/z 155 and 156. Samples are introduced with pneumatic nebulizer .....	253
A-19. Calibration curves for histidine; top curve for ion of m/z=155, bottom curve for ion of m/z=156. Samples are introduced with ultrasonic nebulizer .....	254
A-20. Calibration curve for histidine; the intensity is the sum of that of ions m/z 155 and 156. Samples are introduced with ultrasonic nebulizer .....	255
A-21. Calibration curves for glucose; from left to right, for ions of m/z=181, 163, and 198 respectively. Samples are introduced with pneumatic nebulizer .....	256

- A-22. Calibration curve for glucose; the intensity is the sum of that of ions  $m/z$  163, 181, and 198. Samples are introduced with pneumatic nebulizer .....257
- A-23. Intensity of ions for glucose in 0.1 M of ammonium acetate buffer at different pH. The pH of aqueous glucose solution without buffer is 6.6 .....259

# **Chapter 1. Solid Sample introduction for the Inductively Coupled Plasma**

## **1.1 Introduction**

Although sample introduction is often considered a weak link of analytical atomic spectroscopy and has even been called the "Achilles' heel of atomic spectroscopy", there has been a strong move in recent years to develop improved sample introduction procedures [1]. Nevertheless the practical sample introduction systems in use today primarily handle liquid samples, with only a few developed to handle solid samples directly [2].

The direct analysis of solids is an important priority in analytical methods development for atomic spectroscopy [3-5] because many samples naturally occur in solid form, e.g., those of biological, geological, and metallurgical origin. A number of analytical and practical advantages can be realized if solid samples are introduced directly into an analytical source such as the inductively coupled plasma (ICP). Ideally, when a sample is analysed in its natural state, the time-consuming decomposition step can be omitted and the analysis can be completed without addition of reagents and without any separation and/or concentration steps. Thus the risks of introducing contaminants and of losing the element of interest are considerably reduced.

Langmyhr [3] pointed out two of the main problems encountered when dealing with the direct analysis of solids, namely the relatively small sample size compared to that taken for solution sample analysis and interferences arising from the matrix of the solid samples. A sample analyzed must validly represent the composition of the material of interest, which can be expressed as the relative standard deviation of the sampling operation, i.e., sampling error. Sampling error is inversely proportional to the square root of the number of particles in a sample [6]. It is obvious that when the sample size is reduced, the particle sizes should also be reduced to maintain the same precision for sampling. Smaller particle sizes can be obtained by grinding the sample. However, grinding a sample is a tedious process that may introduce contaminants and/or analyte loss.

Interferences due to the solid matrix introduce systematic errors. This problem can be solved with use of matrix matched standards, but these standards are not as readily available as solution standards. Therefore, standardization becomes complicated for direct solid analysis.

It is not surprising then to find out that the direct analysis of solids is not widely practised. Nevertheless, a number of techniques for the introduction of solids directly into the ICP have been proposed. These techniques can be divided into six categories, namely, powder injection, slurry nebulization, electrothermal volatilization, electroerosion, laser ablation, and direct sample insertion. A brief survey

of the characteristics and the status of development of these techniques is presented in the following sections.

## 1.2 Powder injection

It seems straightforward to inject a powder sample into the plasma. After all, one of the first ICPs was constructed for powder injection, although the goal was crystal growth rather than spectrochemical analysis [7, 8]. The subtle differences are that spectrochemical analysis demands a more consistent powder delivery rate and complete vaporization of the powders in the plasma discharge. To meet these requirements, several powder injection techniques have been proposed [9-14].

Hoare and Mostyn [9] introduced a powder injection assembly consisting of a borosilicate sample container and a mechanical agitator. The assembly was attached to the base of a modified ICP torch. The powdered sample was agitated by vibrating the sample container and a slow argon flow carried the sample to the plasma via a borosilicate capillary tube.

It is obvious that a longer residence time for a particle in the plasma discharge means more heat transfer from the plasma to the particle, and thus a better chance for the particle to vaporize completely. Hoare and Mostyn found that a longer residence time could be obtained by controlling the rate of vibration of the sample container and the argon flow.

This powder injection method proved to be effective for qualitative analysis. The absence of spectral lines from either electrode materials (none required) or associated residual impurities was a particularly valuable feature. However, it was found that vaporization of solids was not an efficient process. Energy transfer from the plasma to the sample particles was poor when sample particles were large and non-conducting. As well, ion lines were less intense compared to liquid sample introduction and neutral atom lines gave the best sensitivity. This means that atomization was not complete, at least during the early stage of injection. Therefore, low injection velocity and small particle size were essential for quantitative analysis.

Lithium salts and alumina were analysed. Lithium salts and standards were prepared by evaporating lithium sulphate solutions and grinding the residue to a fine powder (300 mesh). Alumina was ground with metal oxide. For a charge weight of 100 mg, detection limits were of the order of 1 ppm or better for most elements.

Dagnall et al. [10] described a fluidized-bed chamber for powdered sample introduction. The sample was placed on a sintered glass disc of coarse porosity. An Ar flow passing through the disc carried the particles to the plasma. The chamber was mechanically vibrated to reduce surges of powder. It also facilitated the incorporation of a bleed-off valve to allow a slower flow of carrier gas to the plasma while maintaining a faster flow through the fluidized-bed.

A cyclone chamber, placed on top of the fluidized-bed, was tested for its ability to eliminate large particles or agglomerates. The elimination process made use of the centrifugal force of the tangentially rising carrier gas. However, segregation of particles of varying density was observed, so use of the cyclone chamber was rejected.

Quartz, constricted pyrex, alumina, and tantalum tubes were all tested for optimal powder injection into the plasma from the fluidized bed. The quartz tube was preferred, although a thin walled Ta tube had the interesting ability to preheat the powder if the upper end of the grounded tube was in the high frequency field region. This improved sample vaporization. The Ta tube was ultimately rejected because it slowly degraded at the hot tip end.

It was found that powder feed rate was not constant, but decreased slowly in an exponential manner. To compensate for the changing sample introduction rate, the weight of sample was fixed and intensity was read after a fixed delay time from the start of the carrier gas flow.

Sample matrix that is non-sticking, free from contaminants, and has a low background is optimal for analysis.  $\text{CaCO}_3$ ,  $\text{SiO}_2$ ,  $\text{Al}_2\text{O}_3$ , and  $\text{MgO}$  were tested for this purpose, and  $\text{MgO}$  was found to fit the requirements best and a particle size of less than  $66 \mu\text{m}$  was used.

Calibration curves from 2 to 1000 ppm of beryllium and boron in  $\text{MgO}$  were reported. The curves were linear in the lower concentration range, but sensitivity decreased at

higher concentration. Detection limits were 0.1 and 2.5 ppm for Be and B, respectively. Relative standard deviations (20 samples) for 10 ppm samples were 6.5 % for Be and 10 % for B.

De Silva and Guevremont [13, 14] described a different fluidized-bed sampling system. The system was sealed from the atmosphere, and flushed with argon continuously. Powdered sample was placed in a tube inside the system. When the tube was vibrated vertically with a solenoid (at a rate of up to 10 cycles per second), the sample was suspended in the argon gas. The suspended particles were carried to the plasma by the argon flow. The improvement of this system upon that of Hoare and Mostyn [9] is that the argon flow carrying the particles is combined with a second argon flow before entering the ICP torch. Therefore, changes in the rate of sample introduction are possible by varying the first argon flow while maintaining a constant total carrier gas flow rate.

The system has been applied to the determination of several elements in silica (25  $\mu\text{m}$ ) and two chelating substrates. Nonlinear calibration curves were obtained even with internal standards. Lower limits of practical analysis were approximately 1 ppm, and an accuracy of 5 % or better could be achieved routinely for concentrations of 2 ppm or higher.

Scott [11] introduced a spark elutriation apparatus. Two graphite electrodes were positioned above a finely powdered sample (-200 mesh) contained in a glass or plastic vial. A



repetitive, energetic spark between the electrodes suspended the particles of the powdered sample in a flow of argon gas. This argon flow converged with another carrier gas and entered the plasma. Sample weight was 1 gram.

The acoustic energy of the spark was thought to be instrumental in suspending the particles. The spark may also cause further break-up of the particles to small particles or vapor.

Because of the slow exponential drop-off in emission intensity, signal was measured 30 sec after the beginning of the spark. Segregation effects due to the different particle densities and particle sizes and the preferential elutriation of the finer particles caused the signal drop-off.

Geological samples were analysed. Analytical results for copper agreed well with the values obtained by atomic absorption spectrometry (with dissolution of samples), X-ray fluorescence spectrometry, and mass spectrometry.

Ng and co-workers [12] used a powder injection device of a small volume (~0.3 ml) to introduce small amounts (0.5 to 2.5 mg) of powdered samples. A tangential gas flow created inside the injector device mixed and transported the powder into the ICP. The emission signal was transient in contrast with those of the techniques mentioned above. Therefore, a rapid scanning spectrometer was used for multi-element analysis.

NBS coal fly ash, silicon carbide, whole blood, tomato vegetable dust, pesticide dust, and granular chromatographic-

grade cellulose were examined. Absolute detection limits for chromium, copper, strontium, thallium, vanadium, and zinc were a few ng for the NBS coal fly ash. Reproducibilities of 12 % RSD or less and recoveries of 72 to 110 % were reported for the elements present in the coal fly ash.

It is concluded that the powder injection technique is useful for rapid qualitative analysis. For quantitative analysis, constant powder injection rate is essential, except for the case of total sample injection. Small particle size and low carrier gas flow rate are also required for complete vaporization. With the use of internal standards, reasonable analytical results can be obtained.

### **1.3 Slurry nebulization**

Analytical performance of the powder injection technique suffers because of the difficulty in controlling the powder injection rate. On the other hand, it is well known that pneumatic nebulization of solution samples can be regulated easily. Fine powders suspended in a liquid (i.e., a slurry) can be nebulized in a similar fashion as solution samples, thus powdered sample introduction into the ICP in a controlled manner is possible.

Since the particles in a slurry tend to settle, small particle size (<10  $\mu\text{m}$ ) and constant agitation are required for homogeneous suspensions [15-17]. A more stable suspension

can be obtained if the liquid has high viscosity, which is accomplished by the addition of a thickening agent [18, 19].

Fuller et al. [20] reported direct analysis using slurries. Mineral samples were wet milled with acetone to a mean particle size of less than 6  $\mu\text{m}$  and prepared as slurries. A cross-flow slot type nebulizer [21] was used because the more commonly used concentric and cross-flow nebulizers could not cope with the high solid content of the slurries. The glass nebulizer was based on the Babington design. Continuous nebulization of slurries of over 10 % m/v with the nebulizer coupled with a peristaltic pump was possible.

The analytical performance of this technique can be gauged by the atomization efficiency which is defined as ratio of the signal from the slurry to that of an aqueous solution containing an equivalent concentration of the same element. Generally, the atomization efficiency was found to be low. It was 0.3-0.5 for vanadium and zirconium in mineral samples with a particle size of less than 6  $\mu\text{m}$ . Since the particle size was small, the nebulization efficiencies for the slurries and solution samples should be similar in magnitude. Therefore solution standards were not adequate for calibration and matrix matched standards were required.

Atomization efficiency dropped rapidly to 0.01 if particle size was in the range of 44-63  $\mu\text{m}$ . This reduction occurs because the nebulizer/spray chamber system has poor sample transport efficiency for large droplets and/or

particles ( $>10\ \mu\text{m}$ ). This is critical because it poses an upper limit on the useful particle size.

Ebdon et al. [22, 23] analysed volatile trace metals in coal and coal-ash slurries by ICP-AES with a Babington-type nebulizer. Optimum results were achieved using low power, low injector gas flow, and a high observation height.

Broekaert and co-workers [24] analysed Al, Fe, and Mg in  $\text{TiO}_2$  powder ( $5\ \mu\text{m}$ ), prepared as slurries. A GMK Babington nebulizer, force-fed with a peristaltic pump, was used. They found that calibration with aqueous standards was adequate if Ti was used as an internal standard. Signals for a slurry of  $\text{Al}_2\text{O}_3$  powder ( $0.6\ \mu\text{m}$ ) and an aqueous solution of the same Al concentration were also compared under different nebulization conditions. The analyte signal from the slurry was found to be consistently smaller, which agreed with the report of Fuller et al. [20] on the low atomization efficiency for slurries.

It is concluded that the requirement of small particle sizes for efficient nebulization is a serious limitation of this technique. Improved control in the sample introduction rate and the possibility of using aqueous standards for calibration (with internal standards) are advantageous.

#### **1.4 Electrothermal vaporization**

Electrothermal vaporization (ETV) of liquids for atomic absorption spectrometry (AAS) is well established. However,

the analysis of solids with ETV-AAS is hindered by matrix interferences associated with the solid samples. It is possible to eliminate a number of matrix effects by separating the atomization and excitation processes. ETV-ICP is therefore a potentially viable technique for direct solid analysis.

The ETV-ICP technique is similar to its counterpart in ETV-AAS. Microliters or milligrams of sample are deposited onto a sample-supporting device (usually graphite rods or boats, or tantalum filaments). The sample is then dried, ashed, and vaporized by resistive heating of the sample-supporting device. The aerosol generated is swept into the plasma by a flow of injector gas.

A typical configuration of an ETV sample introduction device involves a graphite rod positioned between two water-cooled terminals connected to a power supply. The assembly is enclosed in a cylindrical glass manifold with a conical top or simply a glass dome. The device usually has three ports: an injector gas inlet, an aerosol outlet, and a sample delivery port. The aerosol outlet is connected to the base of an ICP torch. Injector gas flow rate is comparable to that of the central gas flow for nebulizer/spray chamber systems.

Nixon and co-workers [25] used ETV-ICP to analyse microliters of liquid samples. Since then, two groups have shown this technique to be applicable to direct solid analysis [26,27].

Hull and Horlick [26] reported a calibration curve for Zn using Spex-G standards. Indium was used as an internal standard. A calibration plot for manganese constructed from a series of National Bureau of Standards (NBS) standard reference materials was also reported. The standards included Pine Needles, Tomato Leaves, Spinach, Orchard Leaves, Coal, and Coal Fly Ash. They were mixed with spectroscopic grade graphite in a ratio of 1:1, and the sample weight was 2-3 mg. The results demonstrated linearity regardless of sample matrix.

As mentioned above, ETV-ICP separates the volatilization process from the excitation process. This results in a system with improved analytical capability. For example, the matrix effect of excess chloride on the signal from Pb observed in ETV-AAS was not found in ETV-ICP [26]. The volatilization process can also be simplified to a single stage process. The precaution of matrix effects elimination for AAS, e.g., the charring cycle, is not necessary.

Blakemore et al. [27] used a modified atomic absorption spectrometer atomization chamber to vaporize a standard reference material (Bovine Liver). To ensure homogeneity, the sample was micropulverized by freezing the sample in liquid N<sub>2</sub> and then agitating it in a ball mill. The sample weight was 0.5 mg. The sample was weighed into a graphite microboat which was then placed on the flat portion of the carbon rod of the ETV atomizer. Drying and ashing processes were employed before volatilization. The analytical results for 10

elements agreed well with the certified values. The average analytical precision for triplicate analyses was 12 % RSD, slightly larger than the RSD of 10 % for solution analysis with ETV-ICP. The larger RSD is possibly due to the small sample size leading to larger sampling errors.

A small ETV chamber was described by Tikkanen and Niemczyk [28] for solution samples. It was connected directly to the base of an ICP torch so that the distance the aerosol must travel from the vaporizer to the plasma was minimal (30 cm). The small distance prevented diffusion of the analyte cloud and minimized sample loss to the walls of the delivery system. The volume of the vaporization chamber was also kept small (53 cm<sup>3</sup>) to lessen analyte peak broadening. This concept is certainly applicable for direct solid sampling with ETV.

It is concluded that the ETV-ICP technique is well suited for direct solid analysis. The separation of the volatilization process from the excitation process overcomes some of the problems of matrix effects. The transport of fine aerosol from the ETV chamber to the ICP discharge is also less critical than the powder injection techniques. However, sampling errors due to small sample size may be important.

### **1.5 Electroerosion**

Arcs and sparks have been used successfully as sources for emission spectrometry. Both sources remove fine particles from the surface of electrically conducting samples. This

process is called electroerosion and has been applied to direct solid sampling for the ICP. The separation of sampling from excitation provides the opportunity for independent control of each process, similar to the situation of ETV-ICP.

Jones et al. [29] described an aerosol generator. The device, originally coupled with a dc capillary arc plasma source, was offered as a commercial component for the ICP [30]. A dc arc between a water-cooled tubular anode and the grounded sample ablated material from the sample surface. The aerosol consisted of particles of the order of a micron in diameter which were transported by an argon flow through the hollow anode to the ICP.

The carrier gas was mainly argon, with small percentages of nitrogen and/or oxygen. Flow rate was 1-2 L/min. A 600 V power supply (open circuit voltage) was used. The operating current was 2-8 A. The average voltage drop across the aerosol generator was 50 V. A momentary 25 kV initiator spark started the arc.

Since the cathode spot of the dc arc moved rapidly over the sample surface, the removal of material was nearly uniform over the entire exposed surface. Microscopic examination of a sampled surface revealed shallow pits of a few hundred microns in diameter completely covering the surface. Oscilloscopic observation of the voltage drop across the aerosol generator showed a broad spectrum of pulses with a distribution of frequencies peaking in the neighbourhood of 1 MHz, and voltages ranging up to nearly the open circuit



voltage of the power supply. These pulses corresponded to the formation of the pits from which the aerosol was expelled at high velocities. There was little or no indication of preferred erosion of inclusions or of grain boundaries. Repeated re-arcing of a sampled area did not produce any evidence of differential depletion of volatile elements.

Analytical curves for the determination of copper, molybdenum, chromium, manganese, silicon, nickel, carbon, sulphur, phosphorus, and aluminium in steel alloys with iron as the internal standard, using a dc capillary arc plasma source, were reported. Standard deviations for the elements computed from 22 integrations (3 sec integration time) ranged from 0.40 to 8.5 % RSD. Matrix, interelement, and self-absorption effects were not detectable.

Farnsworth and Hieftje [31] described a radio frequency arc (rf arc) for sample introduction into the ICP. The rf arc made use of the phenomenon that a grounded conductor, placed below the central tube of a modified ICP torch, can attract a stable arc filament from the base of the ICP discharge. At a forward power of 1.5 kW, a 140 W reduction of the rf power was observed when the arc was on, which was presumably directed to the arc filament. The aerosol generated by the arc was carried to the plasma discharge with an argon flow.

Microliters of solution were analysed by placing 100 ng of Cd and Zn on top of a graphite pencil lead which served as an electrode for the arc. The elements were dislodged when the arc was struck, then thermal volatilization was observed.

Complete vaporization was obtained after 40 sec. The relative standard deviations of the measurements were 9.8 % and 19 % for Cd and Zn, respectively.

Aluminium and stainless-steel alloys were prepared as small cylinders (3.2 mm x 3.2 mm). Samples melted within a few seconds of the arc ignition. Elements appeared to distill from the sample in the order of their volatilities. Irreproducible transient signals were observed, which indicates that the arc is not suitable for general analysis of solid alloys.

Nonconducting powders were packed into a small graphite cup for analysis. The rf arc was capable of sampling both volatile and refractory elements from inorganic material, e.g., coal fly ash. However, sample was not totally consumed in the course of a 9 sec burn and sampling was erratic. High organic content samples extinguished the rf arc shortly after its ignition.

Human et al. [32] introduced a spark chamber for solid sampling. A spark between an anode and a conducting sample (the cathode) produced particles from the sample. The particles were then entrained in the carrier gas flow to the ICP discharge. Presently, two commercial instruments that utilized spark aerosol generators are available: the separate sampling and excitation analysis system (SSEA) from Thermo Jarrel-Ash [33] and the conductive solids nebulizer (CSN) from Applied Research Laboratories [34].

The spark chamber of Human et al. [32] consisted of a circular anode section and a thorium-treated tungsten rod as

the counter electrode. The anode was attached to one side of a hollow Perspex cylinder. The cathode (conducting sample with flat surface of >35 mm dia.) was sealed to the other side of the cylinder by an O-ring. An Ar flow of 1 L/min delivered the aerosol from the chamber to the plasma. A voltage-stabilized trigger spark source was used with a discharge voltage of 12 kV (constant). The repetition rate was 50 sparks/sec.

The device was tested on aluminium and brass samples. Detection limits for Cu, Mg, and Zn (in Al alloys) were 3, 2, and 150 ppm. Precision was 4-6 % RSD for Cu in Al alloys. The calibration curves were linear only within a restricted concentration range.

Marks et al. [35] used the SSEAS for the analysis of nickel-based superalloys. The alloys contained major alloying additions of the refractory metals (Ta, W, and Nb) which made dissolution difficult. Detection limits for Cu and Mg were 3 and 2 ppm, respectively.

Broekaert et al. [24] used a medium-voltage spark to sample Al and Al alloys. It was found that the analyte introduction rates increase with both the sparking voltage and the sparking repetition rate. The mean particle sizes were about 1  $\mu\text{m}$ . Detection limits of 0.5 and 0.2 ppm were obtained for Cu and Mg. The precision was approximately 1 % RSD.

Generally, precision for the spark ablation technique falls in the range of 0.5-5 % RSD for various alloy

materials, which is superior to other solid sampling techniques [5]. Accuracies for analysis of alloy standards fall within a few percent relative error. Detection limits for the spark ablation ICP excitation technique in the solid sample extend down to the ppm range, which are comparable to those for solution nebulization, considering the dilution factors for sample dissolution. In addition, only a few micrograms of ablated material were needed. Therefore, the technique is well suited for quantitative analysis of electrically conducting samples.

### 1.6 Laser Ablation

After the invention of the ruby laser by Maiman in 1960 [36] it was soon realized that high powered lasers could be used to vaporize small amounts of materials from the surface of a sample. Several research groups have investigated the use of a laser as a sampling device for ICP-AES [37-39].

It is known that the laser plume contains significant amounts of solid particulate material as well as sample vapor. The ICP, with its high temperature and relatively long sample residence time of introduced species in the plasma, was considered to be effective for further vaporizing the solid fraction of the ablated material and converting it to an atomic state [38].

Carr and Horlick [38] used a ruby laser for solid sampling. A rod type and a disc type sampler have been

developed. The sample chambers were connected directly to the base of the ICP torch. A photodiode array spectrometer was used as a detector because of its multichannel measurement capability as well as providing the option of either time resolving the transient emission signal or integrating the total emission signal. Signal was integrated for 10 s over two consecutive laser shots.

The free running mode of the laser was preferred over the Q-switched mode. This is because about 25  $\mu\text{g}$  of material was removed by the laser in the Q-switched mode while 500  $\mu\text{g}$  was removed in the free running mode. The larger sample size is less susceptible to sample inhomogeneities.

Aluminium samples and NBS naval brass standards were analysed. Precisions of 4 % were obtained. Detection limits were estimated to lie at the sub-nanogram level, and may be improved one-to-two orders of magnitude to picogram levels if a PMT detection system were to be used. An analytical curve based on copper to zinc intensity ratios was determined for the NBS brass samples. The slope of the log-log plot was 1.07 and the overall average RSD was 3.3 %. Analytical curves for the high aluminium samples, based on the intensity ratios of Mn/Si, Mn/Mg, and Si/Mg, were also obtained. The slopes of the log-log plots ranged from 0.53 to 0.87, which indicates that some type of matrix effect was operative. Spatial inhomogeneities of samples were also demonstrated by the fluctuating Mg intensities from different craters of the same sample.

Thompson et al. [39] used a laser microprobe for sampling. It consisted of a ruby laser head mounted in a binocular microscope. The minimum crater size that could be produced was 10  $\mu\text{m}$  in diameter, but diameters  $>300 \mu\text{m}$  were required for satisfactory sensitivities. Gravimetric mass loss determined with a microbalance was approximately 1  $\mu\text{g}$ .

A standard low-alloy steel was analysed. Precision was  $<2 \%$  for iron and nickel. Since nickel was known to be homogeneously distributed in the sample, the precision of this technique was better than 2 %. Precisions for Cu, Cr, and Si were 4.7 %, 9.0 %, and 24.6 %, respectively. The large variation of Si intensity was due to a large sampling error related to a small sample size.

Calibration of minor elements (Ni, Cu, Cr, Mn, Mo, V, P, S) in steel standards showed a strong linear trend, although Si data was scattered due to transport problems (silica may tend to be adsorbed on the chamber surface). Absolute detection limits were on the order of tens of picograms, comparable to that for conventional nebulization (assuming 2 % efficiency).

Abercombie et al. [37] used a pulse-transverse excited  $\text{CO}_2$  laser to vaporize solids samples. When used for geochemical prospecting, the method suffered from inhomogeneity problems because of the small sample size. Thompson et al. reported a similar observation [39].

It is concluded that the laser ablation technique is more universal than the electroerosion technique because it

can handle both conducting and nonconducting samples. In addition, the small sample area examined by the focused laser beam allows local and/or *in situ* microanalysis, yielding information not available by standard macro-analytical techniques. The small sampling area and sample size can, however, introduce significant sampling errors.

Although the method generates transient emission signals similar to that of the ETV-ICP technique, no effect equivalent to the pressure pulse in the ETV technique was observed [39]. Therefore, precisions are potentially better.

### 1.7 Direct sample insertion

The ICP is a high energy source, but powdered samples introduced into the plasma by direct injection methods or slurry nebulization do not vaporize completely unless the particle size is small. The low vaporization efficiency arises because the resident time of the particles in the plasma is limited to a few milliseconds. Heat transfer from the plasma is not fast enough to vaporize large particles (>10  $\mu\text{m}$ ). The direct sample insertion (DSI) technique remedies this problem by placing a sample probe inside the plasma (Figure 1-1). Therefore, the sample, contained in the sample probe, has sufficient time to volatilize. As well, sample introduction efficiency is 100 %, superior to any other method described above.

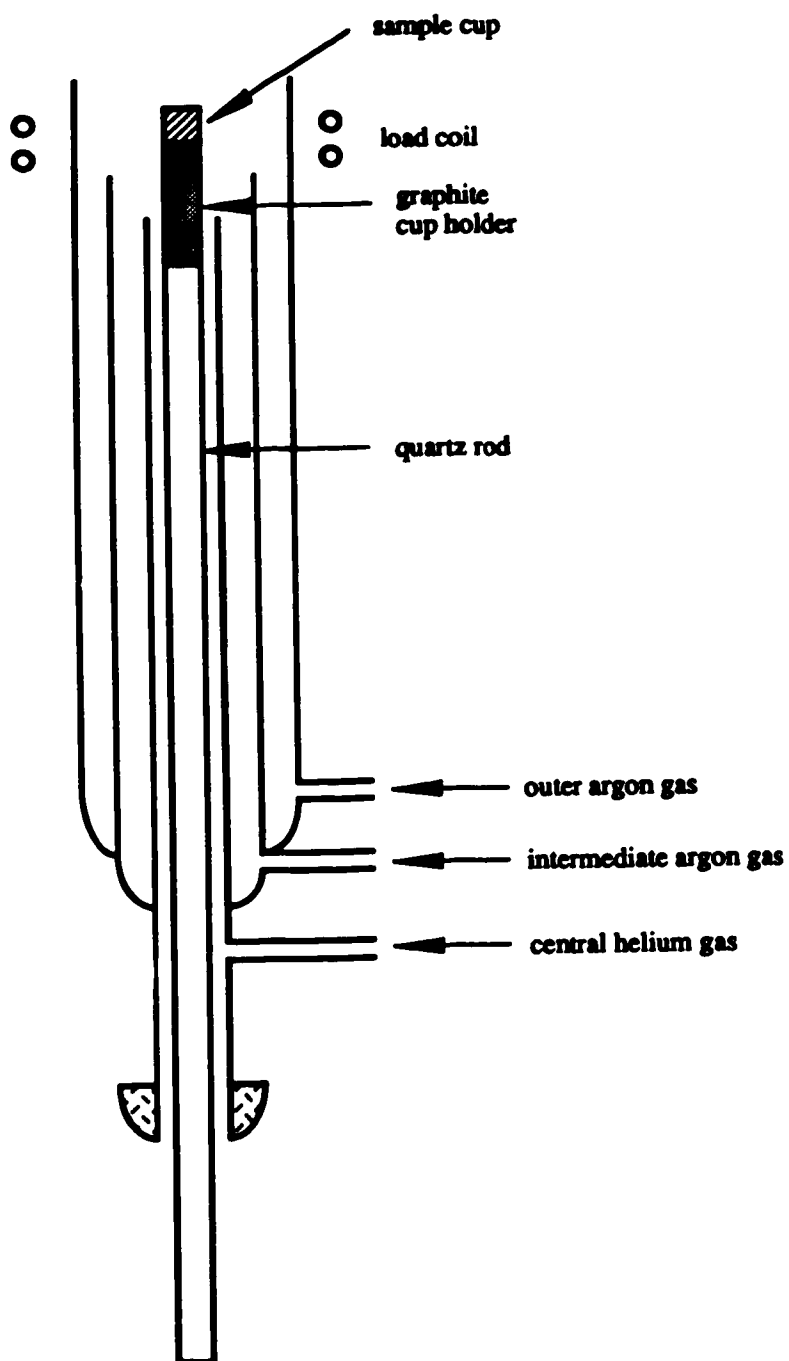


**Figure 1-1.** A typical DSI torch configuration.



The DSI technique is capable of handling small quantities of either liquids (i.e., a few  $\mu\text{l}$ ) or solid samples (i.e., a few mg). Therefore, multi-element analysis can be performed even when limited sample quantities are available. Sample introduction can be achieved with little or no sample pre-treatment, thus reducing or eliminating sample preparation. In addition, by positioning the sample probe at positions successively closer to the plasma, *in situ* sample pre-treatment (drying and ashing) prior to volatilization/atomization of a sample is possible.

Since the first description of a direct sample insertion (DSI) device for the inductively coupled plasma in 1979 by Salin and Horlick [40], several different systems based on this concept have been reported [41-62]. These developments improve on the insertion mechanism, data acquisition method, sample treatment, sample probe, as well as the automation of the device. A thorough review of these reports can be found in chapter 1 of the thesis of Karanassios [63]. However, the development of a DSI system, i.e., both hardware and software, to realize its full analytical potential has only been described recently [44].

Linear calibration curves have been constructed for both liquid and powdered/solid samples (mostly geological and botanical SRMs). The precision reported ranged from 1-25 % RSD. A typical value was in the range of 5-10 %. Detection limits were in the ng to pg range.

The work reported in this thesis focuses on the further development of the DSI device of Shao and Horlick [41]. A microcomputer controlled DSI system has been developed from this device and will be described in the following chapter.

A three dimensional view of the DSI device is shown in Figure 1-2. Details of the system are summarized below. A full description of the system as well as its analytical performance can be found in reference 41.

The frame of the unit is made of plexiglass. It is compact and light weight, and was designed to be attached to a commercial ICP spectrometer (ARL 34000) as a sample introduction module, replacing the original nebulizer/spray chamber solution sample introduction system.

The torch is a modified Fassel type with a central tube of 7 mm internal diameter to accommodate the sample probe. The bottom of the torch is sealed by a glass shutter except during sample insertion so as to maintain the gas pressure in the central tube of the torch and keep the plasma discharge at its normal position. The glass shutter is normally open, i.e., if no power is applied to the solenoid which closes it, it is held open by a spring. This implementation minimizes the chances of impact between the sample cup assembly and the shutter in the case of a solenoid malfunction. During insertion, the glass shutter is opened and the plasma discharge drops to the top of the intermediate tube. When insertion is complete, a teflon stop at the end of the quartz

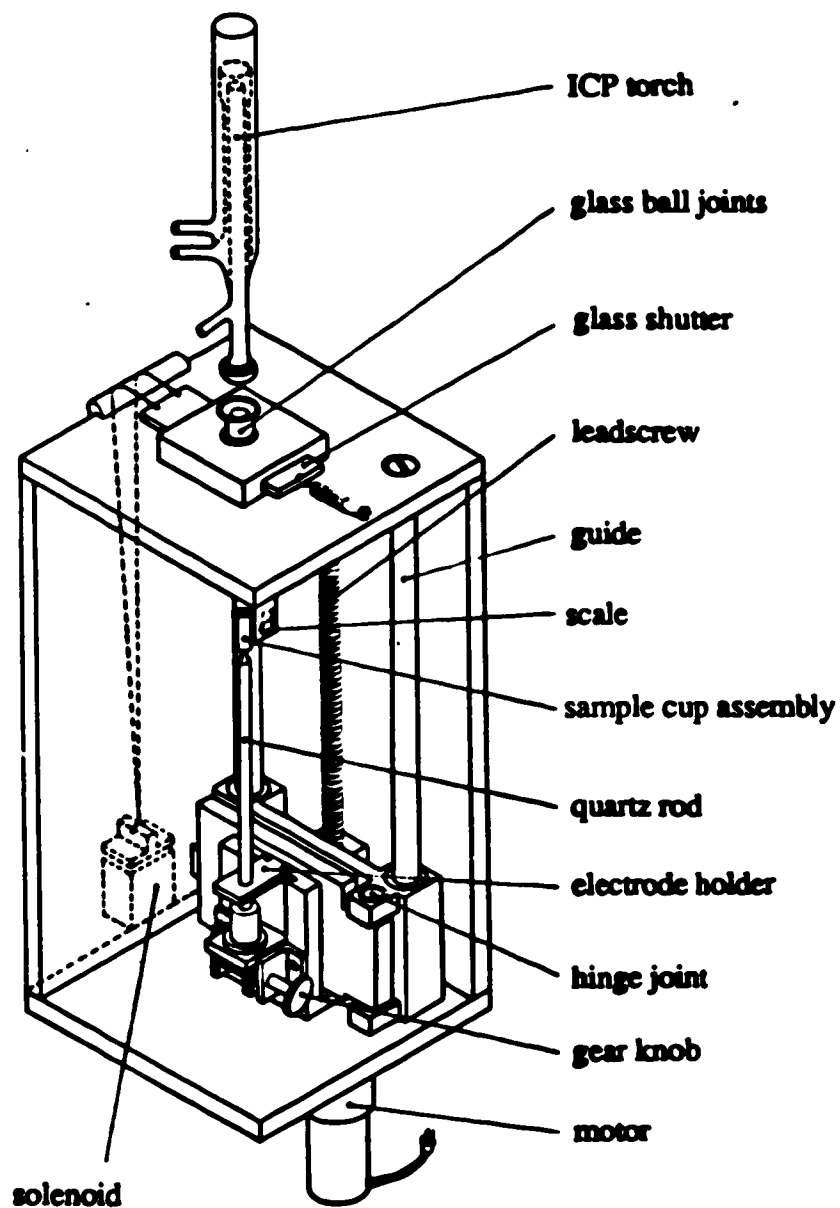


**Figure 1-2.** Three dimensional view of the DSI device of Shao and Horlick.

rod seals the bottom of the central tube and the plasma returns to its normal position.

The sample probe platform is driven by a reversible dc motor which is coupled to a leadscrew with a gear box. The motor is started manually with a switch, and it is stopped with a microswitch positioned at the top of the device. Ashing of a sample is possible by placing another microswitch at an appropriate position. The total time for a full insertion of the sample probe is about 5 seconds. A pair of metal guides ensure that the movement of the elevation platform is precise and reproducible.

The transient signal is integrated with the original readout electronics of the ARL 34000 (integration time: 40 seconds), or it is recorded with a high speed current amplifier (Keithley 427) and a chart recorder. The synchronization of the start of integration and the start of the sample probe insertion is carried out manually since there is no communication between the motor and the computer of the ARL 34000.

Custom-made sample cups as well as graphite sample cups utilized in classical dc arc emission spectroscopy are used as sample probes. The cup sits on top of a quartz rod which is fixed on the sample cup holder. The entire cup holder assembly swings out on a hinge joint in order to facilitate the changing of the sample cup, which is accomplished manually.

The system described above serves as a framework for further development. The insertion sequence and data acquisition were automated with a computer controlled system. A set of software was developed to control these processes and perform signal processing. To facilitate software control, the dc motor was replaced with a stepper motor and custom electronics that can handle transient signals were implemented. A new sample probe has also been designed to allow faster temperature rise and robot cup transfer. The new system is described in detail in the following chapter.

## 1.8 Conclusion

There is considerable research being done on direct solid sampling for the ICP. Sample heterogeneity is a major concern for all approaches because of small sample sizes. Absolute detection limits, however, are often improved over solution nebulization methods. Minimum sample treatment has also been realized, thus loss of sample or contamination are avoided and the time taken for sample analysis is reduced.

The goals of sample introduction are "the reproducible transfer of a representative portion of sample material to the atomizer cell, with high efficiency and with no adverse interference effects" [1]. As yet, there is no clear winner among the methods surveyed. ETV-ICP and DSI-ICP appear to be most promising. Further research to fully develop the analytical potential of each method is necessary. The work

described in the following chapters on the DSI technique is an attempt to realize the potential of one of these methods.

### References

1. R.F. Browner and A.W. Boorn, *Anal. Chem.* **56**, 786A (1984)
2. R.F. Browner and A.W. Boorn, *Anal. Chem.* **56**, 875A (1984)
3. F.J. Langmyhr, *Analyst* **104**, 993 (1979)
4. J.C. Van Loon, H. Haraguchi, and K. Fuwa, "Direct Elemental Analysis of Solids by Inductively Coupled Plasma Emission Spectrometry" in "Inductively Coupled Plasma Emission Spectroscopy", Part 2, P.W.J.M. Boumans, ed., John Wiley & Sons, New York, 1987, pp. 217-243
5. M.W. Routh and M.W. Tikkanen, "Introduction of Solids into Plasmas" in "Inductively Coupled Plasmas in Analytical Atomic Spectrometry", A. Montaser and D.W. Golightly, ed., VCH Publishers, New York, 1987, pp. 431-486
6. H.A. Laitinen and W.E. Harris, "Chemical Analysis", 2nd edition, McGraw-Hill, New York, 1975, pp. 565-582
7. T.B. Reed, *J. Appl. Phys.* **32**, 821 (1961)
8. T.B. Reed, *J. Appl. Phys.* **32**, 2534 (1961)
9. H.C. Hoare and R.A. Mostyn, *Anal. Chem.* **39**, 1153 (1967)
10. R.M. Dagnall, D.J. Smith, T.S. West, and S. Greenfield, *Anal. Chim. Acta* **54**, 397 (1971)
11. R.H. Scott, *Spectrochim. Acta* **33B**, 123 (1978)
12. K.C. Ng, M. Zerezghi, and J.A. Caruso, *Anal. Chem.* **56**, 417 (1984)
13. K.N. De Silva and R. Guevremont, *Spectrochim. Acta* **41B**, 865 (1986)

14. R. Guevremont and K.N. De Silva, *Spectrochim. Acta* **41B**, 875 (1986)
15. J.B. Willis, *Anal. Chem.* **47**, 1752 (1975)
16. W.W. Harrison and P.O. Juliano, *Anal. Chem.* **43**, 248 (1971)
17. M. Kashiki and S. Oshima, *Anal. Chim. Acta* **51**, 387 (1970)
18. C.W. Fuller, *Analyst* **101**, 461 (1976)
19. C.W. Fuller and I. Thompson, *Analyst* **102** 141 (1977)
20. C.W. Fuller, R.C. Hutton, and B. Preston, *Analyst* **106**, 913 (1981)
21. J.F. Wolcott and C.B. Sobel, *Appl. Spectrosc.* **32B**, 591 (1978)
22. J.R. Wilkinson, L. Ebdon, and K.W. Jackson, *Anal. Proc. (London)* **19**, 305 (1982)
23. L. Ebdon and M.R. Cave, *Analyst* **107**, 172 (1982)
24. J.A.C. Broekaert, F. Leis, B. Raeymaekers, and Gy. Zaray, *Spectrochim. Acta* **43B**, 339 (1988)
25. D.E. Nixon, V.A. Fassel, and R.N. Kniseley, *Anal. Chem.* **46**, 210 (1974)
26. D.R. Hull and G. Horlick, *Spectrochim. Acta* **39B**, 843 (1984)
27. W.M. Blakemore, P.H. Casey, and W.R. Collie, *Anal. Chem.* **56**, 1376 (1984)
28. M.W. Tikkanen and T.M. Niemczyk, *Anal. Chem.* **56**, 1997 (1984)
29. J.L. Jones, R.L. Dahlquist, and R.E. Hoyt, *Appl. Spectrosc.* **25**, 628 (1971)



30. R.L. Dahlquist, J.W. Knoll, and R.E. Hoyt, Pittsburgh Conference on Analytical Chemistry and Applied Spectroscopy, Cleveland, Ohio, Abstract No. 49 (1975)
31. P.B. Farnsworth and G.M. Hieftie, *Anal. Chem.* **55**, 1414 (1983)
32. H.G.C. Human, R.H. Scott. A.R. Oakes, and C.D. West, *Analyst* **101**, 265 (1976)
33. R. Gorden, R. Belmore, J. Beaty, and I. Aginsky, "Solid Sampling Literature Manual", Allied Analytical Systems, Waltham, Mass. (1983)
34. D.J. Comaford, J.E. Goulter, and D.B. Tasker, Pittsburgh Conference on Analytical Chemistry and Applied Spectroscopy, Cleveland, Ohio, Abstract No. 902 (1984)
35. J.Y. Marks, D.E. Fornwalt, and R.E. Yungk, *Spectrochim. Acta* **38B**, 107 (1983)
36. T.H. Maiman, *Nature* **187**, 493 (1960)
37. F.N. Abercombie, M.D. Silvester, G. Stoute, Pittsburgh Conference on Analytical Chemistry and Applied Spectroscopy, Cleveland, Ohio, Abstract No. 406 (1977)
38. J.W. Carr and G. Horlick, *Spectrochim. Acta* **37B**, 1 (1982)
39. M. Thompson, J.E. Goulter, and F. Sieper, *Analyst* **106**, 32 (1981)
40. E.D. Salin and G. Horlick, *Anal. Chem.* **51**, 2284 (1979)
41. Y. Shao and G. Horlick, *Appl. Spectrosc.* **40**, 386 (1986)
42. W.E. Pettit and G. Horlick, *Spectrochim. Acta* **41B**, 699 (1986)

43. V. Karanassios, G. Horlick and M. Abdullah, 'Characterization of a direct sample insertion device for ICP-AES', *Spectrochim. Acta*, (submitted)
44. V. Karanassios and G. Horlick, 'A computer-controlled direct sample insertion device for ICP-AES', *Spectrochim. Acta*, (submitted).
45. G.F. Kirkbright and S.J. Watson, *Analyst* **107**, 276 (1982)
46. G.F. Kirkbright and L.-X. Zhang, *Analyst* **107**, 617 (1982)
47. L.-X. Zhang, G.F. Kirkbright, M.J. Cope, and J.M. Watson, *Appl. Spectrosc.* **37**, 250 (1983)
48. N.W. Barnett, M.J. Cope, G.F. Kirkbright, and A.A.H. Taobi, *Spectrochim. Acta* **39B**, 343 (1984)
49. M. Abdullah, K. Fuwa, and H. Haraguchi, *Spectrochim. Acta* **39B**, 1129 (1984)
50. M. Abdullah and H. Haraguchi, *Anal. Chem.* **57**, 2059 (1985)
51. M. Abdullah, K. Fuwa, and H. Haraguchi, *Appl. Spectrosc.* **41**, 715 (1987)
52. E.D. Salin and M.M. Habib, *Anal. Chem.* **56**, 1186 (1984)
53. E.D. Salin and R.L.A. Sing, *Anal. Chem.* **56**, 2596 (1984)
54. M.M. Habib and E.D. Salin, *Anal. Chem.* **57**, 2055 (1985)
55. C.V. Monasterios, A.M. Jones, and E.D. Salin, *Anal. Chem.* **58**, 780 (1986)
56. C.W. McLeod, P.A. Clarke, and D.J. Mowthorpe, *Spectrochim. Acta* **41B**, 63 (1986)
57. A.G. Page, K.H. Madraswala, S.V. Godbole, M.J. Kulkarni, V.S. Mallapurkar, and B.D. Joshi, *Fresenius Z. Anal. Chem.* **315**, 38 (1983)

58. A.G. Page, S.V. Godbole, K.H. Madraswala, M.J. Kulkarni, V.S. Mallapurkar, and B.D. Joshi, *Spectrochim. Acta* **39B**, 551 (1984)
59. D. Sommer and K. Ohls, *Frezenius' Z. Anal. Chem.* **304**, 97 (1980)
60. K. Ohls, *Spectrochim. Acta* **39B**, 1105 (1984)
61. E.R. Prack and G.J. Bastiaans, *Anal. Chem.* **55**, 1654 (1983)
62. A. Lorber and Z. Goldbart, *Analyst* **110**, 155 (1985)
63. V. Karanassios, Ph.D. Thesis, University of Alberta (1988)

## **Chapter 2. Instrumentation for a DSI-ICP System**

### **2.1 Introduction**

The concept of direct sample insertion (DSI) for the inductively coupled plasma (ICP) was first described by Salin and Horlick [1] in 1979. Since then, several different DSI devices based on this concept have been reported [2-26]. The analytical capability of this technique, especially the high sample introduction efficiency and low absolute detection limit, have been demonstrated. A thorough review of these reports can be found in chapter 1 of the thesis of Karanassios [27].

Since the analytical merit of the DSI-ICP technique is well established, a DSI-ICP system should be developed to realize its full analytical potential [5]. A system, based on the DSI device of Pettit and Horlick [3], has been built. It includes both hardware and software designed specifically for this technique. A full description of this system can be found in the thesis of Karanassios [27].

A different DSI system has been developed from the DSI device of Shao and Horlick [2]. The DSI system consists of a DSI device, an ICP spectrometer, a robot arm, readout electronics, a sample cup organizer, and a microcomputer. The microcomputer coordinates the actions of the DSI system. A block diagram of the DSI system is shown in Figure 2-1.

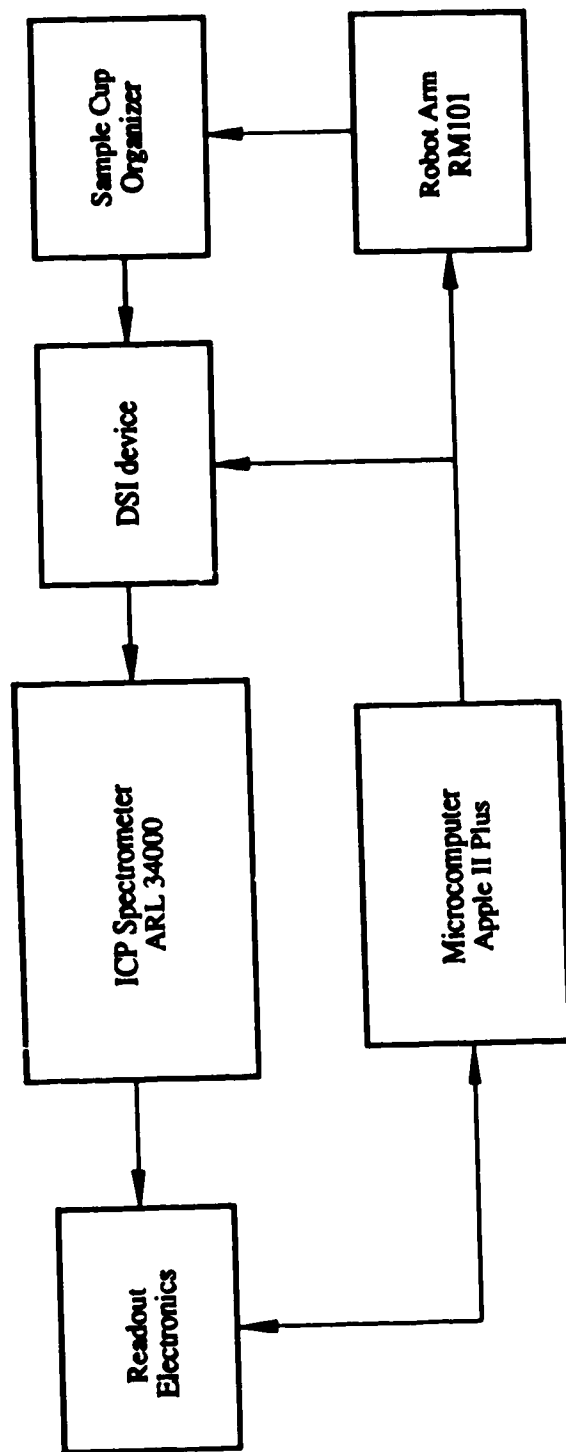


**Figure 2-1.** Experimental set-up of the direct sample insertion (DSI) system.

The DSI device is attached to the bottom of the torch box of a commercial ICP spectrometer, an ARL 34000. It replaces the original nebulizer/spray chamber. Samples are placed in sample cups for insertion. The usual sample size is a few microlitres of solution or a few milligrams of solid. Samples are inserted into the ICP discharge directly for volatilization and excitation. A mechanical driving mechanism is used for insertion.

The ICP spectrometer is a direct reader, i.e., multi-channels of emission signals can be monitored simultaneously. This is critical for the DSI-ICP technique because the signal from discrete samples is transient. A scanning monochromator would not be fast enough for multi-element analysis.

The signals from the photomultiplier tubes (PMT) of the spectrometer are directed to a set of current-to-voltage amplifiers. The original integrators are too slow for the transient signals and thus are by-passed. The signals are amplified and digitized with faster readout electronics and stored on floppy disks for data processing.

A microcomputer controls the insertion sequence of the DSI device and the readout electronics. It also controls a robot arm for sample cup transfer between the DSI device and the sample cup organizer. Custom software has been developed for control and data processing.

Detailed descriptions of each component of the DSI system and the software are provided in the following sections.

## **2.2 The ICP spectrometer**

The ICP spectrometer is a commercial instrument, an ARL 34000. Some modifications of the spectrometer have been implemented. The standard ICP torch was replaced with a modified torch, the DSI-ICP torch. The nebulizer/spray chamber was removed and the DSI device installed. The original integrating readout electronics were replaced with custom electronics.

Typical ICP operating conditions were similar to those described by Shao and Horlick [2]: outer argon gas, 10.5 l/min (40 psi); intermediate argon gas, 0.65 l/min (20 psi); central helium gas, 0.40 l/min (20 psi); forward power, 1.2 kw; reflected power, 0-20 w; and viewing height at 15 mm above the top of the load coil.

## **2.3 The Direct Sample Insertion Device**

The DSI device of Shao and Horlick [2] was modified so that it could be automated. A stepper motor and new gear box replace the old dc motor system. The timing and stepping sequence of the stepper motor are controlled by a micro-computer. The microswitches for positioning of the elevation platform were removed, since the position of the platform is now known by counting the number of steps of the motor. A new

design of the sample cup assembly has also been implemented, but the DSI-ICP torch of Shao and Horlick was unmodified.

### **2.3.1 The DSI-ICP Torch**

The standard Fassel type ICP torch used with solution nebulization systems must be modified for DSI application. A comparison of these two torches and their operating parameters is shown in Figure 2-2. The detailed dimensions of the DSI torch are given in Figure 2-3. The DSI-ICP torch has the same outside diameter as a standard torch, but has an enlarged central tube to accommodate the sample cup assembly. There is also an extra gas inlet to the central tube for the central gas (helium). Helium was used as the central gas to minimize the formation of a filament discharge between the plasma and the sample cup during insertion and retraction of the sample cup assembly [2]. It also reduces the reflected power when the sample cup is fully inserted in the plasma.

### **2.3.2 The Drive**

The original design of the DSI device incorporating a reversible dc motor was not flexible in terms of insertion timing and position. The insertion speed was also slow. The dc motor was replaced by a stepper motor (model PH299-01, Oriental motor, Japan) in the present system. This stepper motor is controlled with an Apple II Plus microcomputer



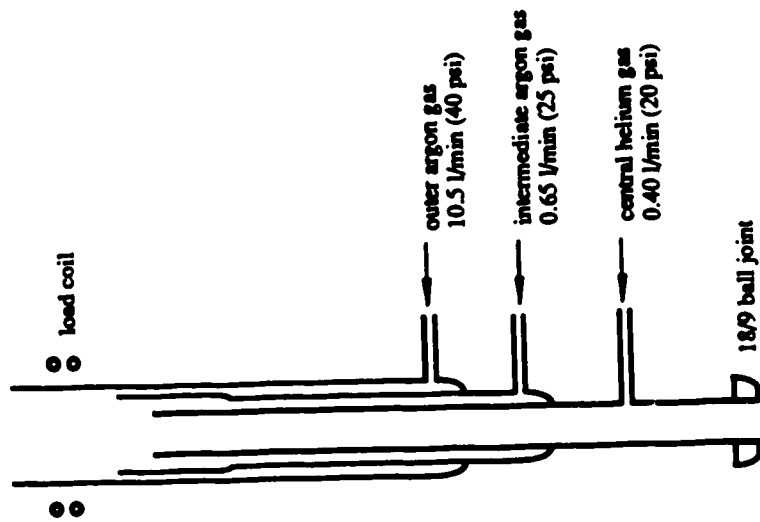
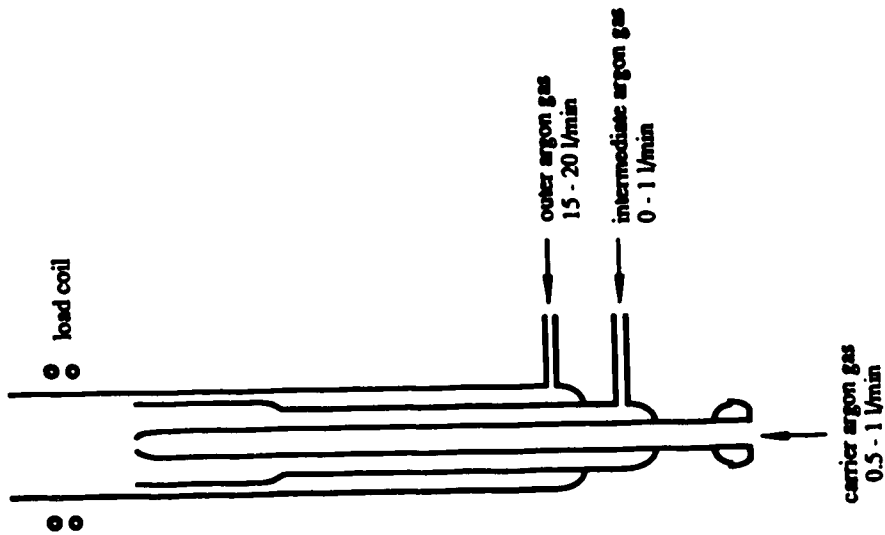


**Figure 2-2.** The modified ICP torch for the DSI device (left) and a typical Fassel type torch (right). Note that the central tube inner diameter of the DSI-ICP torch is enlarged to 0.75 cm to accommodate the sample cup assembly.

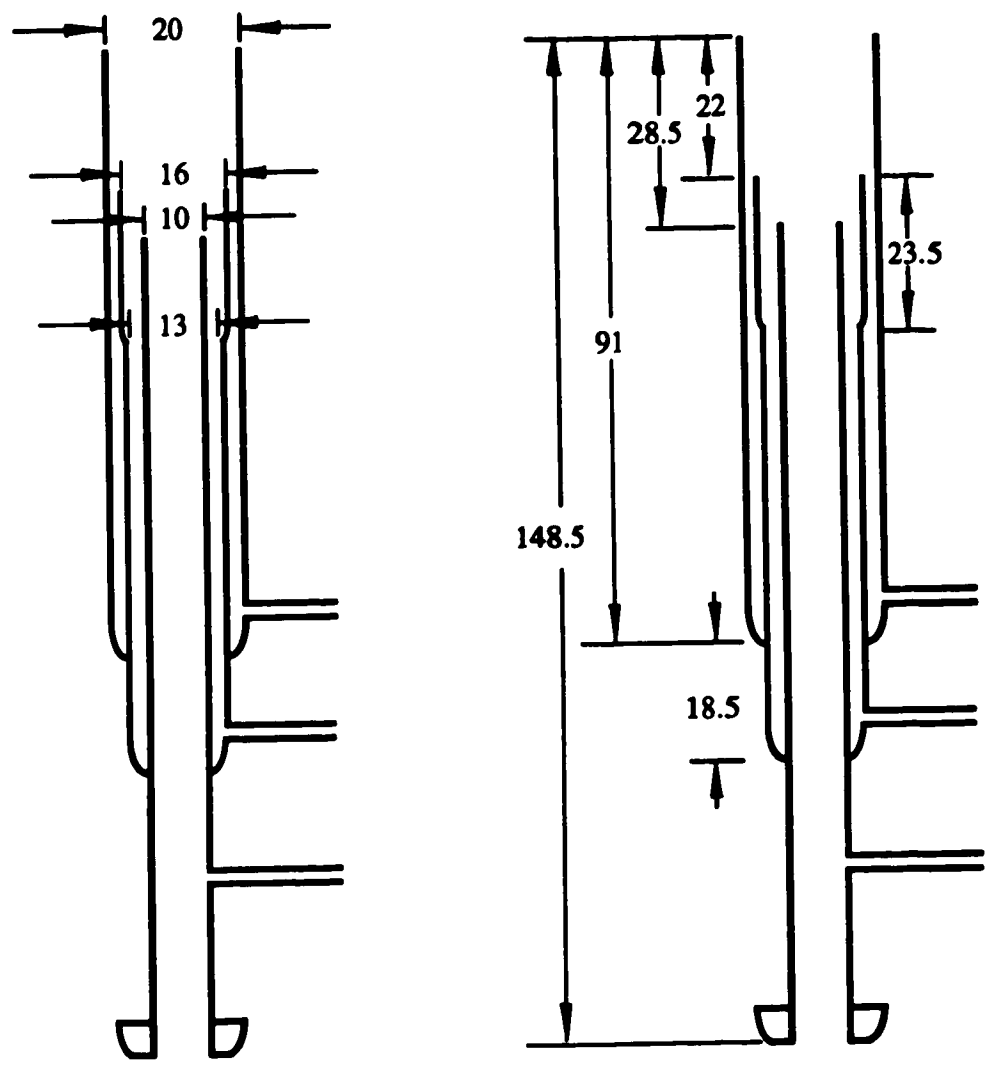


Figure 2-3. Dimensions of the DSI-ICP torch in mm.

through an A6 T/D timer driver board and a R2D34 driver board (Rogers Labs, INC., 2710 South Croddy Way, Santa Ana, CA 92704, U.S.A.).

The stepper motor is coupled to a gear box which is in turn coupled to the leadscrew of the DSI device. It takes 2190 steps of the stepper motor for the elevation platform to traverse the full length of the device (185 mm). At the top speed of 1200 steps/sec, this translates to less than 2 seconds for full insertion or retraction of the sample cup if no drying/ashing or cooling steps are required. A fast insertion speed produces sharp signal peaks and better precision for volatile elements, thus improving analytical performance [4]. However, the speed of insertion is flexible. It can be changed with ease by using a different set of ramp parameters for the motor.

The insertion position of the sample cup is known to better than 0.1 mm by counting the number of steps of the stepper motor. This method is more precise and far more flexible than using a microswitch for positioning, as in the previous design [2]. Precise positioning of the sample cup is essential for reproducible analytical results.

By making use of the temperature gradient along the central tube of the DSI-ICP torch, samples can be dried and ashed *in situ* at various distances from the plasma discharge in the central tube. The optimal dry/ash position and timing depend on the properties of the sample. These parameters can

be adjusted accordingly by setting the runtime parameters of the stepper motor.

### 2.3.3 The Sample Cup Assembly

The sample cup assembly is illustrated in Figure 2-4. The sample cup is made of graphite or tantalum. It sits on top of a graphite cup holder which in turn sits on top of a quartz rod with a cup-shaped top. The assembly is positioned on an adjustable platform attached to the elevation platform of the DSI device. The exact final insertion position of the cup assembly can be adjusted by rotating a gear knob attached to the adjustable platform [2]. The sample cup insertion position is set so that when it is fully inserted, the top of the cup is aligned with the top of the load coil. Throughout the thesis, the position of the cup is measured relative to the top of the load coil, e.g., at full insertion position it is 0 mm below the load coil (blc); before insertion, it is 185 mm blc.

Sample cups and cup holders were machined out of graphite rods (part# 4087 HPND, from SPEX Industries, Inc., Edison, NJ, U.S.A., or equivalent from SCP, Science Division, 2367 Guenette, St Laurent, Quebec, Canada). The dimensions of the sample cup and cup holder are shown in Figure 2-5, along with a commercial dc arc electrode (part# 4004 HPND, from SPEX Industries, Inc.). The cup assembly, consisting of the sample cup plus the cup holder, has the same dimensions as

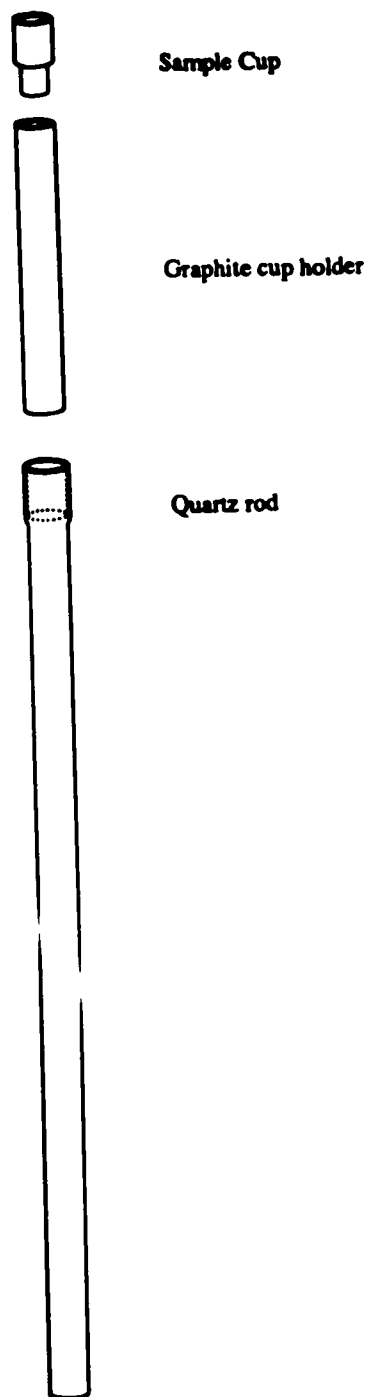


**Figure 2-4.** The sample cup assembly. The lengths of the cup, the holder, and the quartz rod are 8, 33, and 110 mm, respectively. The diameters of the cup and the holder are 5 mm, and the maximum diameter of the quartz rod is 7 mm.

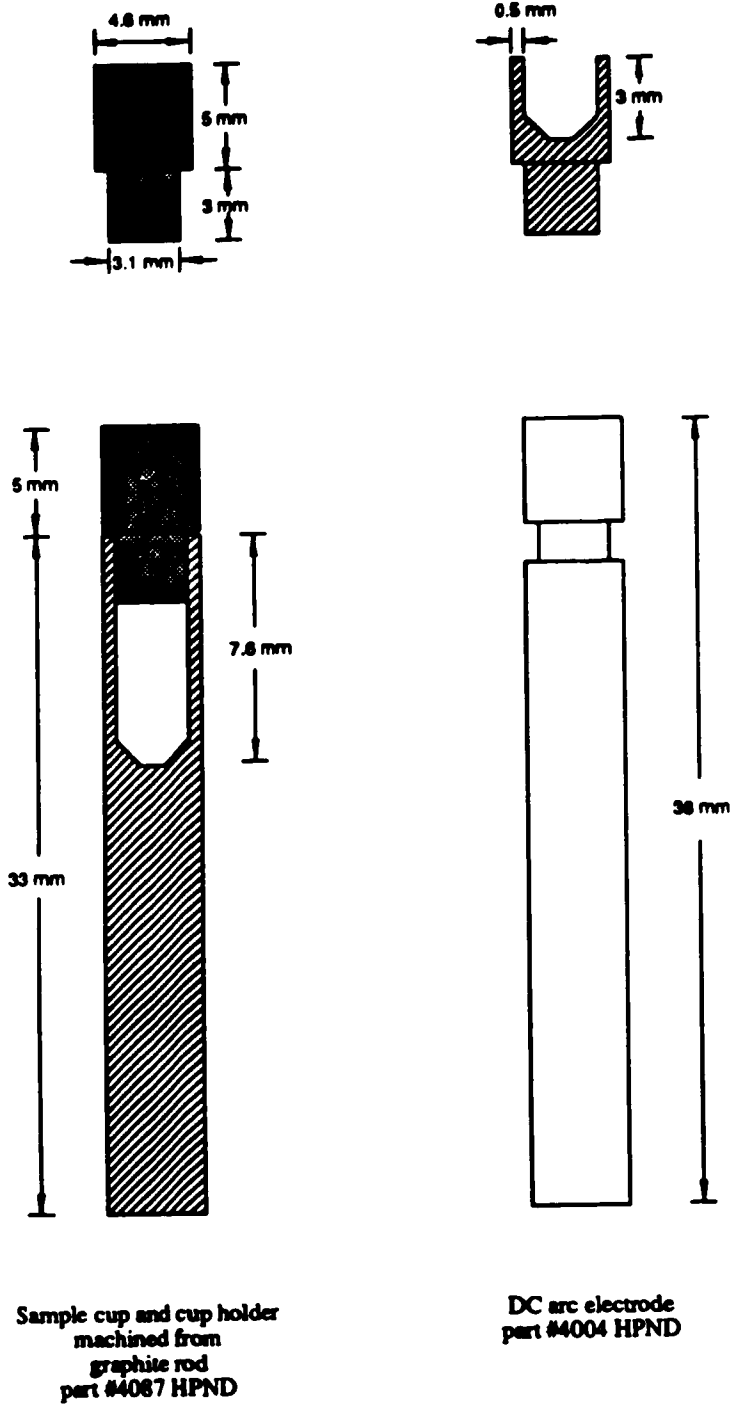


Figure 2-5. Dimensions of the sample cup and the cup holder.  
A dc arc electrode is also shown for comparison.

the dc arc electrode. However, the cup assembly has a lower mass because the upper portion of the cup holder is hollow. Moreover, heat conduction from the sample cup to the cup holder is poor because they are separated. Therefore, the signal characteristics with respect to the temporal behavior of the analyte are different.

The signal from the dc arc electrode has a slower rise time, which is probably due to a lower rate of increase of sample cup temperature. The rate of temperature increase depends on the mass (or heat capacity) of the cup assembly. The dc arc electrode has higher mass, therefore it has a lower rate of heating. The signal from the dc arc electrode also has a smaller peak area.

A new graphite sample cup or graphite cup holder is inserted into the plasma for 60 seconds (i.e. pre-burn) to remove possible contaminants acquired from the machining process. It is allowed to cool down in the torch at half insertion position before being fully retracted. This procedure is required because a sample cup in the plasma discharge can attain a temperature of 2000 K. Immediate retraction of the hot graphite cup from the plasma will result in oxidation of the cup in air, which results in rapid deterioration of the cup. Similar pretreatment is also required for metal (Ta, W) cups.

A sample cup holder can be reused about 50 times although the top portion is oxidized slowly and gradually becomes thinner and more fragile. A graphite sample cup can

be reused a few (~10) times depending on the nature of the sample. Nonvolatile analytes, for example, carbide forming elements like Ni, or powdered botanical samples, do not vaporize from the cup completely. The sample cups have to be discarded after each run for these types of samples to avoid analyte carry-over to the next sample.

## **2.4 Samples**

Discrete samples are used because of the nature of the DSI technique. The size of a sample depends on the capacity of the sample cup. Since the capacity is about 20  $\mu\text{L}$ , the sample size is approximately a few microlitres or a few milligrams for solution and solid samples, respectively.

### **2.4.1 Solution Samples**

Standard solutions were prepared by serial dilution with distilled/deionized water of 1000 ppm standard stock solution from SPEX (SPEX Inc., Edison, NJ, U.S.A.). Solution samples were transferred to a sample cup with an Eppendorf micropipette. The usual sample volume was 10  $\mu\text{l}$ .

The sample was dried at 35 mm below the load coil for 30 to 60 seconds before being fully inserted into the plasma. A sample could also be ashed at a closer position relative to the load coil (usually 16-24 mm b/c) for various periods of



time. The timing and position of the dry/ash process could be controlled with software which will be described later.

#### **2.4.2 Powdered Samples**

Powdered samples were weighed in a small tray with an analytical balance. Standard reference materials were dried in an oven at the recommended temperature before weighing. The sample was transferred to a sample cup through a funnel. After sample transfer, the powdered sample was tamped lightly with a small rod through the funnel.

Powdered samples were dried/ashed in the torch with a similar procedure to that used for aqueous samples.

Standard solutions and/or matrix modifiers could be added on top of the sample with a micropipette. If a large volume of solution ( $>20 \mu\text{L}$ ) was to be added, the solution could be added in portions of 10 or 20  $\mu\text{L}$  and the sample dried with a hot plate between additions. A metal block with an array of holes was placed on top of the hot plate. Graphite cup holders were placed in these holes so that the samples could be dried by placing the sample cups on top of the cup holders. The temperature of the hot plate was 80-90 °C.

#### **2.4.3 Sample Cup Organizer**

Samples were prepared as a group before analysis. The samples were placed in an organizer made of plexiglass with a capacity of 20 sample cups (Figure 2-6). The sample cups were arranged in two rows with 10 cups in each row. The cups were numbered starting from the left side of the front row. These numbers were used by the data recording and data processing software to identify the samples. When the robot arm was employed for cup transfer between the organizer and the sample cup holder of the DSI device, these numbers were also used as indices to locate the proper sample cup in the organizer.

The cup organizer was fixed on the robot table with a holder during analysis, so that the position of each sample cup was known exactly for robot access.

## **2.5 Robot Arm**

The sample cups were transferred from the cup organizer to the DSI cup holder manually or via a robot arm. With the introduction of a robot arm to the system, the DSI device has the potential to be fully automated.

### **2.5.1 The Position Parameters of the Robot Arm**

The robot arm is a Mitsubishi RM-101 Move Master (Mitsubishi Electric Corporation, Mitsubishi Denki Bldg, Marunouchi, Tokyo 100, Japan). It has five degrees of

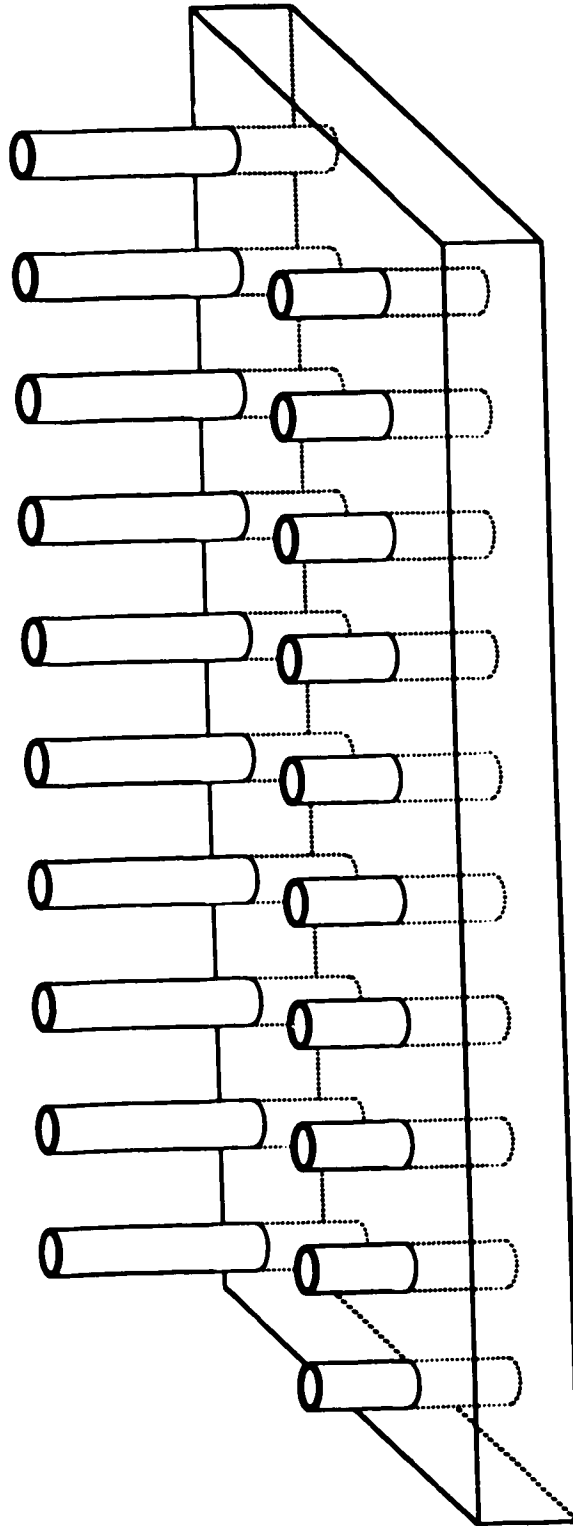


**Figure 2-6.** The sample organizer. Note that the sample cup holders at the front row are about 1 cm shorter than those at the rear row.

freedom: movements of the body, shoulder, elbow, and wrist (counts as two). The movement of these body parts is accomplished with six stepper motors: M1, body rotation; M2, arm pivoting at the shoulder; M3, forearm pivoting at the elbow; M4 and M5, hand rotation or bending at the wrist; M6, end effector open or close.

The home position of the robot arm was defined as: the robot facing the DSI device, the arm at  $80^\circ$  and the forearm at  $-50^\circ$  to the surface of the robot table, and the hand and the end effector parallel to the surface of the table. A schematic diagram of the robot home position is shown in Figure 2-7.

The robot arm was fixed on the robot table so that the relative position of the robot and the sample cup organizer was known exactly and remained stable. The robot table was bolted to the frame of the ARL 34000, therefore the robot to DSI device distance was also fixed. The arrangement of the robot station is shown in Figure 2-8.

The sample cup positions in the organizer and the cup holder were defined in steps of the six stepper motors relative to the home position of the robot. These position parameters were found empirically by moving the robot arm to that position with a program. The direction and increment of the movement of each stepper motor was individually controlled with different keys of the Apple II keyboard so that each joint of the robot could be turned independently to

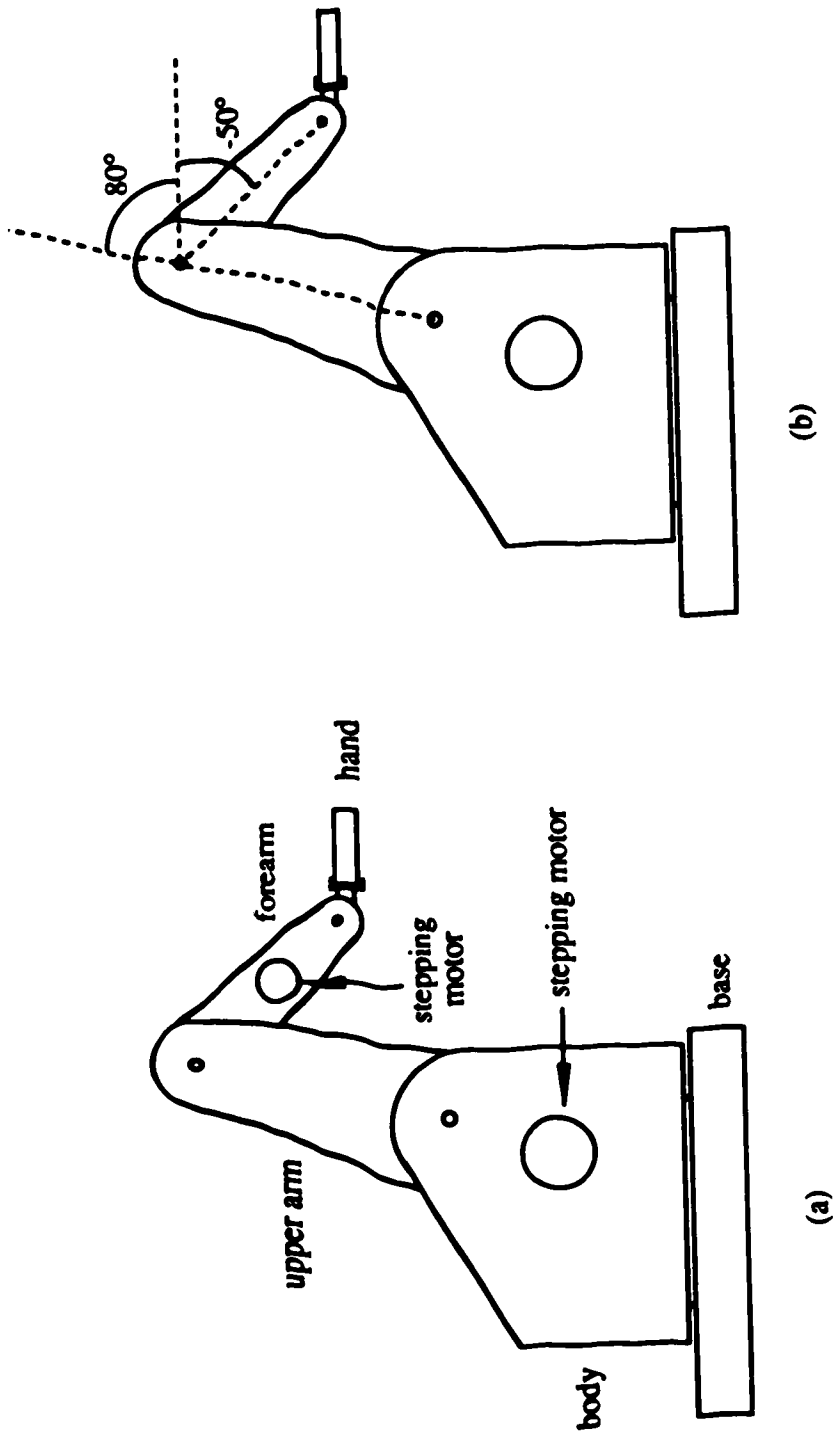


**Figure 2-7.** (a) Schematic diagram of the robot arm RM101 at home position.  
(b) Diagram showing the angles of the forearm and upper arm to the horizon at home position.

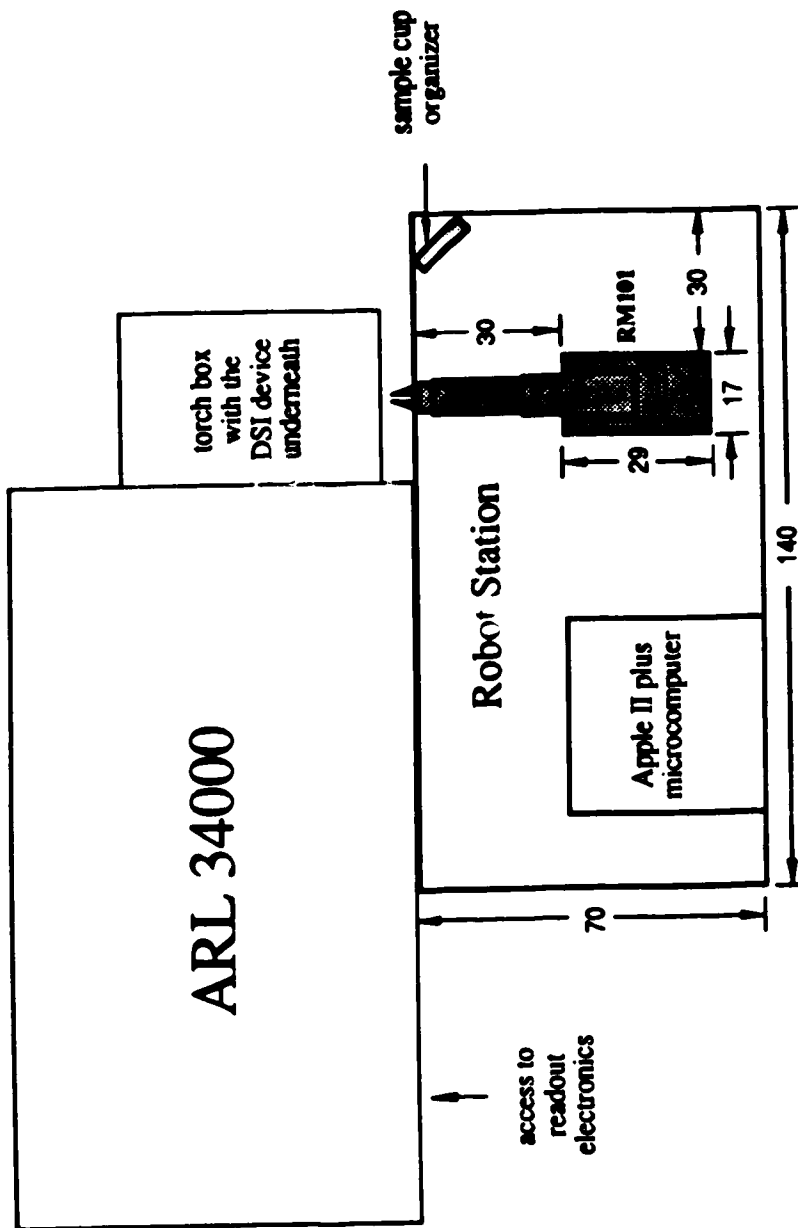


**Figure 2-8.** The robot station and the ARL 34000 spectrometer (Dimensions in cm).  
The height of the station is 71 cm.

lead the robot to the desired position. The overall movements of the six stepper motors were then combined and recorded.

Each sample cup in the organizer has four sets of parameters associated with it. These four sets of parameters represent four positions of the robot arm: (1) the end effector at the position ready to grasp the cup, with fingers open; (2) and (3) the end effector at the position ready to release the cup at the cup holder, with fingers open or closed; and (4) a buffer position above the first three positions to which the robot arm will move to before assuming any of the first three positions. These positions are indexed according to the sample cup number and initialized with the 'position' command into the memory of the robot. The robot can then go to these positions from any original position with a 'movement' command referring to the proper index.

### **2.5.2 The End Effector**

The end effector (i.e. a pair of fingers) attached to the hand of the robot was specifically designed for the sample cup used in this work. The dimensions of the end effector are shown in Figure 2-9. It is made out of aluminum. The end effector is quite long so that it can reach the sample cup on the DSI device with the sample cup assembly in its insertion position. The cup holder assembly does not swing out for sample cup changing when used in conjunction with the robot arm.

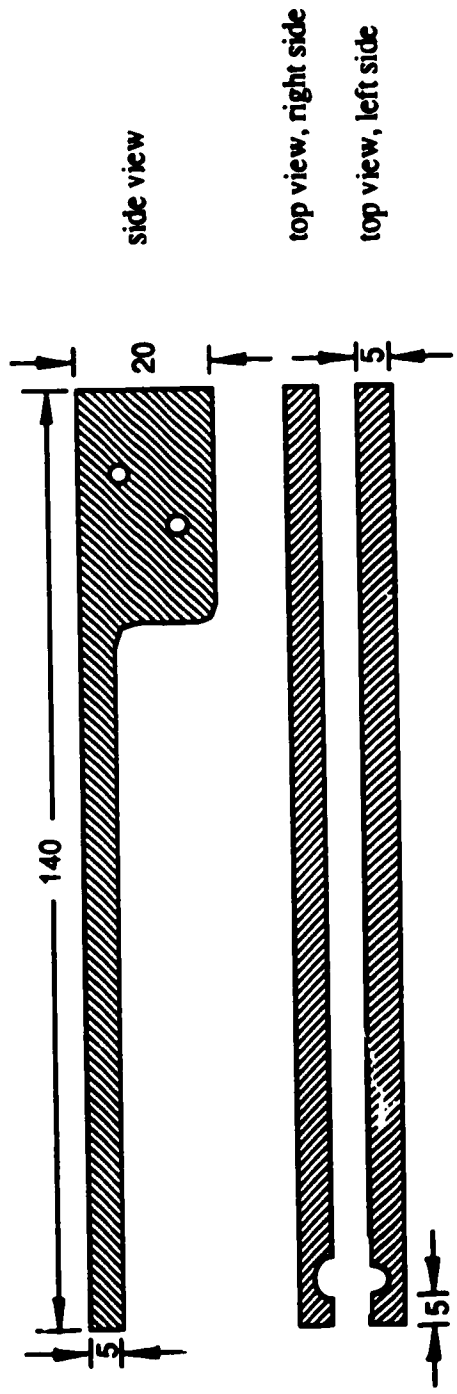


**Figure 2-9.** The end effector for the robot RM 101. The two holes at the right end of the top diagram match the holes on the hand of the robot, so that two sets of nut-and-bolt will secure the end effector to the hand. The side views illustrate that the openings on the left and right side are not equal.



The opening on the left side of the end effector has the same diameter as that of the sample cup, but the opening on the right side is slightly bigger. The purpose of this asymmetric arrangement is that even though the end effector may not be perfectly aligned, the sample cup will still be held tightly and vertically.

## 2.6 Readout Electronics

To obtain quantitative information about an analyte in a sample it is normal, in a direct reader, to integrate the anodic current from the PMT for an emission line of the analyte. However, the emission signal from a DSI-ICP system is transient and different analytes have different vaporization/atomization time behavior as illustrated in Figure 2-10. The readout electronics and associated software of a conventional direct reading ICP spectrometer are designed to have a fixed integration time for all channels. Therefore, setting the integration time for determining multiple elements of a sample simultaneously with a DSI system could be a problem: a short integration time will result in the omission of the tail of the signal of nonvolatile elements, but a long integration time will increase the background for volatile elements. Furthermore, information on the temporal behavior of the vaporization of an individual element is lost with an integration system. This information, though not used extensively at present, could be valuable in understanding

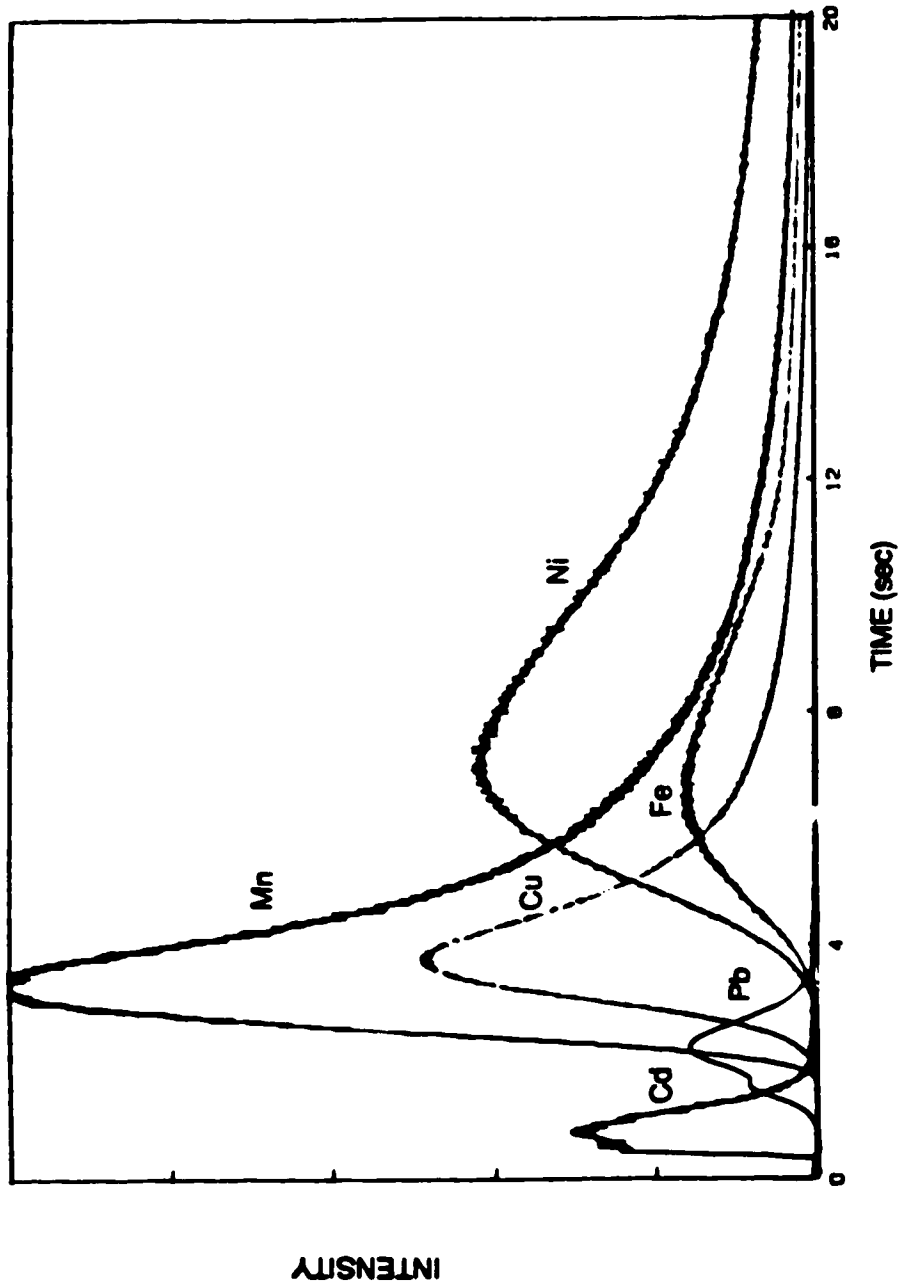


**Figure 2-10.** Temporal behavior of the emitting signal for 10  $\mu\text{L}$  of 100 ppm multi-element standard solution. The pre-amplifier gains for the analytes were: Pb,  $10^6$ ; Mn,  $10^6$ ; Ni,  $10^7$ ; Cu,  $10^6$ ; Fe,  $10^6$ ; Cd,  $10^5$  V/A.

the chemistry of analyte vaporization and also for identification of the various kinds of species of an element in a sample. To obtain the temporal behavior of an analyte, a current amplifier/chart recorder system [2, 6-11, 13, 16], a digital oscilloscope [6], or an analog to digital convertor (ADC)/microcomputer system [4, 13-17, 22] have been used in this and other laboratories.

In this work, a commercial analog-to-digital convertor (ADC) module, AI13, was used to digitize the signal in real time. The details of the ADC and its operation are discussed in the next section. The front end of the ADC was a set of current amplifiers which convert the anodic current from the PMTs to voltage. The voltage is then digitized by the ADC under software control.

Any six of the 34 channels of the ARL 34000 could be monitored by simply connecting the corresponding PMT to a current amplifier whose output was directed to the input of one of the channels of the AI13, as illustrated in Figure 2-11. The current amplifier used was either a Keithley model 427 amplifier or an operational amplifier, AD515 (Analog Devices, Route 1 Industrial Park, P.O.Box 280, Norwood, Mass. 02062, U.S.A.), configured as a current-to-voltage convertor with a 1 or 10 M $\Omega$  feedback resistor and a 220 pF capacitor connected parallel to the resistor. The gain of the OA was 10<sup>6</sup> or 10<sup>7</sup> V/A by selecting either a 1 M $\Omega$  or a 10 M $\Omega$  feedback resistance manually. The gain of the Keithley current amplifier was set to 10<sup>6</sup>, 10<sup>7</sup>, or 10<sup>8</sup> V/A. Although

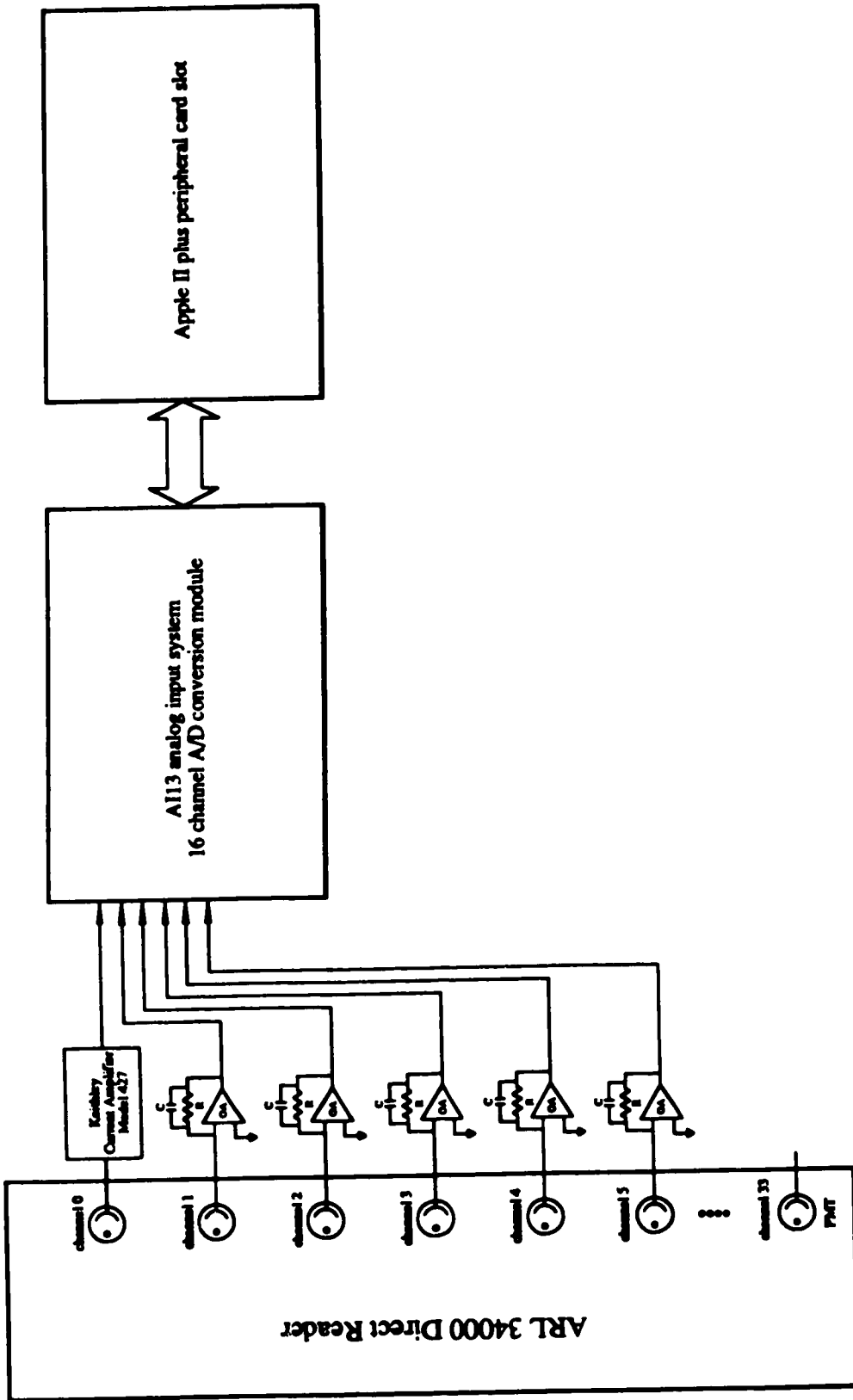


**Figure 2-11.** Readout electronics of the DSI system. The OAs are Analog Devices AD515 FET-input electrometer op amp.  $R = 1$  or  $10$  Mohm.  $C = 220$  pf.

the gains are set manually at present, a simple circuit with software selectable gain can be built for a fully automated system.

The components discussed above should not be viewed as individual objects but rather as parts of the direct sample insertion system. They are designed as a system so that the performance of the DSI device is optimized. These components are coordinated with a microcomputer running software developed specifically for this system.

## **2.7 Computer Hardware and Software**

The microcomputer used in this work is an Apple II Plus with 64 kbyte of memory. This computer has eight expansion slots on the back plane and numerous peripheral cards available for various interfacing purposes [28]. The peripheral cards used in this system include the A6 T/D board for stepper motor control, the AI13 board for analog-to-digital conversion, a Grappler plus parallel printer card for robot communication, a Super Serial Card for plotting on a Hewlett Packard 7470A plotter, a Videoterm 80 column card for text display, a Disk II controller card for two floppy disk drives, and a parallel printer interface card for a Centronic printer.

### **2.7.1 ADC Operation**

A commercial ADC module, AI13 (Interactive Structures Inc., P.O. Box 404, Bala Cynwyd, Pennsylvania, U.S.A.), is used to digitize the signals in real time. The AI13 has sample-and-hold circuitry, sixteen software selectable channels, eight programmable full-scale ranges ( $\pm 5$  v down to 0-100 mv), and 12 bit resolution. Total conversion time is 20  $\mu$ s. A conversion can be initialized with an external trigger or by software.

A BASIC program with an assembly language subroutine was developed to control ADC conversion. The assembly language subroutine was necessary for a fast conversion rate although it is possible to initialize a conversion with high level languages like BASIC. The conversion rate was normally 10 conversion/second/channel, but it could be altered easily by setting a software counter, say, to 100 Hz per channel. Up to six channels can be digitized with the present system. These channels are digitized sequentially at high speed (17.6 kHz), then a software counter serving as a timer counts 0.1 second and the conversion cycle is repeated until the desired number of data points are taken.

Although the AI13 has 16 channels, the number of channels digitized was limited to six. This limit existed because of the limited memory size (64 kbytes) of the Apple II Plus. The memory has to be shared between the main program, several assembly language subroutines, the variables, and the graphic window. Therefore, 6 kbytes of memory assigned for the conversion results is about the upper

limit available. Since a 12-bit ADC conversion result occupies two bytes of memory, the 6 kbytes of memory available can be used to store approximately 3000 data points. With a typical 50-60 seconds observation time and a data conversion rate of 10 Hz per channel, only six channels can be used at a time. Therefore six channels were used and a 3000 data point integer array (each element occupies 2 bytes of memory) was assigned for the conversion result.

The software developed for the DSI system is flexible so that the number of channels can be less than or equal to six. Also, the number of data points taken per channel (the observation time) is only constrained by the condition that the total number of data points (equal to number of channels times number of data points per channel) does not exceed 3000. For example, when monitoring three channels, the observation time can be as long as 100 seconds with a data conversion rate of 10 Hz. Of course, the observation time can be shortened for volatile analytes (by reducing the number of data points per channel) to speed up the observation cycle and the data processing rate.

### **2.7.2 Software**

The software of the DSI system can be divided into three categories: parameter file preparation, analysis of samples, and data processing.

### 2.7.2.1 Parameter Files

A parameter file is generated with a BASIC program to specify the parameters of the AI13, the stepper motor, and the sampler.

#### i. AI13 Parameters

The parameters of the AI13 include the channels to be converted, the number of data points for each channel, and the pre-amplifier gain of each channel. Although it is changed manually, it is important to have the pre-amplifier gain recorded precisely for quantitative analysis of the conversion result. The gain is chosen so that the maximum peak height of the transient signal is within the range of the AI13 and the quantizing error is a minimum.

The proper choice of the pre-amplifier gain requires a knowledge of the sensitivity of the analyte and the approximate amount of the analyte in the sample. The sensitivity of an analyte depends on the rate of vaporization of the analyte in the sample matrix as well as the emission line strength of the analyte. An empirical relationship between peak signal strength and concentration can be measured, and is shown in Figure 2-12. One can consult these data to determine the gain of the pre-amplifier. The intensity in Figure 2-12 is peak height normalized to the full scale of the AI13 at a pre-amplifier gain of  $10^7$  V/A,



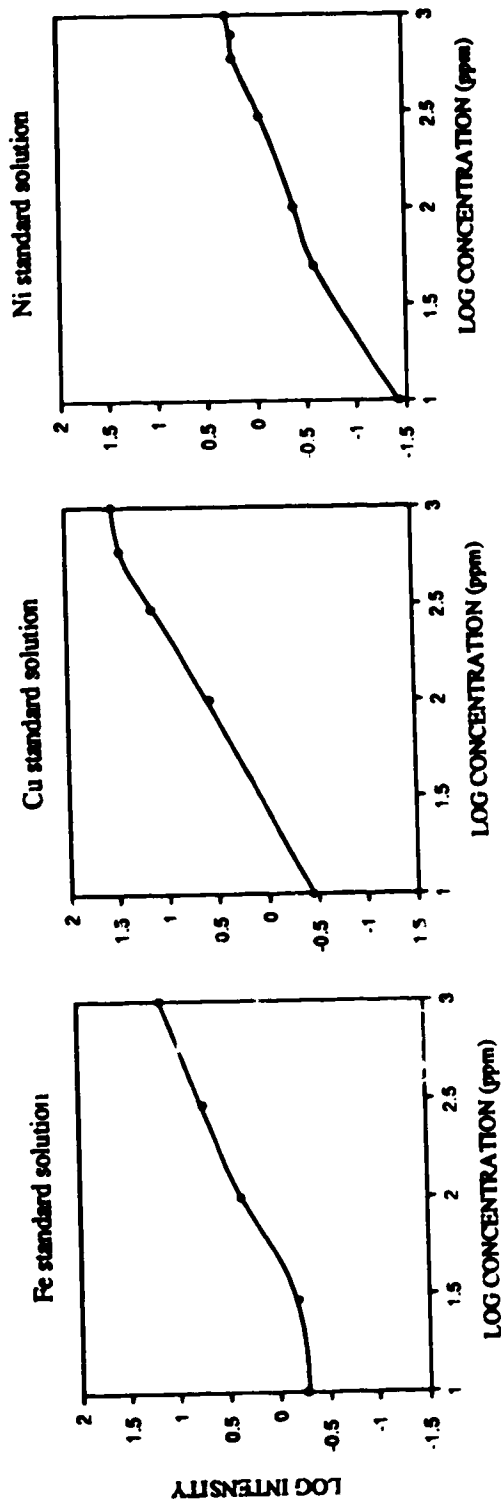


**Figure 2-12.** Calibration curves for Fe, Cu, and Ni standard solutions. The intensities are peak heights normalized to the full scale of the A113 with logarithm of pre-amplifier gain of 7 (V/A).

i.e. logarithm of intensity of '0' corresponds to full scale at gain of  $10^7$  V/A, logarithm of intensity of '1' corresponds to 10 times the full scale, logarithm of intensity of '-1' corresponds to 0.1 times the full scale, and so on. Therefore the optimal gain will be one tenth of  $10^7$  V/A (i.e.  $10^6$  V/A) for logarithm of intensity from 0 to 1, and ten times of  $10^7$  V/A (i.e.  $10^8$  V/A) for logarithm of intensity from -2 to -1. It should be emphasized that the calibration curve for an analyte using peak area as intensity is quite different from that using peak height. The calibration curve for Fe using peak area is shown in Figure 2-13. It is linear over a wide concentration range, while the "calibration" curve for Fe (peak height) is curved (Figure 2-12).

It is, of course, paradoxical to determine the gain according to the amount of the analyte in a sample before the analysis of a sample. If no information is available on the amount of the analyte, the gain is usually set at a lower value, e.g.,  $10^6$  V/A, and adjusted to the optimal value after examining the signal from the first run of the sample. Fortunately, the range of the amount of an analyte in a sample is often known within an order of magnitude.

#### **ii. Stepper Motor Parameters**

The stepper motor parameters include the stages of insertion to be implemented (i.e. drying, ashing, and full insertion), the number of steps taken to reach each stage,

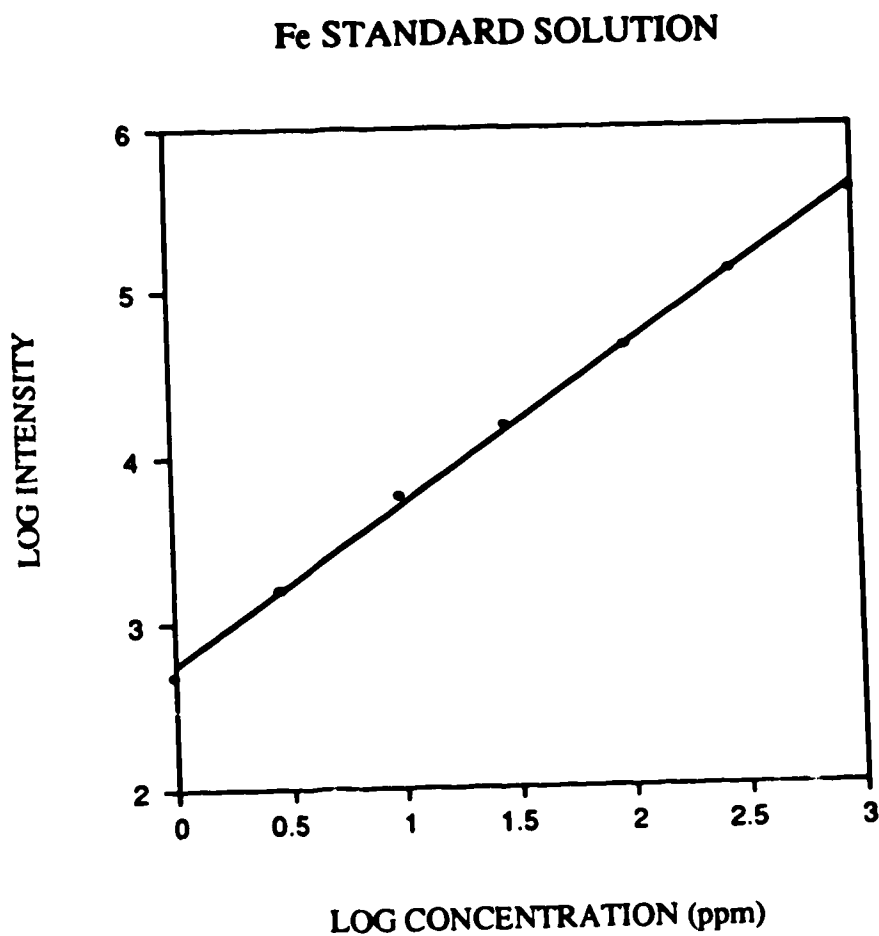


**Figure 2-13.** Calibration curve for Fe standard solution. Intensity is peak area in arbitrary unit. The slope of the curve equals 0.9597. The correlation coefficient equals 0.9994.

and the time delay between stages. The properties of the sample determines these parameters. A simple aqueous solution sample, e.g., well water, needs only a drying stage before full insertion. On the other hand, a powdered botanical sample will need both drying and ashing stages. A typical sequence, starting at 185 mm b/c, is: move 1776 stepper motor steps (sample cup now at 35 mm b/c), pause for 30 seconds (dry), move another 201 steps (18 mm b/c), pause for 60 to 120 seconds (ash) then move 213 steps to fully insert the cup.

### **iii. Sample Parameters**

The parameters of the sample specified in the parameter file include the number of samples, the weight or volume of each sample, the analyte and the pre-amplifier gain for each channel, and the concentration for each analyte.

All the parameters mentioned above are saved in a text file on a floppy disk with a name assigned to this file. This file is recalled for sample analysis and data processing.

### **2.7.2.2 Software for the Analysis Process**

The second set of software handles the analysis process. It contains a BASIC main program and several assembly language subroutines.

### **i. The BASIC Main Program**

The main program is written in BASIC because it is the built-in language of the Apple II Plus. Software development and debugging is simple in this native environment. This program will prompt the user for the parameter file name, load the file, then list the parameters and have the user confirm them. The program then asks for a data file name for this set of samples. The user also has an option to use the robot to transfer the sample cup, or to do this manually. After these routines, the program is ready for sample analysis.

The samples will be analysed sequentially in the order of their sample numbers. After each analysis, the signals are stored on the floppy disk with the data file name indexed according to the sample number. The data file contains the parameter file name as well as the raw data so that the runtime parameters and the analytical data are properly linked. Between samples, the program displays a menu with options to display the signals in a time profile fashion for each analyte, to proceed to next sample, or to exit the program (discontinue analysis). The time profile display option allows the user to monitor the results and make adjustment to some parameters accordingly.

Because of the options available after the analysis of each sample, user intervention is needed to proceed to the next sample. Therefore, the system is not fully automated at

present. A fully automated system would require that the software be able to make some decisions, e.g., select the optimal pre-amplifier gain before analysis. The program should also be able to make proper adjustments of the gain if signal is too strong and goes off scale or is too weak and quantizing error occurs. In order to make such decisions, one needs information and rules. These can be built in the software as a knowledge base and a rule base, which is the concept of an expert system. With a proper knowledge base and a rule base, the parameter file generating process can also be eliminated. The user would enter only the type of sample and the software could determine the proper running parameters for this sample and do the analysis accordingly.

Of course, some problems, like the gain selection, can be solved in other ways. For example, each channel could be digitized at all the gains available so that one of the gains will be optimal for the signal. However, this method generates excess data, which can slow down the analysis and demands more calculation effort during data processing. Therefore a rule based system is probably the best for a fully automated system for DSI.

#### **ii. Assembly Subroutines**

Since BASIC is relatively slow, some assembly language subroutines are employed for the real time applications. These subroutines include a data conversion routine, a

stepper motor ramp data and control routine, a disk space monitoring routine, and two timers for timing during the insertion sequence. These subroutines are loaded into the memory of the computer at system start-up. They are callable from within the main program with BASIC statements.

These subroutines are viewed as modules: once developed, they can be used with any other programs. Therefore, if the main program is modified, there is no need to rewrite the subroutines and considerable programming effort is saved.

### **2.7.2.3 Data Processing**

The third set of software does the data processing of the DSI signals. Several programs were developed to suit different processing requirements.

The first program goes through the indexed data files individually under the request of the user. The program is menu driven. It has the following options: plot the time profile on the screen, plot the time profile on the plotter, do integration and background subtraction of the peak-like signal, access other data files, and exit the program. Before processing a set of data, the program finds the information about the sample in the parameter file which is linked to the data file the user wishes to process. This information is then listed on the screen for reference.

This program is particularly suited for unknown samples, because the user can view the temporal behavior of the signal

first, then decide the integration range. Integration is implemented simply by summing the conversion results in the integration range. Background subtraction of the integrated signal is necessary for quantitative analysis. The background is found by integrating a flat portion of the time profile after the peak shaped emission signal of the analyte. This off-peak background subtraction method is illustrated in Figure 2-14. A permanent record of the temporal behavior can also be plotted. The program can plot several time profiles on a single sheet of paper with or without offset, so that visual comparison is possible for different samples.

A second program automates the data processing sequence. This program only requires the user to input the data file name (without the index) and the analytes to be processed. It will go through all the related data files for each analyte, determine the best integration range for each time profile, and carry out the integration and background subtraction. The results are listed in tabular form for each analyte. For standard addition determination, the program can also perform a linear regression analysis of the integrated signal and determine the content of an analyte in the sample. In the case of the analysis of solid samples, it is difficult to weigh a sample exactly to a certain mass, e.g. 5 mg. If the actual mass of each sample is known but it is slightly different from the nominal mass, e.g., 4.9 mg or 5.2 mg, the program use this actual weight to determine the analyte content.



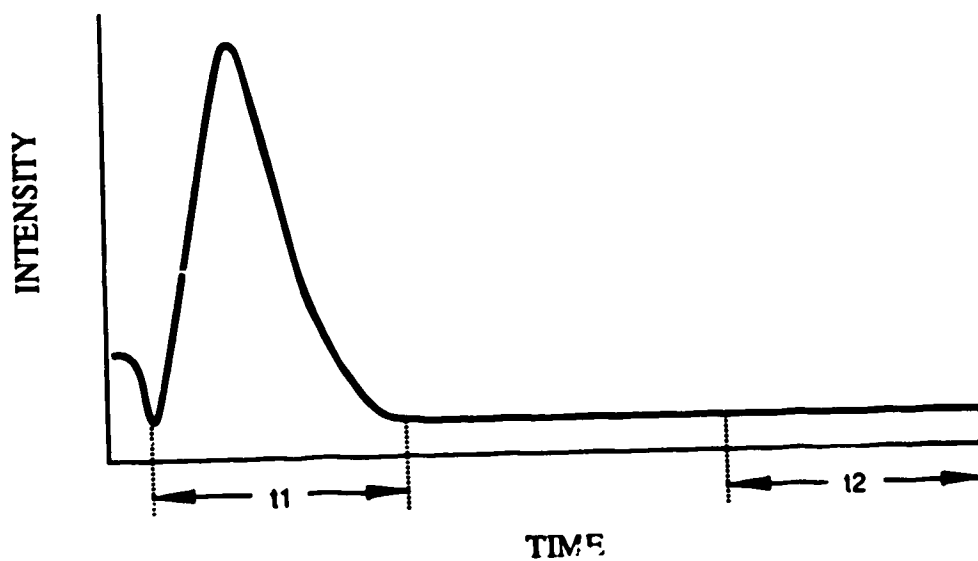


**Figure 2-14.** Off-peak background correction for the peak area of a DSI time profile. Time intervals  $t_1$  and  $t_2$  are equal. The difference between the integrated signals over time interval  $t_1$  and  $t_2$  is the background corrected peak area.

There is also another program to do automatic data processing that is similar to the above program except that the integration range is input by the user. Processing is much faster if the program does not have to determine the integration range of each time profile.

All these data processing programs described could be integrated into a single program with menu selection to enter each different mode of data processing. However, the present state of these programs is the result of the experience gained when processing the DSI data, i.e., further experience on DSI data processing may dictate modification of the data processing operations. Therefore, the programs remain separated as simple programs to make modification less cumbersome.

## **2.8 Conclusion**

A direct sample insertion system has been developed. The system runs under the supervision of a user because the software lacks the necessary information to make decisions. A thorough characterization of the system and the behavior of various analytes in different sample matrixes is required to provide this information. Once this information is available, it can be implemented in a data base which can be accessed by software and a truly intelligent system could be developed from this point.

### References

1. E.D. Salin and G. Horlick, *Anal. Chem.* **51**, 2284 (1979)
2. Y. Shao and G. Horlick, *Appl. Spectrosc.* **40**, 386 (1986)
3. W.E. Pettit and G. Horlick, *Spectrochim. Acta* **41B**, 699 (1986)
4. V. Karanassios, G. Horlick and M. Abdullah, '*Characterization of a direct sample insertion device for ICP-AES*', *Spectrochim. Acta*, (submitted)
5. V. Karanassios and G. Horlick, '*A computer-controlled direct sample insertion device for ICP-AES*', *Spectrochim. Acta*, (submitted).
6. G.F. Kirkbright and S.J. Watson, *Analyst* **107**, 276 (1982)
7. G.F. Kirkbright and L.-X. Zhang, *Analyst* **107**, 617 (1982)
8. L.-X. Zhang, G.F. Kirkbright, M.J. Cope, and J.M. Watson, *Appl. Spectrosc.* **37**, 250 (1983)
9. N.W. Barnett, M.J. Cope, G.F. Kirkbright, and A.A.H. Taobi, *Spectrochim. Acta* **39B**, 343 (1984)
10. M. Abdullah, K. Fuwa, and H. Haraguchi, *Spectrochim. Acta* **39B**, 1129 (1984)
11. M. Abdullah and H. Haraguchi, *Anal. Chem.* **57**, 2059 (1985)
12. M. Abdullah, K. Fuwa, and H. Haraguchi, *Appl. Spectrosc.* **41**, 715 (1987)
13. E.D. Salin and M.M. Habib, *Anal. Chem.* **56**, 1186 (1984)
14. E.D. Salin and R.L.A. Sing, *Anal. Chem.* **56**, 2596 (1984)
15. M.M. Habib and E.D. Salin, *Anal. Chem.* **57**, 2055 (1985)

16. C.V. Monasterios, A.M. Jones, and E.D. Salin, *Anal. Chem.* **58**, 780 (1986)
17. C.W. McLeod, P.A. Clarke, and D.J. Mowthorpe, *Spectrochim. Acta* **41B**, 63 (1986)
18. A.G. Page, K.H. Madraswala, S.V. Godbole, M.J. Kulkarni, V.S. Mallapurkar, and B.D. Joshi, *Fresenius' Z. Anal. Chem.* **315**, 38 (1983)
19. A.G. Page, S.V. Godbole, K.H. Madraswala, M.J. Kulkarni, V.S. Mallapurkar, and B.D. Joshi, *Spectrochim. Acta* **39B**, 551 (1984)
20. D. Sommer and K. Ohls, *Fresenius' Z. Anal. Chem.* **304**, 97 (1980)
21. K. Ohls, *Spectrochim. Acta* **39B**, 1105 (1984)
22. E.R. Prack and G.J. Bastiaans, *Anal. Chem.* **55**, 1654 (1983)
23. A. Lorber and Z. Goldbart, *Analyst* **110**, 155 (1985)
24. Gy. Zaray, J.A.C. Broekaert, and F. Leis, *Spectrochim. Acta* **43B**, 241 (1988)
25. Gy. Zaray, P. Burba, J.A.C. Broekaert, and F. Leis, *Spectrochim. Acta* **43B**, 255 (1988)
26. J.A.C. Broekaert, F. Leis, B. Raeymaekers, and Gy. Zaray, *Spectrochim. Acta* **43B**, 339 (1988)
27. V. Karanassios, 'Development and characterization of direct sample insertion devices for inductively coupled plasmas'. Ph.D. Thesis, University of Alberta (1988)
28. V. Karanassios and G. Horlick, *Talanta* **32**, 601 (1985)

## **Chapter 3. Thermal Properties of the Sample Cup Assembly for a DSI-ICP system**

### **3.1 Introduction**

The analytical signal from a DSI-ICP device is influenced by on the thermal properties of the sample cup assembly. It is important to understand these properties so that proper design of the sample cup assembly can be devised to optimize the analytical performance of the direct sample insertion system.

The maximum temperature of the sample cup is first examined. From this temperature, the input power to the sample cup can be derived. The relationship of the temperature of the sample cup against insertion time is then calculated. This relationship is confirmed by the experimental results. The distribution of the input power among the heat loss processes is also examined and some strategies for future sample cup design are suggested.

### **3.2 Temperature of a sample cup**

The unambiguous determination of the temperature of a sample cup in a plasma would seem to be a straightforward task. However, quite different results obtained with different measurement methods are reported in the literature [1-8].

Abdullah and Haraguchi [1] used 1-3 mg of different metal powders to estimate the temperature of a graphite sample cup. Vaporization of the metal was confirmed by measuring the emission intensity at the analytical line of the metal. They observed the emission signals of copper (bp 2868 K), cobalt (bp 3173 K) and iron (bp 3273 K), but no emission signal was observed from titanium (bp 3533 K) even with insertion times of up to 6 minutes. Therefore, they concluded that the temperature of the cup was about 3200 K. It should be pointed out that the boiling points of the metals quoted by these authors are different from those reported in other sources [9] where we find the following: copper 2567 °C (2840 K), cobalt 2870 °C (3143 K), iron 2750 °C (3023 K) and titanium 3287 °C (3560 K). Since cobalt has a higher boiling point than that of iron, the maximum temperature of the cup could be close to the boiling point of cobalt, i.e. 3140 K, according to their argument.

Substantial vapor pressure of a metal can be achieved below the boiling point of the metal [9]. The temperatures at which cobalt, iron and titanium reach vapor pressures of 1 to 760 mm Hg are listed in Table 3-1. From this table, it can be concluded that the emission signal of an element can be detected at a temperature well below its boiling point. The boiling point is thus only a gauge of the upper limit of the temperature of the cup. The actual cup temperature is probably lower and therefore uncertain as measured by this method.

Table 3-1. Vapor pressures of cobalt, iron, and titanium.

ELEMENT\PRESSURE	TEMPERATURE (°C)				
	1mm	10mm	100mm	400mm	760mm
cobalt	1910	2170	2500	2760	2870
iron	1780	2040	2370	2620	2750
titanium	2180	2480	2860	3100	3260

Since the temperature at which the analyte vaporizes does not necessarily equal the boiling point or any other characteristic temperature of the element, this temperature will be designated "appearance temperature", following the convention of electrothermal furnace atomic absorption spectrometry [10].

Kirkbright and Zhang [2] used the top of a graphite rod to hold solution samples. They suggested that the surface temperature of the graphite rod reached 4000 °C within a few seconds. This conclusion was based on the fact that emission signals from carbide forming elements like boron ( $B_4C$ , bp >3500 °C) and chromium ( $Cr_3C_2$ , bp 3800 °C) were observed within a few seconds after insertion of the sample cup, while those of uranium ( $UC_2$ , 4370 °C), zirconium ( $ZrC$ , bp 5100 °C) and titanium ( $TiC$ , bp 4820 °C) were not observed.

The analytes were placed on the graphite rod as aqueous solutions and the formation of carbides was not actually confirmed by any experimental evidence. The analyte could have been in an oxide form [10] and as such the appearance

temperature of the analyte would have been much lower than that of the corresponding carbides. For example, the appearance temperature of chromium (as chromium oxide  $\text{Cr}_2\text{O}_3$ ) is 1800 K which is less than 4073 K (3800 °C), the boiling point of the carbide quoted by the authors.

The appearance temperature of this oxide was determined with a temperature-voltage calibration graph for an electrothermal atomizer, which was checked with thermocouples [10]. Since both an electrothermal atomizer and a DSI sample cup assembly are composed of the same material (graphite), an analyte should have the same vaporization processes in both systems, i.e., the appearance temperatures are transferable. Therefore, the estimated graphite rod temperature of 4000 K is probably too high.

It is interesting to note that the melting point of chromium oxide is 2539 K and the boiling point is 4273 K, while those of the element chromium are 2130 and 2954 K, respectively. The appearance temperature of Cr is much lower than these temperatures because Cr is vaporized via the following process,



The free energy change for this reaction is positive at room temperature, i.e., the reaction is not favorable. However, as temperature increases, the free energy change decreases. It becomes negative at 1800-1900 K, which agrees with the appearance temperature reported by Campbell and Ottaway [10].



Barnett et al. [3] measured the temperature of four types of graphite cups with a radiation thermometer operating in the range 0.7-1.0  $\mu\text{m}$ . The ICP operating conditions were similar to those of Kirkbright and Zhang [2]. The steady state temperatures found were in the range of 1700 to 1830  $^{\circ}\text{C}$ , depending on the design of the sample cup. These are lower than the temperatures suggested before [2], but are consistent with the appearance temperature noted above. Therefore, direct measurement of the cup temperature appears to be more reliable than using the boiling points of the elements or their compounds for temperature estimation.

Page and co-workers [4] used the melting points of different metals to estimate the physical temperature of a graphite electrode in an argon plasma. They found that the temperature was about 1800  $^{\circ}\text{C}$ . Sommer and Ohls [5] estimated that the maximum temperature attained in their graphite cup was not greater than 3000  $^{\circ}\text{C}$ , based on melting point experiments using tungsten (mp 3410  $^{\circ}\text{C}$ ). Lorber and Goldbart [7] used an optical pyrometer to measure the temperature of a graphite cup inserted horizontally into the plasma at 6 mm above the load coil. They found that the temperature was 1600-2050  $^{\circ}\text{C}$  at forward powers of 1.2-2.2 kW. Prack and Bastiaans [8] calibrated the temperature of an undercut graphite cup electrode on top of a Pyrex tube at different insertion positions. A W/5% Re thermocouple with the thermocouple junction sealed in quartz was used at temperature, below 1000  $^{\circ}\text{C}$  (60-23 mm below the top of the

load coil) and initial points of vaporization (boiling points) of pure lead metal, lead (II) oxide, lead (II) sulfate and cadmium (II) chloride were employed for higher temperatures. The temperature when the cup was level with the top of the load coil was about 1800 °C. These temperatures are consistent with the temperature found by Barnett et al. [3].

Zaray et al. [6] suggested a cup temperature of 3000 K in a 3 kW nitrogen cooled plasma based on melting point experiments using tantalum strips (mp 2996 °C). This high cup temperature could be due to the high input power and the use of a nitrogen mixed gas plasma.

The graphite sample cup is heated by inductive coupling to the magnetic field of the ICP and by thermal conduction from the hot plasma gas. Thus a high forward power will certainly increase the cup temperature. The power density of a N<sub>2</sub> cooled plasma is also higher than that of a Ar plasma [11], which may increase the heat transfer from the plasma to the sample cup. Moreover, nitrogen gas has a higher thermal conductivity than argon. Thus N<sub>2</sub> will increase the rate of heat transfer from the high temperature gas to the low temperature sample cup and, perhaps, result in a higher sample cup temperature. The thermal conductivities  $\kappa$  (W cm<sup>-1</sup> K<sup>-1</sup>) of nitrogen and argon gas are given by the following equations [12, 13]:

for nitrogen,

$$\kappa(T) = 1.26 \times 10^{-4} + 5.18 \times 10^{-7}T - 1.81 \times 10^{-11}T^2 + 4.63 \times 10^{-15}T^3$$

.....(3-1)

and for argon,

$$\kappa(T) = 5.84 \times 10^{-5} + 4.48 \times 10^{-7}T - 9.11 \times 10^{-11}T^2 + 1.29 \times 10^{-14}T^3$$

.....(3-2)

where  $\kappa(T)$  is thermal conductivity at temperature  $T$  (K). At 3500 K, the thermal conductivity ( $\text{W cm}^{-1} \text{K}^{-1}$ ) of nitrogen is  $1.92 \times 10^{-3}$  and that of argon is  $1.06 \times 10^{-3}$ .

To estimate the graphite cup temperature attained in the plasma in our system, a few mg of metal powder were placed in the graphite cup and inserted into the plasma for up to five minutes. Molybdenum powder (mp 2883 K, bp 5833 K) does not melt and the emission signal of Mo is not detected, which indicates that the temperature of the sample cup cannot be higher than 2883 K. Copper powder (mp 1356 K, bp 2840 K) melts and forms a bead at the bottom of the cup. The emission signal of copper can also be measured and it is found that the metal vaporizes completely in 30 seconds. Nickel (mp 1728 K, bp 3003 K) and iron (mp 1808 K, bp 3023 K) have similar behavior except that nickel wets the surface of the graphite cup instead of forming a bead and the emission signal from both elements tails for several minutes. These observations indicate that the temperature of the sample cup is higher than the melting point of iron (1808 K) which is the highest among the three metals. Manganese powder (mp 1517 K, bp 2235 K) melts and based on the time behavior

of the emission signal, vaporization is finished in less than 10 seconds. Since the vaporization of manganese is fast, the sample cup temperature should be close to the boiling point of this metal. The upper limit of the sample cup temperature is therefore estimated to be 2000 K.

The molar heat of vaporization of a liquid at its standard boiling point can be estimated from Trouton's rule [14],

$$\Delta\bar{S}_{\text{vap}} = \frac{\Delta\bar{H}_{\text{vap}}}{T_b} = 88 \text{ J K}^{-1} \text{ mol}^{-1} \quad (3-3)$$

where  $\Delta\bar{S}_{\text{vap}}$  is the molar entropy of vaporization ( $\text{J K}^{-1} \text{ mol}^{-1}$ ),  $\Delta\bar{H}_{\text{vap}}$  is the molar heat of vaporization ( $\text{J mol}^{-1}$ ) and  $T_b$  is the boiling point of the liquid (K). The heat of vaporization of manganese is calculated to be  $197 \text{ kJ mol}^{-1}$ , therefore about 36 J is required to vaporize 10 mg of manganese completely at its boiling point. If the metal is to be vaporized in 10 seconds, the power required is 3.6 W. The heat of vaporization of iron is calculated to be  $266 \text{ kJ mol}^{-1}$  and 48 J is required to vaporize 10 mg of this metal. The energy (or power) required to vaporize the same amount of iron and manganese at their boiling points is approximately the same, which is relatively small compared to the estimated input power of about 110 W to the sample cup (described in a later section). Manganese, however, is completely vaporized in 10 seconds while iron is still vaporizing slowly after 60

seconds. Therefore, the temperature of the sample cup must be close to the *boiling point* of manganese and the *melting point* of iron, 2000 K is a reasonable estimation.

Tantalum sample cups have also been used in our DSI system. The temperature of a metal cup should be measured directly, e.g., with a radiation thermometer. Melting point experiments are not practical due to alloy formation between the sample cup and the metal sample. Furthermore, the vaporization processes of an analyte from a graphite surface are different from that of a metal surface [15], therefore the appearance temperatures described above are not transferable to a metal sample cup. The temperature of the tantalum sample cup has not been measured at present. However, the upper limit is below 3000 °C because tantalum cups (mp 2996 °C, bp 5425 °C) are used for aqueous solution sample introduction without any deterioration.

### **3.3 Input power to the sample cup**

From the maximum temperature of the sample cup, it is possible to estimate the input power to the cup because at this temperature, the input power should be equal to the rate of heat loss from the cup. By calculating the rate of heat loss at the maximum temperature, the input power can be determined.

The sample cup loses heat mainly by radiative heat transfer and heat conduction through the stem of the sample

cup holder to the low temperature end of the holder. The rate of radiative heat transfer is given by the Stefan-Boltzmann law [16],

$$W_r = \epsilon \cdot \sigma \cdot A \cdot T^4 \quad (3-4)$$

where  $W_r$  is the total emissive power (W),  $\epsilon$  is the total emissivity,  $\sigma$  is the Stefan-Boltzmann constant ( $W \text{ m}^{-2} \text{ K}^{-4}$ ),  $A$  is the surface area ( $\text{m}^2$ ), and  $T$  is the temperature (K) of the graphite cup. In the temperature range of 0-3600 °C, the total emissivity of graphite,  $\epsilon$ , equals 0.7-0.8 [9]. Since the emissivity is relatively constant for a large temperature range, the mean, 0.75, is used in the calculation below. The Stefan-Boltzmann constant equals  $5.670 \times 10^{-8} \text{ W m}^{-2} \text{ K}^{-4}$  [9].

The surface area is the sum of the area of the outer cylindrical portion and the the cross-sectional area of the graphite cup (Figure 3-1). The cross-sectional area can be divided into two parts: the surface area of the rim and the cross-sectional area of the hollow portion of the cup. For simplicity of calculation, it is assumed that the hollow portion of the sample cup has an equivalent emitting area as its cross-sectional area. The surface area of the insert of the sample cup is not included because it is hidden in the sample cup holder, i.e., it will be facing surfaces of the same temperature and the net radiative heat transfer is zero. The diameter of the cup is 0.46 cm and the length of the outer cylindrical portion is 0.5 cm. Therefore the area,  $A$ ,

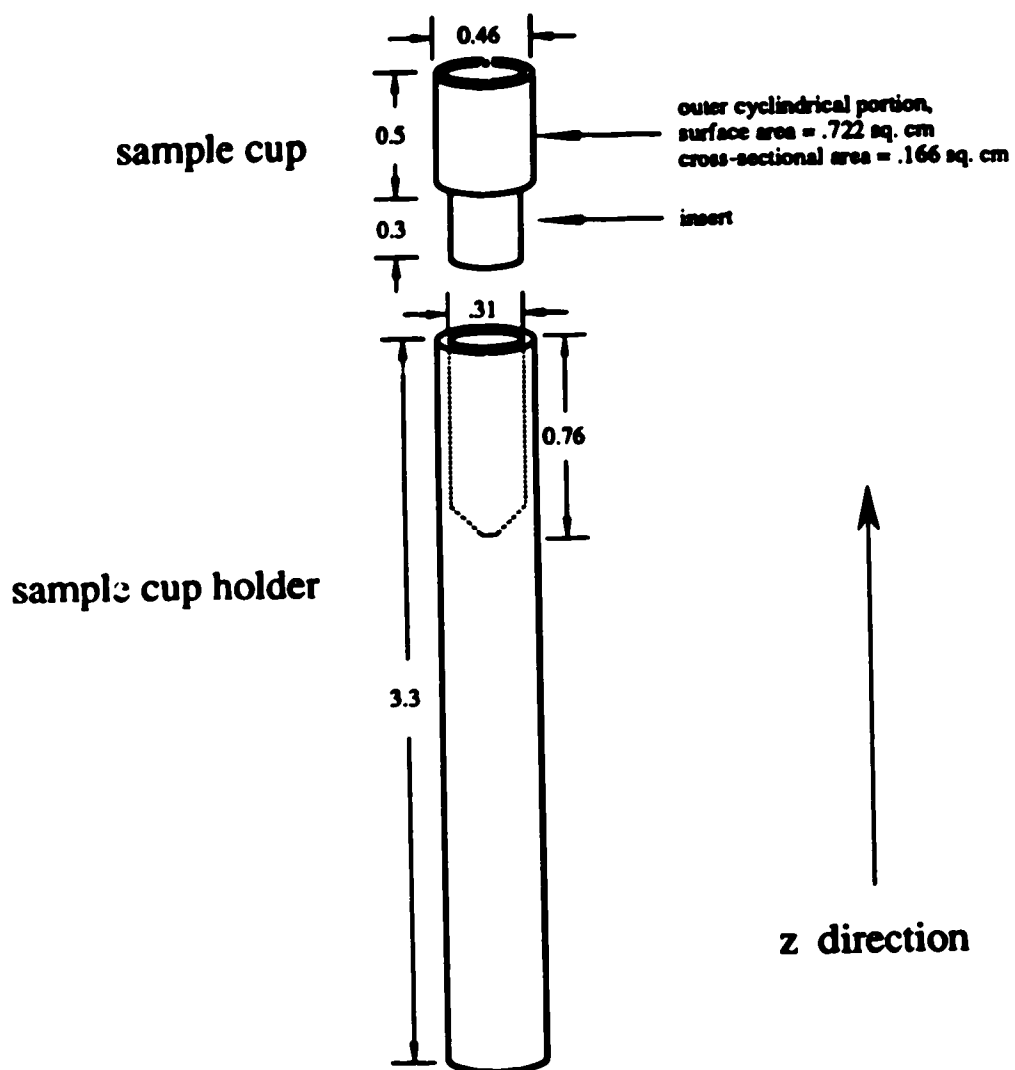


**Figure 3-1.** Dimensions (cm) of the graphite sample cup assembly.

is 0.889 cm<sup>2</sup>. With temperature, T, at 2000 K, the maximum total emissive power is 60.5 W.

If the direction of insertion is defined as the z direction, then the heat loss through conduction is given by the following equation,

$$W_c = \kappa \cdot A' \cdot \frac{dT}{dz} \quad (3-5)$$

where  $W_c$  is the heat conduction rate in the z direction (W),  $\kappa$  is the thermal conductivity of graphite (W cm<sup>-1</sup> K),  $A'$  is the cross-sectional area normal to the heat flow (cm<sup>2</sup>), and  $dT/dz$  is the temperature gradient in the z direction (K cm<sup>-1</sup>). The thermal conductivity of isotropic electrographite is given in reference 12,

$$\kappa(T) = 2.17 - 2.08 \times 10^{-3}T + 9.08 \times 10^{-7}T^2 - 1.34 \times 10^{-10}T^3 \quad (3-6)$$

At 2000 K,  $\kappa = 0.570$  W cm<sup>-1</sup> K. The area,  $A'$ , is the cross-sectional area of the wall of the sample cup holder (Figure 3-1). Since the outer diameter of the cup holder is 0.46 cm and the diameter of the hollow portion of the cup holder is 0.31 cm, the conducting area is 0.0907 cm<sup>2</sup>. The temperature gradient is estimated to be 1000 K cm<sup>-1</sup>. Substituting these values in Equation 3-5, the maximum rate of heat conduction is 51.7 W.

The total heat loss is the sum of the total emissive power and the heat conduction rate, which is 112 W. Therefore the input power is 112 W at 2000 K. It is interesting to



compare the input power to the sample cup to the incident power to the plasma and the heat losses for different processes from the plasma. A brief survey of the literature on the powers of the plasma is presented below.

Bogdain et al. [17] estimated that the output power to the induction coil (i.e. the plasma) was 43 % of the total input power, the rest was lost in the circuits of the r.f. generator. Borgianni et al. [18] used a 4 MHz ICP with maximum input power of 15 kW. The estimated efficiency of power transfer was 35 %. The power of the plasma was distributed among three processes, namely, spectral radiation, conduction through torch walls, and plasma gas enthalpy increase. Their relative values were measured using calorimetric methods and found to be 16%, 30%, and 54 %, respectively. Greenfield and McGeachin [11] found that 40-45 % of the power supplied to the generator reached the plasma, using both direct calorimetric measurement and calorimetric measurement with metallic dummy loads. Barnes and Schleicher [19] developed mathematical models of ICP discharges based on the model of Miller and Aye [20]. They calculated the spatial distribution of gas properties and major energy losses for high temperature ICP discharges. For a typical 27 MHz ICP, the energy losses due to radiation, heat transfer to tube walls, and gas enthalpy increase were 5, 41, and 54 % respectively. Ripson and DeGalan [21] estimated that the input power to the plasma was about 75 % of the generator power for a conventional ICP. The major part of the incident

power was used to heat the argon, with less than 2 % for radiative and conductive heat losses. The power dissipated in the nebulized water was 25 W, with a water mass flow to the plasma of 0.5 mg/s.

The large variation for the powers estimation arises because of the different models of the plasma utilized. If we follow the estimation of Bogdan et al. [17], Borgianni et al. [18], and Greenfield and McGeachin [11], the input power to the plasma is about 40 % of the incident power from the r.f. generator. For our 1.25 kW power supply, the input power to the plasma is 500 W. Without the insertion of the sample cup assembly, most of the energy (95 %) is consumed by the gas enthalpy increase and heat losses through the tube walls. The combined value is 475 W, following Barnes and Schleicher [19] and Ripson and DeGalan [21]. With the insertion of the sample cup assembly, part of the input power is used to heat the sample cup. It is noted earlier that the input power to the sample cup is 112 W, i.e., about 22 % of the total input power to the plasma. Since part of the sample cup holder is in the plasma, in addition to the sample cup, the fraction of power consumed by the sample cup assembly should be even higher. Therefore, the plasma should be cooled considerably by the sample cup assembly.

### **3.4 Temperature rise rate of a sample cup**

With knowledge of the maximum sample cup temperature and the input power to the sample cup, it is possible to calculate the temperature of a sample cup as a function of insertion time. Before we do the calculation, it is of interest to examine the experimental temperature rise rate. The theoretical calculation will be compared to the experimental result in the next section.

When a sample cup is inserted into the plasma, the temperature of the cup will increase and reach a maximum in a certain period of time. It is interesting to compare the heating process for a furnace used in electrothermal furnace atomic absorption spectrometry and that of a DSI system sample cup. The electrothermal furnace is heated by passing current through the furnace. The current is usually ramped up in such a way that the temperature increases linearly. The final temperature is determined by the maximum voltage (and thus current) applied. The DSI sample cup, on the other hand, is inserted into a constant temperature environment (the plasma). The input power to the sample cup is approximately constant throughout the heating process while the heat loss from the sample cup through radiation and conduction processes increases with temperature. Therefore, the temperature rise rate decreases as temperature increases and the temperature reaches a maximum at which the input power equals the rate of heat loss.

The temperature rise rate of a sample cup can be modeled with a knowledge of the sample cup temperature as a function

of insertion time. Since different analytes have different appearance temperatures (and thus appearance times), a set of seven analytes were chosen to provide these data. A list of these temperatures and times, along with the suggested oxide forms of the analytes on the surface of the furnace at the appearance temperatures is given in Table 3-2.

**Table 3-2.** Appearance temperatures and appearance times of candidate elements undergoing graphite-furnace atomization.

element	oxide	appearance temperature (K)	appearance time (sec)
Cd	CdO	850	0.048
Pb	PbO	1000	0.322
Zn	ZnO	1100	0.375
Mn	Mn <sub>3</sub> O <sub>4</sub>	1600	1.326
Cu	Cu <sub>2</sub> O	1730	1.424
Fe	Fe <sub>2</sub> O <sub>3</sub>	1750	2.512
Ni	NiO	1800	2.179

It should be pointed out that the temperatures were not measured in this laboratory, instead, they are the appearance temperatures reported by Campbell and Ottaway [10] for an electrothermal furnace. (L'vov [22] has compiled a list of appearance temperatures from different research groups. The average temperatures for each element were also calculated. The temperatures reported by Campbell and Ottaway [10] are

slightly higher than the average temperatures [22]. However, only the temperatures from this group, instead of the average, is chosen for consistency.) It is assumed that the appearance temperatures for an electrothermal furnace are approximately transferable to our DSI-ICP sample cup. By definition, the temperature of the sample cup equals the appearance temperature.

The appearance times were measured experimentally. The amount of the analyte used was 1  $\mu\text{g}$  (100 ppm  $\times$  10  $\mu\text{l}$ ) of the element in nitrate form. The sample cup was heated at a position 35 mm below the top of the load coil (blc) for 30 seconds before insertion to a position level with the top of the load coil. The origin of the time axis is defined as the point when the cup is first level with the top of the load coil, which occurs 0.345 sec after the start of insertion of the cup from 35 mm blc. The appearance time is the time when the emission signal of an analyte is initially observed.

A plot of appearance temperature (i.e. graphite sample cup temperature) as a function of appearance time (i.e. insertion time) is shown in Figure 3-2. The solid line is a fit of the experimental data, which is calculated from the following relationship,

$$T(t) - T(0) = \frac{T(\infty) - T(0)}{1 + c \left\{ \frac{1}{t} \right\}^n} \quad (3-7)$$

where  $T(t)$  is the temperature at time  $t$ ,  $T(0)$  is the initial temperature,  $T(\infty)$  is the maximum temperature of the sample cup, and  $c$  and  $n$  are constants to be found empirically. Equation 3-7 is based on the fact that when  $t = 0$ ,  $T(0) = T(t)$  and when  $t = \infty$ ,  $T(t) = T(\infty)$ . Also, the rate of increase of  $T(t)$  is reduced as  $t$  increases.

The initial temperature,  $T(0)$ , is assigned to be 823 K (550 °C) which is the intercept on the temperature axis for a curve fit of the first three data points in Figure 3-2, assuming that the initial rate of temperature rise is linear. The temperature is consistent with the calibration curve of Prack and Bastiaans [8]. The maximum temperature,  $T(\infty)$ , is 2000 K as discussed earlier. Rearranging Equation 3-7 and substituting the values of  $T(0)$  and  $T(\infty)$ , we get,

$$\frac{1177}{\{T(t) - 823\}} - 1 = c \left\{ \frac{1}{t} \right\}^n \quad (3-8)$$

If we do a linear regression on the logarithm of the left hand side term of the above equation against the logarithm of  $1/t$ , the following relation is obtained,

$$\ln \left\{ \frac{1177}{\{T(t) - 823\}} - 1 \right\} = -1.402 \times \ln(t) - 0.02935 \quad (3-9)$$

The solid curve in Figure 3-2 is obtained by plotting  $T(t)$  against  $t$  from Equation 3-9. The curve shows that the temperature rise rate decreases as temperature increases as expected.

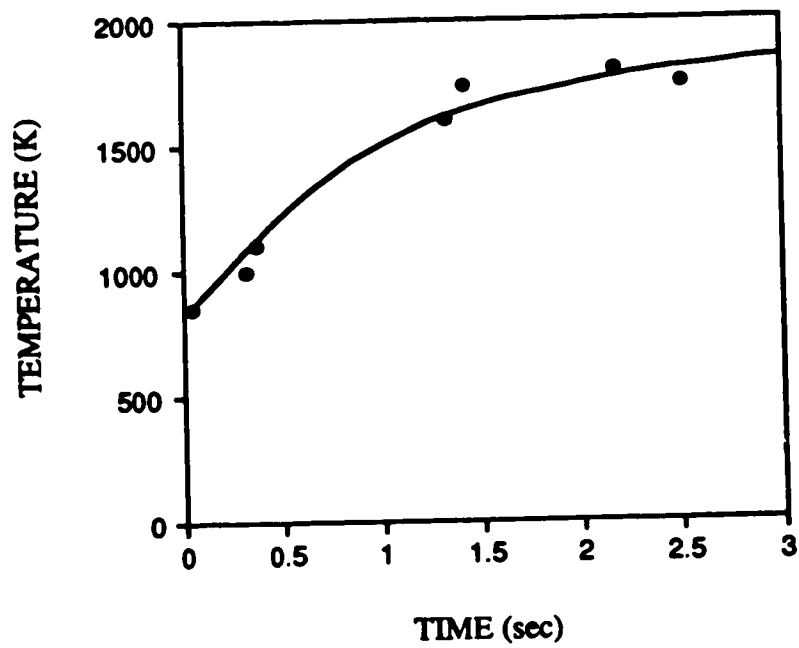


**Figure 3-2.** Graphite sample cup temperature rise curve.  
The solid line is a curve-fit of the experimental results.

### 3.5 Theoretical calculation of the temperature of a sample cup as a function of insertion time

The net power gained by the sample cup at time  $t$  is the difference between the input power and the sum of the radiation and conduction heat losses, which is given by,

$$W_c(t) = W_{in} - (W_r(t) + W_c(t)) \quad (3-10)$$

where  $W_{in}$  is the input power to the sample cup, which is equal to the sum of the radiation and conduction heat losses at maximum cup temperature, i.e.,  $W_r + W_c$ ;  $W_r(t)$  is the rate of radiation heat loss at cup temperature  $T(t)$ , which can be calculated from Equation 3-4;  $W_c(t)$  is the rate of conduction heat loss at cup temperature  $T(t)$ , which can be calculated by substituting Equation 3-6 and the relation between  $dT/dz$  and  $T(t)$  into Equation 3-5. The temperature gradient,  $dT/dz$ , is expected to change with  $T(t)$ . It can be represented by the following equation,

$$\frac{dT}{dz} = T(t) - T'(t) \quad (3-11)$$

where  $T'(t)$  is the temperature of the base of the sample cup holder. (The temperature of the base of the sample cup holder is represented by  $T'$  in this thesis). The distance,  $dz$ , is assigned to be 1 cm. It is assumed that  $T'(t)$  increases linearly with the sample cup temperature,  $T(t)$ , so that



$$T'(t) - T'(0) = \frac{T'(\infty) - T'(0)}{T(\infty) - T(0)} \times (T(t) - T(0)) \quad (3-12)$$

where  $T'(0)$  and  $T(0)$  represent the initial temperatures, and  $T'(\infty)$  and  $T(\infty)$  represent the maximum temperatures of the base and the cup, respectively.  $T'(0)$  is estimated to be 500 K according to the calibration curve of Prack and Bastiaans [8].  $T'(\infty)$  is estimated to be 1000 K.  $T(0)$  and  $T(\infty)$  are 823 K and 2000 K, respectively, as estimated earlier. Substituting the values of the temperatures in Equation 3-12, we get,

$$T'(t) = 0.4248 \times T(t) + 150.4 \quad (3-13)$$

From Equations 3-11 and 3-13, the temperature gradient is

$$\frac{dT}{dz} = 0.5752 \times T(t) - 150.4 \quad (3-14)$$

The rate of conduction heat loss is obtained by substituting Equations 3-6 and 3-14 into 3-5,

$$W_c(t) = -29.60 + 0.1416T - 1.209T^2 + 4.920T^3 - 6.992T^4 \quad \dots (3-15)$$

where  $T$  is equivalent to  $T(t)$ , the temperature of the sample cup.

The net energy gained by the sample cup raises the temperature of the cup, so that

$$W_c dt = C_p dT = m \cdot c \cdot dT \quad (3-16)$$

where  $C_p$  is the heat capacity of the graphite sample cup ( $J K^{-1}$ ),  $m$  is the mass of the cup (g), and  $c$  is the specific heat capacity of graphite ( $J g^{-1} K^{-1}$ ). The mass of the graphite cup is  $0.1399 \pm 0.0012$  g. The specific heat capacity of graphite is  $0.7119 J g^{-1} K^{-1}$  [9]. Substituting these values and Equations 3-4, 10, and 15 into 3-16, we obtain,

$$dT = \{1423 - 1.422T(t) + 1.214 \times 10^{-3}T(t)^2 - 4.940 \times 10^{-7}T(t)^3 + 3.225 \times 10^{-11}T(t)^4\} dt \quad \dots (3-17)$$

Integrating the above equation gives the temperature of the sample cup at time  $t$ ,

$$T(t+\Delta t) = T(t) + \{1423 - 1.422T(t) + 1.214 \times 10^{-3}T(t)^2 - 4.940 \times 10^{-7}T(t)^3 + 3.225 \times 10^{-11}T(t)^4\} \times \Delta t \quad (3-18)$$

A program was developed to calculate  $T(t)$ .  $T(0)$  is assigned a value of 823.15 K and  $\Delta t$  a value of 0.001 second. The relation between  $T(t)$  and  $t$  is shown in Figure 3-3. The experimental data is also shown for comparison. The first 3 seconds of the heating curve are shown in Figure 3-3a. The theoretical calculation agrees well with the experimental results. The plot in Figure 3-3b for a full 10 seconds shows that the temperature increases sharply in the first 2 seconds, then the rate reduces. The temperature reaches 2000 K after a few seconds and then remains constant.

### 3.6 Distribution of the input power among different processes

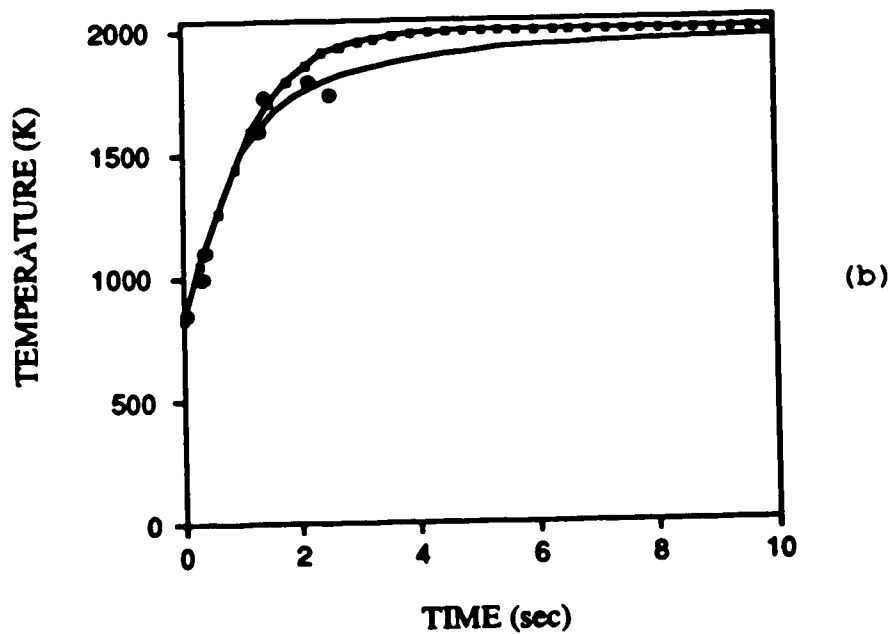
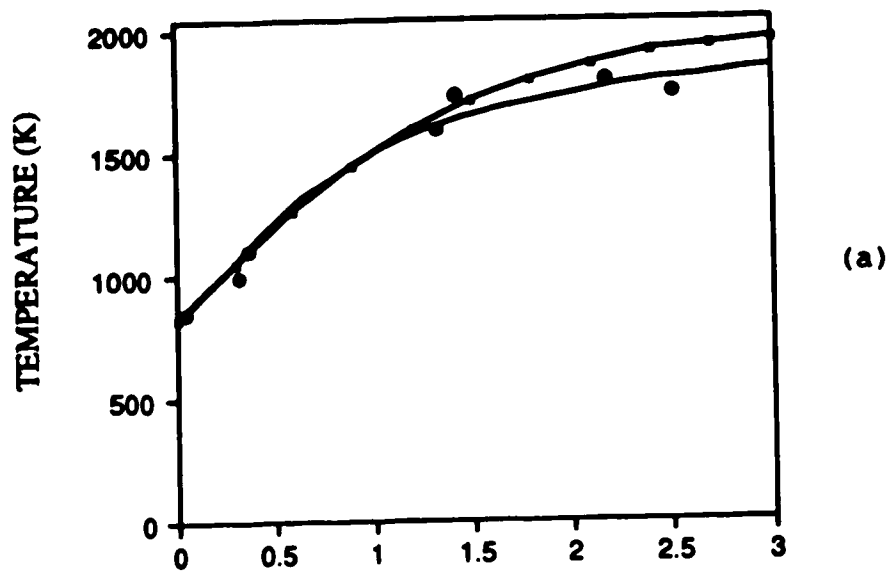


**Figure 3-3.** The theoretical temperature rise curves for a graphite sample cup. ● is experimental results, — is the fit of the experimental results, and ■ is the theoretical calculation. (a) first 3 seconds of the curve. (b) first 10 seconds of the curve.

The total input power is distributed between the processes of temperature rise, radiative heat transfer, and heat conduction. Both the rate of radiative heat transfer and that of heat conduction increase with temperature, and it is evident from Equation 3-10 that the net power gained by the sample decreases with temperature. These relationships are illustrated in Figure 3-4. It is interesting to note that, when the temperature is lower than 1500 K, the heat conduction process consumes more energy than the radiative heat transfer process does, while the largest portion of energy contributes to the sample cup temperature rise. Although the power consumed by heat conduction increases approximately in a linear fashion against temperature, and that of radiative heat transfer increases exponentially, the energy drained by these two processes is equal only at about 1900 K for this particular system configuration. It is obvious that heat conduction determines the rate of temperature rise of the sample cup, while radiative heat transfer determines the temperature attainable.

The power distribution as a function of time is shown in Figure 3-5. The power gained by the sample cup follows an exponential decrease against time, and it is virtually equal to zero after 5 seconds. This is consistent with the temperature rise curve shown in Figures 3-2 and 3-3.

The initial rate of temperature rise is  $796 \text{ K s}^{-1}$  which is obtained by calculating the slope of the first 0.6 seconds of the curve of Figure 3-2. Therefore, from Equation 3-16,

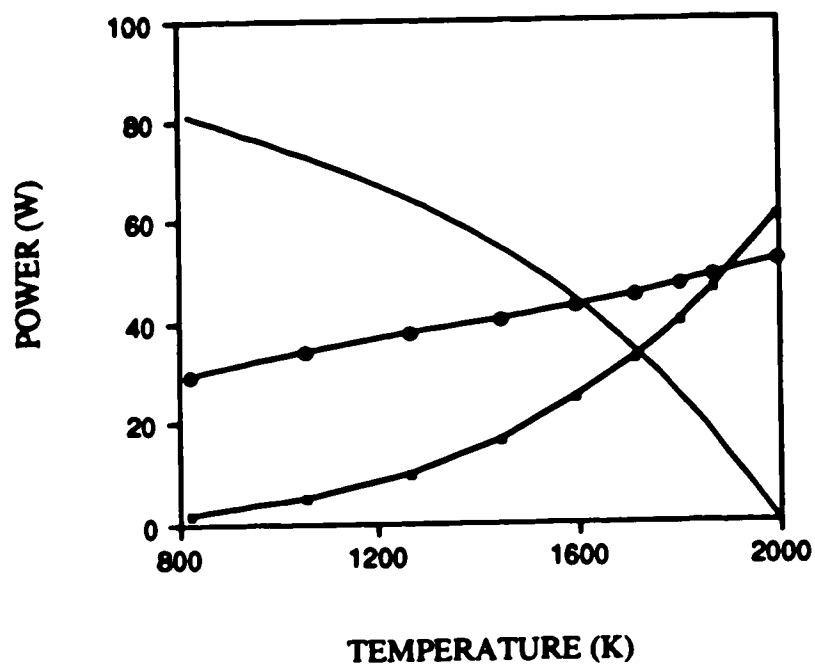


**Figure 3-4.** Distribution of the input power to a graphite sample cup among different processes as a function of temperature of the sample cup. — is net power gain by the sample cup, which raises the cup temperature. ◆ is the rate of conduction heat loss. ■ is the rate of radiative heat loss.

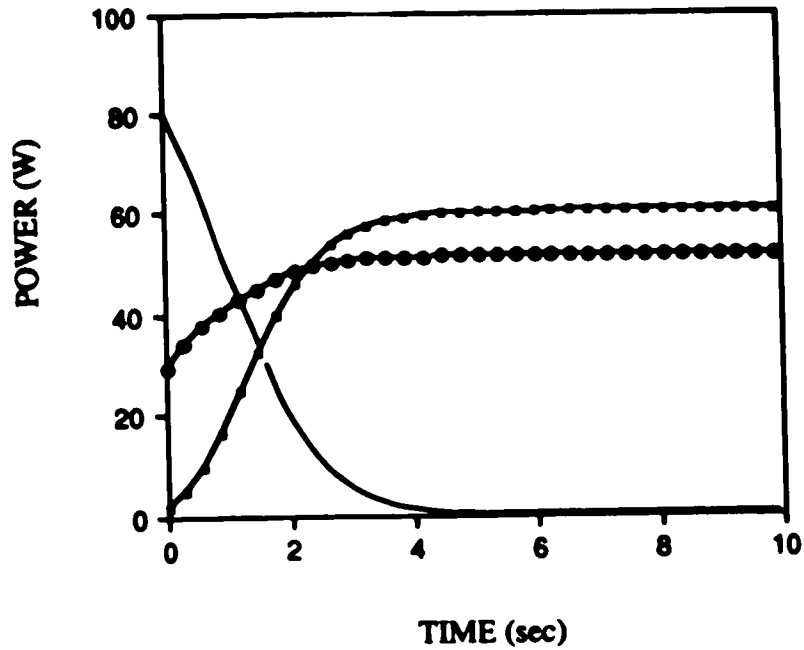


**Figure 3-5.** Distribution of the input power to a graphite sample cup among different processes as a function of insertion time. — is net power gain by the sample cup, which raises the cup temperature. ● is the rate of conduction heat loss. ■ is the rate of radiative heat loss.

the initial power gain of the sample cup is 79 W. This value agrees with the value of 73 W at 0.3 seconds (temperature of cup equals 1055 K) calculated from Equation 3-10. The rates of conduction heat loss and radiative heat loss at that moment are 34 and 5 W respectively. The rate of conduction heat loss is about half of the power gained by the sample cup, and it is about 7 times that of the radiative heat loss. If conduction heat loss is eliminated by using a heat insulator as the sample cup holder, the temperature of the sample cup will certainly rise faster. A hypothetical temperature rise curve that has no heat conduction loss process is shown in Figure 3-6. The initial rate of temperature rise is  $1052 \text{ K s}^{-1}$  and the power is 105 W. The maximum temperature attainable is about 2330 K, which is not a substantial increase from the original 2000 K due to the exponential increase in radiative heat loss with temperature.

If radiative heat loss is assumed to be negligible, the initial rate of temperature rise is about the same as the experimental result. However, the maximum temperature is about 3000 K, which is a significant increase from the original value. The temperature rise curve under this assumption is shown in Figure 3-7.

### **3.7 Conclusion**

The rate of temperature rise depends on the following factors: (1) the thermal conductivity and conducting area of

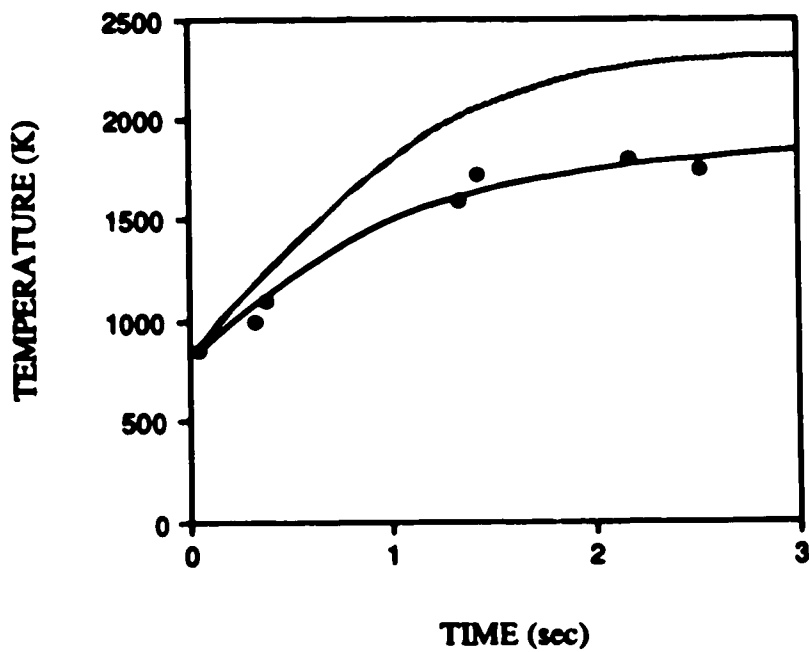


**Figure 3-6.** Hypothetical sample cup temperature rise curve with no conductive heat loss (gray line). Experimental results are shown for comparison.



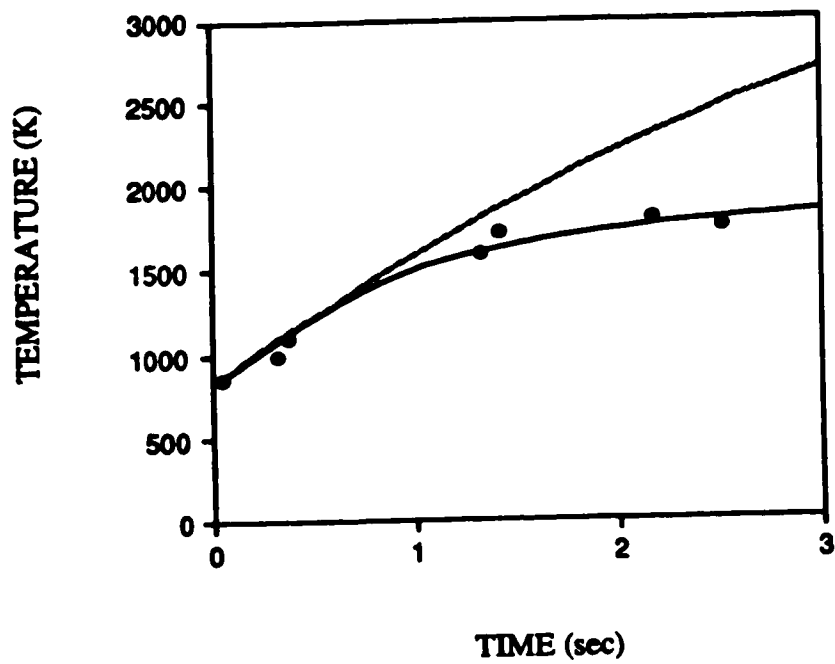


**Figure 3-7.** Hypothetical sample cup temperature rise curve with no radiative heat transfer (gray line). Experimental results are shown for comparison.

the cup holder, (2) the heat capacity and emitting area of the sample cup, and (3) the emissivity of the sample cup material. It can be increased by carefully choosing the proper material and design of the cup holder and the sample cup.

Refractory materials with low thermal conductivity, such as silicon carbide ( $\text{SiC}$ , mp 2700 °C and  $\kappa = 0.4 \text{ W cm}^{-1} \text{ K}^{-1}$  at 25 °C) and aluminium oxide ( $\text{Al}_2\text{O}_3$ , mp 2015 °C and  $\kappa = 0.30 \text{ W cm}^{-1} \text{ K}^{-1}$  at 25 °C), compare favorably to graphite (mp 3700 °C,  $\kappa = 1.1\text{--}1.9 \text{ W cm}^{-1} \text{ K}^{-1}$  at 25 °C). However, these materials are not easily machinable, while graphite can be readily machined to different shapes. Therefore graphite is the material of choice for a sample cup holder. In light of this factor, a small heat conducting area should be considered to limit the conduction heat loss. An undercut graphite cup with a thin stem or the hollow cup holder described earlier are ideal. (The conducting area of an undercut graphite electrode is 0.031 cm<sup>2</sup> if the stem diameter is 2 mm, and it is 0.071 cm<sup>2</sup> if the stem diameter is 3 mm. On the other hand, the conducting area of the hollow cup holder is 0.091 cm<sup>2</sup>. It can be reduced to 0.064 cm<sup>2</sup> if the wall thickness is reduced to 0.5 mm from the original 0.75 mm.)

The material of a sample cup is usually graphite or a high melting point metal, e.g., tantalum and tungsten. The specific heat of graphite is 0.712 J g<sup>-1</sup> K<sup>-1</sup> at 25 °C, while that of tantalum and tungsten are 0.140 and 0.136 respectively. However, the weight of a graphite cup is

0.14 g, but the weight of a tantalum and tungsten cup of similar shape is about 1.40 g. Therefore, the heat capacity of a metal cup is actually 2 times greater than that of a graphite cup. Thus the graphite cup will have a faster temperature rise than a metal cup.

The maximum cup temperature attainable depends mainly on the radiative heat loss from the sample cup. The emissivities of unoxidized tantalum and tungsten are 0.21 and 0.23 at 1500 °C, which are about a quarter that of graphite (0.7-0.8). Therefore, a metal cup with an unoxidized surface is more favorable than a graphite cup. However, if the surface is oxidized, which happens after prolonged use of the sample cup, the emissivity of the metals will be increased and the advantage of their lower rate of radiative heat transfer is lost.

The radiating area of the sample cup can be cut down to increase the maximum temperature attainable. However, a 50 percent cut on the area only translates to a 19 percent increase of the temperature. The area (and thus the volume) cannot be reduced drastically, considering the volume of sample that should be handled.

The maximum temperature attainable is determined by the radiative heat loss which is proportional to the fourth power of temperature. Since the magnitude of this heat loss increases quickly with temperature, the maximum temperature is self-limiting in the range of 2000-3000 K. However, higher

temperature may be obtained with the use of a  $N_2$  cooled plasma and higher input power.

The purpose of the calculation in this chapter is to estimate the relative importance of different heat transfer processes operative in the sample cup assembly. Some approximations have been utilized for the simplicity of the calculation. These include: assigning the emitting area of the hollow portion of the sample cup as its cross-sectional area; estimation of the temperature gradient along the sample cup holder; assuming constant input power (should be changing with temperature); and assuming constant heat capacity of the sample cup against temperature. Additionally, the calculation of conduction heat loss treated the sample cup and the sample cup holder as a single unit, but they are actually two separate units with relatively poor heat conduction between them. This is evident when the sample cup assembly is inserted rapidly into the plasma. The sample cup starts glowing before the sample cup holder does, although the time lag is only one or two seconds. Again, if the cup assembly is withdrawn rapidly from the plasma, the cup holder ceases to glow before the sample cup does. The conclusion drawn, however, should still be valid, because the trend of the processes should remain unchanged.

**References**

1. M. Abdullah and H. Haraguchi, *Anal. Chem.* **57**, 2059 (1985)
2. G.F. Kirkbright and Zhang Li-Xing, *Analyst* **107**, 617 (1982)
3. N.W. Barnett, M.J. Cope, G.F. Kirkbright and A.A.H. Taobi, *Spectrochim. Acta* **39B**, 343 (1984)
4. A.G. Page, S.V. Godbole, K.H. Madraswala, M.J. Kulkarni, V.S. Mallapurkar and B.D. Joshi, *Spectrochim. Acta* **39B**, 551 (1984)
5. D. Sommer and K. Ohls, *Fresenius Z. Anal. Chem.* **304**, 97 (1980)
6. Gy. Zaray, J.A.C. Broekaert and F. Leis, *Spectrochim. Acta* **43B**, 241 (1988)
7. A. Lorber and Z. Goldbart, *Analyst* **110**, 155 (1985)
8. E.R. Prack and G.J. Bastiaans, *Anal. Chem.* **55**, 1654 (1983)
9. R.C. Weast, M.J. Astle, and W.H. Beyer, Editors, "*CRC Handbook of Chemistry and Physics*", 64th ed., CRC Press, Florida, 1983
10. W.C. Campbell and J.M. Ottaway, *Talanta* **21**, 837 (1974)
11. S. Greenfield and H.McD. McGeachin, *Anal. Chim. Acta* **100**, 101 (1978)
12. S. Wu, C.L. Chakrabarti, and T.J. Rogers, *Prog. Anal. At. Spectrosc.* **10**, 111 (1987)
13. Y.S. Touloukian, P.E. Liley, and S.C.Saxena, "*Thermal Conductivity, Nonmetallic Liquids and Gases, Thermophys-*

- cal Properties of Matter*", Vol 3, IFI/Plenum, New York, 1970
14. F. Daniels and R.A. Alberty, *"Physical Chemistry"*, 4th ed., John Wiley & Sons, New York, London, Sydney, Toronto, 1975
  15. C.W. Fuller, *Analyst* **99**, 739 (1974)
  16. C.O. Bennett and J.E. Myers, *"Momentum, Heat, and Mass Transfer"*, 2nd ed, McGraw-Hill, Inc., 1974
  17. B. Bogdain, H. Linn, and H. Gast, *ICP Inf. Newsl.* **2**, 269 (1977)
  18. C. Borgianni, M. Capitelli, F. Cramarossa, L. Triolo, and E. Molinari, *Combust. Flame* **13**, 181 (1969)
  19. R.M. Barnes and R.G. Schleicher, *Spectrochim. Acta* **30B**, 109 (1975)
  20. R.C. Miller and R.J. Ayen, *J. Appl. Phys.* **40**, 5260 (1969)
  21. P.A.M. Ripson and L. DeGalan, *Spectrochim. Acta* **38B**, 707 (1983)
  22. B.V. L'vov, *Spectrochim. Acta* **33B**, 153 (1978)

## Chapter 4. Characterization of DSI-ICP-AES

### 4.1 Introduction

The ability of DSI-ICP-AES to analyse small amounts of discrete samples and to implement *in situ* sample treatment under the plasma, making use of the temperature gradient in the central channel of the ICP torch, are considered advantages of this technique. However, since vaporization/atomization of an analyte strongly depend on the matrix of the sample and the interaction/reaction between the surface of the sample cup and the sample, sample treatment becomes necessity, which is similar to the situation encountered in electrothermal atomization absorption spectrometry (ETA-AAS) [1].

It is important to understand the effect of sample treatment on sample vaporization, so that proper choice of the treatment may be selected. The effect of dry/ash processes, including the ashing height and the manner of desolvation (external or *in situ*), are described in this chapter. The vaporization of an analyte was monitored via the emission time profile, digitized in real time with the ADC described in Chapter 2. Mechanisms of vaporization are presented to explain the temporal behavior of the analyte vaporization.

The detection limits of some elements are also reported, which shows the typical capability of the DSI-ICP system for trace element determination.

#### 4.2 *In situ* sample treatment (drying and ashing)

Since both the DSI-ICP system and ETA-AAS atomize discrete samples in a sample cup or a furnace by raising the temperature of the sample cup or the furnace, the sample processing cycles of these two methods have many aspects in common. Some ideas and nomenclatures of ETA-AAS can be readily transferred to DSI-ICP-AES.

In electrothermal atomic absorption spectrometry, *in situ* sample treatment is possible and necessary. A sample goes through a drying step and an ashing (pyrolysis) step before being atomized. The drying step is to remove solvent and excess acids from the sample. The drying temperature should be high enough to dry the sample in a minimum time without splattering. A temperature just below the boiling point of the solvent is normally suggested. The drying time required, in seconds, can be calculated by a simple rule of thumb as being equal to 1.5-2 times the sample volume as measured in microliters [1].

The ashing cycle is frequently the most important experimental factor to be controlled. The sample is heated at the highest temperature possible without significant loss of the analyte so that the matrix is broken down or vaporized



prior to the atomization stage. The problems of inter-element interferences and background light scattering or absorption are thus reduced. The ashing time depends on the sample matrix: as a general rule, a time period similar to that of the drying cycle is sufficient. The optimum ashing temperature is determined experimentally by plotting the analytical signal as a function of ashing temperature. It has a wide range for different analytes. As an example, the ashing temperatures range from 400 °C for Tl to 1600 °C for Ge in a matrix of nitrate and fluoride of metal [2] with an ashing time of 45 seconds.

For the DSI technique, since there is a temperature gradient along the central tube of the DSI-ICP torch [3], the sample can also be thermally processed *in situ* at various temperatures, i.e., at various distances from the plasma, before being inserted into the plasma for atomization. In this work, the sample is inserted sequentially to two different positions below the plasma for various periods of time before atomization, which is analogous to the drying and ashing steps of ETA-AAS.

The drying process was usually implemented at 35 mm below the top of the load coil (blc), with a drying time of 30 seconds. When a sample cup is inserted to this position, its temperature will rise gradually from room temperature to about 500 K which is sufficient to remove the solvent from the samples without analyte loss. Splattering was not

observed because the sample cup temperature increased at a slow rate.

After the drying process, the sample cup is moved closer to the plasma for ashing. The ashing time is usually 60 or 120 seconds. The optimum ashing temperature (height) is determined by inserting the sample to different heights for fixed periods of time and then monitoring the analytical signal upon full insertion. The closest distance to the plasma, measured in mm b/c, without analyte loss, is taken as the ashing position. The optimum ashing height depends on the analyte and the sample matrix. For example, the analytical signal for Cu in 10 mg of Pine Needles as a function of ashing height, with an ashing time of 120 seconds, is shown in Figure 4-1. The optimum height is found to be 16 mm b/c. However, with the addition of 10  $\mu$ l of concentrated nitric acid to the sample, the optimum ashing height shifted to 18 mm b/c as shown in Figure 4-2, although the maximum intensities in both situations are the same. Nitric acid was added because its oxidizing properties might enhance matrix decomposition during the ashing cycle.

Different analytes in the same matrix have different optimal ashing heights (temperatures) due to different volatilities of the analytes. For example, the optimal ashing height for Pb in 10 mg of Pine Needles with 10  $\mu$ l of concentrated nitric acid is 22 mm b/c (Figure 4-3), which is lower than that for Cu (16 mm b/c). The difference arises because Pb is more volatile than Cu [4].

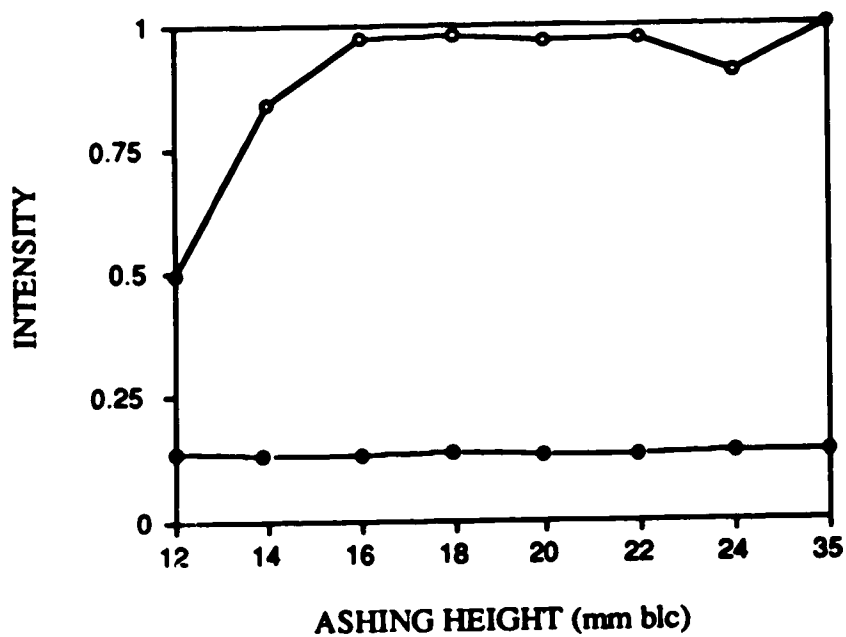


**Figure 4-1.** Signal for Cu from 10 mg of Pine Needles as a function of ashing height. Ashing time is 120 s.  
○ is peak area and ● is background.

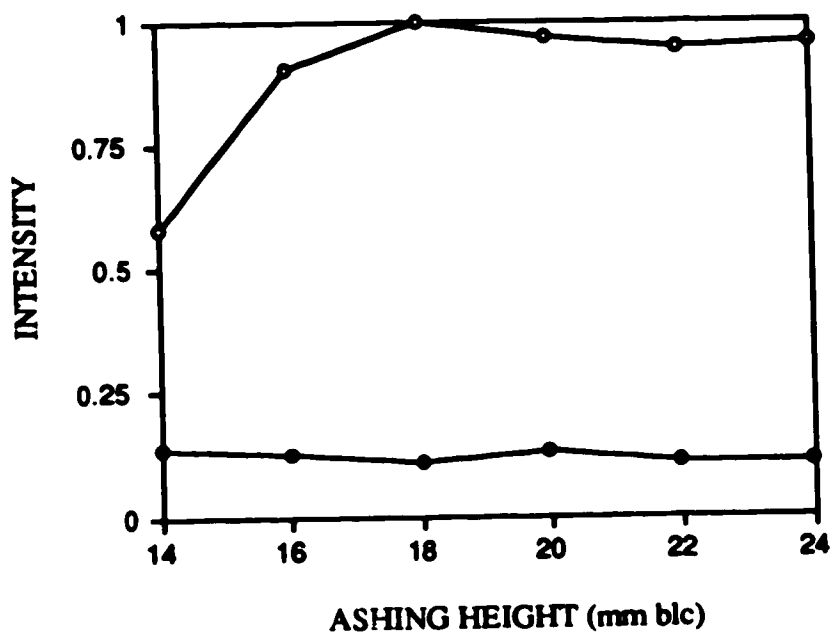


**Figure 4-2.** Signal for Cu from 10 mg of Pine Needles with concentrated nitric acid as a function of ashing height. Ashing time is 120 s.  $\circ$  is peak area and  $\bullet$  is background.

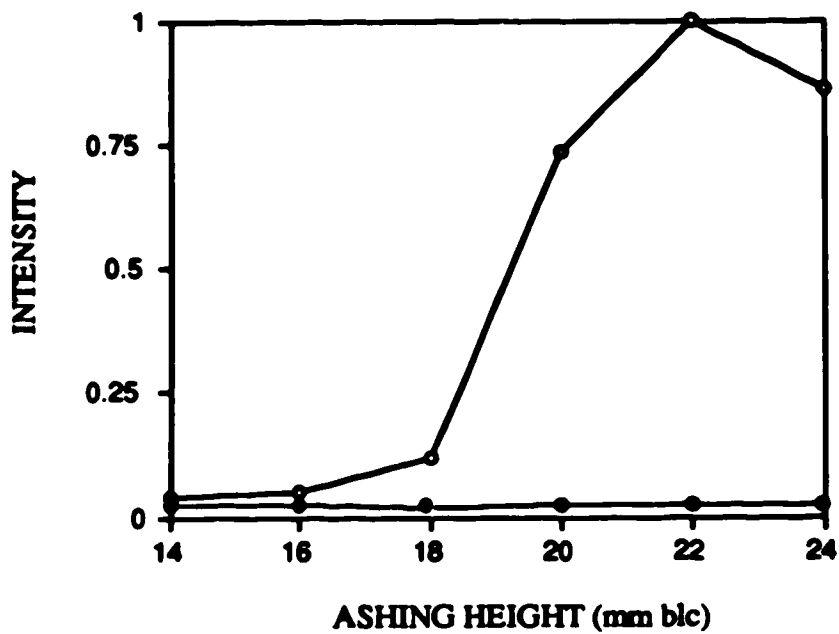


**Figure 4-3.** Signal for Pb from 10 mg Pine Needles with concentrated nitric acid as a function of ashing height. Ashing time is 120 s.  $\circ$  is peak area and  $\bullet$  is background..

The effect of a matrix modifier on the analytical signal depends on the analyte. Ten microliters of concentrated nitric acid was added to 10 mg of Pine Needles, and the sample was ashed at 18 mm b/c for 60 or 120 seconds. The signal was compared to that of the sample ashed at the same height for 60 seconds. It was found that the analytical signal for Cu was virtually independent of the addition of acid. However, the signal for Pb was reduced by half with acid if ashed for 60 seconds, and was reduced to about 10 percent if ashed for 120 seconds (Figure 4-4).

The ashing height for an analyte is usually found empirically. For multi-element analysis, the optimal height for the most volatile element will be selected to avoid loss of analyte. For example, ashing at 22 mm b/c will be used for the analysis of Pb and Cu in Pine Needles with concentrated nitric acid.

#### 4.3 Desolvation of Samples (*in situ* and external)

Solution samples were desolvated *in situ* and externally, and the effect of desolvation was monitored with the emission time profile. For *in situ* desolvation the sample is spiked in the sample cup and inserted into the ICP torch immediately for drying. External desolvation is the process in which the sample is allowed to dry in air before insertion.

The method of desolvation of a solution sample can have a significant effect on the temporal behavior of the signal

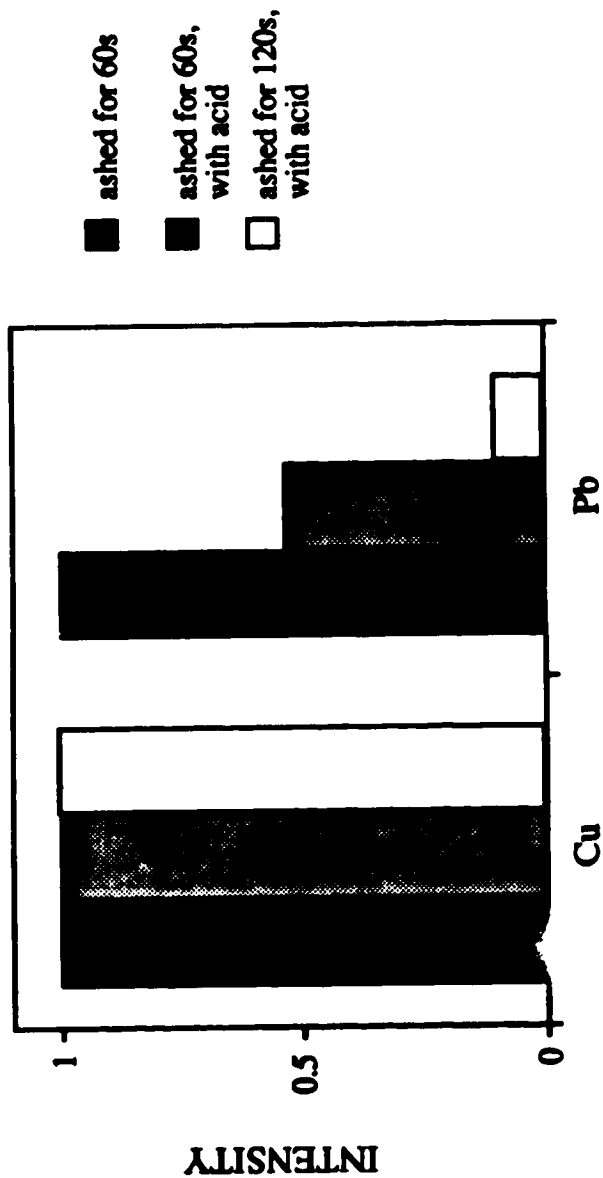


**Figure 4-4.** The effect of concentrated nitric acid on signals for Cu and Pb in 10 mg of Pine Needles. The samples were dried at 35 mm b1c for 30 s then ashed at 18 mm b1c.

of an analyte. Depending on the matrix of the sample, the peak intensity may also be altered by the desolvation process. These effects were not expected initially because the drying step should simply remove the solvent, without changing the matrix significantly.

#### 4.3.1 Samples with desolvation but without ashing

Solution samples were desolvated *in situ* and externally, then the samples were inserted into the plasma directly without an ashing step.

The time profiles of Fe and Pb in nitrate and chloride forms, with *in situ* desolvation, are shown in Figure 4-5. The samples were 10  $\mu$ l of a 100 ppm solution of the analyte, i.e., the total amount was 1  $\mu$ g. The solutions were dried at 35 mm h<sub>2</sub>O for 30 seconds before being inserted into the plasma.

The time profile for Fe in the nitrate form shows only one peak, while that of the chloride form shows a small peak followed by a broad peak similar to that of the nitrate. It has been suggested in the ETA-AAS literature that  $\text{Fe}(\text{NO}_3)_3$  is converted to  $\text{Fe}_3\text{O}_4(\text{s})$  at 585 K. The oxide is then reduced by the graphite of the furnace to  $\text{Fe}(\text{s})$  at 1500 K, and  $\text{Fe}(\text{s})$  subsequently vaporizes [5]. Another suggested mechanism is that the oxide is reduced by carbon directly to the gaseous species,  $\text{Fe}(\text{g})$ , at 1700 K [6]. The time profile of  $\text{Fe}(\text{NO}_3)_3$



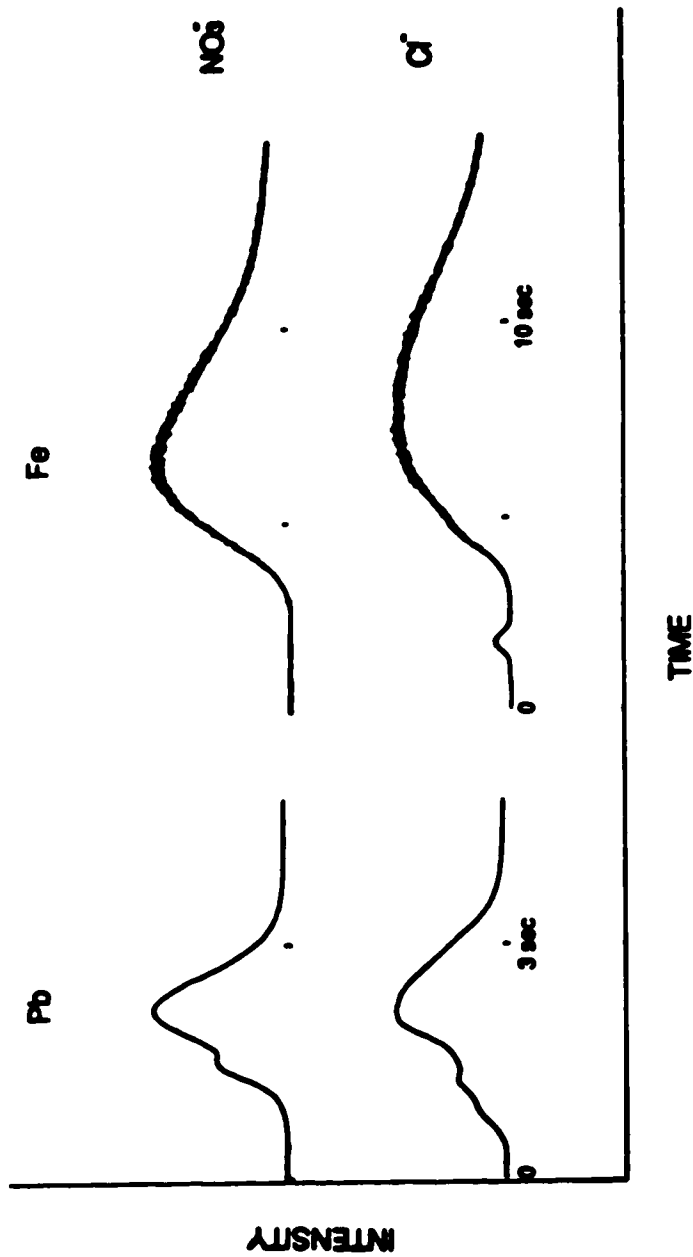


**Figure 4-5.** Emission intensity-time profiles for atomization of 10  $\mu\text{L}$  of 100 ppm of Pb and Fe in nitrate and chloride forms. The samples were dried in situ at 35 mm blc for 30 s before full insertion. No ashing cycle was used.

shows only one peak, therefore, both reactions may take place simultaneously.

$\text{FeCl}_3$  has a different vaporization process. The small peak is likely due to the sublimation of the chloride [5]. It is reported that at 590 K,  $\text{FeCl}_3$ , in the form of  $\text{Fe}_2\text{Cl}_6(l)$ , is reduced to  $\text{FeCl}_2(l)$ , and at or above 674 K,  $\text{Fe}_2\text{Cl}_6(g)$  vaporizes from the solution of  $\text{FeCl}_2$  in  $\text{Fe}_2\text{Cl}_6(l)$  [7]. The second peak has a similar shape as that of the nitrate, which may be due to the hydrolysis of the chloride leading to the production of oxide and thus having the same vaporization process as the nitrate.

$\text{Pb}(\text{NO}_3)_2$  shows two peaks (Figure 4-5) which are possibly from two species.  $\text{Pb}(\text{NO}_3)_2$  decomposes to  $\text{PbO}(s)$  at 925 K [8]. In the absence of a reducing agent,  $\text{PbO}(s)$  sublimes to  $\text{PbO}(g)$  [9]. In the presence of carbon, the oxide is reduced to  $\text{Pb}(l)$  which vaporizes as  $\text{Pb}(g)$  at about 1000 K [5] or it is reduced to  $\text{Pb}(g)$  directly [6]. It is also found that molecules of  $\text{PbO}$  begin to appear earlier than lead atoms in ETA-AAS [10]. Therefore, the two-peak time profile observed is likely due to two vaporization processes: (1)  $\text{PbO}(s)$  without direct contact with the graphite surface sublimes as oxide which decomposes to Pb in the plasma, this process accounts for the first peak; (2) the oxide with direct contact with graphite is reduced and vaporized as metal vapour, which is the second peak.

$\text{PbCl}_2$  has a more complicated time profile with three peaks. The first peak is probably due to the sublimation of

$\text{PbCl}_2$  [10]. The chloride is also hydrolysed to oxide [5]. Therefore the second and third peaks are similar to those of the nitrate.

External desolvation of a sample before analysis results in different temporal behavior than that for *in situ* desolvation. The emission time profiles of the same Pb and Fe solutions described above but with external desolvation are shown in Figure 4-6. The experimental conditions are the same except that the sample solutions were dried in air first. The resulting time profiles generally have simpler shapes. This observation may arise because the external desolvation takes a considerably longer time than the *in situ* desolvation, the analyte thus has the chance to form a thin layer on the graphite surface inside the sample cup. Therefore the dominant vaporization mechanism is one that involves interaction between graphite and the analyte. On the other hand, *in situ* desolvation is fast and the analyte is desolvated to polycrystalline forms on the bottom of the cup instead of forming a thin layer. Therefore at least two vaporization processes are possible: the analyte vaporizes by itself, and the analyte interacts with graphite and the resulting product vaporizes.

$\text{Fe}(\text{NO}_3)_3$  has a sharper peak with external desolvation. It may be due to the larger surface area leading to a higher rate of vaporization, i.e., more  $\text{Fe}_3\text{O}_4(\text{s})$  interacts with the graphite surface at a time. The peak area of the small peak of  $\text{FeCl}_3$  is reduced considerably.

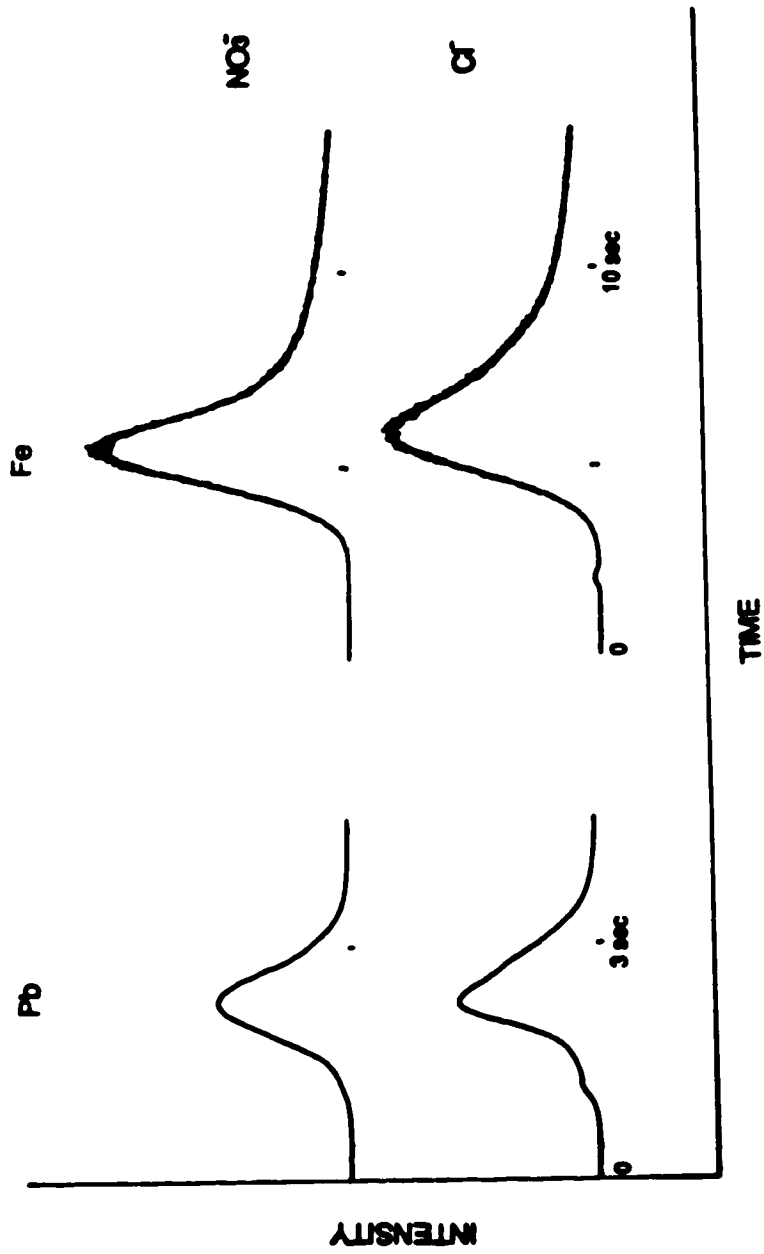


**Figure 4-6.** Emission intensity-time profiles for atomization of 10  $\mu\text{L}$  of 100 ppm of Pb and Fe in nitrate and chloride forms. The samples were dried externally, then heated at 35 mm b/c for 30 s before full insertion. No ashing cycle was used.

$\text{Pb}(\text{NO}_3)_2$  has a smooth peak instead of the double peak observed earlier. The difference arises because the better surface contact favors oxide reduction, therefore,  $\text{PbO}$  sublimation is not observed. On the other hand,  $\text{PbCl}_2$  has two peaks. The appearance time of the first peak matches that of the peak attributed to oxide sublimation for samples with *in situ* desolvation. The oxide is probably formed by the hydrolysis of the chloride. The second peak is the vaporization of the metal which is the product of the oxide reduction by carbon.

#### 4.3.2 Samples with desolvation and ashing

The temporal behavior of an analyte is altered by the introduction of an ashing cycle, in addition to the method of desolvation described above.

Emission time profiles for Cu are shown in Figure 4-7. The sample was 10  $\mu\text{l}$  of 100 ppm Cu in the form of  $\text{Cu}(\text{NO}_3)_2$ . With external desolvation but without ashing, two peaks were observed.  $\text{Cu}(\text{NO}_3)_2$  decomposes at 1220 K to  $\text{CuO}_{(s)}$  [8]. This oxide is in equilibrium with its gas phase species,  $\text{CuO}_{(g)}$ , at 873-1223 K [9]. The oxide is, however, more stable in the form of  $\text{Cu}_2\text{O}_{(s)}$  at a temperature above 800 K. This oxide will be reduced to  $\text{Cu}_{(g)}$  by carbon at temperatures above 1800 K [6,11]. The two peaks in the time profile possibly arise from the vaporization of  $\text{CuO}$  and the reduction of  $\text{Cu}_2\text{O}$ .

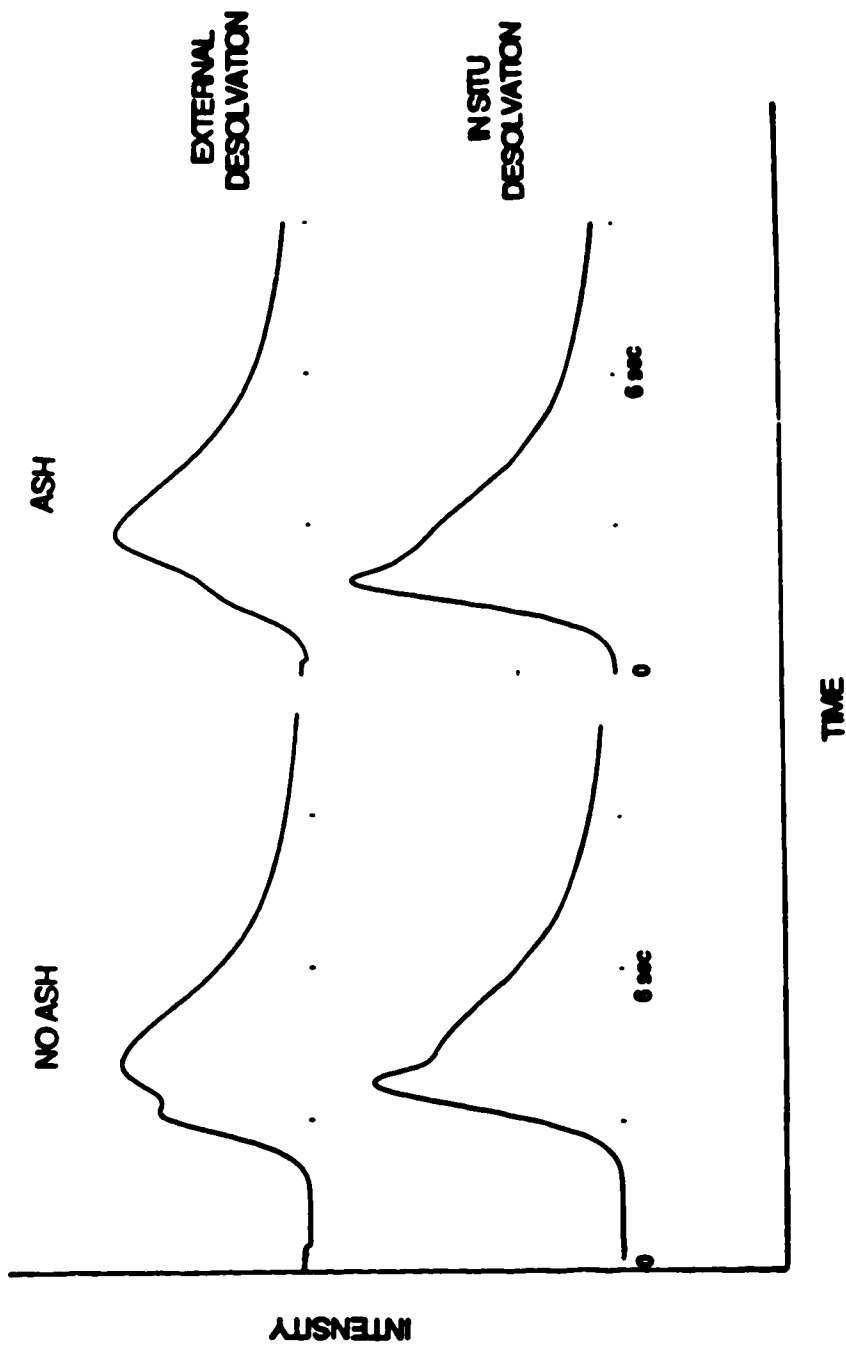


**Figure 4-7.** Emission intensity-time profiles for atomization of 10  $\mu\text{L}$  of 100 ppm of Cu in nitrate form. All samples were heated at 35 mm b/c for 30 s. The time profiles on the left hand side were for samples without ashing cycle. The time profiles on the right hand side were for samples with 60 s ashing at 18 mm b/c.

If the  $\text{Cu}(\text{NO}_3)_2$  solution is externally desolvated and ashed at 18 mm hlc for 60 seconds, the intensity of the first peak is reduced. The reduction is probably due to the transformation of  $\text{CuO}$  to  $\text{Cu}_2\text{O}$  and also due to the possible loss of  $\text{CuO}$  as gas phase species during the ashing cycle.

If the  $\text{Cu}(\text{NO}_3)_2$  solution is desolvated *in situ*, the time profiles from samples with or without ashing have a large first peak followed by a second peak similar to that of the externally desolvated samples. This observation is in contrast to the observation that the intensity of the first peak is reduced in the case of external desolvation with ashing described above. The first peak is larger because the sample now desolvates to a polycrystalline form. The oxide from the decomposition of the  $\text{Cu}(\text{NO}_3)_2$  crystal has less contact with the graphite surface, and thus is more readily vaporized as an oxide.

Emission time profiles for  $\text{Fe}(\text{NO}_3)_3$  with or without ashing are shown in Figure 4-8. They are consistent with those shown in Figures 4-5 and 4-6. The ashing cycle has no effect on the shape of the time profiles. This is because Fe has only one vaporization mechanism which involves carbon.

The time profiles for  $\text{Pb}(\text{NO}_3)_2$  are shown in Figure 4-9. The time profiles without ashing are the same as those in Figures 4-5 and 4-6. However the time profiles with ashing have smaller peak area than that without ashing. The reduction in peak area is because  $\text{PbO}$  is lost via sublimation

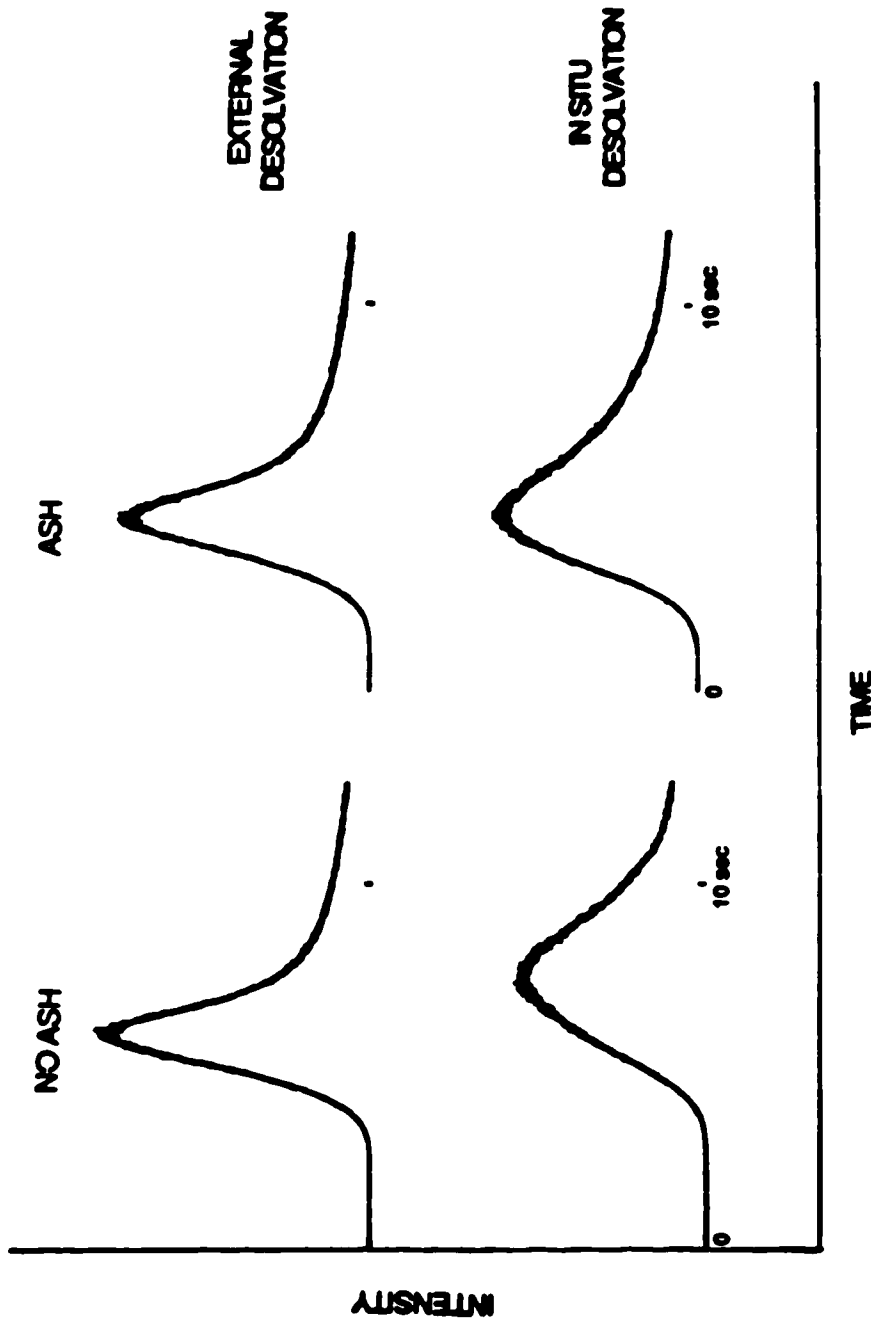


**Figure 4-8.** Emission intensity-time profiles for atomization of 10  $\mu\text{L}$  of 100 ppm of Fe in nitrate form. All samples were heated at 35 mm b/c for 30 s. The time profiles on the left hand side were for samples without ashing cycle. The time profiles on the right hand side were for samples with 60 s ashing at 18 mm b/c.



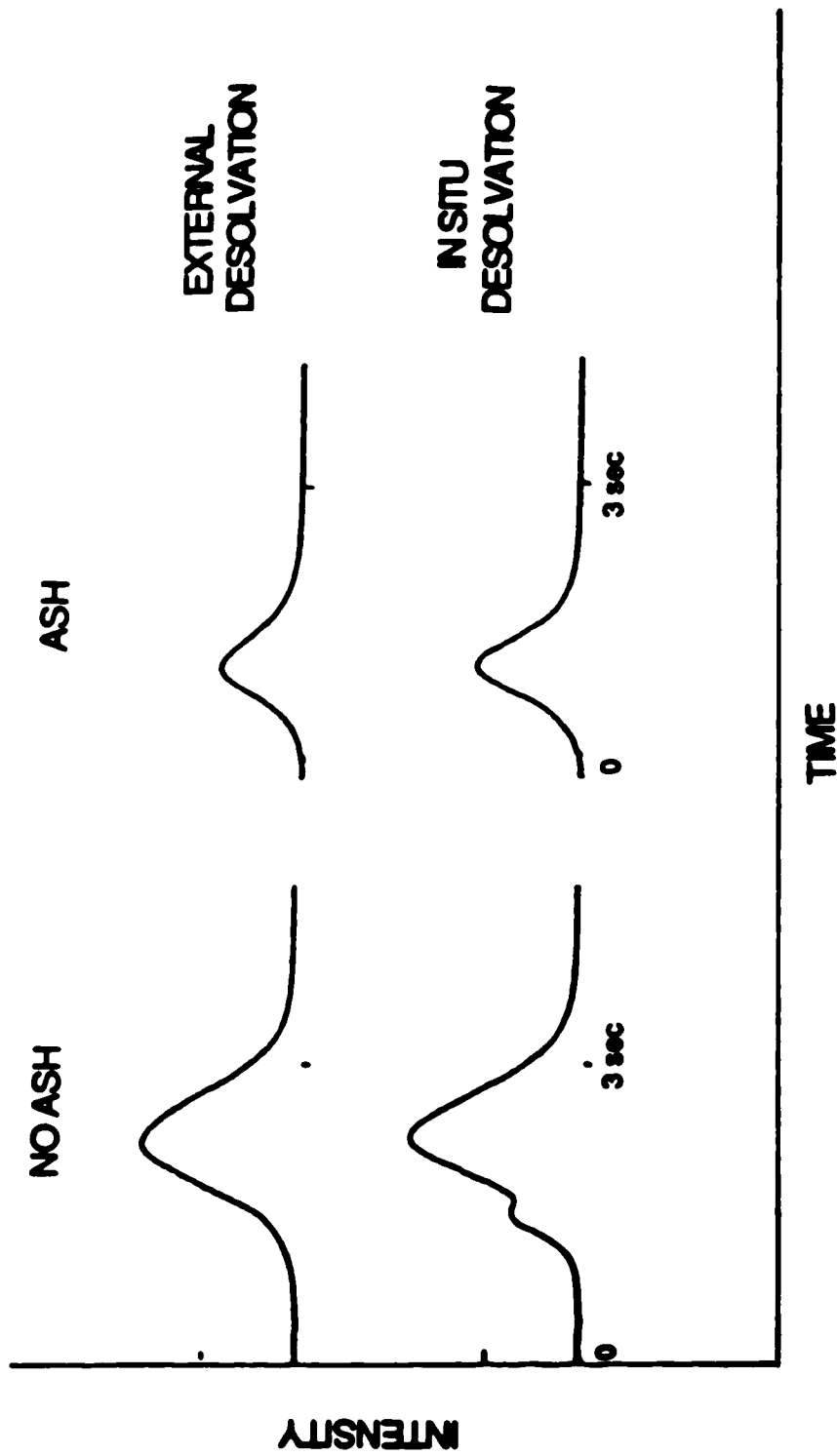


**Figure 4-9.** Emission intensity-time profiles for atomization of 10 µL of 100 ppm of Pb in nitrate form. All samples were heated at 35 mm blc for 30 s. The time profiles on the left hand side were for samples without ashing cycle. The time profiles on the right hand side were for samples with 60 s ashing at 18 mm blc.

during the ashing cycle. The smooth peak is from the reduction of the PbO by carbon as described above.

The temporal behavior of Ni shows a much stronger dependence on the ashing cycle than the elements described above. The time profiles for Ni are shown in Figure 4-10. The sample was 10  $\mu$ l of 100 ppm of Ni in the form of NiCl<sub>2</sub> solution. The time profile with external desolvation but no ashing shows a small peak prior to a large peak. The small peak is presumably from the vaporization of NiCl<sub>2</sub>. NiO is formed by the hydrolysis of the chloride [5]. The oxide is reduced and vaporized by the same mechanism as Fe<sub>3</sub>O<sub>4(s)</sub> [5,6]. However, the second peak has a shoulder on its tailing portion. Therefore, there appears to be at least one more vaporization process in addition to that of oxide reduction. This mechanism is probably carbide formation discussed below.

NiCl<sub>2</sub> solution with external desolvation and ashing shows a smooth time profile which is different from that of the sample with external desolvation but no ashing. The difference is possibly due to the formation of Ni<sub>3</sub>C during the ashing cycle. The Gibb's free energy of the following reaction,



can be calculated from the listed Gibb's free energy of formation of each component [12,13]. It is positive at temperatures below 800 K but becomes negative at or above this temperature: at 298 K and 800 K, the Gibb's energy is 260 kJ mol<sup>-1</sup>, and -19 kJ mol<sup>-1</sup> respectively. Therefore, at the

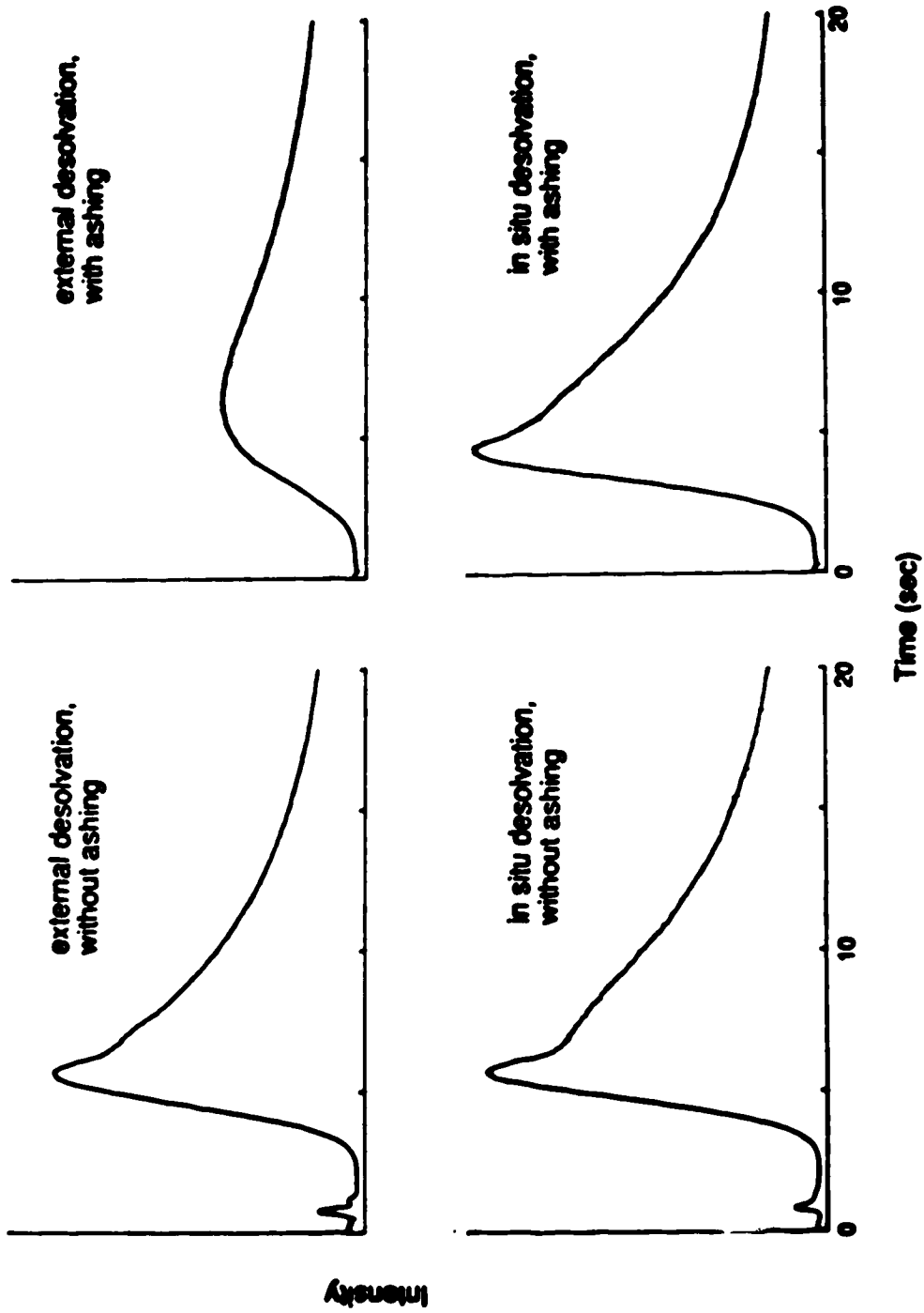


Figure 4-10. Emission intensity-time profiles for atomization of 10  $\mu$ L of 100 ppm of Ni in chloride form. All samples were heated at 35 mm b/c for 30 s. The time profiles on the left hand side were for samples without ashing cycle. The time profiles on the right hand side were for samples with 60 s ashing at 18 mm b/c.

ashing temperature of about 1000 K, nickel carbide forms favorably from its oxide in a graphite sample cup under standard conditions. The carbide vaporizes slowly, therefore the peak is flat and broad. The shoulder of the second peak of the time profile with external desolvation but no ashing also possibly arises due to carbide formation.

The time profiles of sample with *in situ* desolvation have similar shapes and are independent of the ashing cycle, except that the one without ashing has a small peak from  $\text{NiCl}_2$  sublimation. These time profiles are also similar to that of the sample with external desolvation and no ashing. Therefore, Ni is vaporized via the same mechanism of oxide reduction described above. It is interesting to note that the sample with *in situ* desolvation and ashing still has a relatively sharp peak which is opposite to that of the sample with external desolvation and ashing. This difference can also be explained with the argument that a polycrystalline residue is formed instead of a thin layer.

Loss of Ni during the ashing cycle is not observed, which is in contrast to that reported by Campbell and Ottaway [6]. This observation indicates that the considerably smaller peak for the sample with external desolvation and with ashing does not arise because of analyte loss during the ashing cycle.

#### 4.3.3 Conclusion

The temporal behavior and the signal of an analyte strongly depends on the method of sample treatment and the sample matrix. To obtain consistent results, the sample and its standards must be treated in the same way and the matrices of the sample and standard should be matched. Different analytes have different optimal sample treatment requirements. For example, Fe has a sharper peak with external desolvation and ashing. However, Ni will form a carbide with this treatment, and has better sensitivity with *in situ* desolvation. The best sample treatment for each analyte should be determined empirically.

#### 4.4 Detection limits

The detection limits for some elements are listed in Table 4-1. The detection limits were determined by measuring the peak intensity (area) of an analyte 10 times with a concentration within the range of 1-10 times of the background equivalent concentration, and that of the background (also 10 times) in the same integration range. The background equivalent concentration of an analyte, BEC, is calculated by

$$\text{BEC} = I_B \times \frac{C_H}{I_H - I_B} \quad (4-1)$$

where  $I_B$  is the background intensity, and  $I_H$  is the peak intensity of the analyte of concentration  $C_H$ . The detection limit, DL, is calculated by

$$DL = 3\sigma_{I_B} \times \frac{C_H}{I_H - I_B} \quad (4-2)$$

where  $\sigma_{I_B}$  is the standard deviation of the background.

**Table 4-1.** Absolute and relative detection limits for Cd, Zn, Cu, Pb, and Fe\*.

element	concentration (ppb)	absolute amount (pg)
Cd	0.12	1.2
Zn	0.45	4.5
Cu	1.4	14
Pb	2.1	21
Fe	3.0	30

\* 10  $\mu$ l of standard solutions of concentration within the range of 1-10 times of the background equivalent concentration were used. The solutions were dried at 35 mm b/c for 120 seconds before insertion.

For example, the peak area of Pb was obtained by integrating the time profile of 10  $\mu$ l of 10 ppb of Pb from 1.9 to 3.4 seconds, time 0 being the point when the sample cup starts to rise from 35 mm b/c (see Figure 4-11). The background was obtained by integrating the signal from an empty cup with the same integration range.

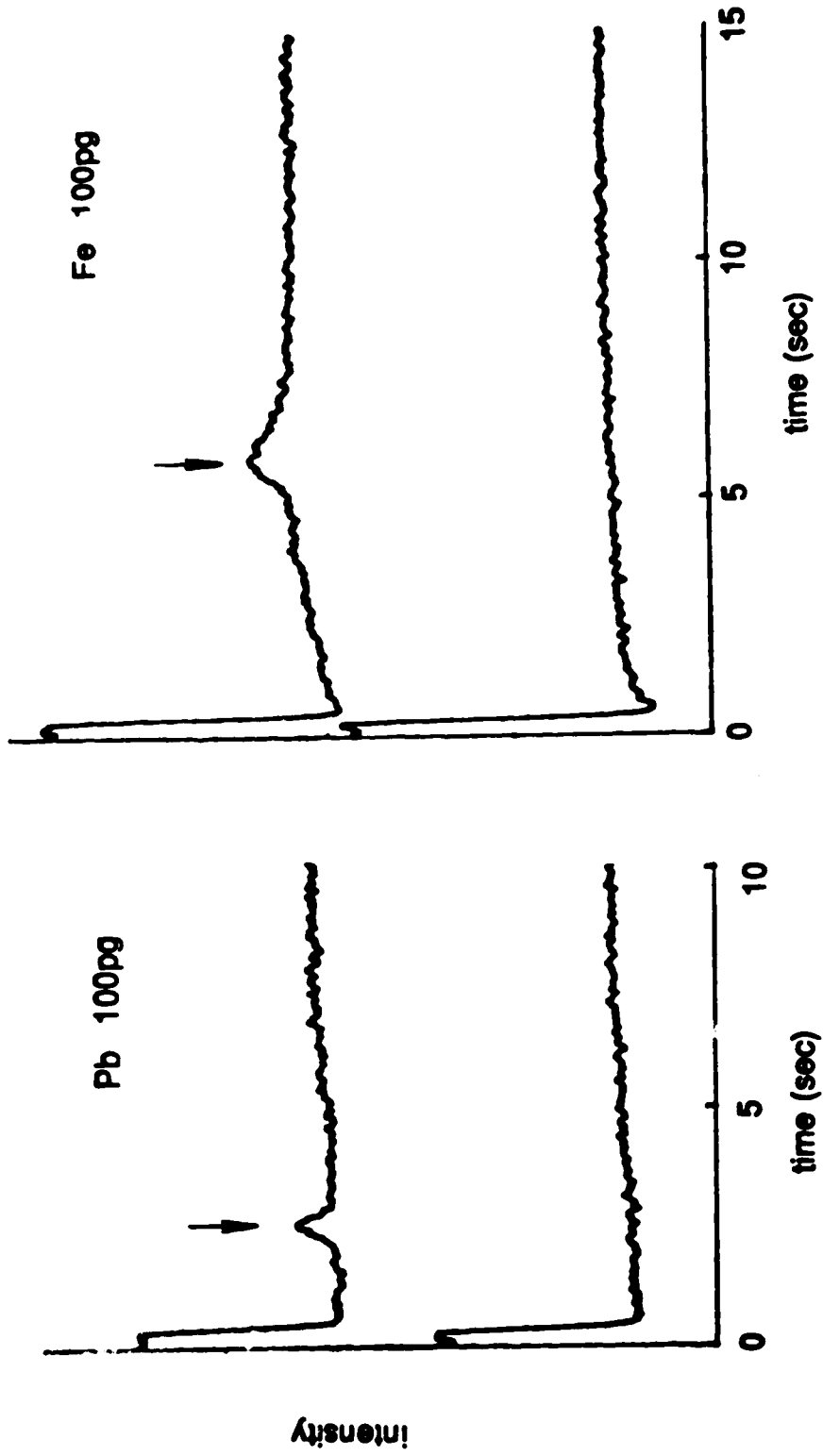


**Figure 4-11.** Emission intensity-time profiles for Pb and Fe at concentration close to the detection limits. The time profiles of their blanks are shown on the bottom for comparison.

It is interesting to note that the detection limit will be larger if the peak is broader. This increase occurs because a broader peak has a larger integration range. The background intensity is thus larger, which leads to a higher standard deviation of the background, although the relative standard deviation remains the same. From Equation 4-2, the detection limit becomes larger. Therefore it is important to have a fast temperature rise and high sample cup temperature so that the peak of an analyte is as sharp as possible and thus the detection limit is optimal.

The time profiles of Pb, Fe, Zn, and Cd and their respective background time profiles are shown in Figures 4-11 and 4-12. The arrows indicate the peaks. Note that the background drops after the sample cup is inserted into the plasma.



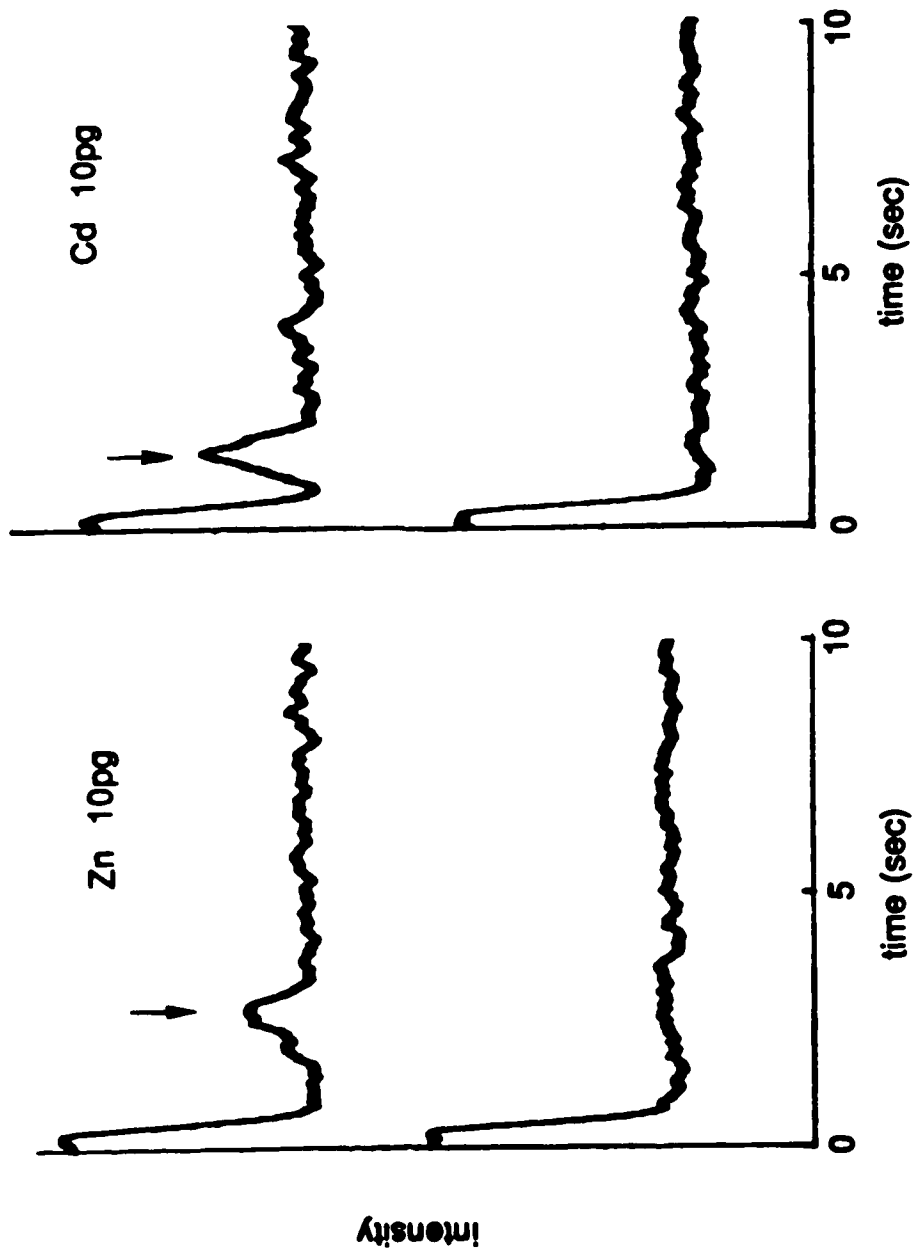


**Figure 4-12.** Emission intensity-time profiles for Zn and Cd at concentration close to the detection limits. The time profiles of their blanks are shown on the bottom for comparison.

**References**

1. C.W. Fuller, "Electrothermal Atomization for Atomic Absorption Spectrometry", The Chemical Society, Burlington House, London, 1977
2. J.Y. Marks and G.G. Welcher, "Determination of Trace Elements of Metallurgical Interest in Complex Alloy Matrices by Nonflame Atomic Absorption Spectroscopy", Flameless Atomic Absorption Analysis: An Update, ASTM STP 618, American Society for Testing and Materials, 1977, pp. 11-21.
3. E.R. Prack and G.J. Bastiaans, *Anal. Chem.* **55**, 1654 (1983)
4. Y. Shao and G. Horlick, *Appl. Spectrosc.* **40**, 386 (1986)
5. R.E. Sturgeon, C.L. Chakrabarti, and C.H. Langford, *Anal. Chem.* **48**, 1792 (1976)
6. W.C. Campbell and J.M. Ottaway, *Talanta* **21**, 837 (1974)
7. C.M. Cook, Jr., *J. Phys. Chem.* **66**, 219 (1962)
8. C. Duval, "Inorganic Thermogravimetric Analysis", 2nd ed., Elsevier Publishing Co., New York, 1963
9. L. Brewer and D.F. Mastick, *J. Chem. Phys.* **19**, 834 (1951)
10. E.M. Sedykh and Yu.I. Belyaev, *Prog. Anal. At. Spectrosc.* **7**, 373 (1984)
11. C.W. Fuller, *Analyst* **99**, 739 (1974)
12. I. Barin and O. Knacke, "Thermochemical Properties of Inorganic Substances", Springer-Verlag, Berlin, Heidelberg, New York, 1973

13. I. Barin, O. Knacke, and O. Kukaschewski, *"Thermochemical Properties of Inorganic Substances, Supplement"*, Springer-Verlag, Berlin, Heidelberg, New York 1977

## Chapter 5. Analysis of Powdered Botanical Samples

### 5.1 Introduction

An ideal situation for quantitative analysis would be if a calibration curve of an analyte could apply to the analysis of all types of samples. However, the presence of concomitants in a sample can cause interferences, i.e., systematic errors in the analytical signal. For example, both the intensities and the shapes of the peak-like signal for the same amount of Pb in standard  $\text{Pb}(\text{NO}_3)_2$  solution and Pine Needles are different (Figure 5-1). Moreover, the signal for the standard addition of this standard solution to the Pine Needles is not the sum of the above signals but about twice the magnitude of that of the Pine Needles. These results are summarized in Table 5-1.

It is evident that the matrix of the botanical sample has a significant effect on the Pb signal. A calibration curve established with standards of a certain matrix is therefore not applicable for the determination of the unknown concentration of an analyte in samples of a different matrix. This is demonstrated by the comparison of the calibration curves of standard Pb solution and standard addition of Pb to Pine Needles (Figure 5-2).

Matrix effects can be reduced or corrected by various means [1]. One major approach, called matrix matching, is the use of reference samples whose chemical composition and

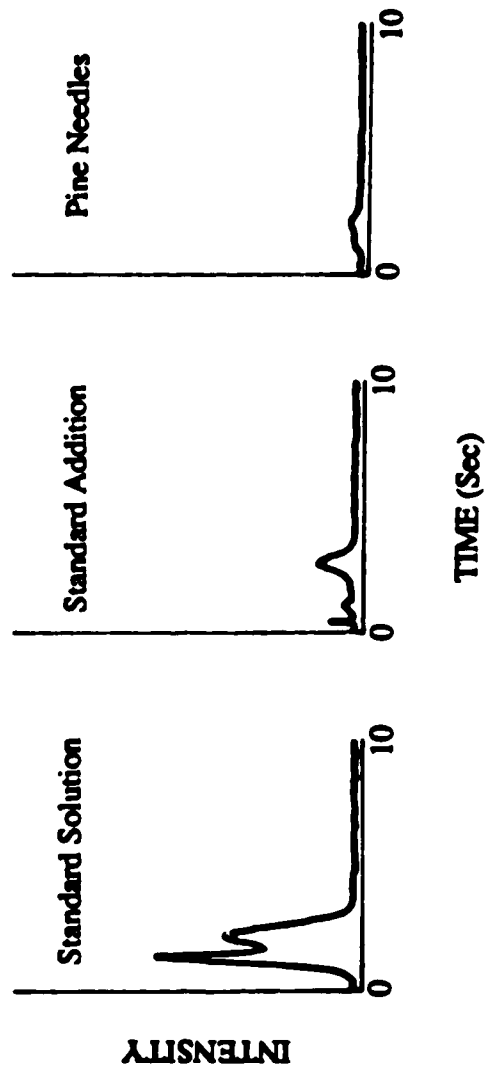


**Figure 5-1.** Signal for Pb from 10  $\mu\text{L}$  of 10 ppm standard solution, 10 mg of pine needles (Pb content is 10.8 ppm), and standard addition of the standard solution to the Pine Needles.

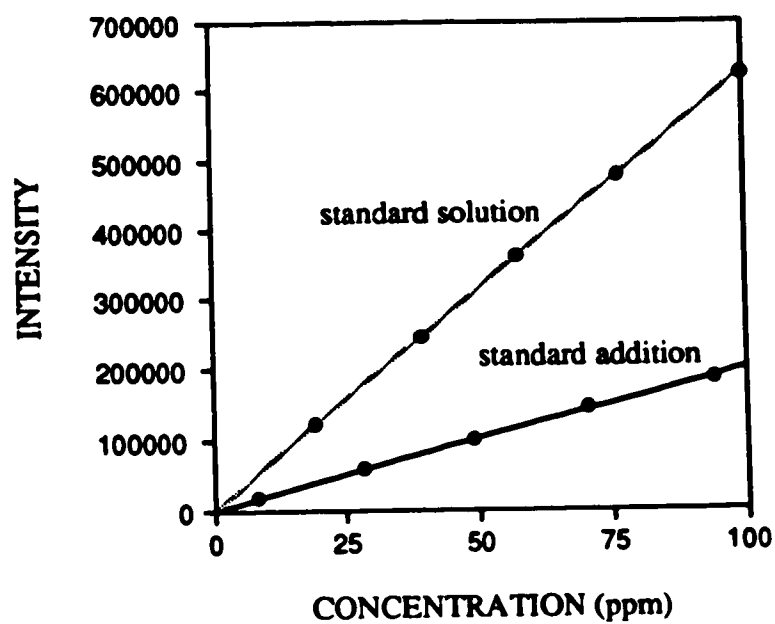


**Figure 5-2.** Calibration curves for Pb standard solution and standard addition analysis of Pine Needles. The curve for standard addition analysis is corrected to pass through origin, so that the slopes can be compared.

physical properties match those of the samples as closely as possible. Other approaches include the internal standard technique, the isoformation technique, and the standard addition technique.

**Table 5-1.** Comparison of the Signals for Pb from NBS SRM 1575 Pine Needles, Standard Solution, and Standard Addition.\*

Sample	Intensity (arbitrary unit)	Intensity Ratio
Pine Needles	4989	1.0
Standard Pb Solution	56924	13.9
Standard Addition	9185	2.2

\* Volume of 10 ppm of Pb Standard Solution was 10  $\mu$ L. Weight of pine Needles was 10 mg. Certified Value of Pb in Pine Needles is  $10.8 \pm 0.5$  ppm.

The internal standard technique measures the analytical signal of the analyte relative to the signal emitted by an internal standard element of fixed concentration. The internal standard is either a major constituent of the sample and the standard, or an element which is not present in the sample and is added specifically. In some cases the background signal can also be used as internal standard. A plot of the ratio of the analyte signal to that of the internal standard against concentration is used for the calibration curve. For this approach to work, it must be carefully

established that the analyte and the internal standard experience the same matrix effect and that the effect is multiplicative.

The isoformation technique refers to procedures that eliminate the effects of the differences in crystallographic structure between the sample and standards on the analytical results. Fusion with a flux and dissolution of a solid sample are some of the well-known procedures.

The standard addition technique is the procedure in which successive known amounts of the analyte are added to aliquots of the sample. A calibration curve is constructed with the signals of the samples plotted against the added concentrations. The analytical result is found by extrapolating this curve to intercept the negative concentration axis.

In this Chapter, matrix matching and standard addition techniques are examined for the analysis of powdered botanical samples using DSI-ICP-AES. Matrix modification with the addition of NaF solution to the samples is also studied.

## **5.2 Experimental**

Standard solutions were prepared by serial dilution of 1000 ppm standard stock solution from SPEX (SPEX Inc., Edison, NJ, U.S.A.) with distilled/deionized water.

The powdered botanical samples are Pine Needles (Standard Reference Material 1575 from the National Bureau of



Standards), Orchard Leaves (NBS SRM 1571), Spinach (NBS SRM 1570), Tomato Leaves (NBS SRM 1573), and Pepperbush (NIES SRM No.1, Japan). The samples were dried in an oven according to the instructions for each material, then they were weighed into a sample cup with an analytical balance. Standard solution and/or matrix modifier were added on top of the sample and allowed to be absorbed by the sample before analysis.

The samples were usually dried/ashed in the central tube of the ICP torch below the plasma before insertion for measurement. This step decomposed the matrix of the samples. During the dry/ash process, the botanical samples were charred and smoke was observed at the bottom of the ICP torch. The sample was sintered into a bead, which prevented splattering of the sample upon final insertion into the plasma.

### **5.3 Matrix Matching Method**

The chemical composition and physical properties of a solution sample and a powdered botanical sample are quite different, which contributes to the difference in sensitivity of an analyte as mentioned earlier. However, the botanical standard reference materials are generally similar to each other. Therefore the sensitivity of an analyte from the various SRMs should be similar. Calibration curves for analytes in these SRMs can be used to test this hypothesis.

If good calibration curves are obtained, then real botanical samples can be analysed by the DSI technique directly with no sample pretreatment.

### 5.3.1 Experimental

The weight of the Standard Reference Materials used was 5.0 mg. The samples were placed in a graphite sample cup, then dried/ashed at 35 mm b/c in the central tube of the DSI-ICP torch for 120 seconds. No further ashing was used in order to avoid loss of volatile analytes, e.g. Pb and Cd.

A total of eight elements was measured, which were divided into two groups because the DSI readout electronics handles only six channels at a time. The first group included Al, Cu, Fe, Mn, and Zn. The second group consisted of As, Cd, Cu, Pb, and Zn. The elements Cu and Zn were measured in both groups to monitor the behavior of the samples. It was found that the behavior of these two elements in both groups was the same.

The pre-amplifier gains for the analog-to-digital convertor, AI13, are listed in Table 5-2. The integration time for each channel was 50 seconds, and the sampling rate was 10 Hz.

All five of the SRMs (namely, Tomato Leaves, Orchard Leaves, Spinach, Pine Needles, and Peppercorn) were used. Each sample was measured with five replicates in each group. Therefore, there is a total of 125 sets of signals for each

group (5 elements), i.e., 62500 data points or ~120 kbyte. This shows that the amount of data gathered and required to be processed with the DSI technique is large.

**Table 5-2.** The pre-amplifier gains of the AI13 for the eight elements of the SRMs.

element	gain (V/A)
Al	$10^7$
As	$10^7$
Cd	$10^7$
Cu	$10^7$
Fe	$10^7$
Mn	$10^5$
Pb	$10^8$
Zn	$10^6$

### 5.3.2 Results and Discussion

The calibration curves for the elements, Al, As, Cd, Cu, Fe, Mn, Pb, and Zn, are shown in Figure 5-3. The intensities are peak areas. The elements can be divided into two categories: volatile and non-volatile. For the volatile elements such as Pb, Cd and Cu (Figure 5-3a, 5-3b and 5-3c), the analytes vaporized completely during the measurement time period. These elements generally have an acceptable calibration curve. Therefore, the matrix matching method appears to be applicable for volatile elements.

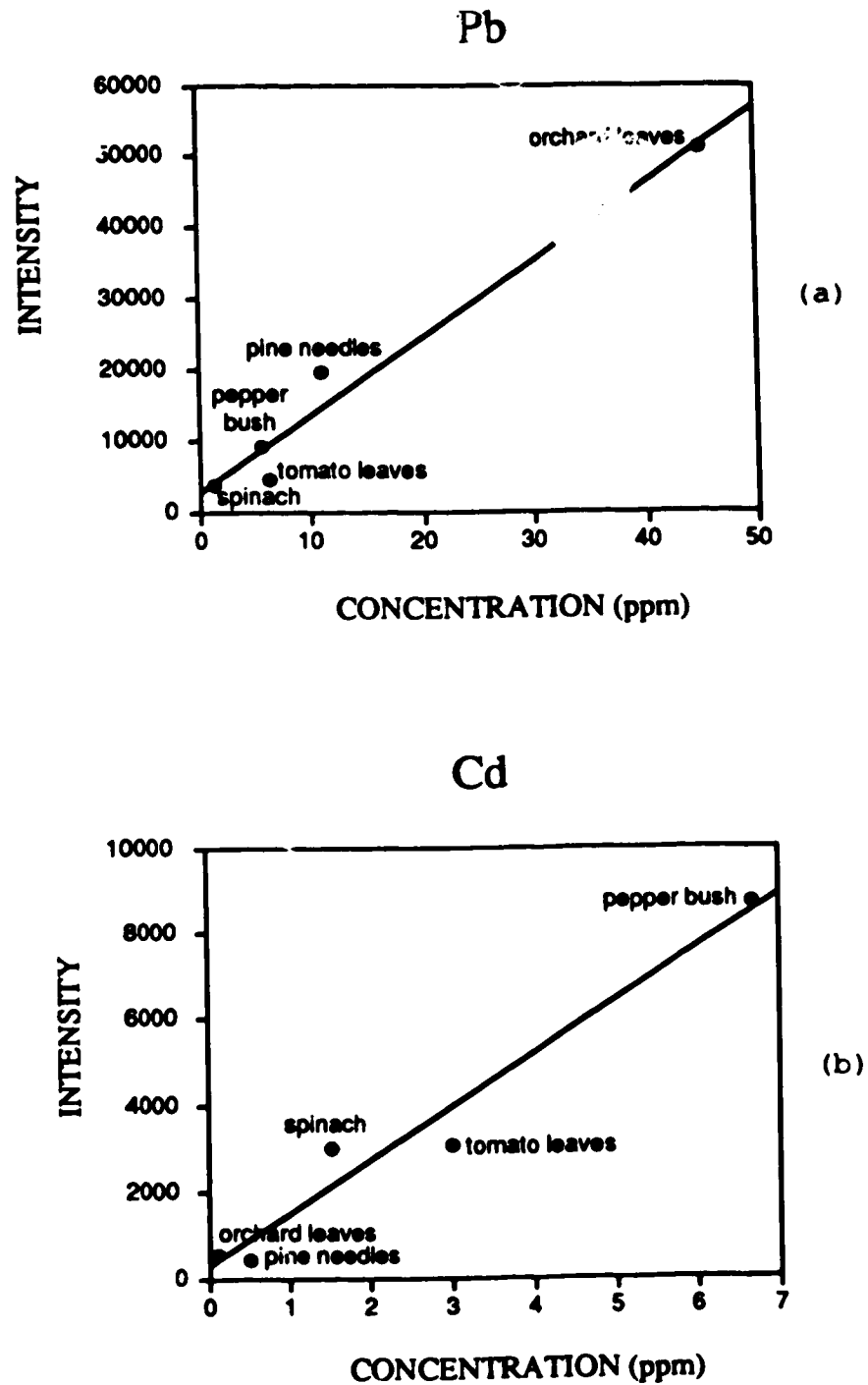


**Figure 5-3.** Calibration curves for Standard Reference Materials. (a) Pb, (b) Cd.

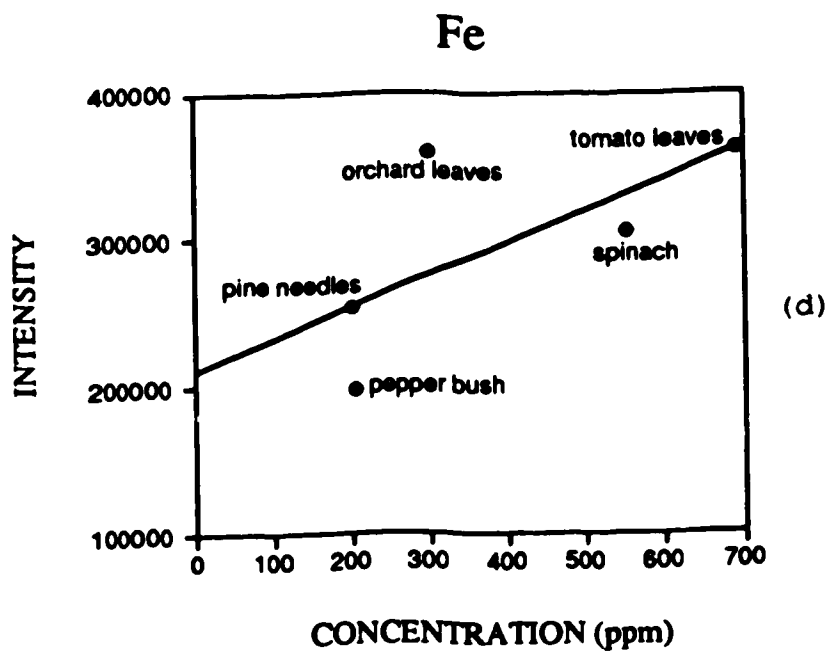
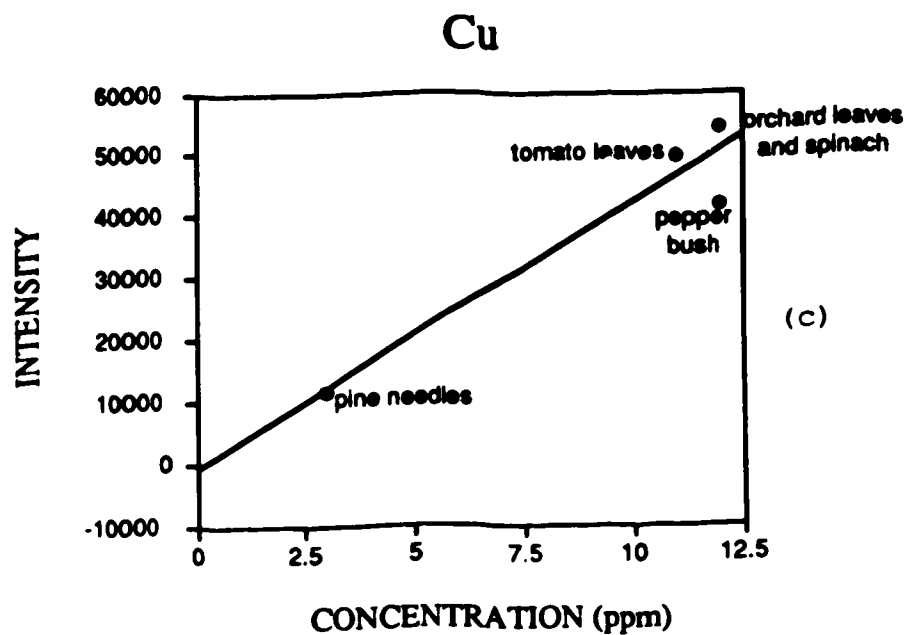


**Figure 5-3.** Calibration curves for Standard Reference Materials. (c) Cu, (d) Fe.

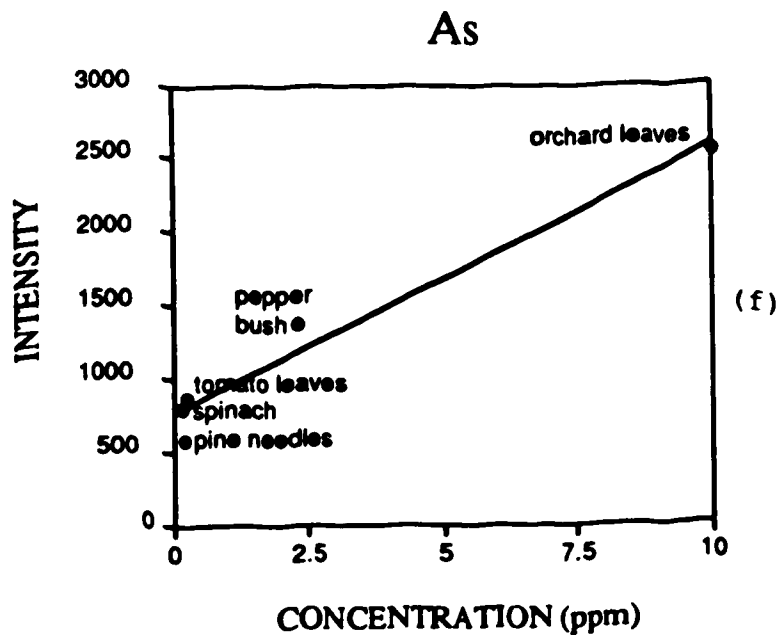
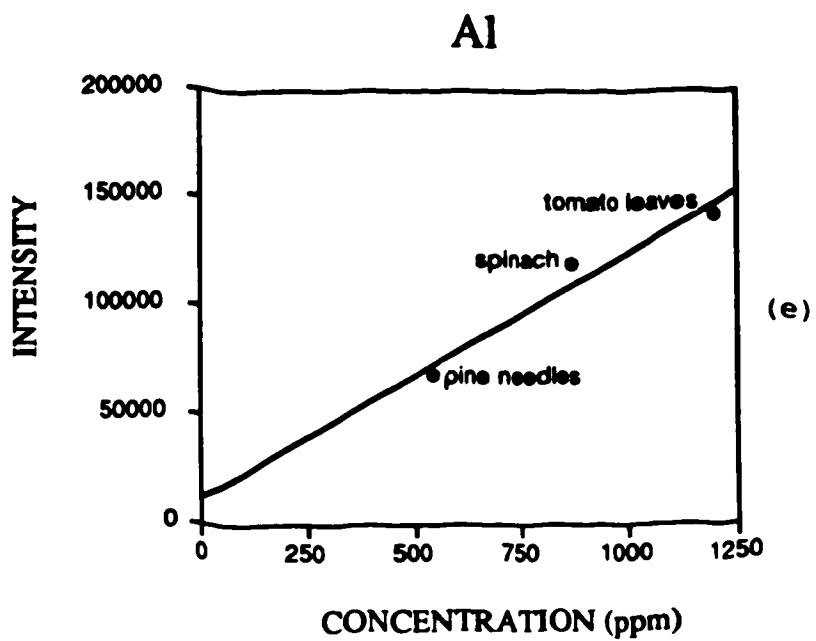


**Figure 5-3.** Calibration curves for Standard Reference Materials. (e) Al, (f) As.

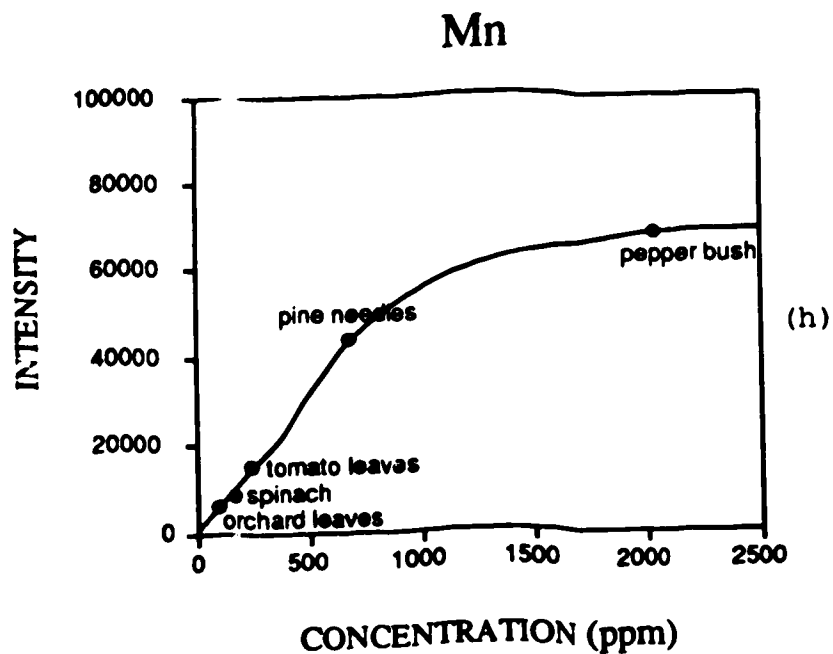
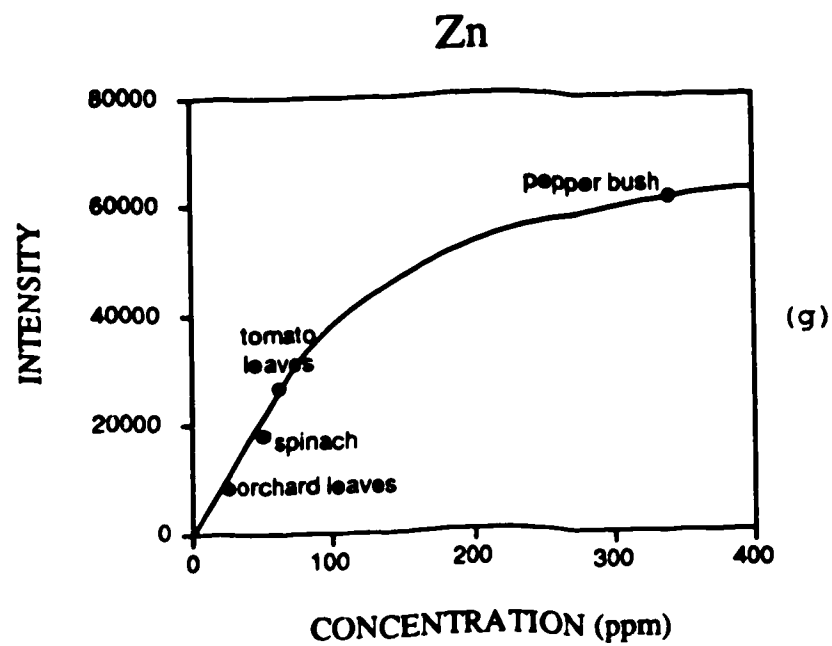


**Figure 5-3.** Calibration curves for Standard Reference Materials. (g) Zn, (h) Mn.

The temporal behavior of the signal for an analyte from different samples is quite different, as illustrated in Figure 5-4. However, the temporal behavior seems to have little effect on the quality of the calibration curve if the analyte was completely vaporized. For example, the calibration curve of Cu (Figure 5-3c) has a correlation coefficient of 0.95 and that of Pb (Figure 5-3a) is 0.98.

For elements that are not completely vaporized during the observation period, the intensities are not well correlated. For example, the correlation coefficient for the Fe calibration curve (Figure 5-3d) is 0.68.

Two exceptions were found. Zn and Mn appeared to be completely vaporized, as shown in Figure 5-4e and 5-4f, but their calibration curves (Figure 5-3g and 5-3h) are curved at higher concentration. (The data points that are not well correlated to other data points are labeled with open circles.) It is noted that the curved portion of the calibration curve corresponds to high concentration of the analyte (340 ppm of Zn in Pepperbush, and 675 and 2030 ppm of Mn in Pine Needles and Pepperbush). Therefore, high emission intensity (peak height) may have saturated the PMT. The anodic current of the PMT at the peak of the signal can be calculated with the following equation,

$$i = \frac{x}{4095} \times \frac{5}{G} = \frac{x}{819 \times G} \quad (5-1)$$



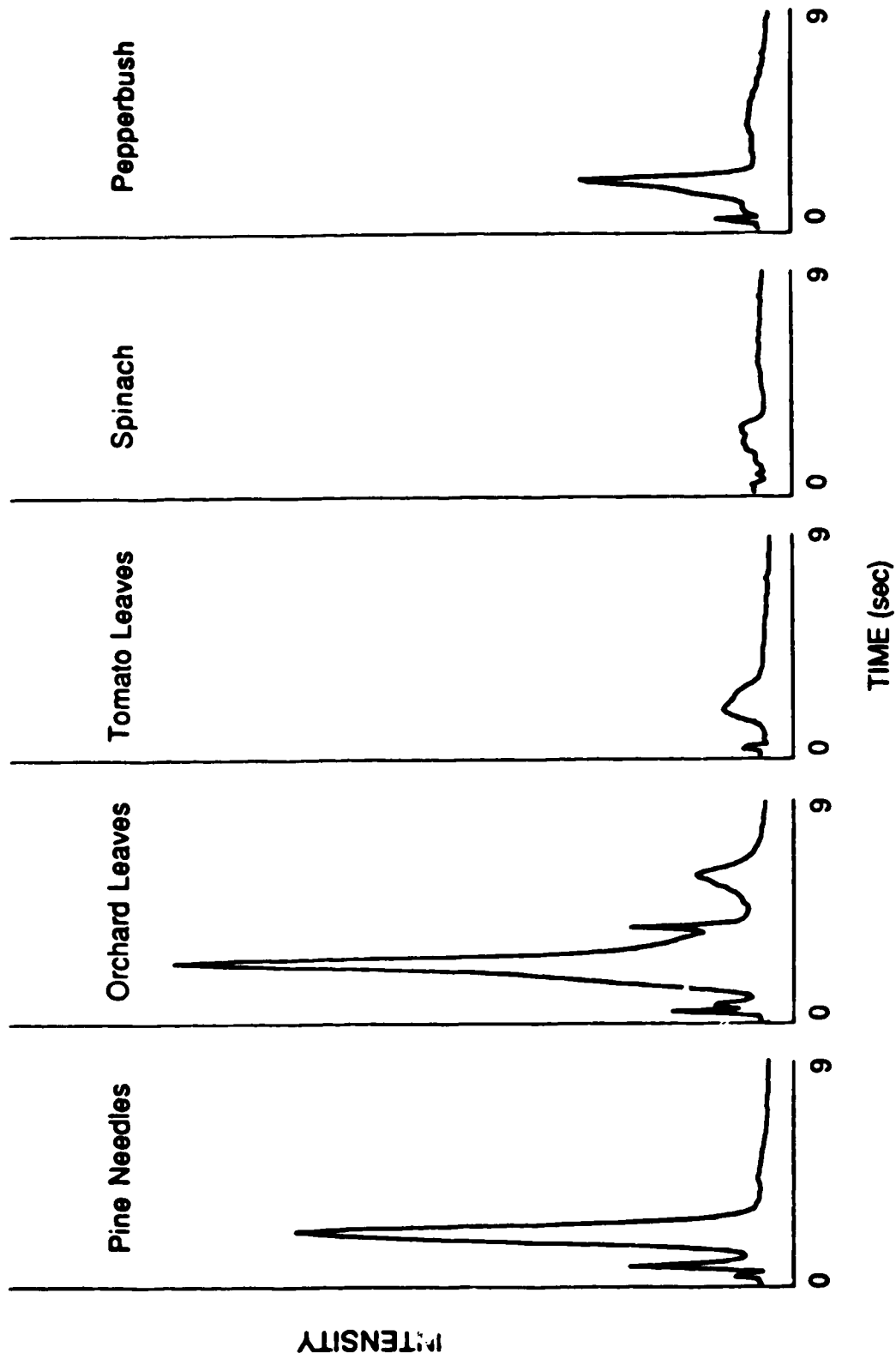


**Figure 5-4(a).** Signal for Pb from standard reference materials of botanical matrices.

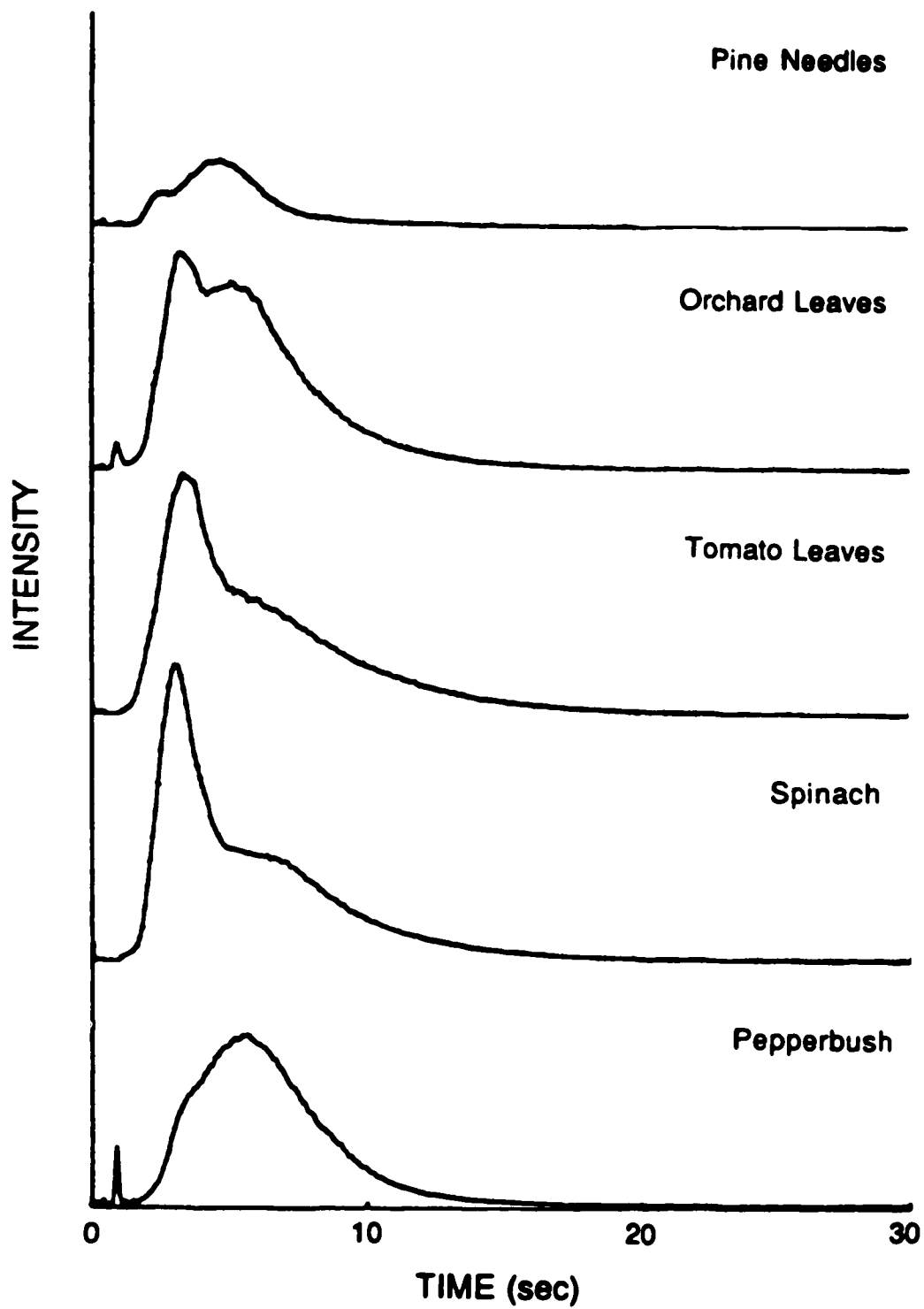


**Figure 5-4(b).** Signal for Cu from standard reference materials of botanical matrices.

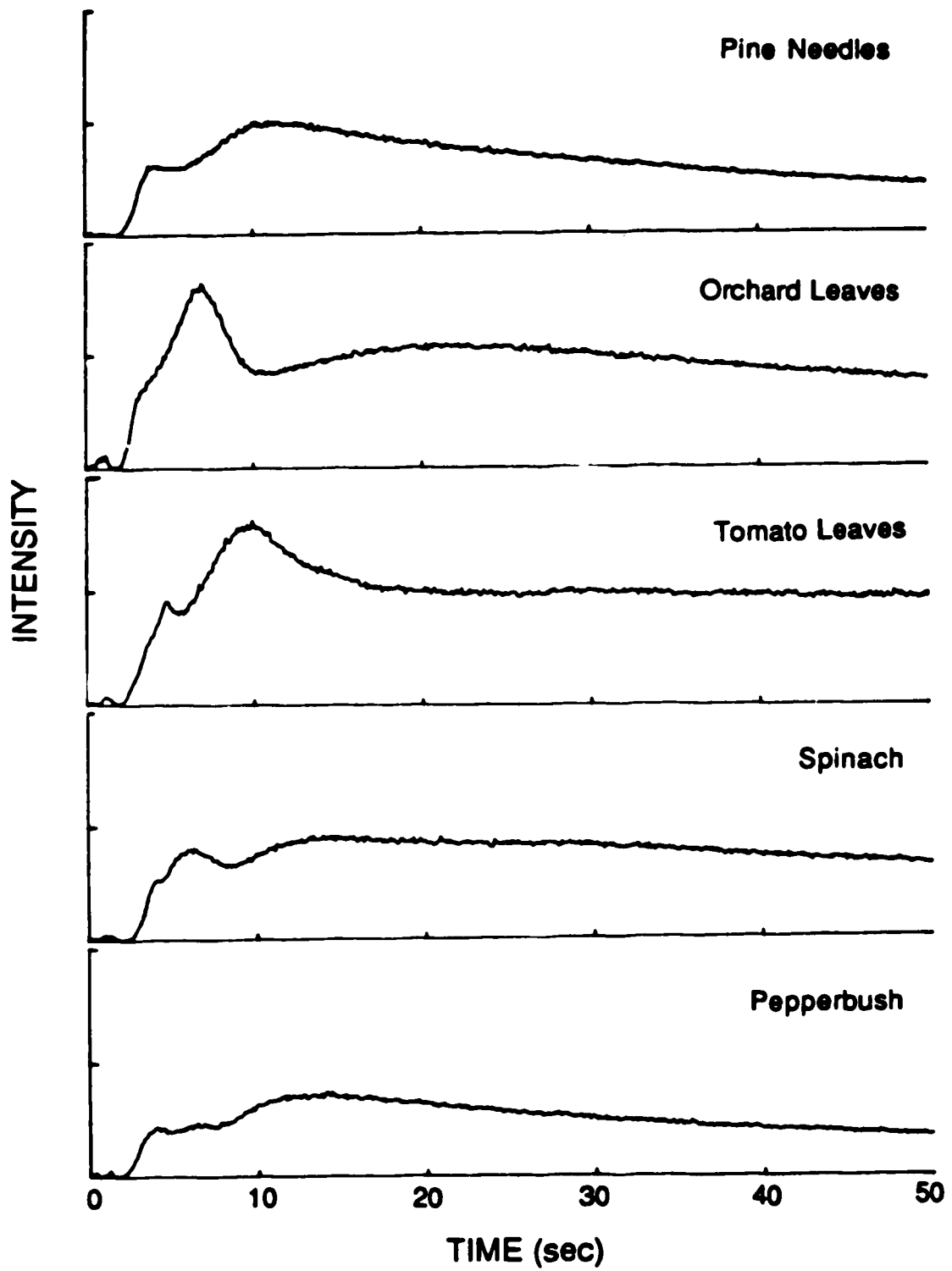


**Figure 5-4(c).** Signal for Fe from standard reference materials of botanical matrices.

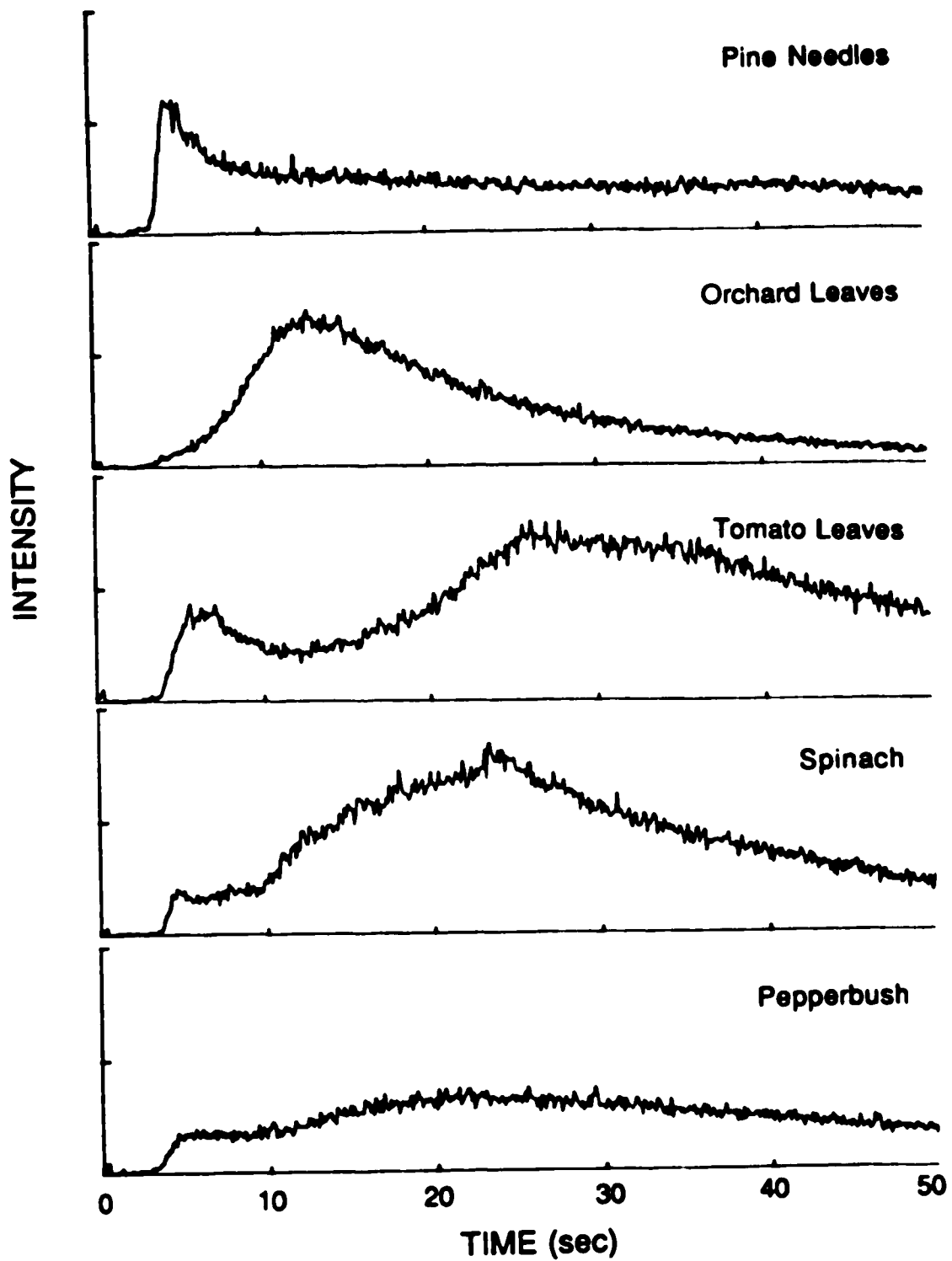


**Figure 5-4(d).** Signal for Al from standard reference materials of botanical matrices.

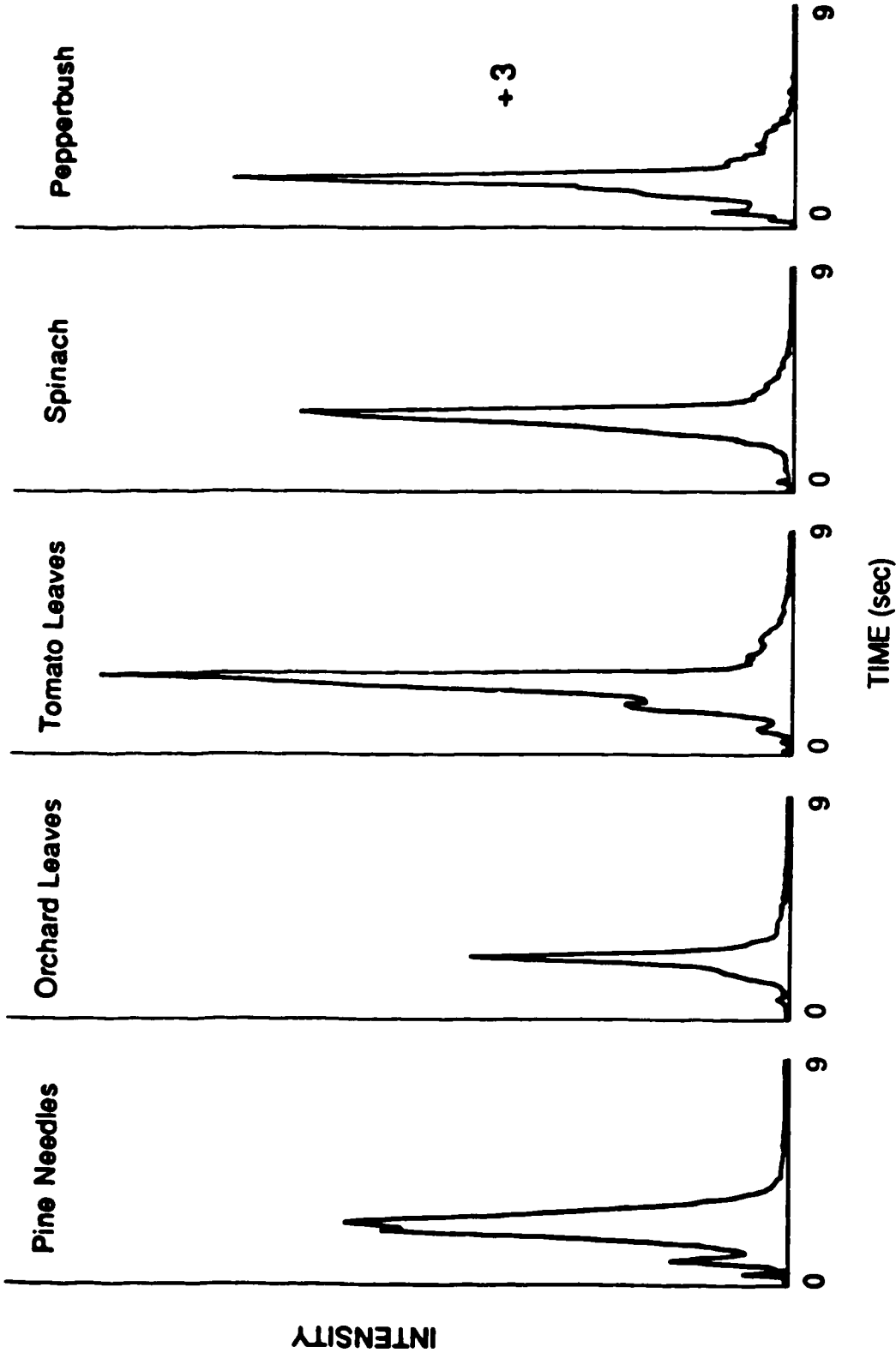


**Figure 5-4(●).** Signal for Zn from standard reference materials of botanical matrices.

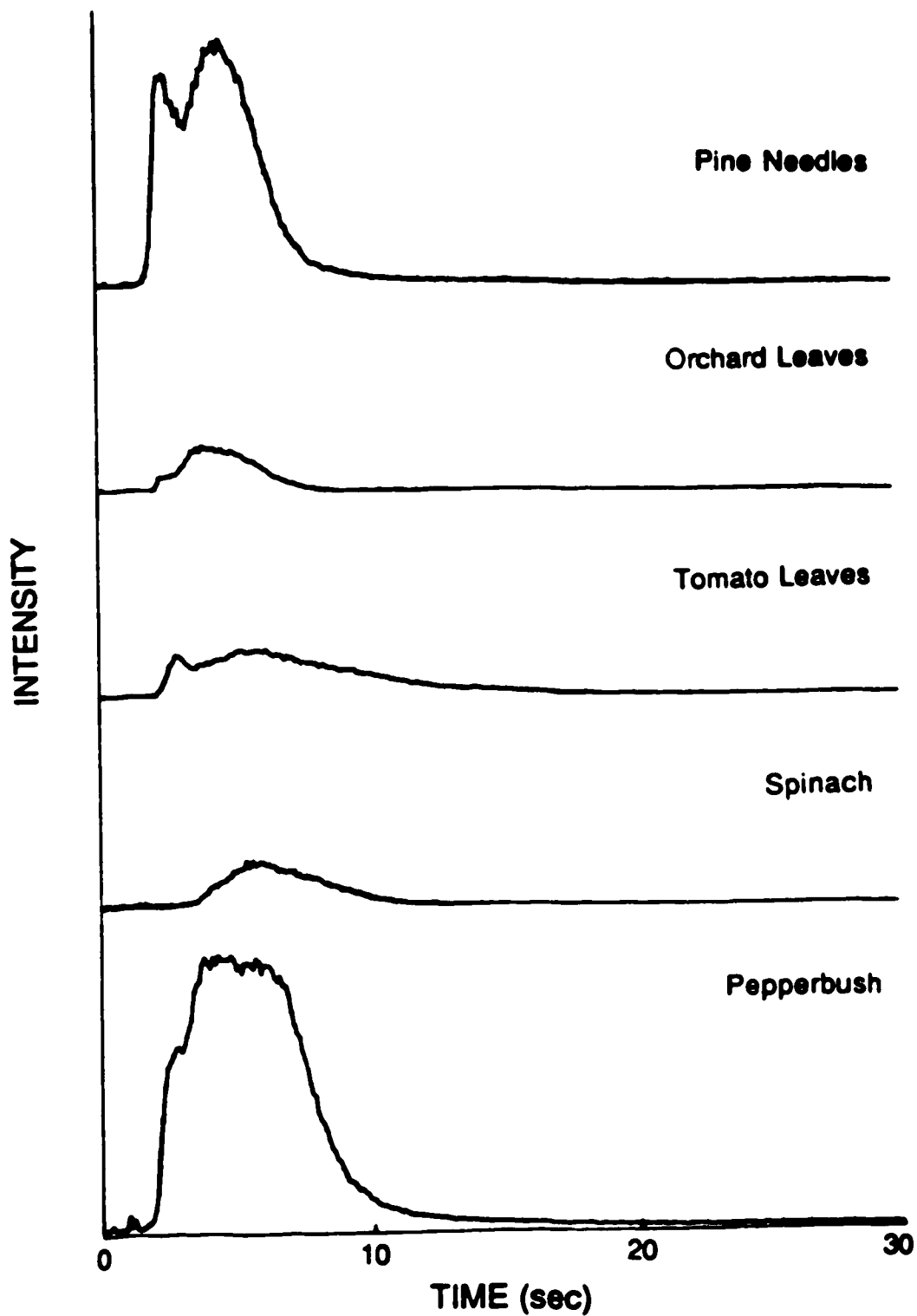


**Figure 5-4(f).** Signal for Mn from standard reference materials of botanical matrices.

where  $i$  is the anodic current of the PMT in A,  $x$  is the digitized result at the peak,  $G$  is the gain of the pre-amplifier in V/A, 4095 is the full scale of the ADC (12 bits), and 5 (V) is the full scale of the input voltage of the ADC. For example, the peak height of Mn in Peppercorn is 1200 and the gain is  $10^5$  V/A. Substituting these values in Equation 5-1, the anodic current is calculated to be  $1.46 \times 10^{-5}$  A. This result indicates that the PMT is saturated since the usual maximum operating current of a PMT is between  $10^{-7}$  to  $10^{-6}$  A. The peak currents of Zn and Mn were plotted against concentration of the analytes and these plots are shown in Figure 5-5a and 5-5b. It is obvious that the curved calibration curves in Figure 5-3g and 5-3h are due to PMT saturation.

It is interesting to note that the peak height calibration curve for Zn in Figure 5-5a is linear for the lower concentration samples, which is also true for the peak area calibration curve in Figure 5-3g. This similarity is because Zn is a volatile element. For the less volatile element Mn, the low concentration samples have the same peak height, but the peak areas are proportional to the analyte concentration as shown in Figure 5-3h and 5-5b.

### 5.3.3 Conclusion

The method of matrix matching is applicable for the elements that are completely vaporized within the observation

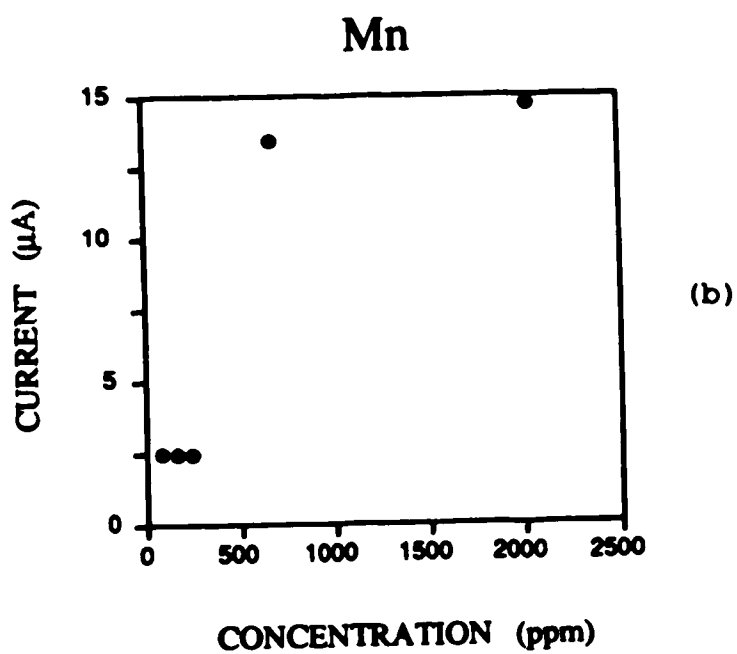
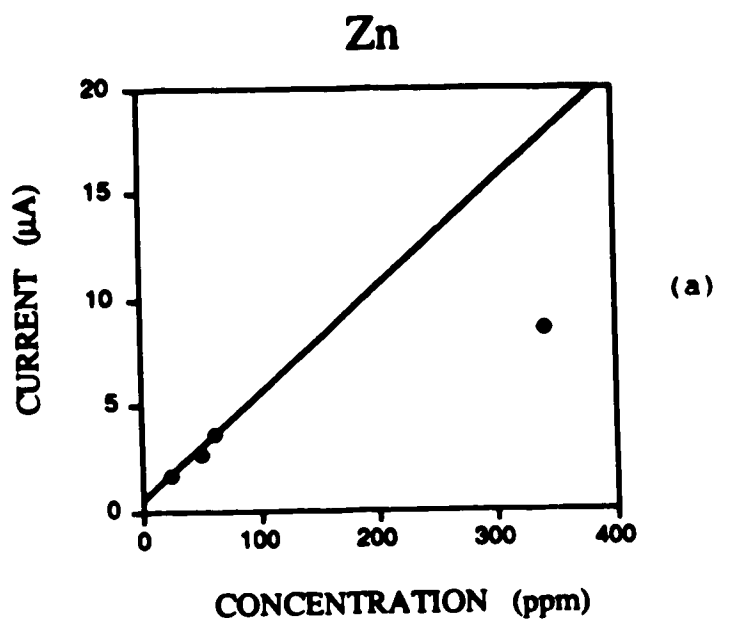


**Figure 5-5.** Calibration curves for (a) Zn and (b) Mn.  
Intensity is peak height (anaodic current of the PMT).



period. Since peak area correlates better with concentration than peak height does, it seems that recording the signal with an integrator is sufficient. However, it is important to determine whether an element is vaporized completely, and whether it vaporizes too fast such that the PMT is saturated. In both cases, even an integrated signal will give an erratic result. Therefore, it is necessary to digitize the temporal behavior of the signal in real time, which is then integrated by summing the ADC results in the region of the peak.

#### **5.4 Standard Addition Method**

Since the matrix of a botanical sample cannot be removed completely during the dry/ash cycle, standards with a matrix that closely matches that of the sample should be used for quantitative analysis. The matrix matching method described in section 5-3 works well. However, the concentration range of the available standards may not be adequate. For example, the concentration of Cu in Pine Needles is 3 ppm, that in Tomato Leaves is 11 ppm, and those in Orchard Leaves, Spinach, and Peppercorn are the same: 12 ppm. The range of concentration is less than one order of magnitude. In fact, there are practically two values of concentration (3 and 12 ppm) only. The problem of a small concentration range and/or uneven distribution of concentration of an analyte in the calibration curve can be solved by the standard addition method.

### 5.4.1 Experimental

Standard solution was added to a known amount of powdered sample. The usual volume of standard solution was 10  $\mu\text{L}$ , and the sample weight was 5 or 10 mg. The standard solution was added on top of the powdered sample and was allowed to soak into the sample. The sample was then dried at 35 mm b/c for 30 seconds and ashed at 22 mm b/c for another 120 seconds in the central tube of the DSI-ICF torch. The measurement time was 100 seconds for each element, and the conversion rate was 10 Hz. Three elements, Cu, Fe, and Pb, were analysed simultaneously. Each sample was analysed three times. The unknown concentration was determined from the negative intercept on the concentration axis of the standard addition calibration curve.

With a 10  $\mu\text{L}$  spike and a sample weight of 10 mg, the concentration in the sample can be read directly from the negative intercept of concentration axis of the calibration curve. The logic is shown in the following equation,

$$C_{\text{sample}} = \frac{C_{\text{soln}} \times 10 \mu\text{L}}{10 \text{ mg}} = \frac{C_{\text{soln}} \times 10 \text{ mg}}{10 \text{ mg}} = C_{\text{soln}} \quad (5-2)$$

where  $C_{\text{sample}}$  and  $C_{\text{soln}}$  are the concentration of the powdered sample and that of the standard solution, respectively. The concentrations are usually expressed in ppm.

Since the weight of the samples analyzed in the next section was 5 mg, the concentration is two times that of the negative intercept on the concentration axis.

#### **5.4.2 Results and Discussion**

The results for the determination of Cu, Fe, and Pb in Orchard Leaves and Pine Needles are listed in Table 5-3 and 5-4. The confidence intervals of the standard addition results are calculated by the method described in references 2 and 3. The calibration curves were constructed so that the concentration range of the standard solution was selected to include the 'unknown' concentration of the botanical sample. The concentration of the standard solutions was also evenly distributed [2]. The calibration curves of Orchard Leaves are shown in Figure 5-6 as an example.

Since Cu and Pb are vaporized completely during the observation period, the signal is corrected for background with the off-peak background correction method (Chapter 2). However, Fe is not completely vaporized. Therefore, off-peak background correction is not possible. The intensity in the calibration curve is thus the integrated signal for the whole 100 seconds observation time. Incomplete vaporization is a problem for the determination of this analyte.

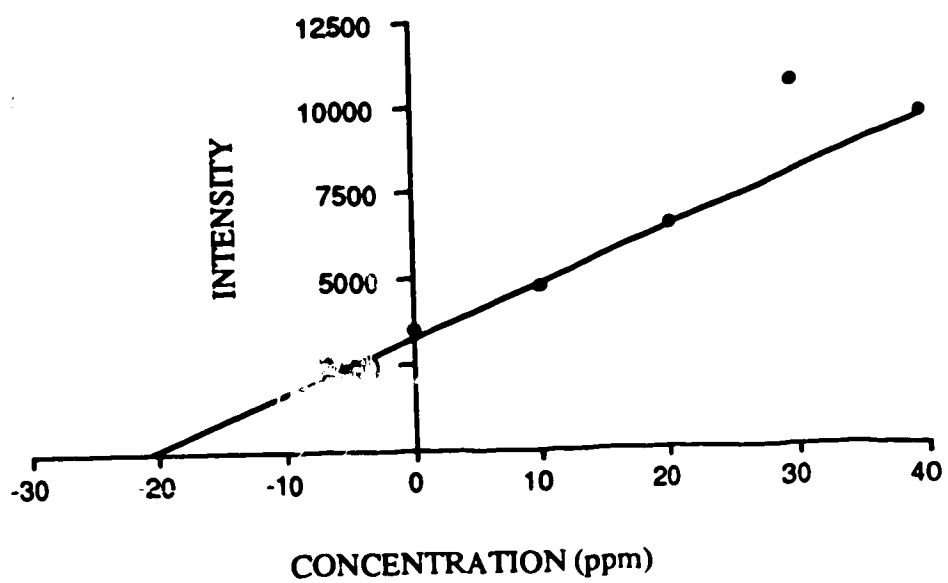


**Figure 5-6.** (a) Calibration Curve for the standard addition analysis of Pb in Orchard Leaves

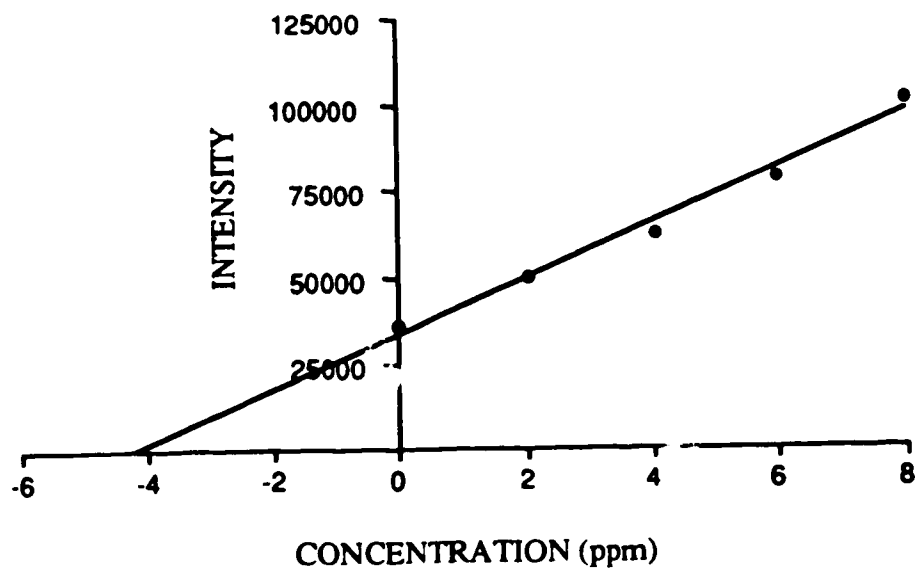


**Figure 5-6. (b) Calibration Curve for the standard addition analysis of Cu in Orchard Leaves**

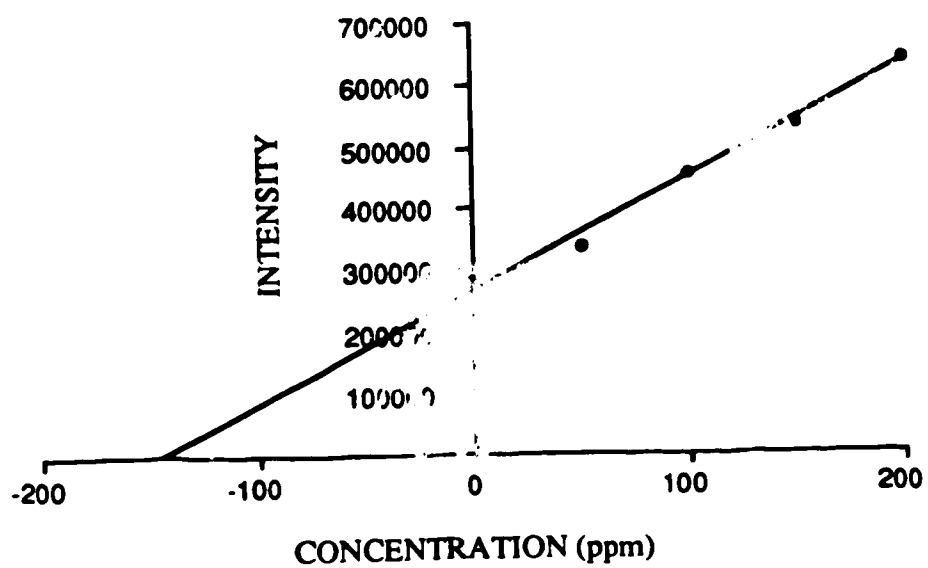


**Figure 5-6.** (c) Calibration Curve for the standard addition analysis of Fe in Orchard Leaves

**Table 5-3. Standard Addition Result for Orchard Leaves  
(NBS SRM 1571)**

element	experimental result (ppm)	certified value (ppm)
Cu	$8 \pm 1$	$12 \pm 1$
Fe	$288 \pm 28$	$300 \pm 20$
Pb	$41 \pm 3$	$45 \pm 3$

**Table 5-4. Standard Addition Result for Pine Needles  
(NBS SRM 1575)**

element	experimental result (ppm)	certified value (ppm)
Cu	$3.0 \pm 0.4$	$3.0 \pm 0.3$
Fe	$144 \pm 12$	$200 \pm 10$
Pb	$9.8 \pm 2.0$	$10.8 \pm 0.5$

#### 5.4.3 Limitations and Assumptions of the Standard Addition Method

The full composition of a real sample is usually not known, and the matrix may not be completely removed during the ashing process. With the standard addition method, it is assumed that the standard added to the sample is in the same

matrix as the original analyte, therefore it will be interfered with to the same extent as the analyte [4]. This assumption is usually true for solution samples because the standard is readily mixed with the solution. However, the standard added to a solid sample may still have different chemical composition as well as physical properties from that of the original analyte. The analytical results described above and the modification of sensitivity of the added standard described in section 5.1 show that the added standard seems to behave as the original analyte. Thus the aqueous standard is absorbed into the matrix of the sample, and seems to interact with the matrix in the same manner as the original analyte and is converted to the same form during the ashing process. This process is crucial for the success of the standard addition method for powdered samples.

The standard addition method corrects for effects which modify the elemental sensitivity. It assumes that the added standard responds in the same way as the analyte element in the sample [4-9]. However it does not correct for blank interference, i.e., cross sensitivity and/or background interference of the plasma. Cross sensitivity occurs when the instrument is unable to resolve the line of interest from the lines or bands produced by the concomitants. Background interference occurs when the background radiation underlies the line of interest [7]. Therefore, simultaneous background correction is necessary for accurate results. Due to the construction of a direct reader spectrometer (the ARL 34000



in this work), it is not possible to perform simultaneous background correction for these analyses because of the transient nature of the signals. The off-peak background correction method (chapter 2) corrects for the background interference but not the cross sensitivity. It is expected that a diode array spectrometer could solve this problem.

The other assumption of the standard addition method is that the calibration curve is linear in the region of measurement. The assumption is satisfied with a carefully chosen standard concentration range. The linearity is checked conveniently because the additions are evenly spaced in concentration.

#### **5.4.4 Correction for the Variation of Sample Weight**

Liquid samples are usually measured by volume. Therefore, it is relatively easy to obtain an exact amount of a solution sample with volumetric apparatus. On the other hand, solid samples are usually measured by weight. It is quite tedious to weigh ten or fifteen samples to exactly the same mass, e.g., 10.0 mg, for standard addition analysis. This problem is solved mathematically in this work.

A nominal weight of the sample is defined, for example, 10.0 mg. The samples are weighed so that their weights are close to the nominal weight. As an example, a hypothetical set of samples is listed in Table 5-5. None of the sample weights is exactly equal to the nominal weight, but they are

close to it and are known. This situation is typical for powdered sample weighing.

**Table 5-5. A Hypothetical Set of Samples.**

Sample Number	Weight of Samples (mg)
1	9.8
2	9.3
3	9.7
4	10.5

The samples are spiked with standard solutions as usual and the emission intensities are measured. The data collected are subjected to linear regression analysis as if the sample weights are exactly the nominal weight. The emission intensity of each sample is then modified with the following equation,

$$I_{\text{new}} = I_{\text{old}} + \left(1 - \frac{\text{weight of sample}}{\text{nominal weight}}\right) \times A \quad (5-3)$$

where  $I_{\text{new}}$  and  $I_{\text{old}}$  are the calculated and original intensities, and  $A$  is the intercept of the regression curve on the intensity axis (it corresponds to the emission intensity of the sample without standard addition). If we call the new set of intensities  $I'$ , linear regression analysis of  $I'$  yields a new intercept  $A'$ . Substituting the original set of intensities  $I_{\text{old}}$  and  $A'$  in Equation 5-3 yields

another set of data  $I''$  and  $A''$ , and so on. This iteration process can be performed to a fixed number of times or until the difference between two successive intercepts is smaller than a certain preset value. In this work, 10 repetitions were performed, i.e., the unknown concentration was calculated from the intercept and slope of the tenth linear regression analysis.

Let's consider a hypothetical case: a set of samples are analysed with standard addition method, with 10  $\mu\text{L}$  of standard solution spiked on the top of each sample. The concentration of the standards are 0, 10, 20, and 30 ppm. The nominal weight of the sample is 10.0 mg. The content of a sample is 15 ppm and the sensitivity is 100 p. Therefore, the slope of an ideal standard addition calibration curve is 100 and the intercept on the intensity axis is 1500. A set of ideal intensities can be calculated (Table 5-6). If the sample weights are not exactly the same as the nominal weight, the 'measured' intensities and the resulting slope and intercept will be different from that of the ideal case. The 'measured' intensities are calculated from the standard concentration, the sensitivity, and the sample weights of the samples, assuming that no other error of measurement occurred. The data obtained are analysed with the successive approximation method described above, and the calculated intensities are listed in Table 5-6. At the third cycle of iteration, the correct result for the slope and intercept are obtained.

Table 5-6. Successive Approximation for Hypothetical Standard Addition Results.

conc (ppm)	weight (g)	Ideal		Measured Intensity	Calculated Intensity				
		Intensity	Intensity		1st cycle	2nd cycle	3rd cycle	4th cycle	5th cycle
0	9.8	1500	1470	1470	1500.15000	1499.99925	1500.00000	1500.00000	1500.00000
10	10.5	2500	2575	2575	2499.62500	2500.00188	2499.99999	2500.00000	2500.00000
20	9.3	3500	3395	3395	3500.52500	3499.99738	3500.00001	3500.00000	3500.00000
30	9.7	4500	4455	4455	4500.22500	4499.99888	4500.00000	4500.00000	4500.00000
intercept		1500	1507.5	1507.5	1499.96250	1500.00019	1500.00000	1500.00000	1500.00000
slope		100	97.75	97.75	100.01125	99.99994	100.00000	1000.00000	100.00000

conc (ppm)	weight (g)	Ideal		Measured Intensity	Calculated Intensity				
		Intensity	Intensity		6th cycle	7th cycle	8th cycle	9th cycle	10th cycle
0	9.8	1500	1470	1470	1500.00000	1500.00000	1500.00000	1500.00000	1500.00000
10	10.5	2500	2575	2575	2500.00000	2500.00000	2500.00000	2500.00000	2500.00000
20	9.3	3500	3395	3395	3500.00000	3500.00000	3500.00000	3500.00000	3500.00000
30	9.7	4500	4455	4455	4500.00000	4500.00000	4500.00000	4500.00000	4500.00000
intercept		1500	1507.5	1507.5	1500.00000	1500.00000	1500.00000	1500.00000	1500.00000
slope		100	97.75	97.75	100.00000	100.00000	100.00000	100.00000	100.00000

A second case is shown in Table 5-7. The sample weights in this case show greater deviation from the nominal weight, and all of them are lower than the nominal weight. The successive approximation method can still obtain the correct result, although more iterations (8 times) are required. But a lower value will be obtained without the correction.

The success of this correction process depends on the linearity of the calibration curve and the absence of blank interference (i.e., the calibration curve must pass through origin if the concentration of the sample is zero), which are also the requirements of the standard addition analysis. Therefore, no additional assumption is made for the calculation.

#### 5.4.5 Conclusion

The standard addition method obviates the requirement of matching standards. The results listed in Table 5-3 and 5-4 show that it is applicable to the analysis of powdered botanical samples. However, it is important to have a linear calibration curve and proper correction for the blank interference. Furthermore, the problem of incomplete analyte volatilization needs to be addressed. The matrix modification method described in the next section is one of the approaches to solve this problem.



### 5.5 Matrix Modification with NaF

For some elements, e.g. Fe, volatilization is not complete during the period of measurement (Figure 5-4c). Thus quantitative analysis of these analytes is difficult. Moreover, the sensitivities of nonvolatile elements are usually poor [10-12]. One of the methods to improve the volatilization behavior of an analyte is chemical modification of the sample matrix [10,11,13-16]. The modifiers have included use of fluorocarbon (0.1% Freon) in the injector gas [10], AgCl [13,14], NH<sub>4</sub>Cl, AgCl, BaF<sub>2</sub>, and PTFE [15], and NaF [11,16].

Abdullah and co-workers [16] in this group investigated the use of KCl, KF, NaCl, and NaF as modifiers for Al, Ca, Sr, and Zr solution samples. Both NaF and KF enhanced the signals of the most nonvolatile element Zr, while the chlorides failed. However, the largest enhancement was observed when NaF was used. In addition, with KF, a high vaporization rate was observed even during the initial stages of sample insertion, which may lead to loss of sensitivity and extinguishment of the plasma. Therefore, NaF was chosen as the modifier for their analysis of solution samples and B in powdered CaSO<sub>4</sub> [16]. In this work, NaF was used for the analysis of powdered botanical samples. Both nonvolatile elements (B, Cr, and Fe), and volatile elements (Pb and Cu) are analysed for comparison.

### 5.5.1 Experimental

Stock NaF solution was prepared from analytical grade NaF as received. Since the solution is saturated at about 1 M, the concentration of the stock solution was 0.8 M to avoid crystallization of the compound.

Orchard Leaves (SRM 1571) was analysed by the standard addition method. The sample weight was 5 mg. The sample was spiked with 10  $\mu$ L of standard solution and 40 to 80  $\mu$ L of 0.8 M of NaF solution. The NaF solution was added in 20  $\mu$ L portions with an Eppendorf micropipette. Since the capacity of the sample cup is only  $\sim$ 20  $\mu$ L, the sample was dried in between solution addition, which is accomplished by placing the sample cup on top of a graphite rod which is inserted in a metal block that was heated by a hot plate at about 90  $^{\circ}$ C.

Standard solutions with and without NaF were analysed along with the powdered sample for comparison.

The samples were dried at 35 mm b/c for 60 seconds and ashed at 18 mm b/c for 120 seconds. The observation time was 60 seconds and sampling rate was 10 Hz.

Pre-amplifier gains for the channels of B, Cu, Fe, and Pb were equal to  $10^7$  V/A, that of Cr was  $10^8$  V/A.

Upon insertion of the sample cup into the plasma, the plasma turned bright yellow for about 10 seconds due to the vaporization of Na into the plasma. The usual background drop at the point of insertion was also absent with the introduction of NaF. Outside of these observations, the



background signal was not changed compared to a regular insertion.

### **5.5.2 Determination of the Amount of NaF Required**

The signal for B from 5 mg of Orchard Leaves without a matrix modifier is virtually indistinguishable from the background (Figure 5-7). With the addition of an increasing amount of NaF, the signal increases accordingly. The signal splits into two peaks: the first peak is sharper and its area increases with NaF concentration, while the second peak is broader and the area levels off as the amount of NaF increases. The first peak is due to B contained in the NaF solution because the appearance time and the shape of this peak are consistent with that of B from the NaF solution (Figure 5-7). Impurities of Al, Ca, Sr, and Zr in spectroscopic and analytical reagent grade NaF are also documented in reference 16. A calibration curve was constructed for the intensity of the B signal against the volume of 0.8 M of NaF solution (Figure 5-8), showing the linear relation between the B signal to the amount of NaF.

The signals from more volatile analytes in Orchard Leaves, i.e., Cu and Pb, with various amounts of NaF are shown in Figure 5-9 and 5-10. The Cu signal becomes sharper as more NaF is added, indicating that the volatilization rate is improved (Figure 5-9). The signal shape for Pb changes considerably with the addition of NaF. The appearance time

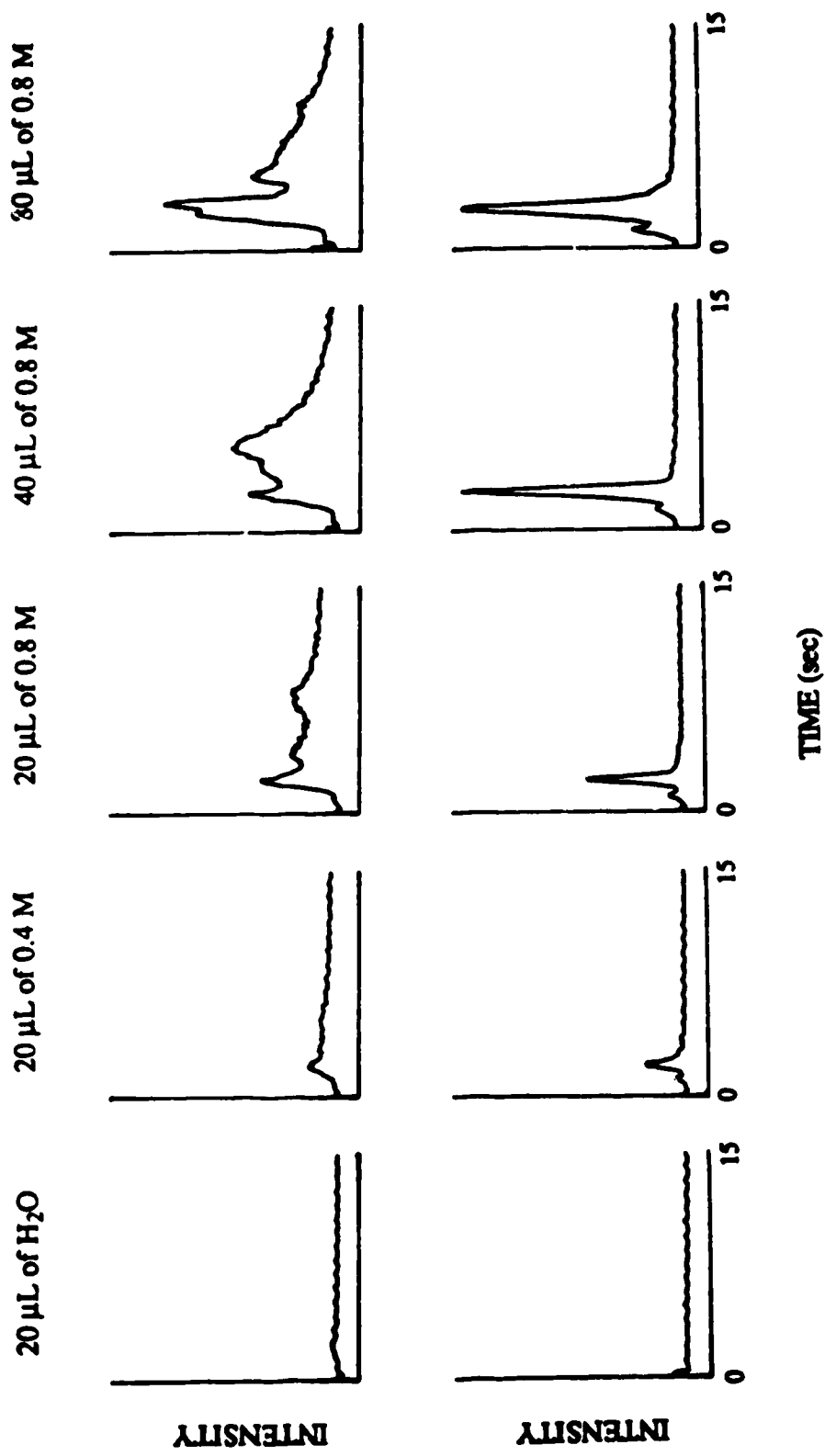


**Figure 5-7.** Signal for B from 5 mg of Orchard Leaves with increasing amount of NaF added (top row) and signal for the corresponding NaF solutions (bottom row). The concentrations of the NaF solutions are given on the top of each column.

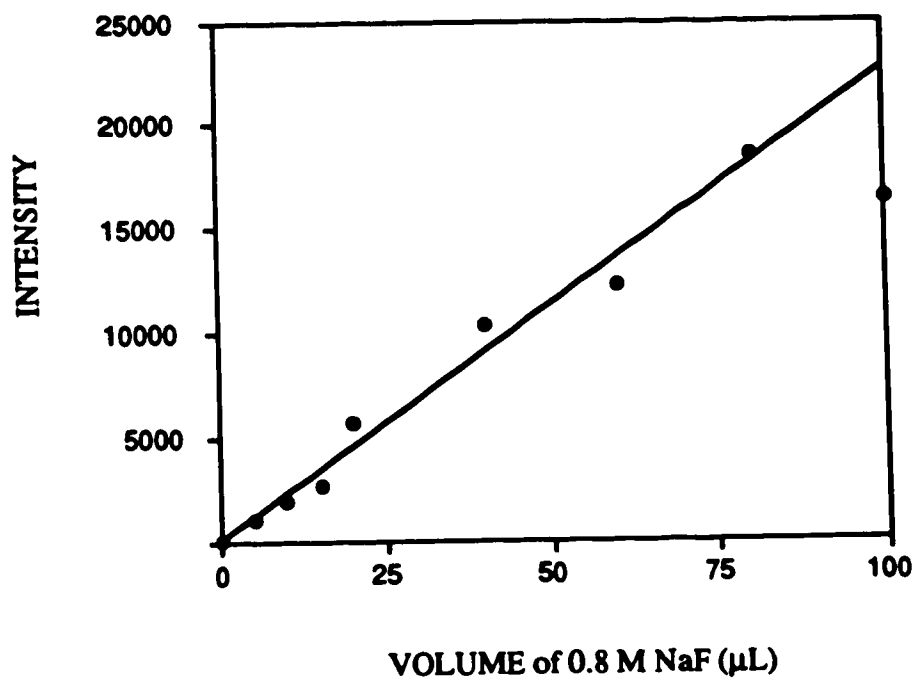
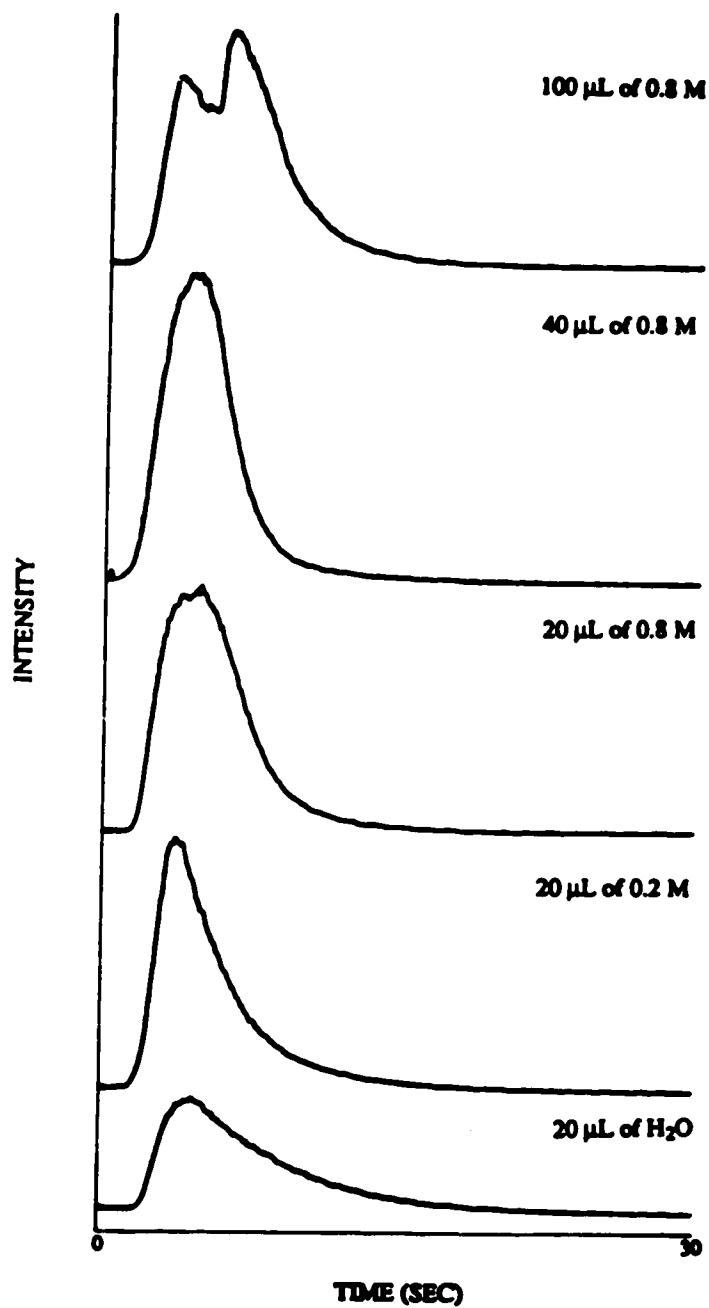
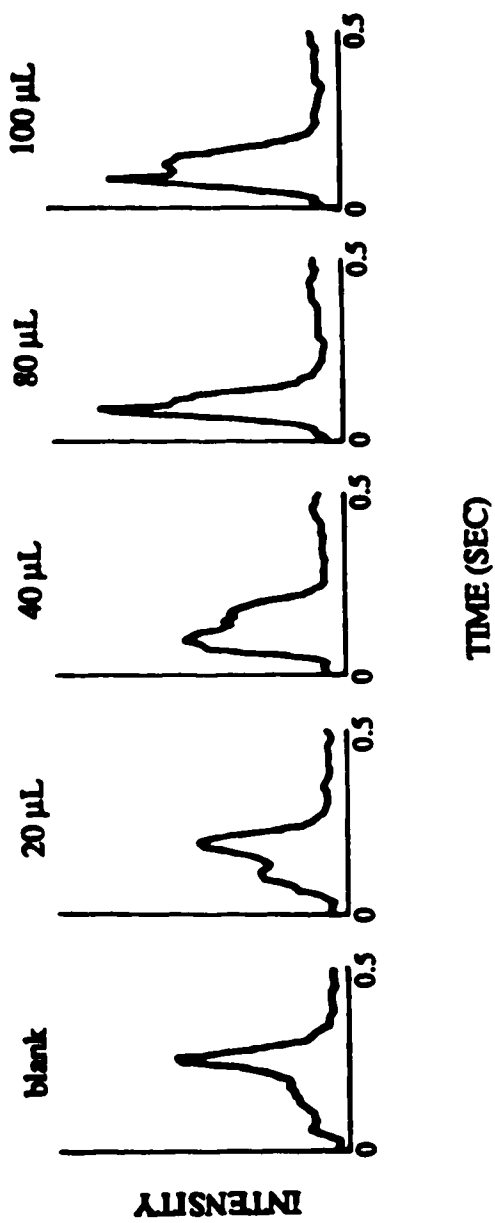


Figure 5-8. Calibration curve for B in NaF solution.



**Figure 5-9.** Signal for Cu from 5 mg of Orchard Leaves with various amounts of NaF added.



**Figure 5-10.** Signal for Pb from 5 mg of Orchard Leaves with various amounts of NaF added.

of the signal of Pb is not appreciably reduced, however, the peak is early shifted by  $\sim 0.2$  seconds on the time axis (Figure 5-10). This phenomenon is interesting, considering the high volatility of Pb itself.

The intensities of B, Cu, Fe, Cr, and Pb from 5 mg of Orchard Leaves as a function of added volume of 0.8 M NaF solution are shown in Figure 5-11. The sensitivity of B is improved 25 times with the addition of 40  $\mu\text{L}$  or more of 0.8 M NaF solution. The sensitivities of both Cu and Fe are improved by about a factor of 2. The enhancement of the sensitivity for B, Cu, and Fe levels off at a volume of NaF equal to or larger than 40  $\mu\text{L}$ . The sensitivities of Cr and Pb, however, were not enhanced. The lack of enhancement of Cr may be due to the low concentration of Cr in Orchard Leaves (certified value = 2.6 ppm), so that the change of sensitivity is not readily detected. In the case of Pb, the analyte is volatile and thus no enhancement of volatilization by NaF is really expected. The distribution of Pb in Orchard Leaves is not as homogeneous as other elements, which may explain the fluctuation of the Pb signal shown in Figure 5-11.

The optimal volume of 0.8 M NaF solution for the enhancement of volatility of B, Cu, and Fe is 40  $\mu\text{L}$ , while that of Cr and Pb is undetermined. In the next section, B, Cu, and Pb were analysed simultaneously, and the volume of NaF solution added was 40  $\mu\text{L}$ . Cr and Fe were analysed as a group, and the volume of NaF solution was 80  $\mu\text{L}$ .

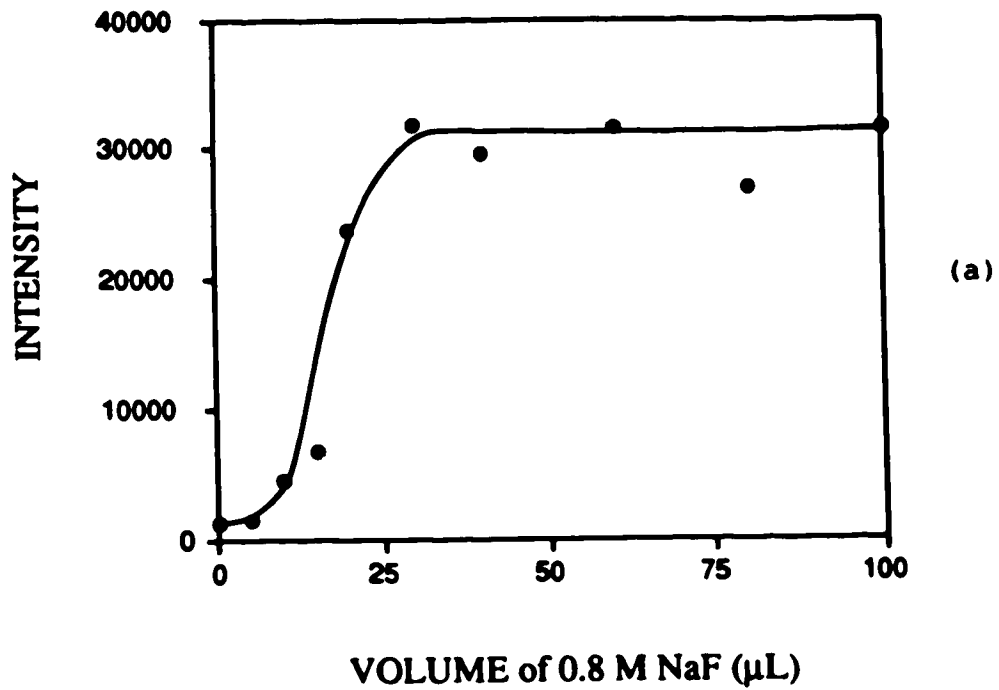


**Figure 5-11.** Relationship between analytes intensities from 5 mg of Orchard Leaves to the volume of 0.8 M NaF solution. (a) B.

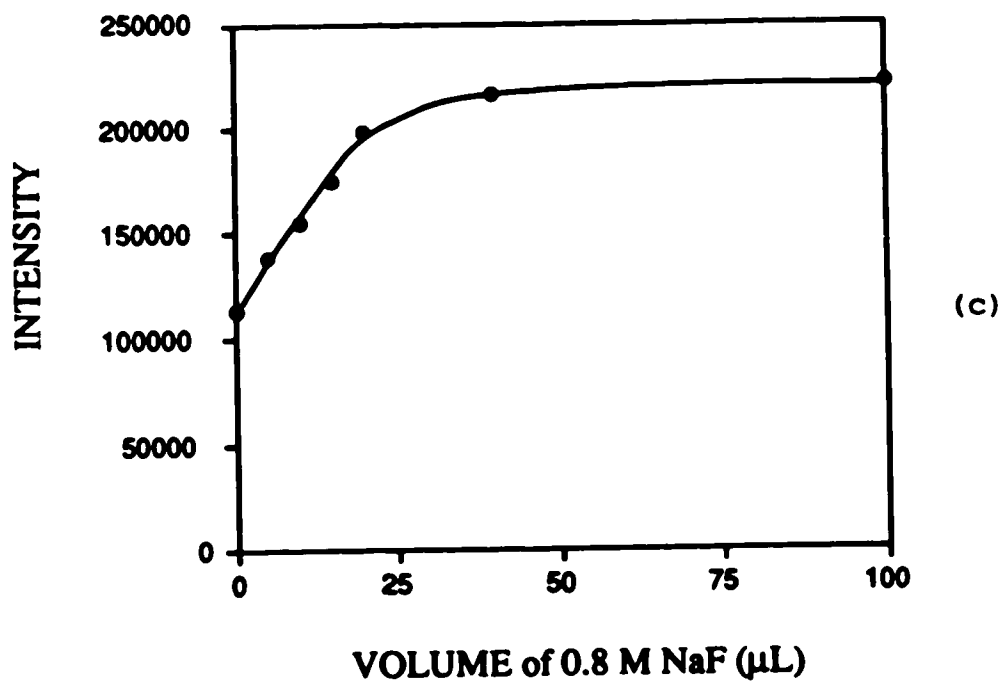
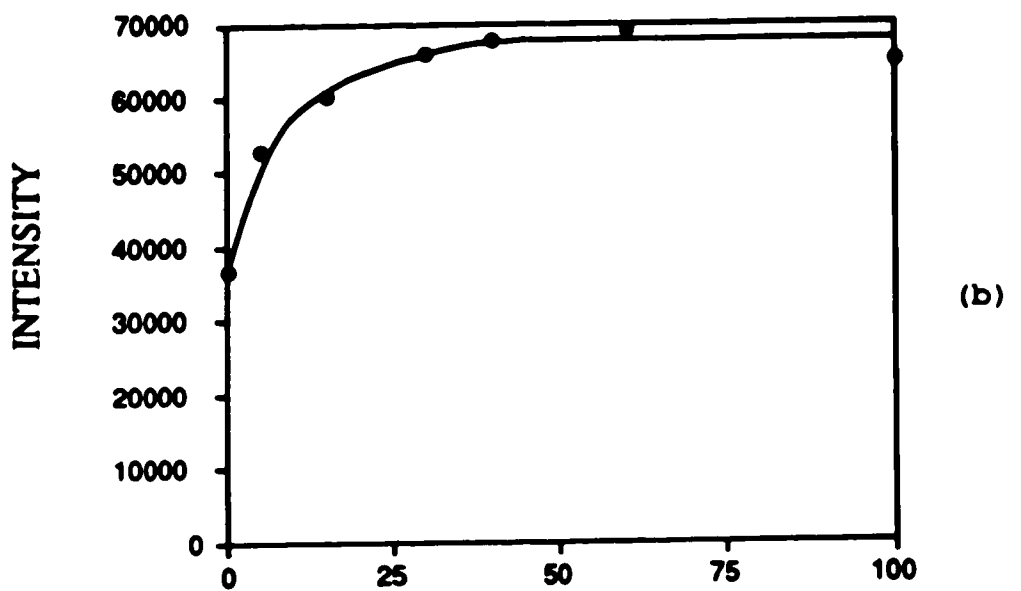
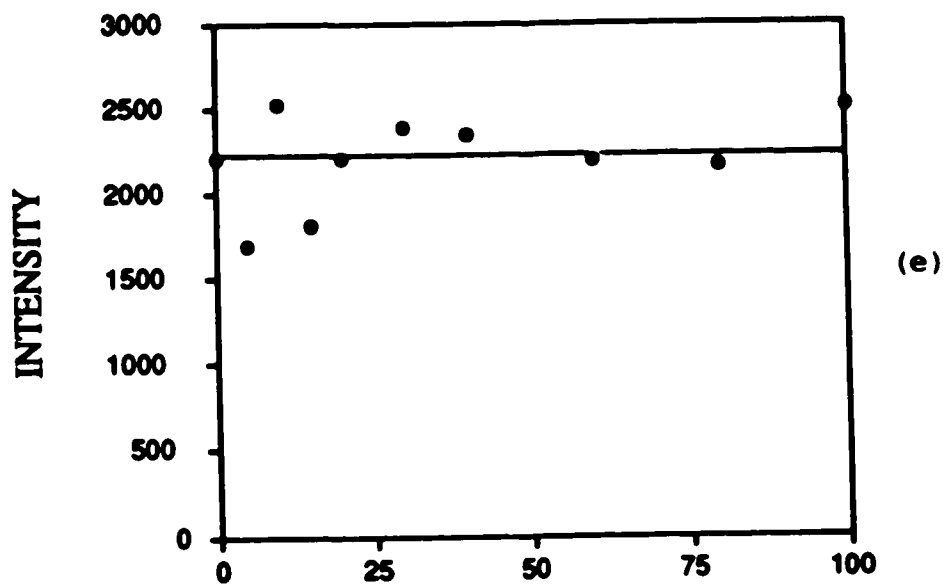
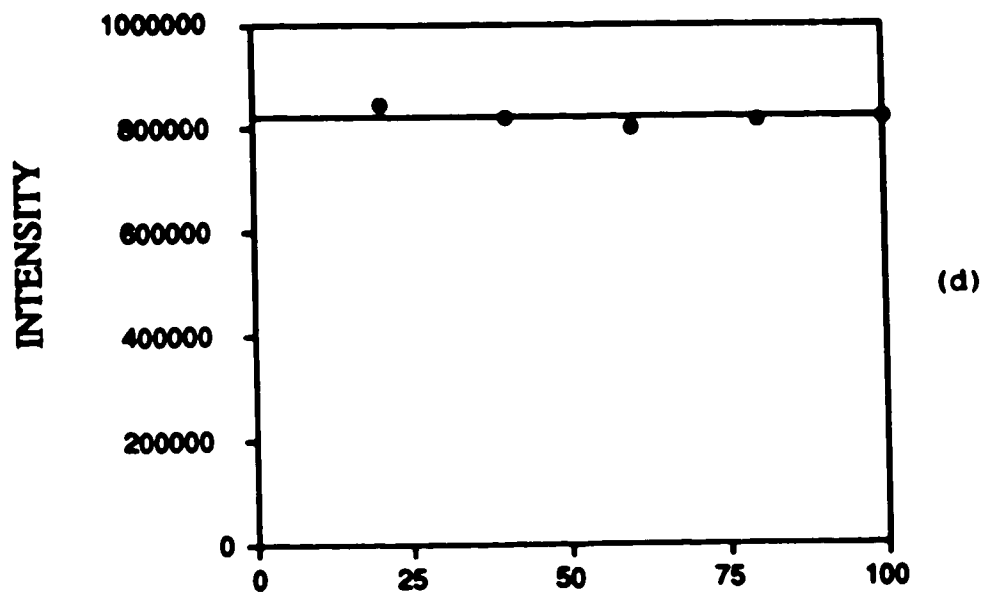


**Figure 5-11.** Relationship between analytes intensities from 5 mg of Orchard Leaves to the volume of 0.8 M NaF solution. (b) Cu, (c) Fe.





VOLUME of 0.8 M NaF ( $\mu$ L)

**Figure 5-11.** Relationship between analytes intensities from 5 mg of orchard leaves to the volume of 0.8 M NaF solution. (d) Cr, (e) Pb.

### 5.5.3 Results and Discussion

The results of standard addition analysis of Orchard Leaves with NaF as a chemical matrix modifier are shown in Table 5-8.

**Table 5-8.** Standard addition results for Orchard Leaves (NBS SRM 1571) with NaF matrix modifier added.

element	experimental result (ppm)	certified value (ppm)
B	19	33 ± 3
Cu	10	12 ± 1
Pb	38	45 ± 3
Fe	310	300 ± 20
Cr	5	2.6 ± 0.3

The corresponding calibration curves for the standard addition analyses are shown in Figure 5-12. Since the sample weight is 5 mg and the standard solution volume is 10  $\mu$ L, the negative intercepts on the concentration axis of the curves are at half of the concentration in the samples.

For the analysis of B, the calculated value is 41 ppm from the curve. However, as described in the last section, NaF contains B as a contaminant and thus it is necessary to correct for it. The amount of B was determined with a calibration curve of B standard solution with the same amount

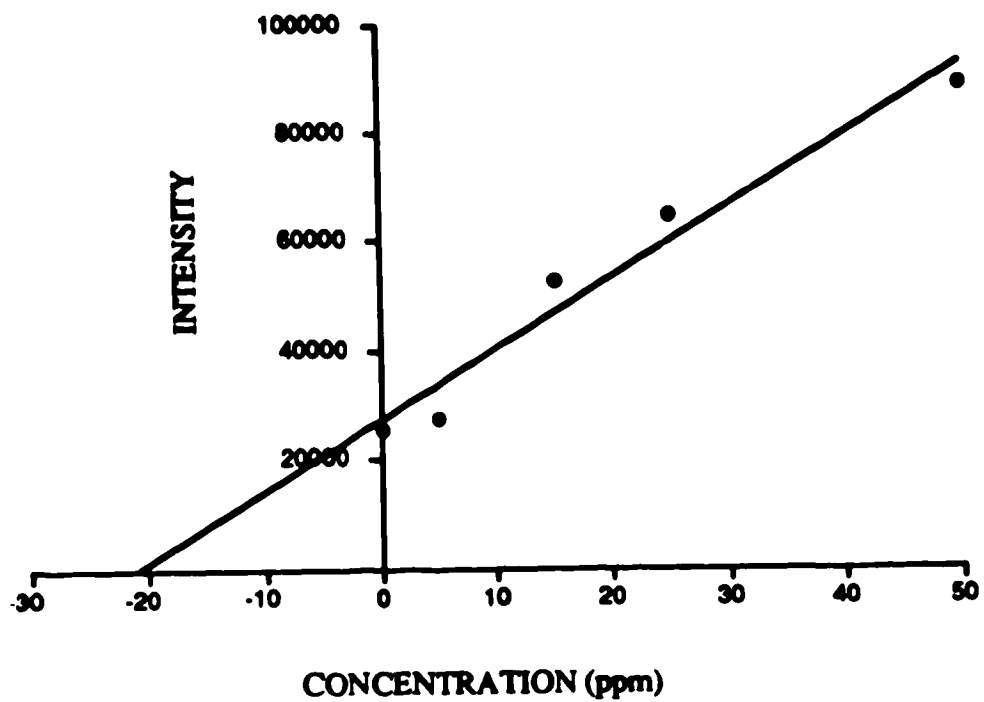


**Figure 5-12.** Calibration curve for standard addition analysis of Orchard Leaves with NaF matrix modifier.  
(a) B, volume of 0.8 M of NaF is 40  $\mu$ L.

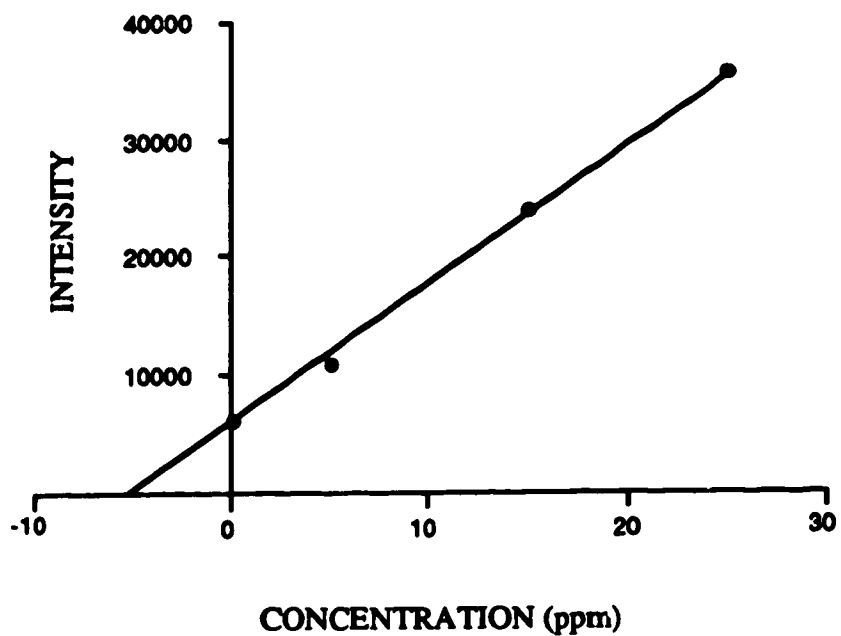


**Figure 5-12.** Calibration curve for standard addition analysis of Orchard Leaves with NaF matrix modifier. (b) Cu, volume of 0.8 M of NaF is 40  $\mu$ L.

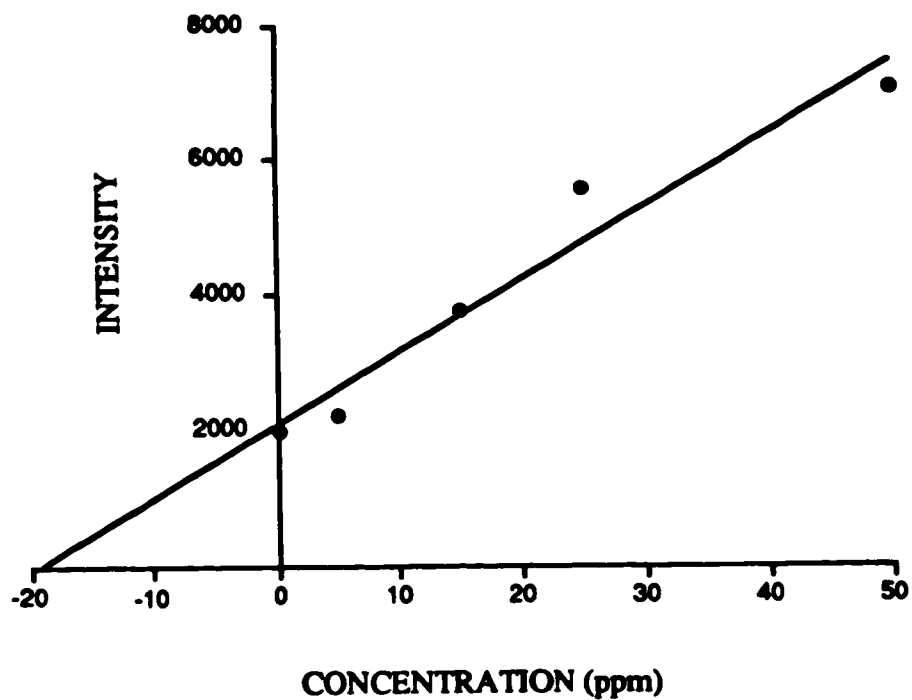


**Figure 5-12.** Calibration curve for standard addition analysis of Orchard Leaves with NaF matrix modifier. (c) Pb, volume of 0.8 M of NaF is 40  $\mu$ L.

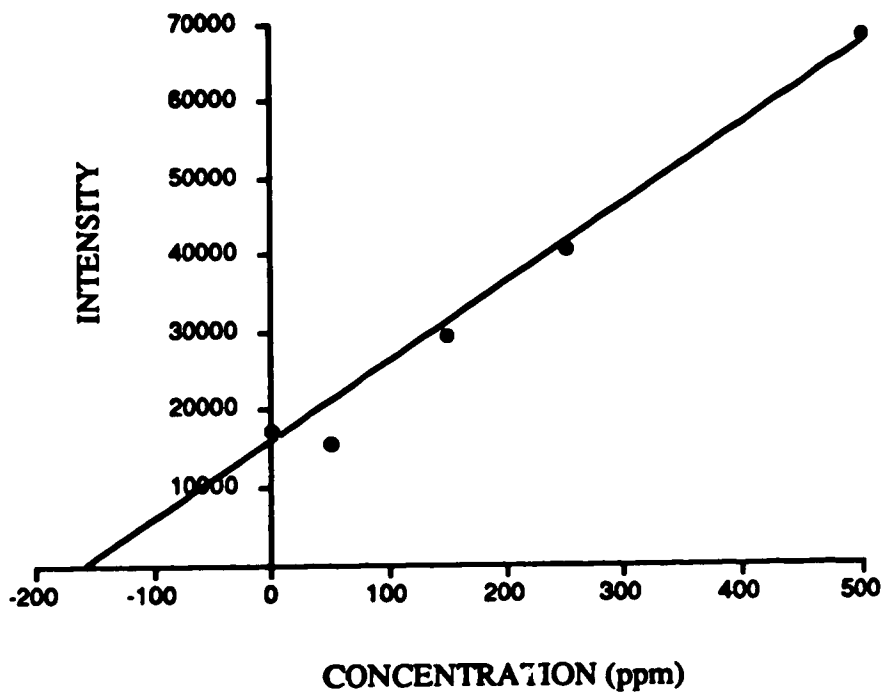


**Figure 5-12.** Calibration curve for standard addition analysis of Orchard Leaves with NaF matrix modifier.  
(d) Fe, volume of 0.8 M of NaF is 40  $\mu$ L.

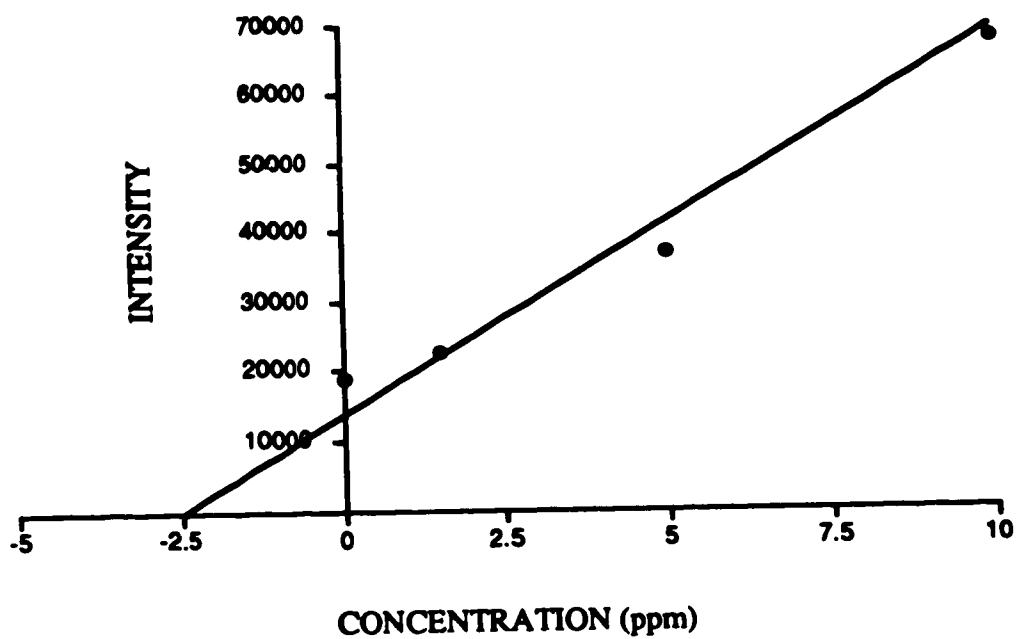


**Figure 5-12.** Calibration curve for standard addition analysis of Orchard Leaves with NaF matrix modifier.  
(e) Cr, volume of 0.8 M of NaF is 40  $\mu$ L.

of NaF added (40  $\mu$ L of 0.8 M of NaF), which is shown in Figure 5-13. It was found that the content of B in 40  $\mu$ L of 0.8 M of NaF solution is equivalent to 10  $\mu$ L of 11 ppm B standard solution. The corrected concentration of B in Orchard Leaves is therefore equal to 19 ppm. The corrected result is lower than the certified value because the slope of the calibration curve for the B standard solution with NaF is larger than that of the standard addition, as shown in Figure 5-14, i.e., the result is over-corrected. One of the methods to solve the contaminant problem is to use the simulation technique: standard addition analysis (with NaF added) of a sample of the same matrix as Orchard Leaves but with no B content. The intercept obtained can be used to correct for that of the analysis of Orchard Leaves. Of course, the usage of pure chemicals is the most desirable means. However, the question of 'how pure is pure?' [17] arises as the sensitivity of an analytical method increases.

#### **5.5.4 Comparison of the sensitivities of standard solutions and those of standard addition analysis**

The sensitivities of some elements in the botanical samples were lower than those in aqueous standard solutions. However, with the addition of NaF as a matrix modifier, the sensitivities are improved. It is interesting to compare these two sets of sensitivities to determine whether they have converged because of the enhancement. If so, the ideal



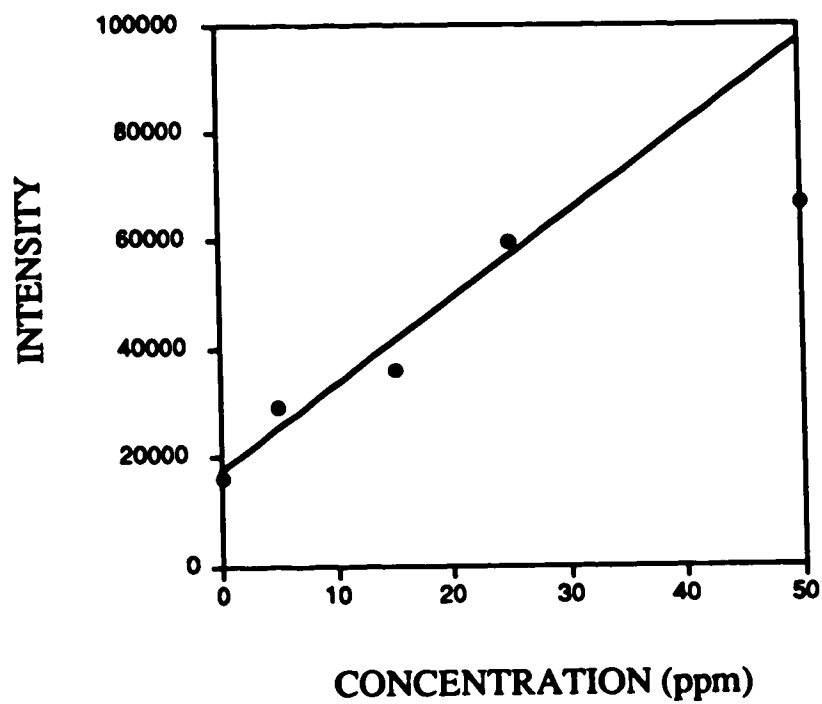


**Figure 5-13.** Calibration curve for B standard solution with NaF added. The volume of the standard solution is 10  $\mu\text{L}$  and that of the 0.8 M NaF solution is 40  $\mu\text{L}$ .

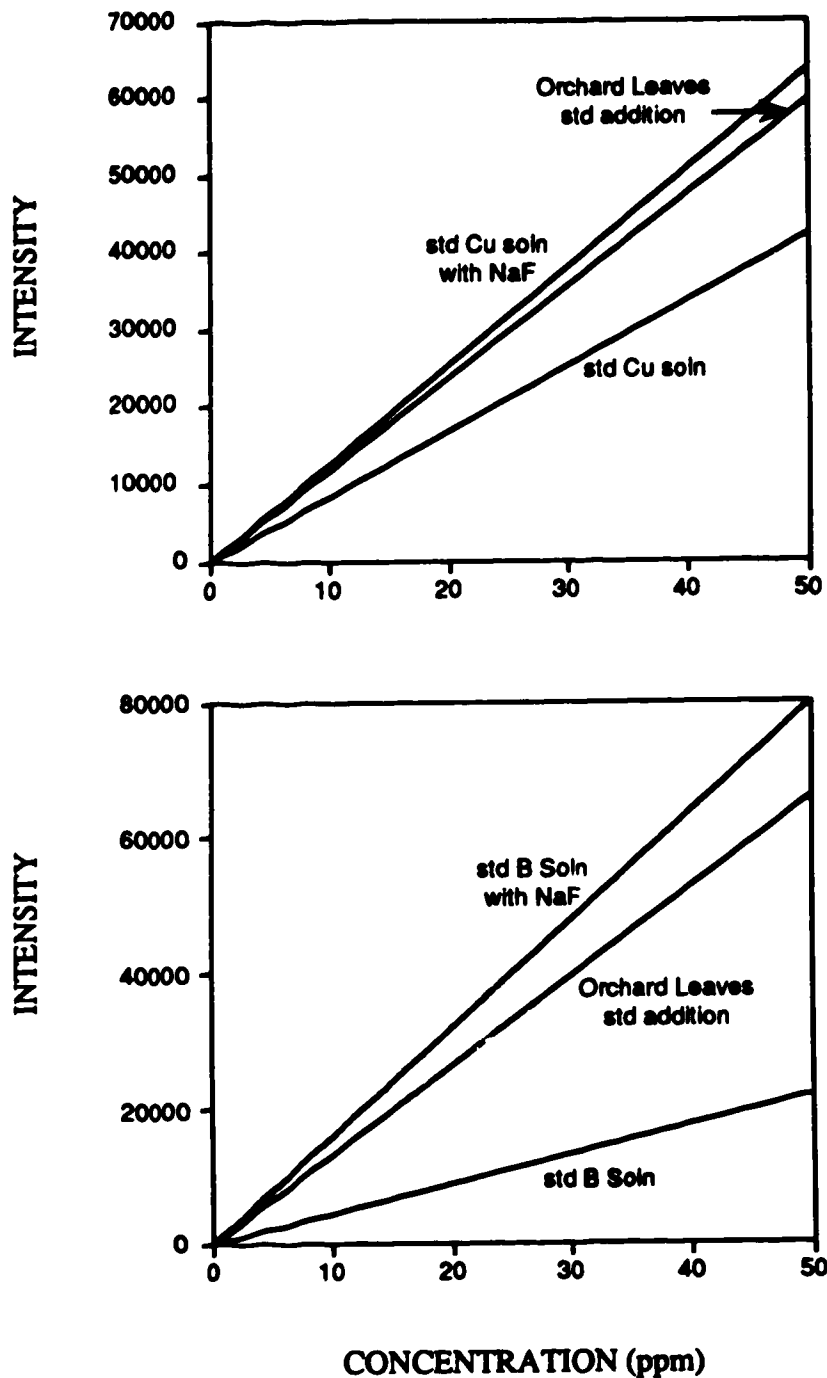


**Figure 5-14.** Calibration curves for standard solutions with and without NaF, and standard addition analysis of Orchard Leaves with NaF. The curves are forced to pass through origin so that the slopes can be compared. (a) Cu, (b) B.

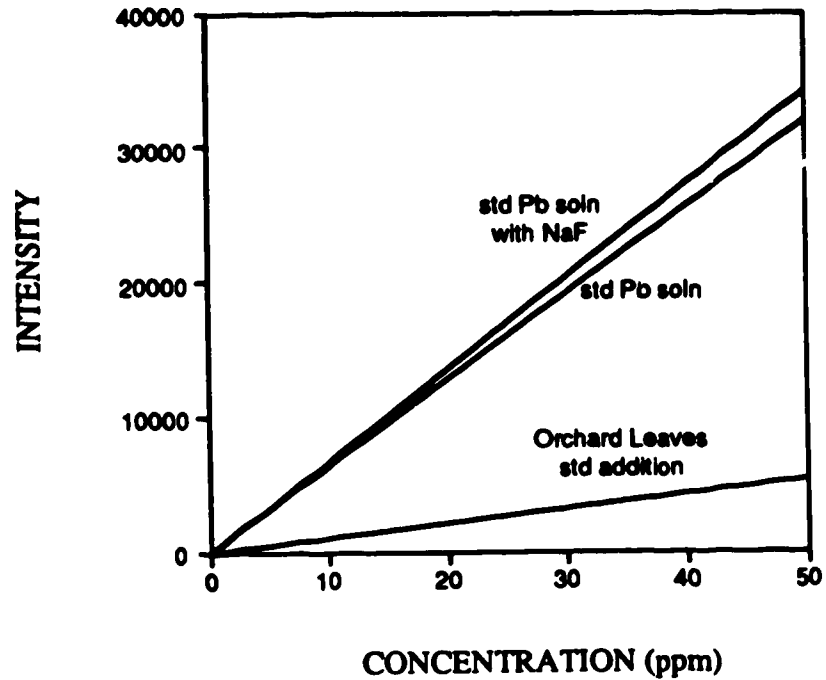


**Figure 5-14.** Calibration curves for standard solutions with and without NaF, and standard addition analysis of Orchard Leaves with NaF. The curves are forced to pass through origin so that the slopes can be compared.  
(c) Pb.

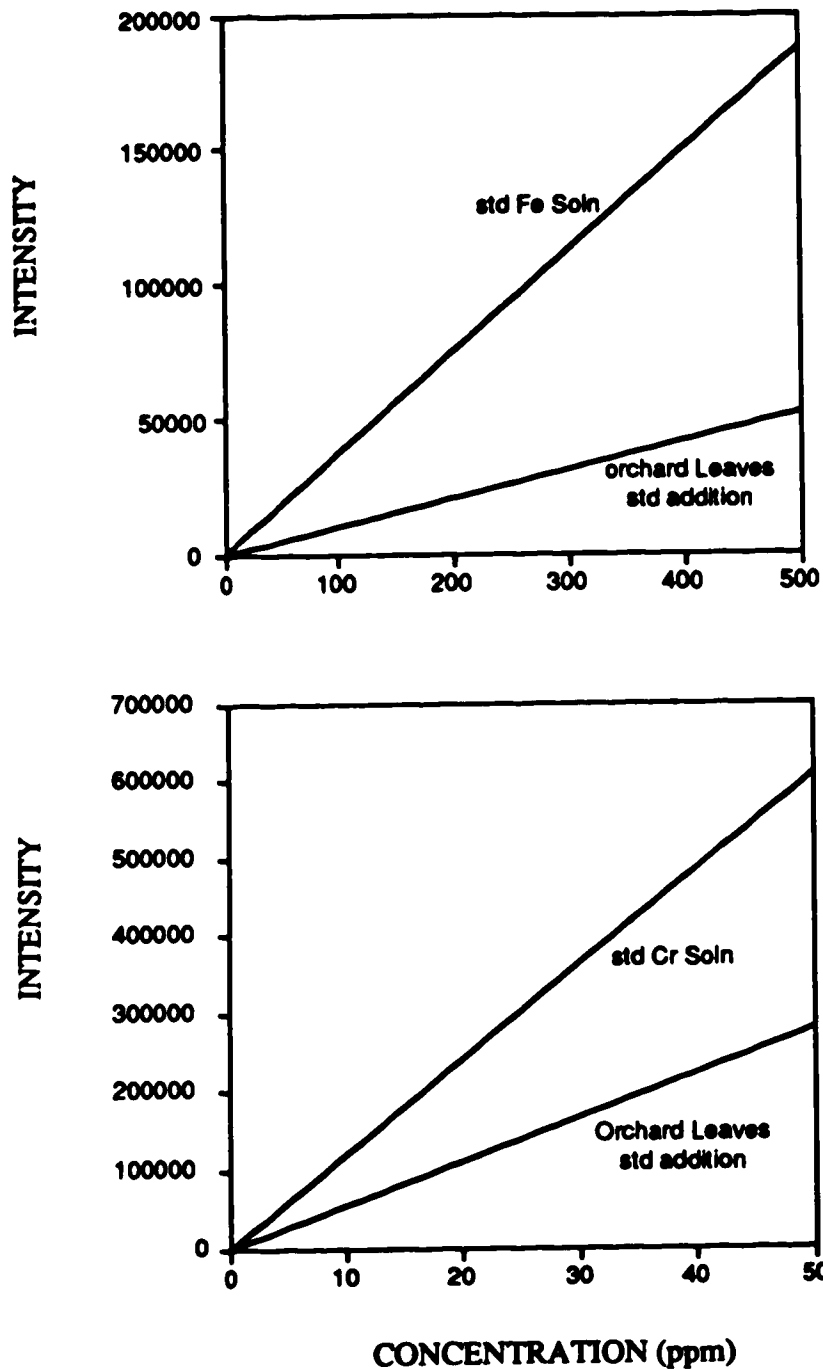


**Figure 5-14.** Calibration curves for standard solutions with and without NaF, and standard addition analysis of Orchard Leaves with NaF. The curves are forced to pass through origin so that the slopes can be compared. (d) Fe, (e) Cr.

situation of constructing a calibration curve from aqueous standard solutions for the analysis of samples with different matrices may be practical.

The calibration curves of the standard solutions, the standard solutions with NaF, and the standard addition analysis with NaF are shown in Figure 5-14. The amounts of NaF added to the standard solution and the botanical sample are the same for an analyte. The behavior of the analytes can be classified into three groups. The first group includes Cu and B: the sensitivity of the standard solution with NaF and that of the standard addition analysis are comparable, while the sensitivity for the standard solution without NaF is lower. The second group contains Pb only: the sensitivity is not enhanced with the addition of NaF for both the botanical sample and the standard solution, therefore sensitivities for the standard solution with and without NaF are comparable and much higher than that of the standard addition analysis.

The third group consists of Fe and Cr: addition of NaF to the standard solution reduces the sensitivity, and the signal fluctuates so much that a calibration curve cannot be constructed. The signal of the analytes from standard solutions with and without NaF are shown in Figure 5-15. For all analytes, the volatility is improved with the addition of NaF because the peaks are sharper. The integrated intensities for B, Cu, and Pb are also increased to various extents, but that of Fe and Cr are decreased and not reproducible. The behavior of Fe and Cr may be due to the fast vaporization of

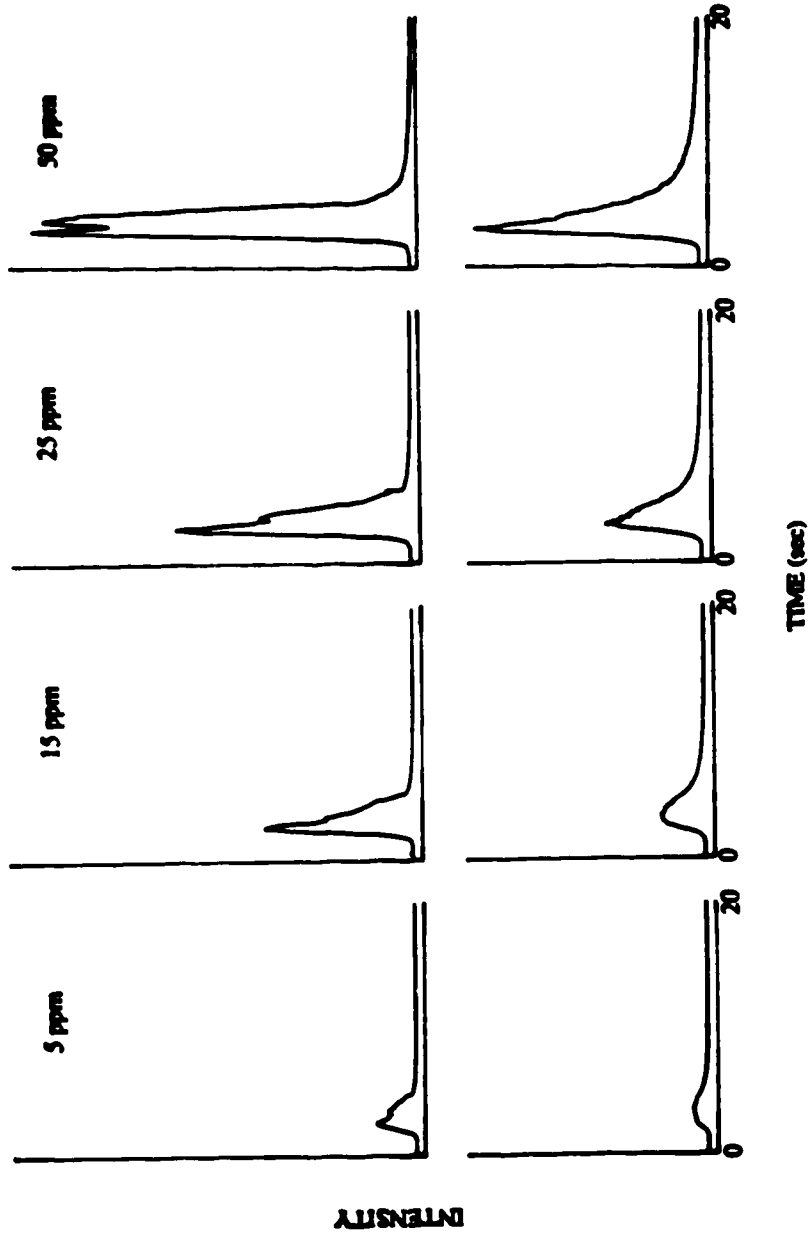


**Figure 5-15(a).** Signal for 10  $\mu\text{L}$  of Cu standard solutions with 40  $\mu\text{L}$  of 0.8 M NaF solution added (top row) and without NaF added (bottom row). The concentration of the Cu solution is shown on the top of each column.

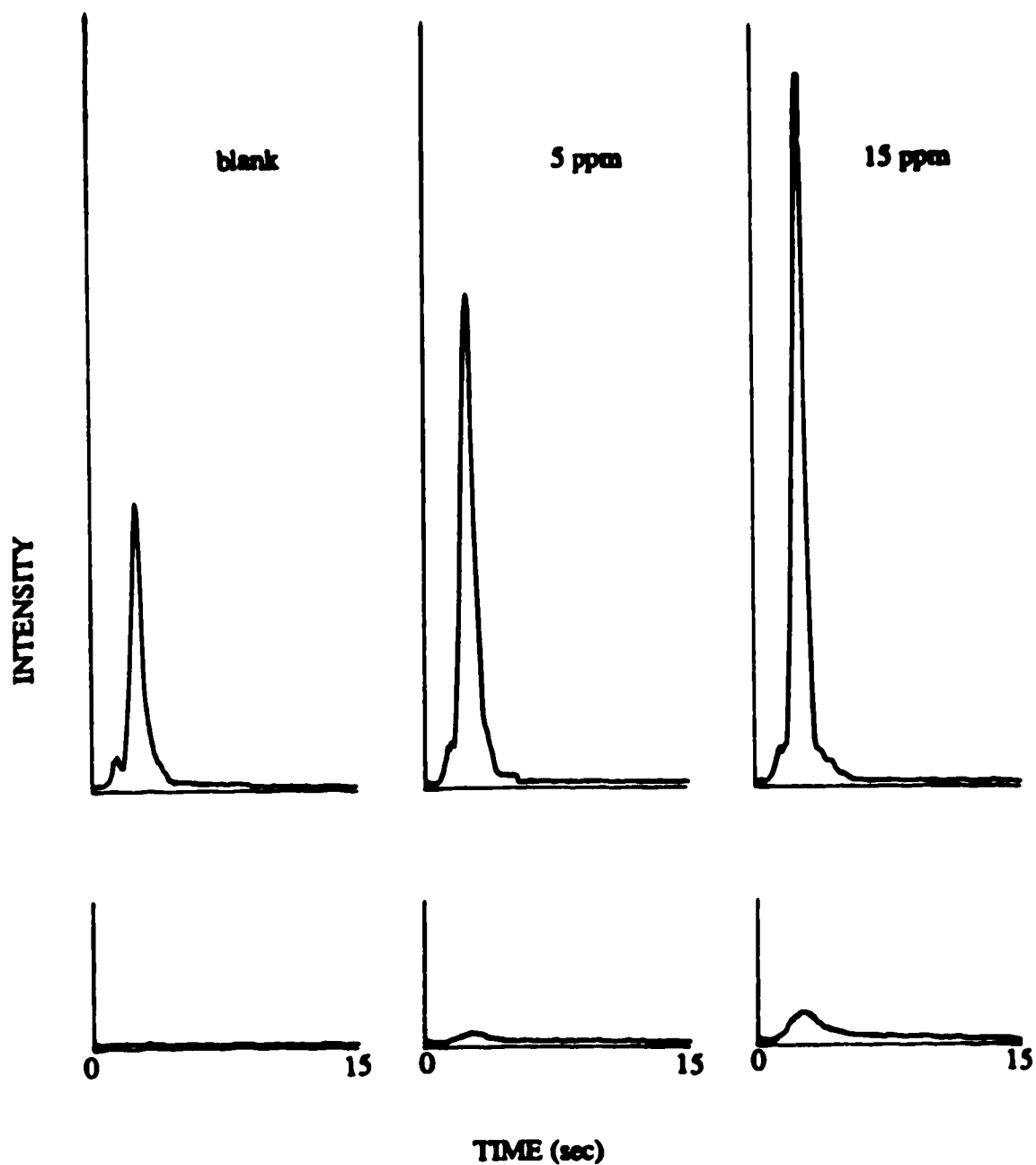


**Figure 5-15(b).** Signal for 10  $\mu\text{L}$  of B standard solutions with 40  $\mu\text{L}$  of 0.8 M NaF solution added (top row) and without NaF added (bottom row). The concentration of the B solution is shown on the top of each column.

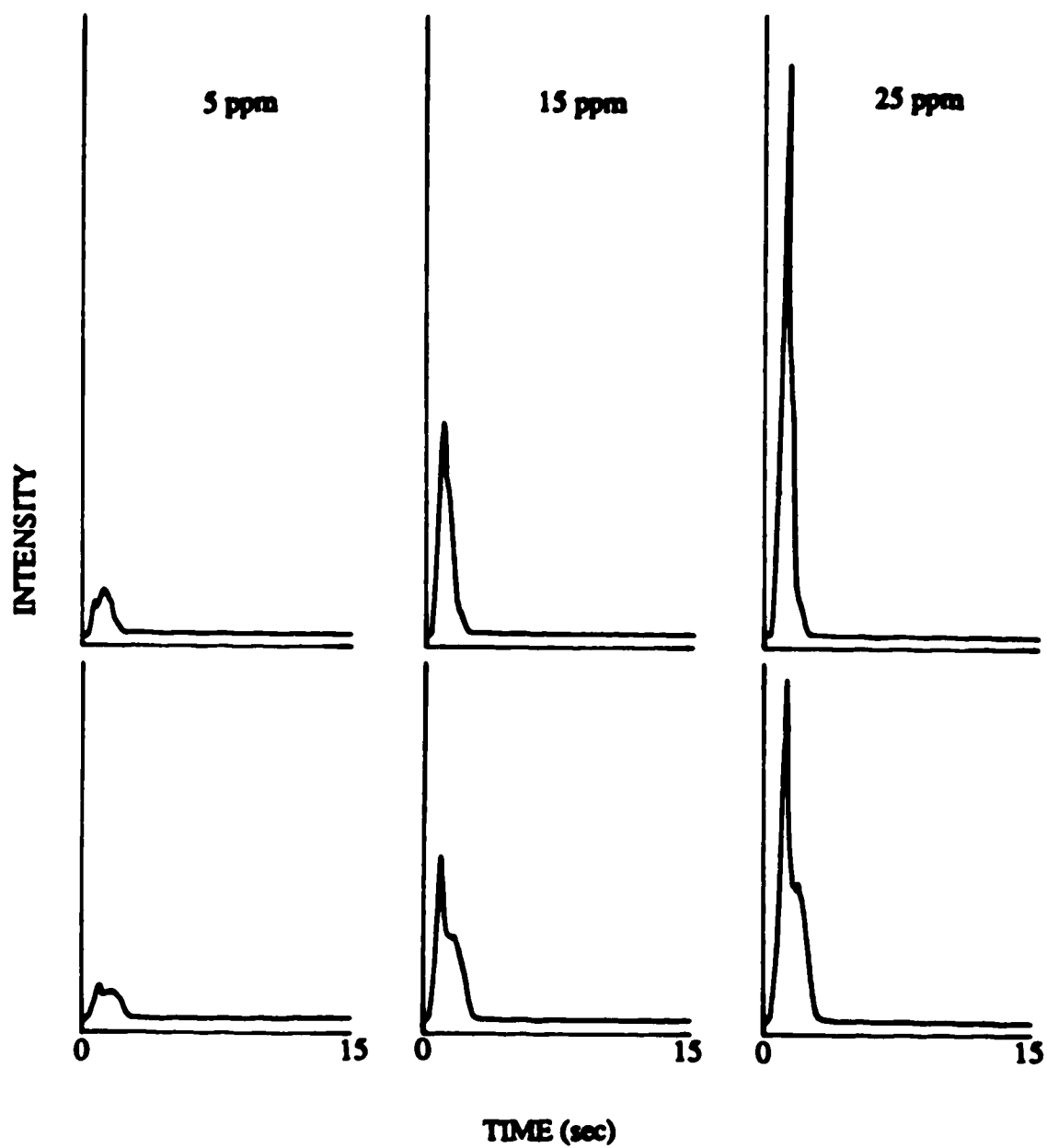


**Figure 5-15(c).** Signal for 10  $\mu\text{L}$  of Pb standard solutions with 40  $\mu\text{L}$  of 0.8 M NaF solution added (top row) and without NaF added (bottom row). The concentration of the Pb solution is shown on the top of each column.



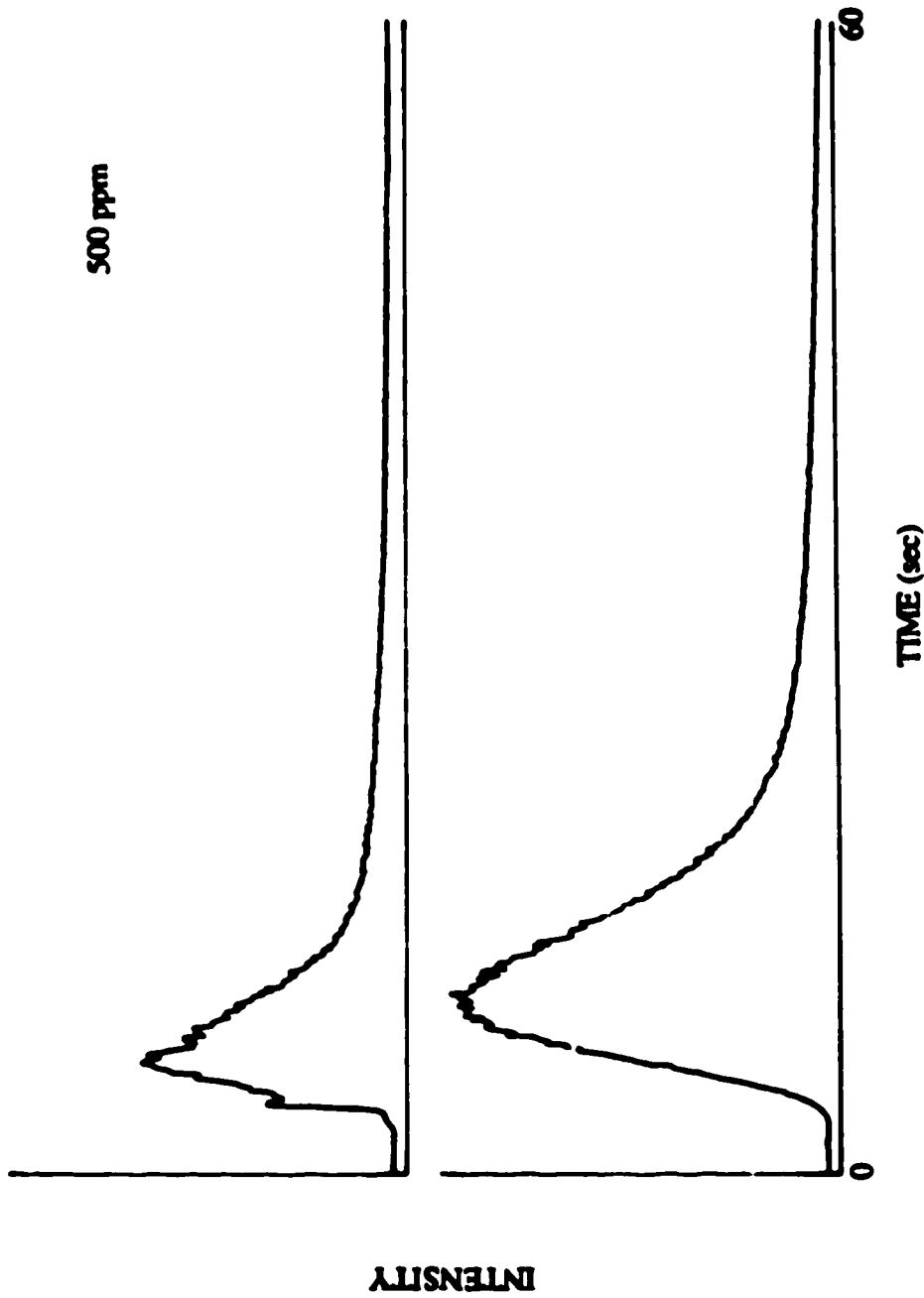


**Figure 5-15(d).** Signal for 10  $\mu\text{L}$  of Fe standard solution with 80  $\mu\text{L}$  of 0.8 M NaF solution added (top) and without NaF added (bottom). The concentration of the Fe solution was 500 ppm.

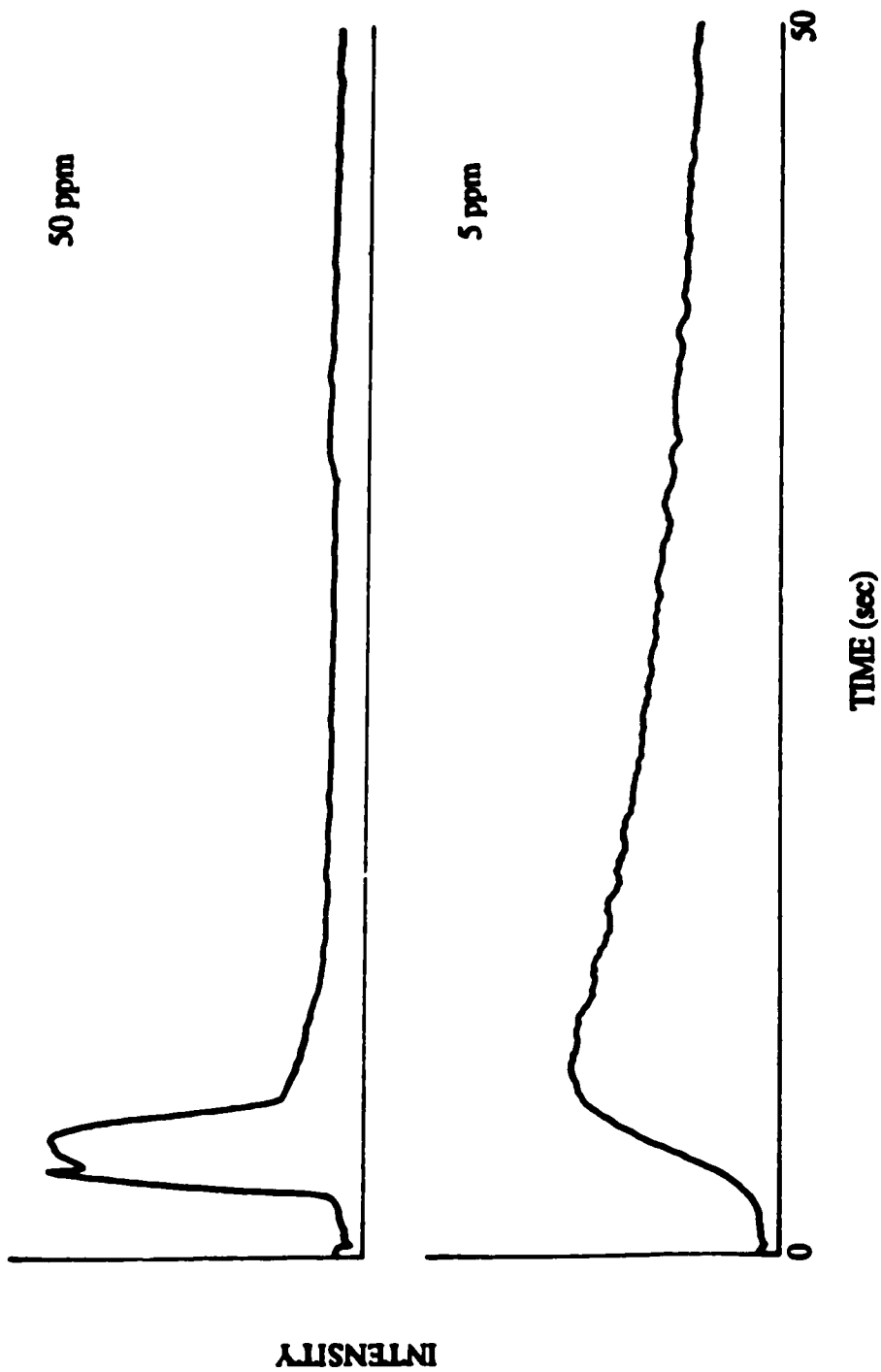


**Figure 5-15(e).** Signal for 10  $\mu\text{L}$  of Cr standard solution with 80  $\mu\text{L}$  of 0.8 M NaF solution added (top) and without NaF added (bottom). The concentrations of the Cr solution were 50 and 5 ppm.

the fluorides so that some analytes do not pass through the central channel of the plasma and are not detected. For the third group, sensitivity for a standard solution is higher than that of the standard addition analysis.

The sensitivities for B and Cu in botanical samples are enhanced so that they are higher than those for the standard solutions. For these analytes, the idea of using a standard solution calibration curve (with NaF added) for solid sample analysis is possible, provided that the analytical procedure is fine tuned to have the two sensitivities converge. For other analytes, although the addition of NaF enhances the sensitivity of the analyte in the botanical sample it is still lower than that of a standard solution. Therefore a standard solution calibration curve for solid sample analysis is not possible for these analytes.

#### 5.5.5 Conclusion

The method of matrix modification combined with standard addition analysis allows the quantitative analysis of some nonvolatile elements, e.g. B and Cr. The sensitivities of the analytes Cu and Fe are also increased, which may provide better detection limits for these analytes.

## **5.6 Semi-quantitative Survey**

For some analyses, an order of magnitude approximation to analyte concentration is sufficient, i.e., a semi-quantitative analysis. Moreover, the time required for the analysis is preferably short. The survey mode of the DSI system is designed to meet this requirement.

A set of calibration curves is constructed by analysing standards with a similar matrix as the sample. The concentrations of the standards increase in steps of an order of magnitude, so that a small number of standards can cover a large range of concentration. The signal is integrated with the original electronics of the ARL 34000, so that as many as 34 channels can be monitored at a time and the amount of data generated is considerably smaller than that of the real time ADC mode. The samples are analysed in the same manner, and the concentration of an analyte is obtained directly from the calibration curve. Since the analytical procedure and the data processing are simplified, semi-quantitative information of as many as 33 elements (Cd occupies 2 channels) can be obtained in a short period of time.

### **5.6.1 Experimental**

Since the powdered botanical samples are charred during the dry/ash stage, a standard with a carbon base matrix should be adequate for the semi-quantitative analysis of the

samples. The SPEX G standard 1002 is employed in this work. It contains 49 elements at concentrations of 1, 10, 100, and 1000 ppm in #4061 graphite.

The NBS SRMs Pine Needles, Orchard Leaves, Tomato Leaves, and Spinach were analysed. The weight of the botanical samples and the SPEX G standard was 5 mg. The samples were dried/ashed at 35 mm h<sub>2</sub>O for 120 seconds before insertion into the plasma.

All 34 channels of the ARL 34000 were monitored with the original integrating electronics of the instrument. There were two integration periods, both 30 s. The first period started at the point of insertion, which covered the peak of the signal. The second one started right after the first one, which was for background subtraction. Some analytes, e.g. Fe, were not completely vaporized in the first 30 s observation window, therefore the second 30 s observation window would be integrating the tail of the signal. Over-correction for the signal occurred in these cases. However, since the purpose of the analysis is to obtain semi-quantitative information of the analytes, the error is acceptable.

Each sample was analysed six times.

### 5.6.2 Results and Discussion

The calibration curves for the SPEX G standards are summarized in Table 5-9. The curves are double logarithmic plots, with intensity in mV and concentration in ppm. Only

the analytes that have reasonable sensitivities are listed in the table. The analytes that are not listed included: nonvolatile elements (Zr, Si, Mo, Tl, V), elements that emit in the vacuum UV region (N, P, S, C, Hg) and channels that are not operational (Ag, Sr). The calibration curves of some of the elements that are not listed (Mo, V, S, and P) are shown in Figure 5-16. Those of Al, Cr, Cu, and Zn are shown in Figure 5-17 for comparison.

The results of the analysis of Pine Needles, Orchard Leaves, Tomato Leaves, and Spinach are listed in Table 5-10 to 5-13. The experimental results agree with the certified values within an order of magnitude, which is satisfactory for a semi-quantitative analysis. The survey mode is therefore a quick method to obtain a large amount of preliminary information about the elemental composition of a sample.

## 5.7 Conclusion

Four methods for the direct analysis of powdered botanical samples with little or no sample pretreatment were presented. The DSI technique is sufficiently sensitive for analyte concentrations in the ppm range. The sample size is small, which is important for biochemical and clinical analysis. However, proper standards covering a wide range of concentrations are not available. The standard addition method solves the problem, but the analytical procedure is

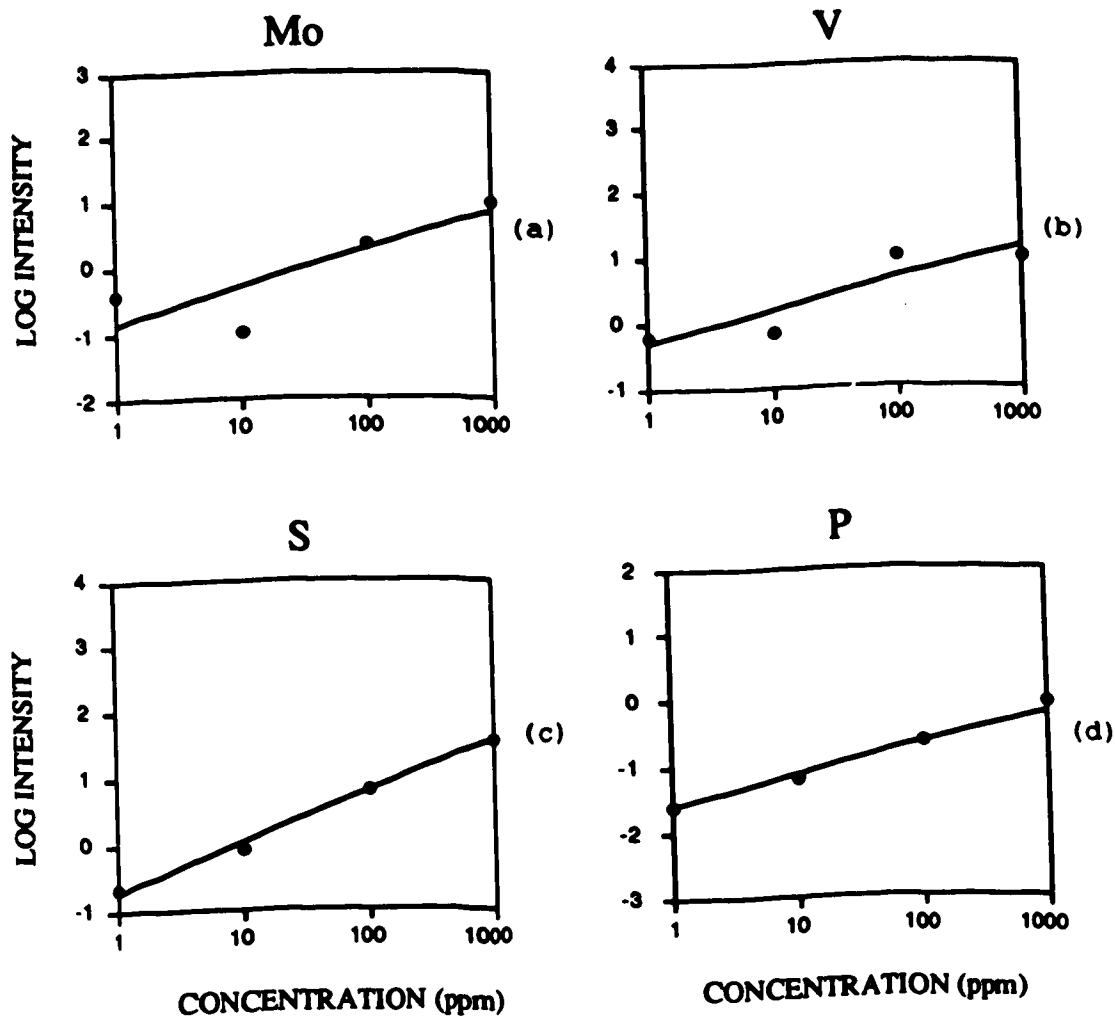


**Figure 5-16.** Calibration curves for (a) Mo, (b) V, (c) S, and (d) P for SPEX G standards. Note that the sensitivities are low and the slopes for the log-log plots are much less than one for the nonvolatile elements (Mo and V) and elements with emission lines in the vacuum UV region (S and P).

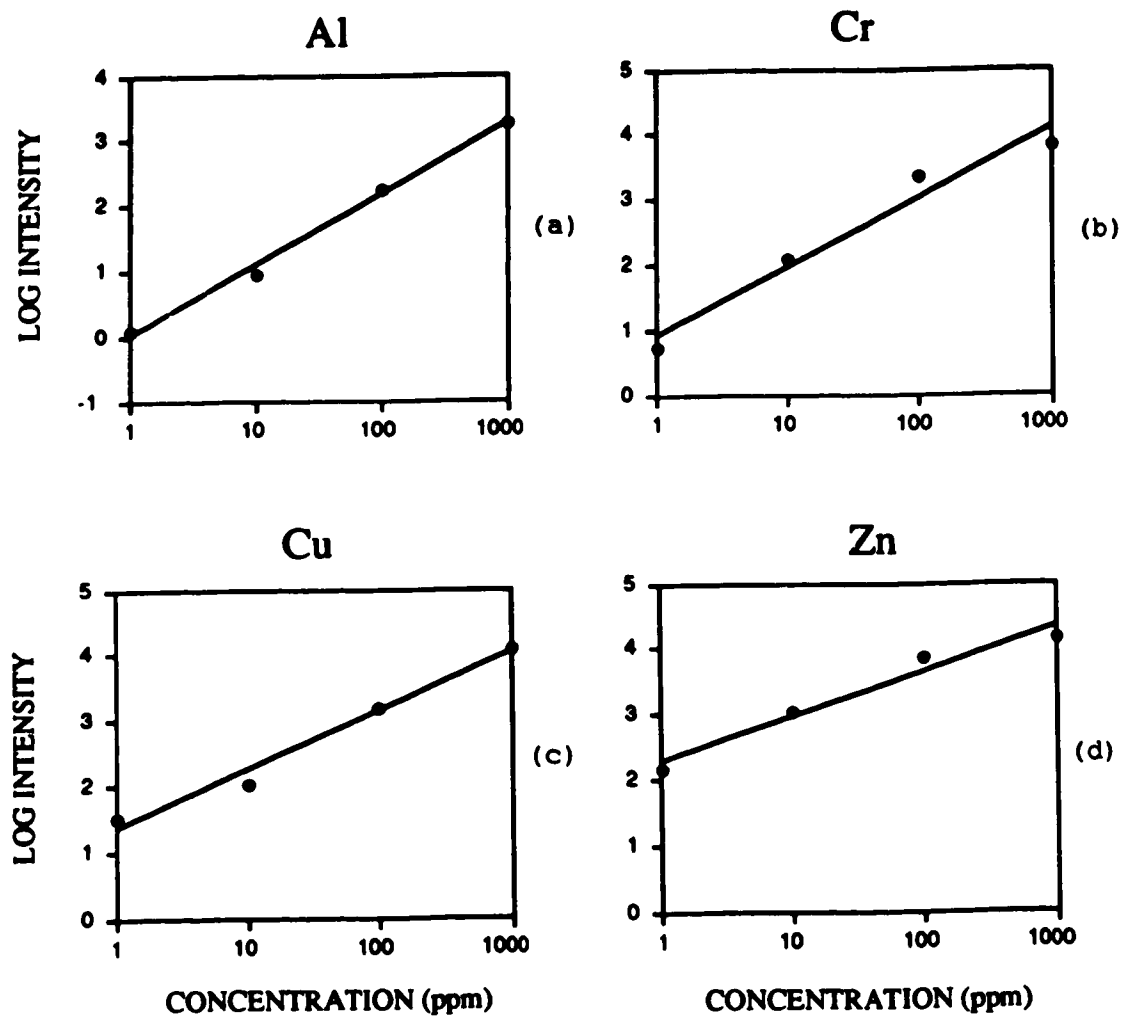


**Figure 5-17.** Calibration curves for (a) Al, (b) Cr, (c) Cu, and (d) Zn from SPEX G standards.



tedious. With matrix modification, some analytes can be analysed with a standard solution calibration curve, which may lead to a simple and fast method for direct powdered sample analysis. More work is needed to optimize the experimental conditions and matrix modifier combination so that a truly universal calibration curve can be established for all samples.

**Table 5-9. Calibration Curves for Semi-Quantitative Analysis**

Element	slope	intercept	correlation coefficient
Al	1.0785	0.0240	0.9972
As	1.0330	0.6934	0.9999
B	0.7921	0.6100	0.9966
Ba	0.9677	-0.5041	0.9471
Ca	1.2110	-0.7779	0.9451
Cd	0.9901	0.9296	0.9975
Cr	1.0560	0.9196	0.9798
Cu	0.8841	1.3801	0.9898
Fe	1.1986	0.9469	0.9910
Ge	1.0150	0.3124	0.9909
In	0.9450	0.9251	0.9997
K	1.0724	-0.1304	0.9996
Li	0.8913	1.5609	0.9973
Mg	0.9165	0.8661	0.9999
Mn	1.0277	1.8814	0.9981
Na	0.9020	0.8737	0.9980
Ni	0.9046	0.7700	0.9974
Pb	0.8817	0.7366	0.9995
Sb	0.9437	1.0974	0.9994
Sn	0.9942	1.0442	0.9989
Zn	0.6758	2.3017	0.9812

**Table 5-10. Semi-quantitative Analysis of Pine Needles  
(NBS SRM 1575)**

element	certified value (ppm)	experimental result (ppm)
Al	545 ± 30	300
Ca	4100 ± 200	3000
Cr	2.6 ± 0.2	3
Cu	3.0 ± 0.3	6
Fe	200 ± 10	150
K	3700 ± 200	4000
Ni	(3.5)	1
Pb	10.8 ± 0.5	3
Sb	(0.2)	0.4

**Table 5-11. Semi-quantitative Analysis of Orchard Leaves  
(NBS SRM 1571)**

element	certified value (ppm)	experimental result (ppm)
B	33 ± 3	6
Ca	2.09 ± 0.03%	1%
Cr	2.6 ± 0.3	6
Cu	12 ± 1	30
Fe	300 ± 20	330
K	1.47 ± 0.03%	1%
Mg	6200 ± 200	4000
Mn	91 ± 4	100
Ni	1.3 ± 0.6	1
Pb	45 ± 3	20
Sb	2.9 ± 0.3	3
Zn	25 ± 3	20

**Table 5-12. Semi-quantitative Analysis of Tomato Leaves**  
(NBS SRM 1573)

element	certified value (ppm)	experimental result (ppm)
B	(30)	10
Ca	3.00 ± 0.03%	1%
Cr	4.5 ± 0.5	4
Cu	11 ± 1	20
Fe	690 ± 25	330
K	4.46 ± 0.03%	1%
Mg	(0.7%)	0.4%
Pb	6.3 ± 0.3	2
Zn	62 ± 6	70

**Table 5-13. Semi-quantitative Analysis of Spinach**  
(NBS SRM 1575)

element	certified value (ppm)	experimental result (ppm)
Al	870 ± 50	200
B	(30)	20
Ca	1.35 ± 0.03%	1%
Cr	4.6 ± 0.3%	7
Cu	12 ± 2	40
Fe	550 ± 20	330
K	3.56 ± 0.03%	1%
Mn	165 ± 6	150
Ni	(6)	1
Pb	1.2 ± 0.2	1
Zn	50 ± 2	60

### References

1. P.W.J.M. Boumans, ed., '*Inductively Coupled Plasma Emission Spectroscopy, Part 1*', John Wiley and Sons, New York (1987)
2. W.E. Harris and B. Kratochvil, '*An Introduction to Chemical Analysis*', Saunders College Publishing, Philadelphia (1981)
3. R.L. Anderson, '*Practical Statistics for Analytical Chemists*', Van Nostrand Reinhold Co., New York (1987)
4. W.I. Price, '*Spectrochemical Analysis by Atomic Absorption*', Heyden & Son Ltd., London/Philadelphia/Rheine (1979)
5. D.A. Skoog and D.M. West, '*Principles of Instrumental Analysis*', 3rd ed., Holt, Rinehart and Winston, New York (1971)
6. R. Mavrodineanu, ed., '*Analytical Flame Spectroscopy, Selected Topics*', Macmillan and Co. Ltd., London and Basingstoke (1970)
7. E.L. Grove, ed., '*Analytical Spectroscopy Series, vol 1: Analytical Emission Spectroscopy, Part II*', Marcel Dekker Inc., New York (1972)
8. W.J. Blaedel and V.W. Meloche, '*Elementary Quantitative Analysis, Theory and Practice*', 2nd ed., Harper and Row, New York/Evanston/London (1963)
9. Bownan and Willis, *Anal. Chem.* **39**, 1210 (1967)

10. G.F. Kirkbright and Zhang Li-Xing, *Analyst* **107**, 617 (1982)
11. Y. Shao and G. Horlick, *Appl. Spectrosc.* **40**, 386 (1986)
12. V. Karanassios, G. Horlick, and M. Abdullah, 'Characterization of a DSID for ICP-AES', *Spectrochim. Acta*, (submitted)
13. A.G. Page, K.H. Madraswala, S.V. Godbole, M.J. Kulkarni, V.S. Mallapurkar, and B.D. Joshi, *Frezenius' Z. Anal. Chem.* **315**, 38 (1983)
14. A.G. Page, S.V. Godbole, K.H. Madraswala, M.J. Kulkarni, V.S. Mallapurkar, and B.D. Joshi, *Spectrochim. Acta* **39B**, 551 (1984)
15. G. Zaray, P. Burba, J.A.C. Broekaert, and F. Leis, *Spectrochim. Acta* **43B**, 255 (1988)
16. V. Karanassios, M. Abdullah, and G. Horlick, 'The Application of Chemical Modification to a Direct Sample Insertion Device for ICP-AES', *Spectrochim. Acta*, (submitted)
17. L.B. Rogers, *J. Chem. Ed.* **63**, 3 (1986)

## **Chapter 6. Concluding Remarks and Future Experiments**

A computer-controlled direct sample insertion system for the ICP has been developed, as described in Chapter 2. Characterization of the DSI technique was presented in Chapter 4. The manner of sample pre-treatment (drying and ashing) was found to have a considerable influence on the temporal behavior of analyte emission. The capability of the system for the direct analysis of powdered samples with little or no sample pretreatment has been demonstrated. The results were reported in Chapter 5.

The thermal properties of the sample cup assembly have also been examined (Chapter 3). Several directions for improving the sample cup temperature rise rate and the maximum sample cup temperature were proposed based on this study. These include utilization of a small cross-sectional area of the sample cup holder to limit conductive heat loss, selection of the sample cup and cup holder materials, and employment of a mixed gas plasma (e.g., a N<sub>2</sub> cooled ICP) with higher input power.

Several areas of further development of the DSI system are proposed in the following sections. These include automation of the DSI system, increase of the sample cup temperature, elimination of the effects of the sample cup (i.e., interaction between the sample and the cup wall and maximum temperature attainable for the sample), utilization

of a photodiode array spectrometer as signal detection system, and consideration of sample throughput.

### **6.1 A fully automated DSI system**

A more detailed characterization of the system is desirable. This includes the effects of the insertion sequence and timing; the interaction between the analyte and the sample matrix and the sample cup surface; the temperature rise rate and the maximum temperature attainable for the sample cup; the ICP operating parameters, e.g., forward power, gas flow rates, mixed gas, observation zone, and selection of ion lines or neutral atom lines for detection. This information could be stored in a data base for user consultation so that the optimal experimental parameters for the analysis of a particular type of sample could be selected. If a fully automated system was implemented, the data base could serve as a knowledge base for an expert system, as proposed in Chapter 2.

For a truly automated system, automatic sample preparation and transfer are in order. A robot is an ideal choice for this task. At present, our robot has limited ability for sample transfer. The position of each sample cup in the cup organizer and the DSI device must be known and fixed. Moreover, error checking and correction are not implemented. A robot with visual sensors would be much more intelligent, provided that proper software is available. Only



the approximate position of a sample cup would then be required, because the robot would be able to correct for the error. This would save the operator the tedious sample cup position calibration. The real benefit of a robot with sensors is that it could also perform sample preparation. Locating a sample vial and dispensing sample from it to a sample cup would not be viable without visual feedback.

### **6.2 Ohmic heating of the sample cup**

The maximum temperature attainable for the sample cup has a significant effect on the analyte volatilization. It was shown that the final sample cup temperature is about 2000 K in our system, which is relatively low compared to that of electrothermal vaporization atomic absorption spectrometry. Refractory elements are thus not vaporized effectively. A combination of ohmic heating and inductive heating for the sample cup might improve its maximum temperature [1]. A tungsten wire could perhaps be placed inside the sample cup holder for electrothermal heating of the sample cup.

### **6.3 Consumable sample cup and the capillary sampler**

The sample cup interacts with the sample as well as limiting its temperature. To eliminate these effects, a wall-less sample probe has been proposed by Blain and Salin [2]. Pallet samples were placed on top of a holder and inserted

into the plasma. A consumable sample cup has been discussed in this group [3]. The most obvious implementation would be a graphite cup combined with an oxygen mixed gas plasma. The graphite cup would be burned in the oxidative atmosphere in a controlled fashion, the sample then being exposed to the plasma gas directly. Complete vaporization of the sample should be possible since the residence time of the sample in the plasma would be much longer than that of powder injection methods [4].

The idea of introduction of a solid sample into the plasma without the hindrance of the sample cup can also be realized with a capillary sampler (see Figure 6-1). This technique involves sampling powders or liquids with a capillary tube by dipping the tube into the samples, the tube is then inserted into the ICP torch to a position just under the plasma discharge, and the sample is injected into the plasma with a flow of Ar gas through the capillary tube. Preliminary results were obtained using a capillary tube with external and internal diameters of 0.08 and 0.04-0.05 cm respectively. For a sample length of 0.1 cm, the volume of the sample is about  $2 \times 10^{-4}$  cm<sup>3</sup>, which is 1 mg of sample if sample density is 5 g/cm<sup>3</sup>. The on/off of the injector gas flow was controlled manually with a switch originally used for the nebulizing gas of the ARL 34000. Preliminary experimental results for injecting powdered geochemical reference samples [6] are shown in Figures 6-2 and 6-3.

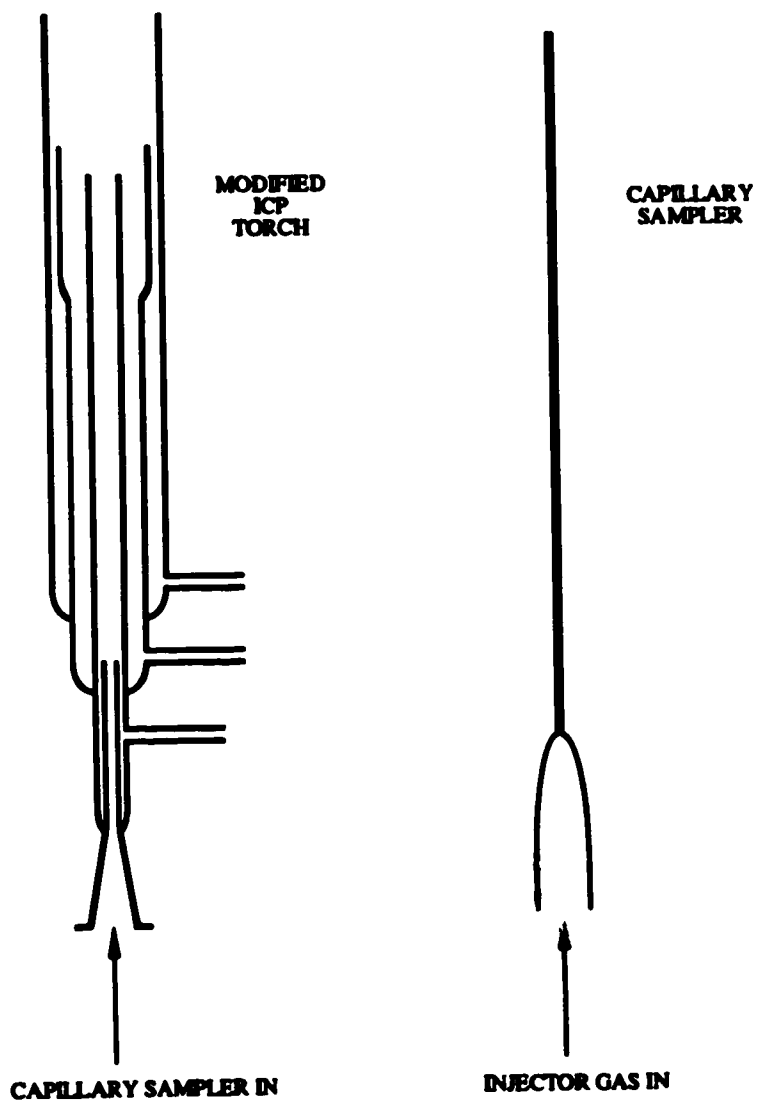
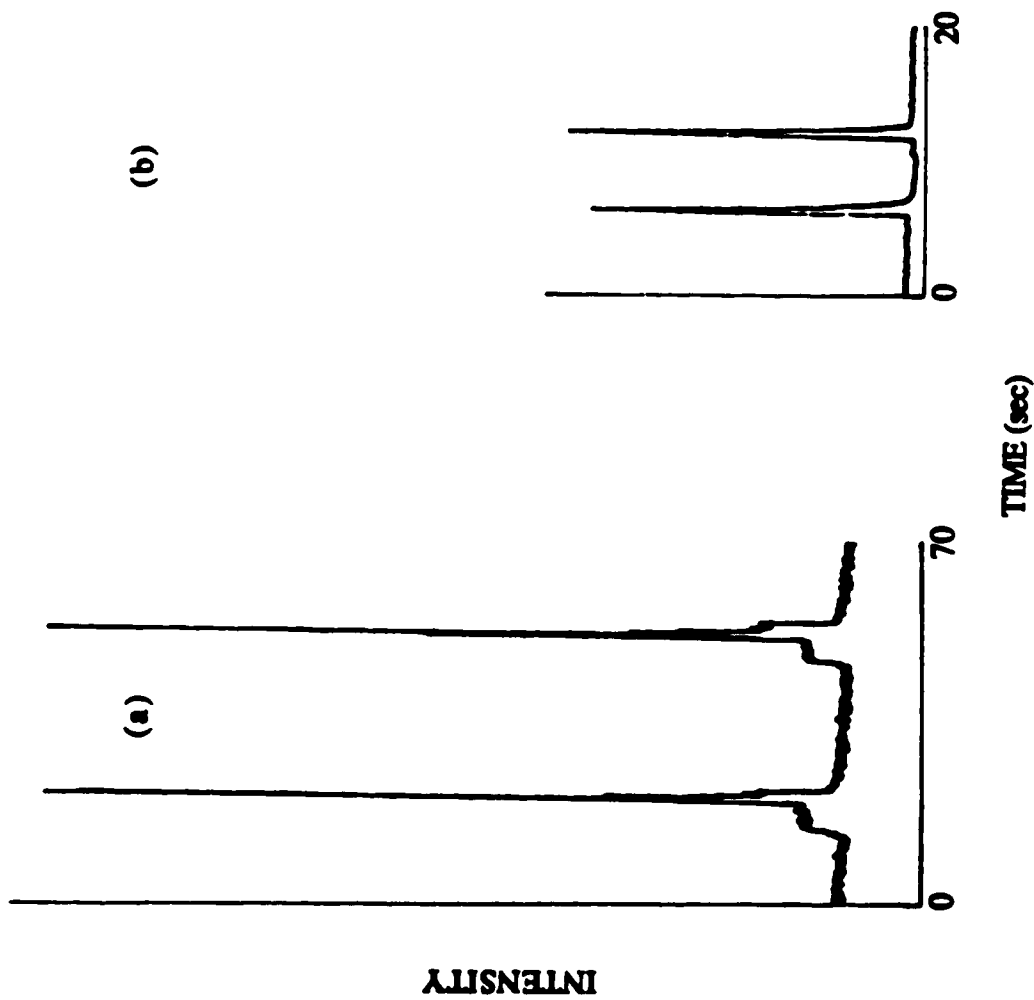
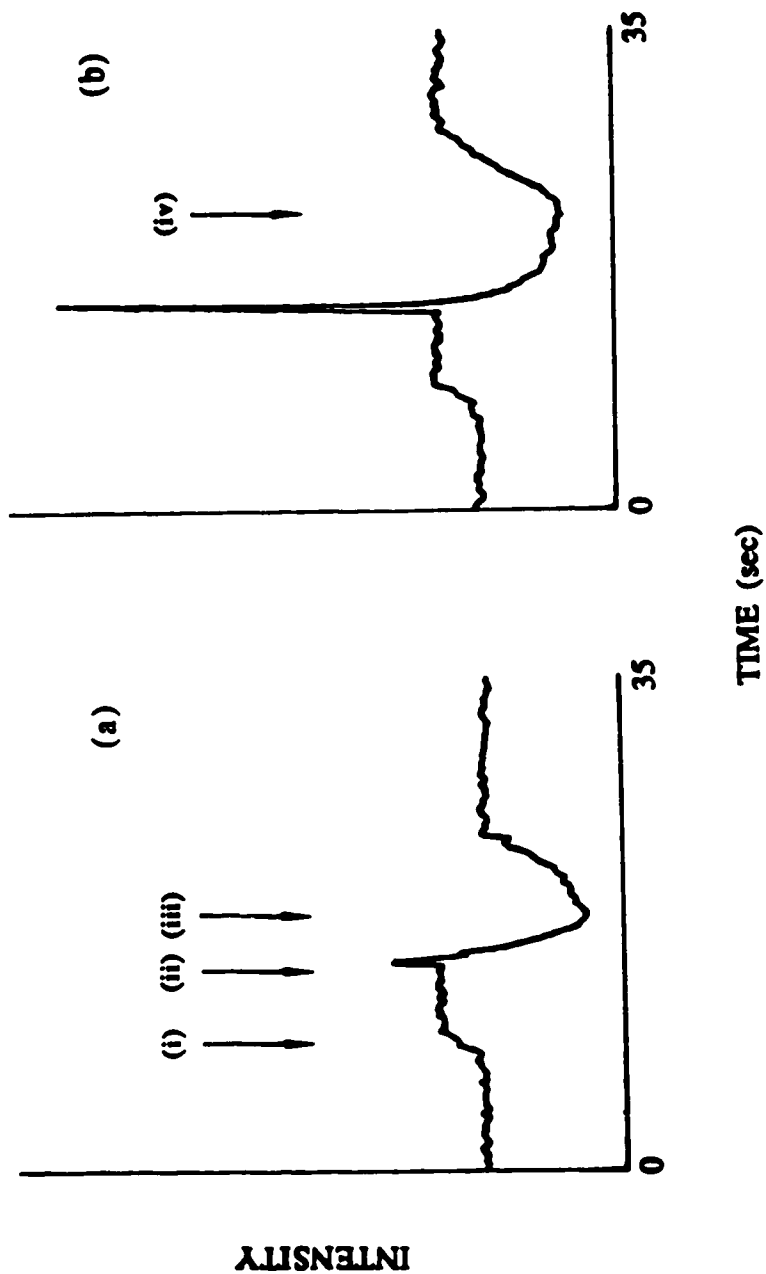


Figure 6-1. A modified ICP torch and the capillary sampler.



**Figure 6-2.** Temporal behavior of the signal for two consecutive runs of (a) Ca from calcium carbonate and (b) Zn in GSD-1, with the capillary sampler.



**Figure 6-3.** Temporal behavior of the signal for Ni in (a) GSD-2 (5.5 ppm) and (b) GSD-1 (76 ppm). Background intensity changes with (i) capillary sampler inserted into the ICP torch, (ii) Ar injector gas turned on, (iii) Ar injector gas turned off and the capillary sampler withdrawn from the torch, and (iv) Ar injector gas turned off and the capillary sampler remained inserted into the torch.

The capillary sampler injects powdered samples directly into the plasma, which eliminates the need for a sample cup. Powders are not transported through tubing as other powder injection methods, therefore transport efficiency is 100 %. The measurement cycle is relatively short because sample weighing into a sample cup and dry/ash cycles are not necessary. The small sample size, however, may cause serious sampling errors. This can be overcome with repeat measurement. A capillary sampler with multiple capillary tubes that allows injector gas flows through the tubes sequentially would make repeat measurement fast and simple.

#### **6.4 Photodiode array spectrometer**

The best analytical lines for the DSI-ICP technique may not be the same as that for the conventional nebulizer/spray chamber configuration. A photodiode array (PDA) spectrometer [5] is more flexible in selecting an analytical line than a polychromator, while maintaining the multichannel capability. In addition one would like the option of either time resolving the transient emission signal or integrating the total emission signal. To this end, the PDA spectrometer represents an ideal measurement system for the DSI technique.

### **6.5 Sample throughput**

The ability of *in situ* desolvation and ashing of a sample is considered an advantage of the DSI technique. However, these processes can be time-consuming, e.g., the combination of a typical 60 sec drying and 120 sec ashing process is three times as long as a 60 sec measurement window. For maximum sample throughput it is necessary to dry/ash the samples outside the plasma torch. An oven or a hot plate can be used to dry/ash a set of samples efficiently. Moreover, the dry/ash conditions for the whole set of samples are identical and can be easily controlled.

**References**

1. Kuniyuki Kitagawa, Private discussion (1985)
2. L. Blain and E.D. Salin, FACSS XV, Abstract No. B33 (1988)
3. G. Horlick, Group meeting (1987)
4. H.C. Hoare and R.A. Mostyn, *Anal. Chem.* **39**, 1153 (1967)
5. G. Horlick, *Appl. Spectrosc.* **30**, 113 (1976)
6. X. Xie and M. Yan, "*Geochemical Reference Samples, Drainage Sediment GSD 1-8 from China*", *Geostandards Newsletter* **9**, 83 (1985)



## **Appendix A. Liquid sample introduction system for APCI/MS/MS**

### **A.1 Introduction**

Atmospheric pressure chemical ionization mass spectrometry (APCI/MS) is a sensitive analytical technique for the detection of trace compounds in ambient air [1-4]. Recently APCI has also been adopted as an interface for high performance liquid chromatography and mass spectrometry (HPLC/MS) [5-7]. Therefore, APCI/MS is a versatile technique for the analysis of trace organics in both liquid and gas phases.

The main reagent ion in APCI is the hydronium ion/water clusters,  $\text{H}_3\text{O}^+(\text{H}_2\text{O})_n$ . It is generated by ionization of moist air, typically with a corona discharge, which initiates a sequence of ion/molecule reactions and results in the hydronium ion [8], with  $n = 5-8$  [9]. Analyte molecules are protonated by the hydronium ions. The reduced fragmentation resulting from the mild ionization provides insufficient structural information for identification of unknown compounds [10,11]. Fortunately, APCI produces abundant molecular ions which is well suited for a tandem mass spectrometer (MS/MS).

A triple-quadrupole mass spectrometer was used in this work. The first quadrupole serves as a mass filter which selects the molecular ion (parent ion). Collision activated

dissociation (CAD) of the parent ion takes place in the second quadrupole, and a family of daughter ions is produced. The lower mass daughter ions are rich in structurally significant fragmentation information. This information is extracted with the third quadrupole for the identification of the parent ion [12]. In this manner, both separation and identification of a sample consisting a mixture of several compounds can be carried out simultaneously with APCI/MS/MS.

An efficient way to introduce liquid samples to the APCI, so as to match the analytical efficiency of the instrument, is described below. The sample introduction system consists of a concentric nebulizer, a spray chamber, and a heated tube. The rate of sample aerosol generation and delivery to the APCI is fast, on the order of a few seconds. Moreover, sample can be nebulized continuously and sample changing is simple and fast.

An ultrasonic nebulizer coupled with a heated tube has also been used for sample introduction, because ultrasonic nebulizer has a better nebulization efficiency and generates smaller aerosol.

## **A.2 Experimental**

### **A.2.1 The mass spectrometer**

The APCI/MS/MS is a TAGA 6000e triple quadrupole mass spectrometer (Sciex, Thornhill, Ontario). A schematic diagram

of the APCI source is shown in Figure A-1. Ions are generated in a small cylindrical region (the wall-less reactor) between the tip of the corona discharge needle and the interface plate aperture. A continuous flow of dry nitrogen from the interface gas plenum through the interface plate aperture prevents moisture and neutral molecules from entering the MS. Ions are drawn into the MS by the potential difference between the discharge needle and the interface plate and vacuum orifice. Typical operating parameters for the TAGA 6000e are listed in Table A-1.

Experiments were performed in several modes of operation. For MS scan, quadrupole 1 (Q1) was scanned over the desired mass range. Q2 and Q3 were set in RF-only total ion mode, with the collision gas turned off.

For the multiple conventional scan mode, several masses were monitored in Q1 for a period of time, with Q3 in total ion mode.

Operation in the MS/MS mode involved opening the valve of the CAD gas inlet to Q2, adjusting the collision gas (N2) thickness to  $3 \times 10^{14}$  molecules/cm<sup>2</sup>, switching Q1 to transmit only the parent ion of interest, and scanning Q3.

### **A.2.2 The sample introduction system**

A heated tube/pneumatic nebulizer/spray chamber system was employed to introduce aqueous samples into the APCI. The

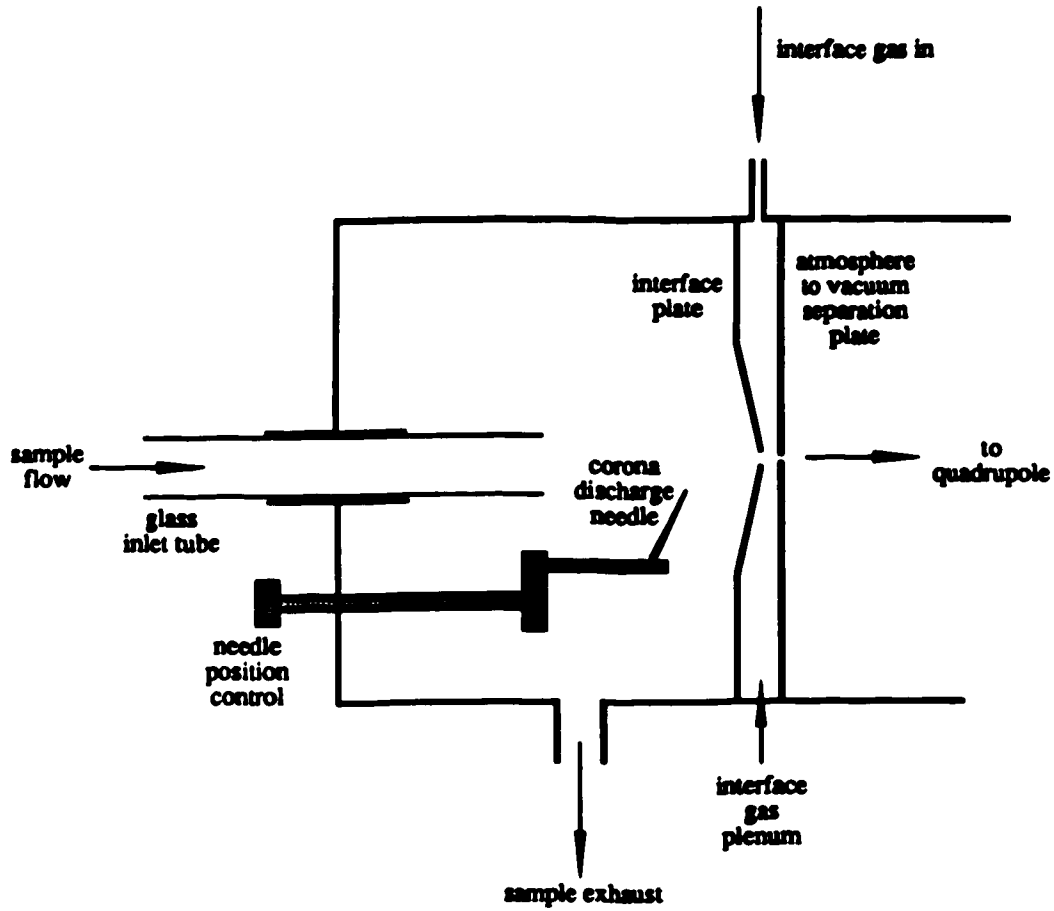


**Figure A-1.** Schematic diagram of the APCI source of the TAGA 6000e.

Table A-1. Operating parameters for the TAGA 6000e.

	code	description	value
APCI source	DI	discharge current	1 $\mu$ A
	SAF	sample gas flow rate	off
	BAF	bypass gas flow rate	off
	IN	interface plate voltage	700 V
Lens	OR	orifice lens	55 V
	CB	cluster breaker lens	50 V
	R0	AC entrance rod	30 V
	IQ	interquad lens	30 V
Quadruple mass filters	DM1	Quad 1 delta mass	0.4
	RE1	Quad 1 resolution	120
	R1	Quad 1 rod offset	28 V
	DM3	Quad 3 delta mass	0.1
	RE3	Quad 3 resolution	140
	R3	Quad 3 rod offset	28 V
Quadruple 2	CGT	collision gas thickness	$3 \times 10^{14}$ cm <sup>-2</sup>
	CG	collision gas type	N <sub>2</sub>
	R2	Quad 2 rod offset	30 V
Measurement Control Parameters	C	count control mode	10
	MCL	measurement count limit	1260
	MO	mass offset	0.01
	MTL	measurement time limit	0.1 sec
	PE	period between scans	0 sec
	TH	threshold value	10 count/s
	TT	total time limit for scans	variable
	STEP	amu increment	1
	FP	Faraday plate	60 V
	MU	multiplier voltage	-3400 V

design of the heated tube is based on that of Henion [5]. A schematic diagram of the heated tube is shown in Figure A-2. The heated tube consists of two concentric tubes. Nichrome wire was wound around the narrow region of the inner tube for heating. The resistance of the wire is  $20 \Omega$ . The typical voltage across the wire was  $22 V_{\text{rms}}$ , supplied by a transformer. Sample aerosol and nebulizing gas were introduced into the inner tube directly from the spray chamber. Typical solution sample uptake rate was 1 ml/min, with a nebulizing gas ( $N_2$ ) flow rate of 0.6 L/min at 34 psi. The auxiliary gas ( $N_2$ ) flow was 8 L/min at 20 psi. When the gases passed through the narrow region of the tube, they were heated by the tube wall. The temperature distribution inside the APCI is shown in Figure A-3. The sample aerosol was believed to be completely desolvated because the temperature of gases at the outlet of the inner tube reached  $200^\circ\text{C}$ .

The idea of the nebulizer/spray chamber system is borrowed from ICP spectrometry. A Meinhard concentric nebulizer was used. The spray chamber was a Scott type, with the direction of the aerosol outlet modified from the vertical to the horizontal position, so that it could be coupled with the inlet of the heated tube directly. The sample uptake rate was not controlled, therefore excess solvent was condensed in the inner tube after prolonged measurement ( $> 1$  hour). This problem can be overcome by using a peristaltic pump in front of the nebulizer to reduce sample uptake. A condenser [13] positioned between the spray chamber

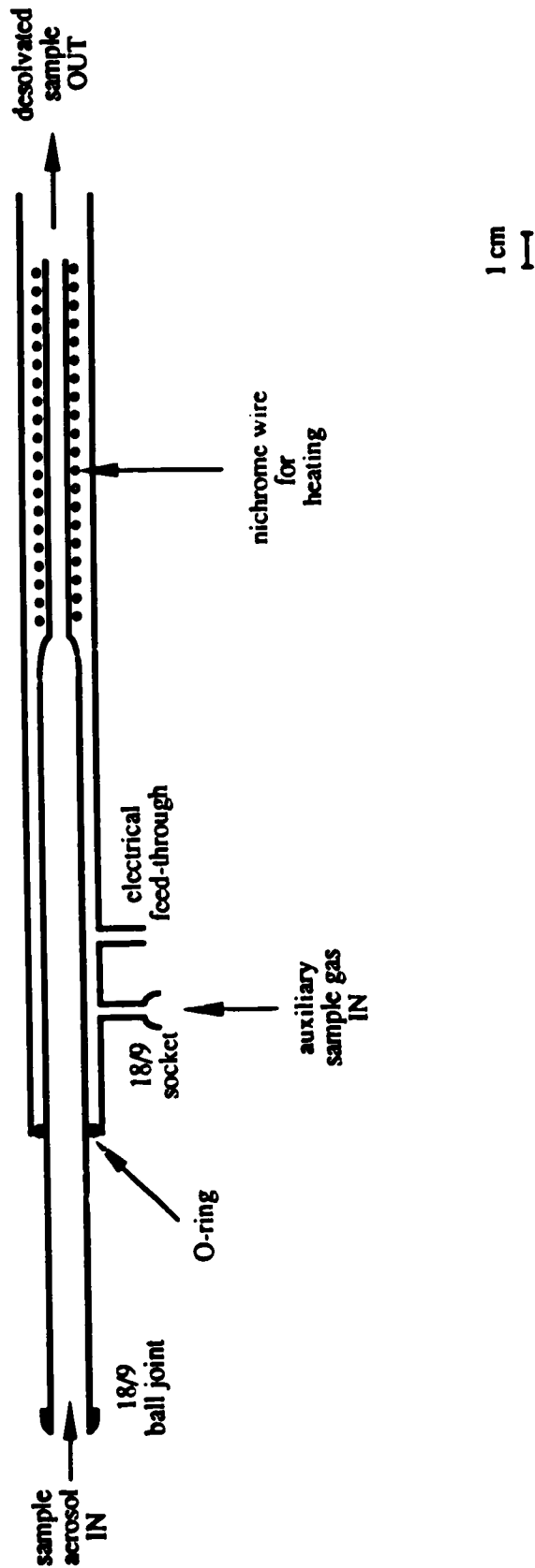
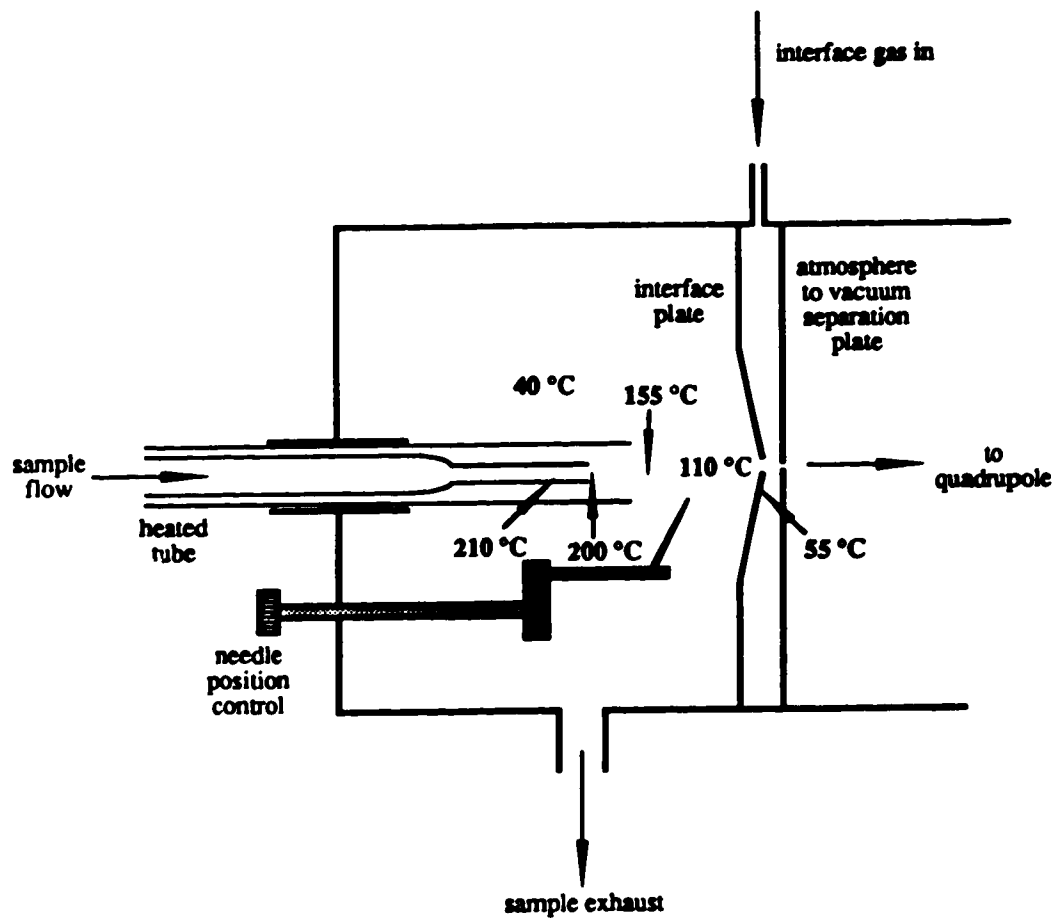


Figure A-2. Heated tube for sample aerosol desolvation.



**Figure A-3.** Temperature distribution in the APCI source with the heated inlet tube.



and the heated tube can also reduce the amount of solvent entering the APCI.

An batch type ultrasonic nebulizer system was also used for aerosol generation. The radio frequency generator (model UNPS-1, Plasma-Therm Inc.) delivers an output power of 50 W maximum, with an output impedance of 50  $\Omega$ . Typical output power was 35 W. The output frequency is tunable from 1350 to 1400 kHz, and it was tuned so that the reflected power was minimum. The ultrasonic transducer (model CPMT, Channel Product Ltd.) has a nominal frequency of 1.4 MHz. The maximum drive voltage and current are 50  $V_{rms}$  and 1  $A_{rms}$  respectively.

The nebulizer chamber is based on the design of Belchamber [14]. The size of the nebulizer is 4 cm in diameter x 24 cm in length. A schematic diagram of the chamber is shown in Figure A-4. The typical volume of sample solution was 20 ml. When the power of the rf generator is turned on, a fountain of sample solution rises above the transducer and a fine mist of analyte droplets is produced. This mist is then swept out of the chamber to the heated tube by a tangential flow of nitrogen carrier gas. The carrier gas enters through a side arm about halfway up the chamber. Typical carrier gas flow rate was 0.7 L/min at 20 psi.

### **A.3 Qualitative Analysis**

The APCI source produces analyte ions by protonation of the analyte molecules with a group of reagent ions, the

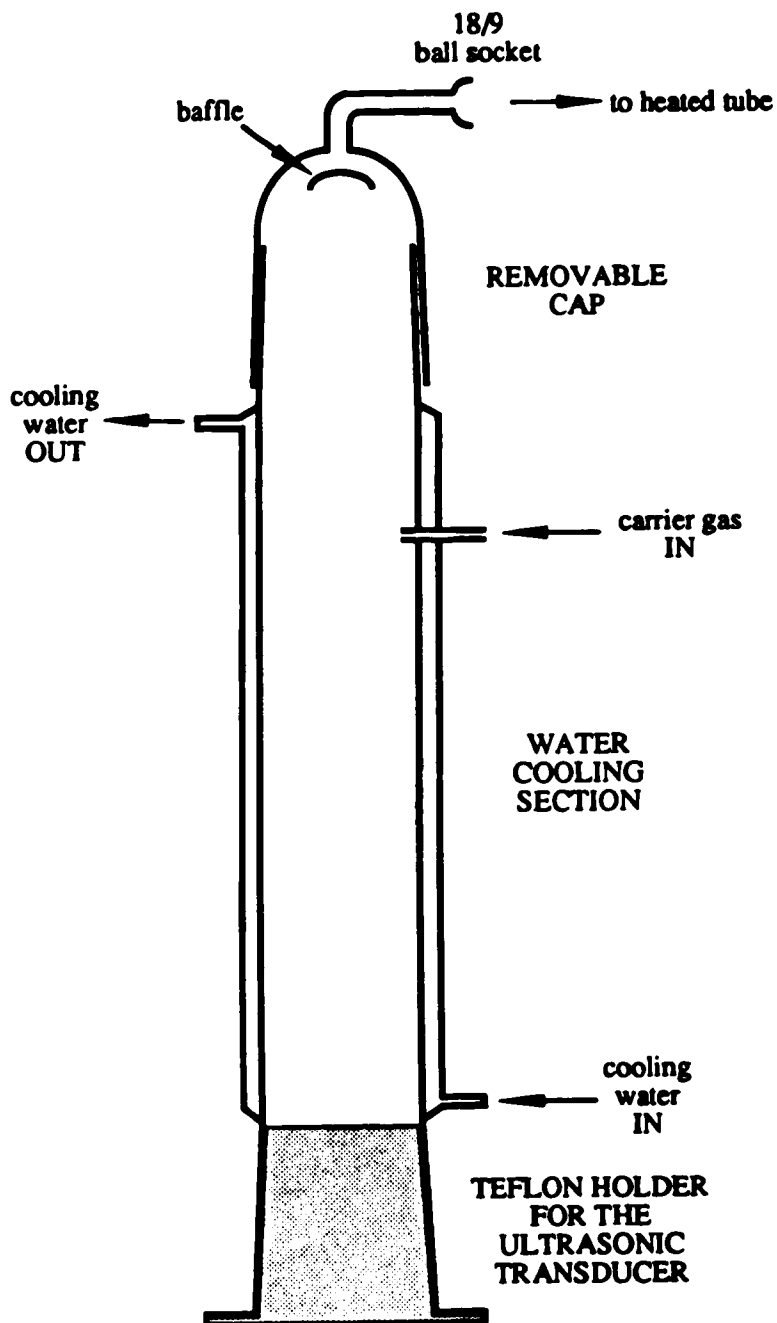


**Figure A-4.** The ultrasonic nebulizer assembly.

hydronium ion clusters. A typical background spectrum is shown in Figure A-5. The major peaks are  $m/z$  36, 37, 54, 55, 72, and 73. These are peaks for  $H_2O^+(H_2O)_n$  and  $H_3O^+(H_2O)_n$  ions clusters with  $n = 1-3$  respectively. The number of water molecules in the cluster,  $n$ , is smaller than that of the most stable clusters, i.e. 5-8. This is because cluster ions that drift through the dry interface gas undergo extensive thermal declustering [2]. It should be noted that the intensity is plotted on a logarithm scale, therefore, the most intense peaks, e.g.  $m/z$  37, are at least 3 orders of magnitude larger than other background peaks. In fact, the intensity of  $m/z$  37 is about 3000000 count/s, which possibly saturates the channel electron detector.

The APCI/MS is a sensitive technique for the detection of organic molecules in ambient air. Spectra of some volatile organic compounds are shown in Figure A-6. The samples were contained in a vial, which was placed in front of the air sample inlet tube of the APCI. The vaporized sample was carried into the APCI by the air flow, generated by the air pump.

The major peaks for ethanol spectra are  $m/z$  47 and 93, which are  $M+1$  and  $2M+1$  respectively. The peak at  $m/z$  65 is  $M+19$ , the protonated molecular ion-water molecule cluster. The peaks found in the APCI background spectrum are reduced in intensity, because of the ion molecule reaction between ethanol and the hydronium ions.

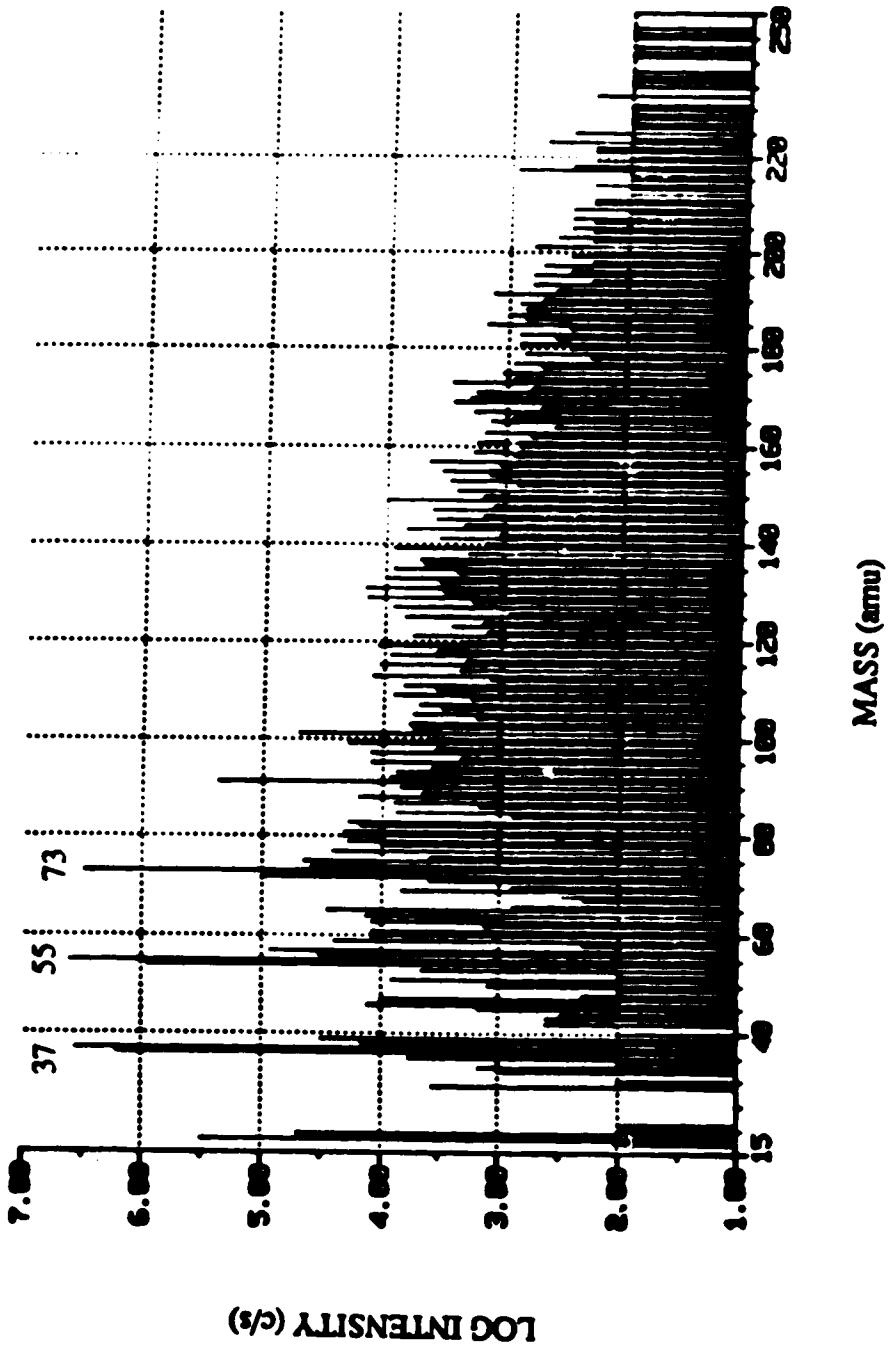
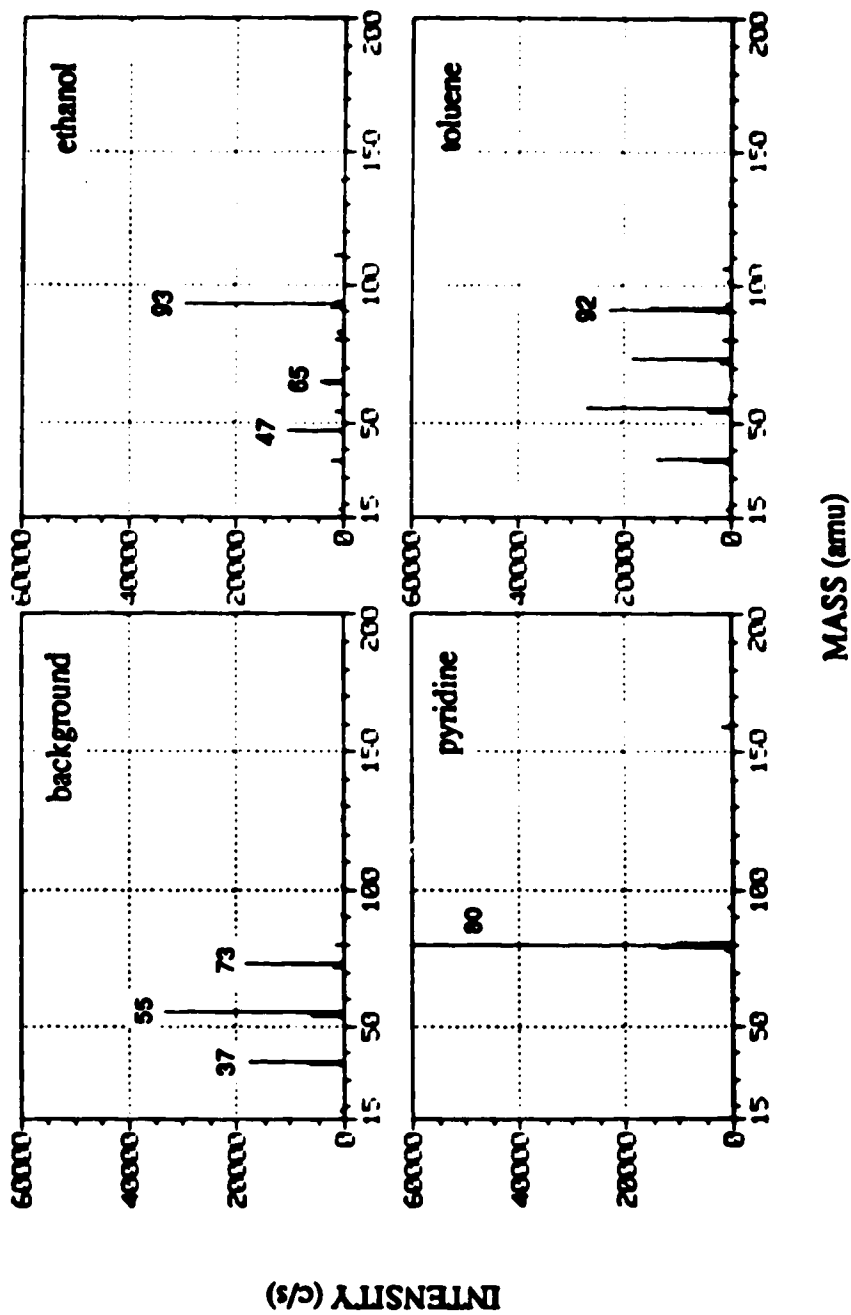


Figure A-5. Background spectrum of the APCI.



**Figure A-6.** Mass spectra for ethanol, pyridine, and toluene. The background spectrum is included for comparison.

The major peak for pyridine spectra is  $m/z$  80, the  $M+1$  ion. The actual peak intensity is about 1000000 c/s. The spectrum only shows the lower part of the peaks, so that the clean background is emphasized. Hydronium ions were not detected in the presence of pyridine vapour.

The spectrum of toluene consists of peaks for  $M$  and  $M+1$  ( $m/z$  92 and 93) as well as those of hydronium ions. The sensitivity of an analyte depends on its gas phase basicity (GB) and the hydration energy of the ion [15]. The lower sensitivity of toluene is due to its low GB (182.0 kcal/mole, compared to 213.1 and 180.2 kcal/mole for pyridine and ethanol, respectively [16]) and poor hydration of carbon bases. Sensitivity enhancements of compounds of GB lower than 200 kcal/mole were obtained at high temperatures in the APCI [17].

The spectra in Figure A-6 show the ability of APCI/MS for the detection of volatile organic compounds, with various degrees of sensitivity. However, samples of low vapour pressure, e.g. trace organic in aqueous solution, will be difficult to analyse. This problem is overcome with the nebulizer/spray chamber/heated tube solution introduction system. The spectrum of 0.001 M of glucose ( $C_6H_{12}O_6$ ) in aqueous solution shown in Figure A-7 was obtained with this mode of sample introduction. The major peaks are  $m/z$  163, 181, and 199, which are  $(M+1)-18$ ,  $M+1$ , and  $(M+1)+18$  respectively.

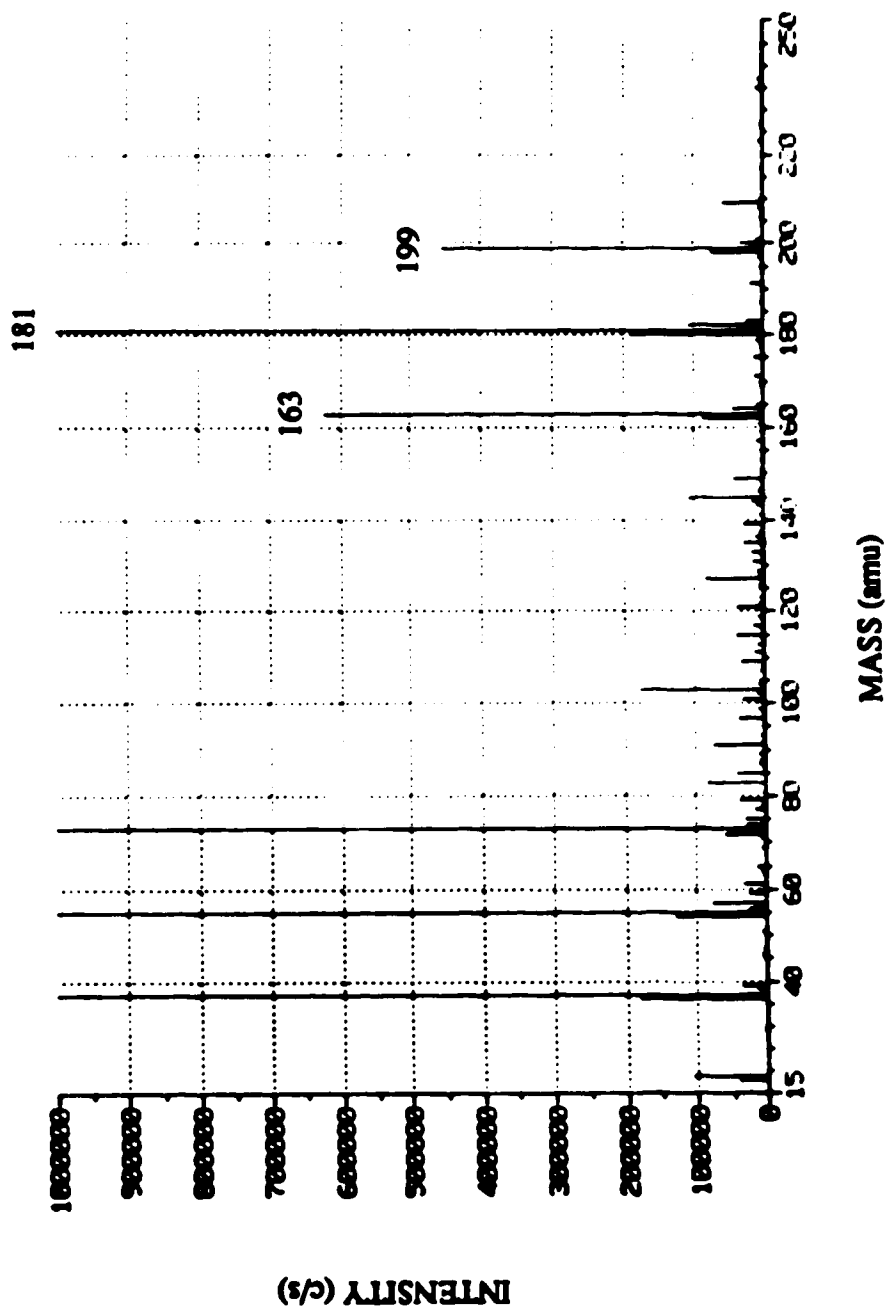


**Figure A-7.** Mass spectrum for 0.001 M of aqueous glucose solution with the nebulizer/spray chamber/heated tube as the sample introduction system.

A more dramatic example is shown in Figure A-8. Coffee from the cafeteria was diluted 1:2 with water and nebulized in the APCI. The dilution is to reduce the amount of coffee introduced, so that peak of  $m/z$  195 is not saturated. This peak corresponds to the  $M+1$  ion of caffeine (1,3,7-trimethylxanthene,  $MW = 194$ ). The ion of  $m/z$  195 is identified by comparing its CAD spectrum to the library stored in the fixed disk of the PDP 11/23 microcomputer of the TAGA 6000e. The CAD spectra of  $m/z$  195 and that of caffeine in the library are closely matched (Figure A-9).

A library of CAD spectra of 21 amino acids (listed in Table A-2) have been built for the identification of these organic compounds in aqueous solution. The library of each compound consists of a conventional mass spectrum and a CAD spectrum of the molecular ion. The concentration of each amino acid was adjusted so that the intensity of the molecular ion peak in the conventional mass spectrum was in the range of  $10^5$  to  $10^6$  count/sec. This ensured positive identification of the ion and sufficient amount of molecular ions available for CAD. The conventional mass spectrum and the CAD spectrum of tyrosine are shown in Figure A-10 as an example.

Two sets of lens setting were used to obtain these spectra. The first set (IN=650, OR=40, CB=33) have lower ion energy, and was used for the molecular ion spectrum collection. The second set (IN=700, OR=70, CB=60) have higher



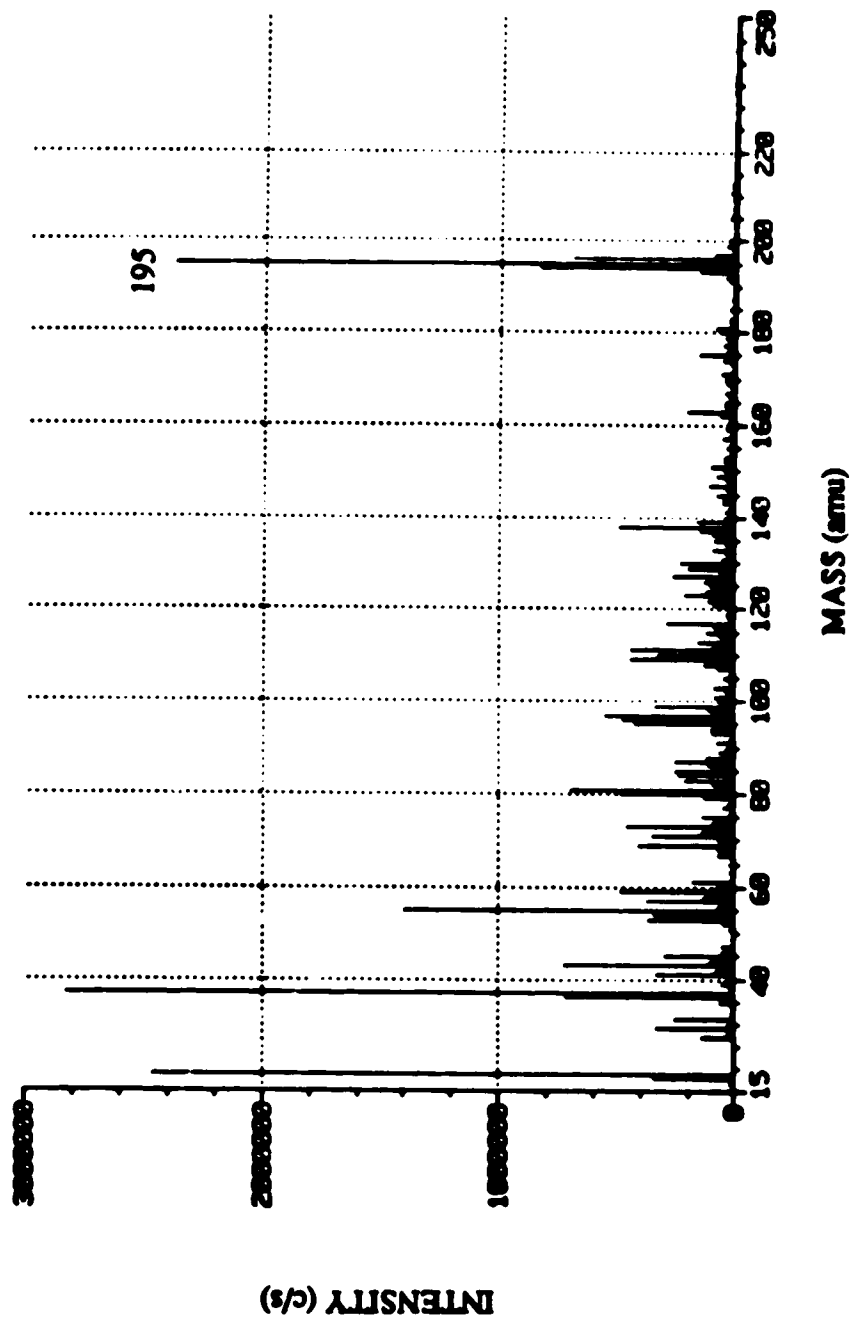


Figure A-8. Mass spectrum for coffee. The peak at  $m/z$  195 is from caffeine.

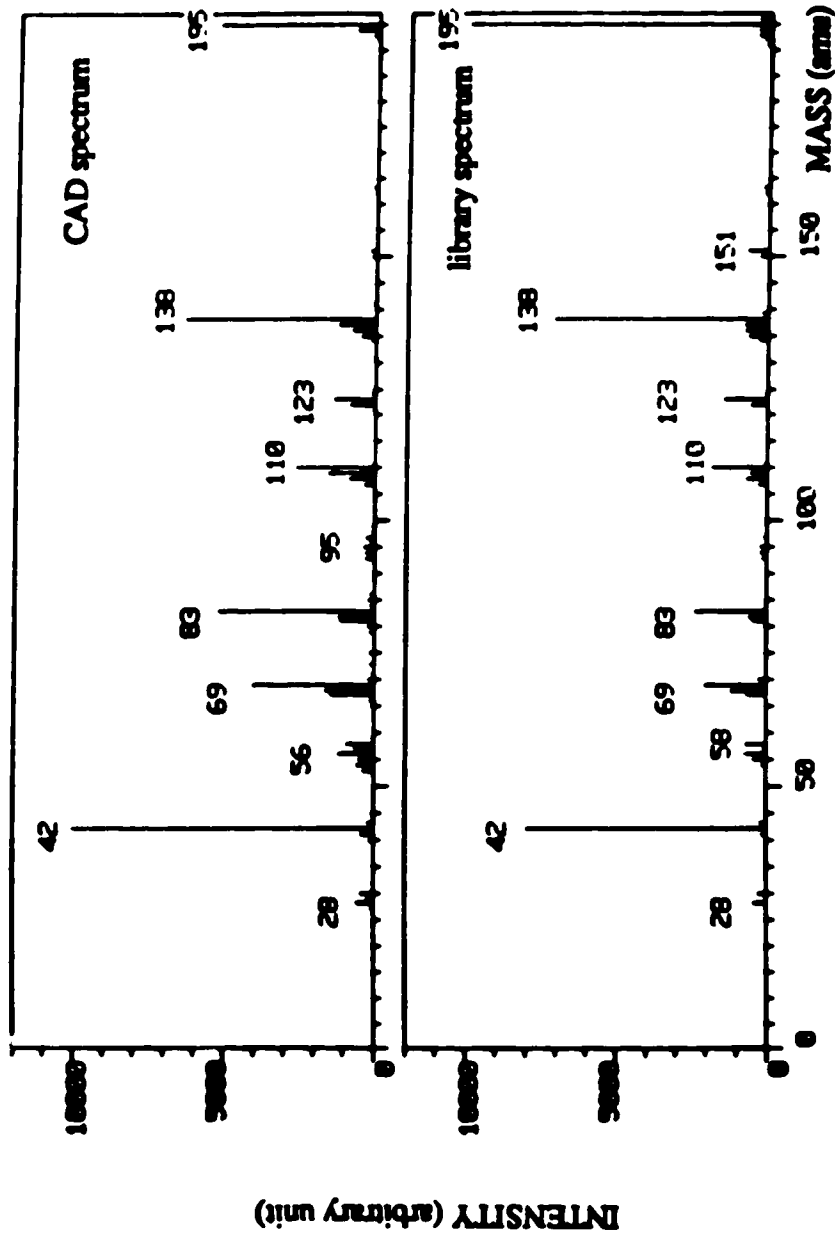


Figure A-9. CAD spectrum for m/z 195 from coffee obtained experimentally (above) and CAD spectrum for caffeine stored in the spectrum library (below).

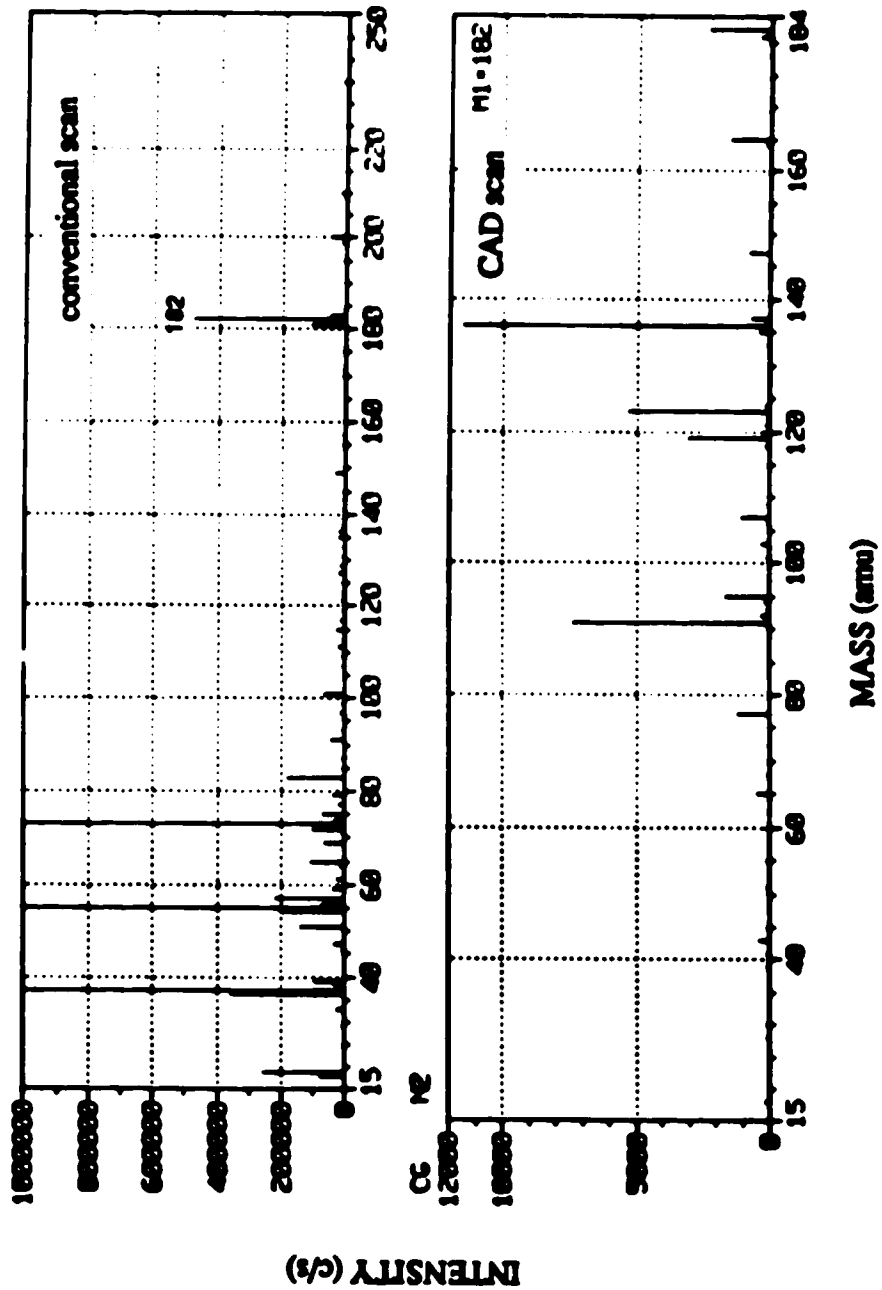


Figure A-10. Mass spectrum (above) and daughter spectrum for tyrosine.

**Table A-2.** List of the candidate amino acids and their molecular weights.

Amino acid	Molecular weight
DL-Alanine	89.09
L-Arginine	174.21
DL-Aspartic acid	133.10
L-(+)-Cysteine	121.15
L-Glutamic acid	147.13
Glycine	75.07
L-(-)-Histidine	155.16
DL-Leucine	131.18
DL-iso-Leucine	131.18
L-(+)-Norleucine	131.18
L-(+)-Lysine monohydrochloride	182.65 (146) *
DL-Methionine	149.22
DL-Phenylalanine	165.19
L-Proline	115.13
DL-Serine	105.09
DL-Threonine	119.12
DL-Tryptophan	204.22
L-(-)-Tyrosine	181.19
DL-Valine	117.15
L-(+)-Norvaline	117.15

\* without hydrochloride

ion energy, required for CAD. If the second set was used for the conventional scan, fragmented ions would be observed as well as the molecular ion (Figure A-11).

The ability of the APCI/MS/MS to identify compounds in a mixture was demonstrated by analysis of a mixture of four amino acids: glycine, histidine, tryptophan, and tyrosine, with the system. The conventional mass spectrum of this sample was shown in Figure A-12. The molecular ions of these amino acids are readily identified in the mass spectrum. The identification of the acids are confirmed by their CAD spectra (Figure A-13).

Isomers are difficult to identify, however. Valine and norvaline have the same molecular weight, and their CAD spectra are similar with only subtle difference (Figure A-14). This is because the fragmentation mainly occurs at the carboxyl group, not in the hydrocarbon segment. Another example is the isomers of leucine (Figure A-15). Separation of the isomers before analysis is necessary in these cases.

#### **A.4 Quantitative Analysis**

For a conventional scan, there is usually more than one ion originated from a single analyte. Therefore, it is necessary to consider all the dominant ions for quantitative analysis.

The major ion species of histidine are  $m/z$  155 and 156, the molecular ion and the protonated molecular ion.

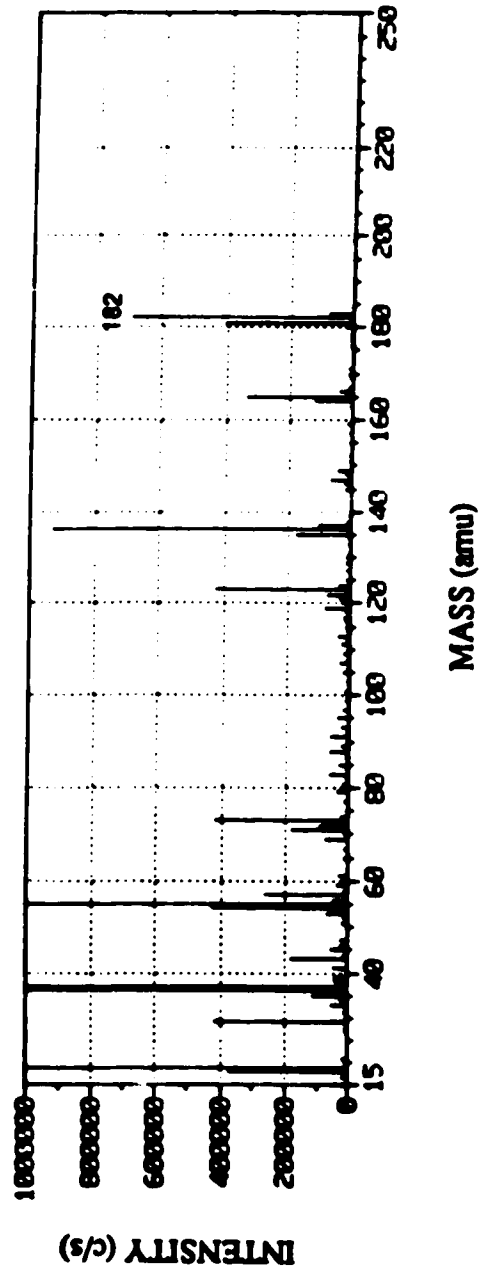


Figure A-11. Mass spectrum for the same tyrosine solution in Figure A-10. Higher ion energy was used.

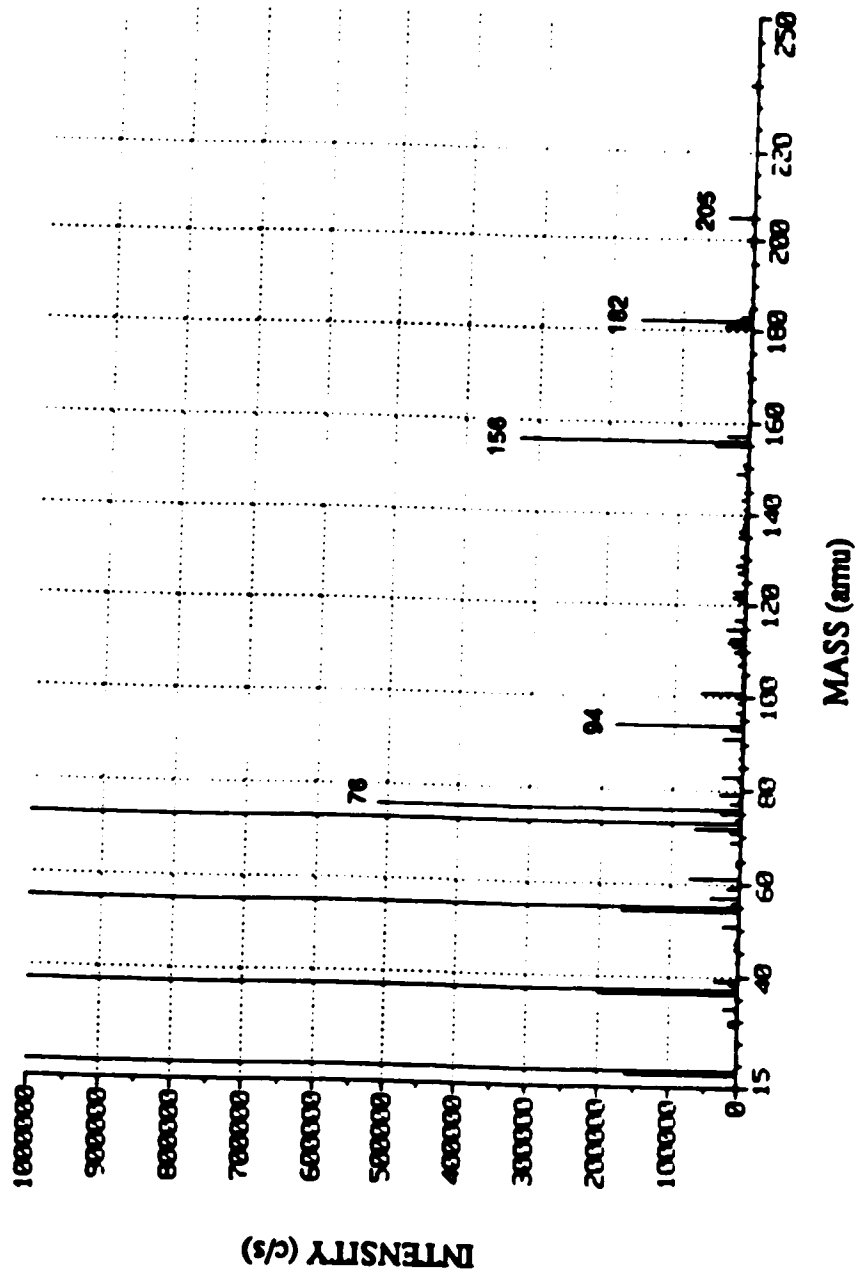
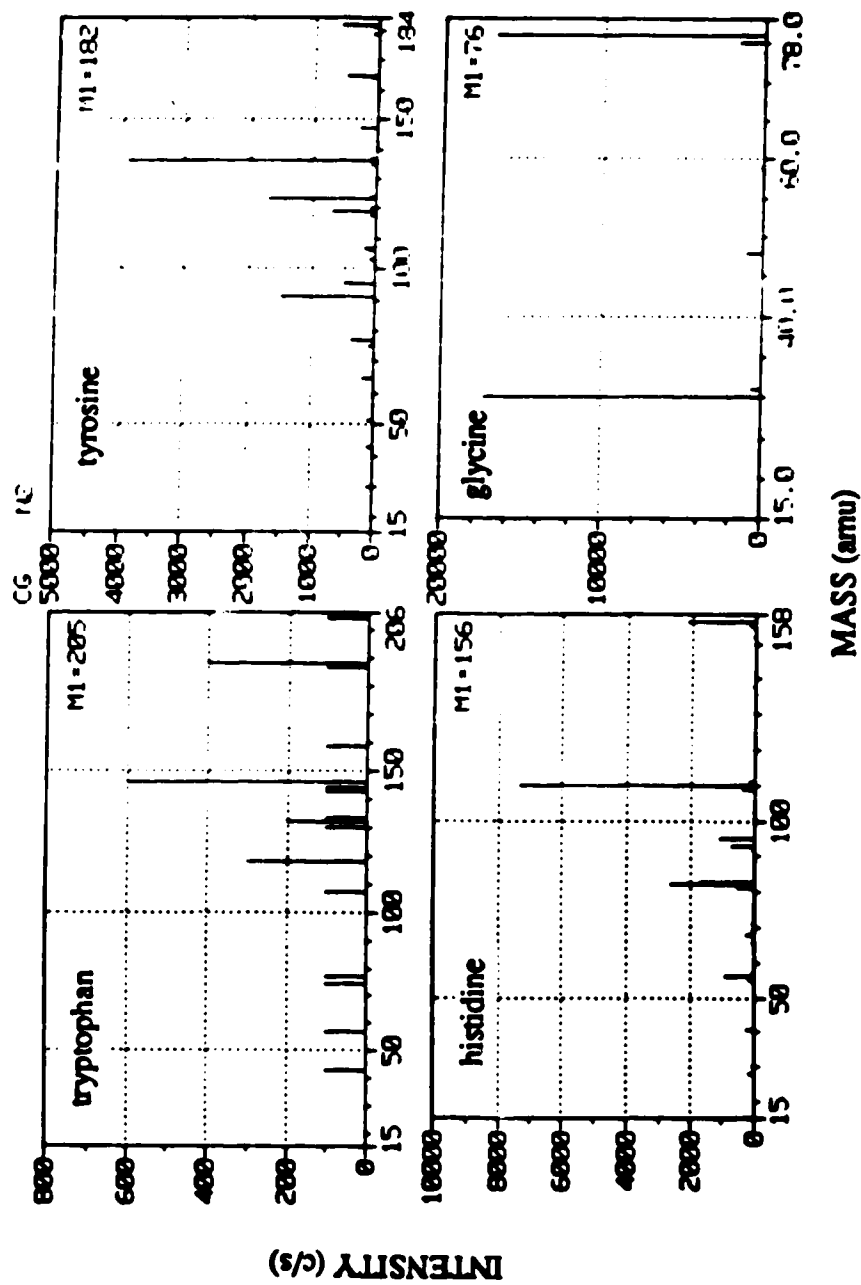
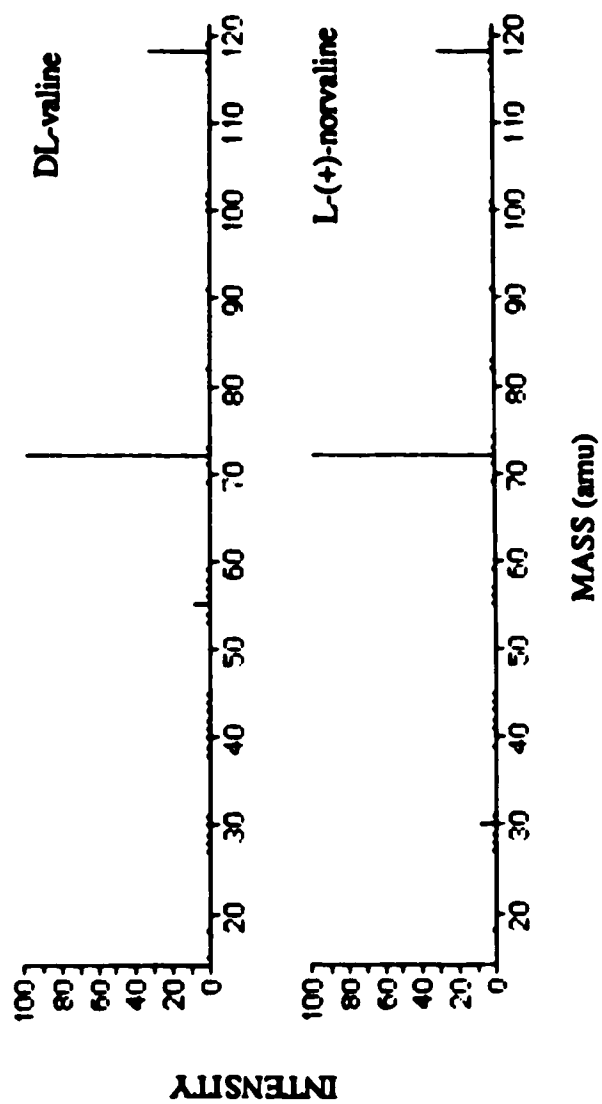


Figure A-12. Mass spectrum for a mixture of four amino acids: glycine (M=75), histidine (M=155), tryptophan (M=204), and tyrosine (M=181).



**Figure A-13.** CAD spectra for glycine, histidine, tryptophan, and tyrosine in a mixture of the amino acids.





**Figure A-14.** CAD spectra for valine and norvaline.

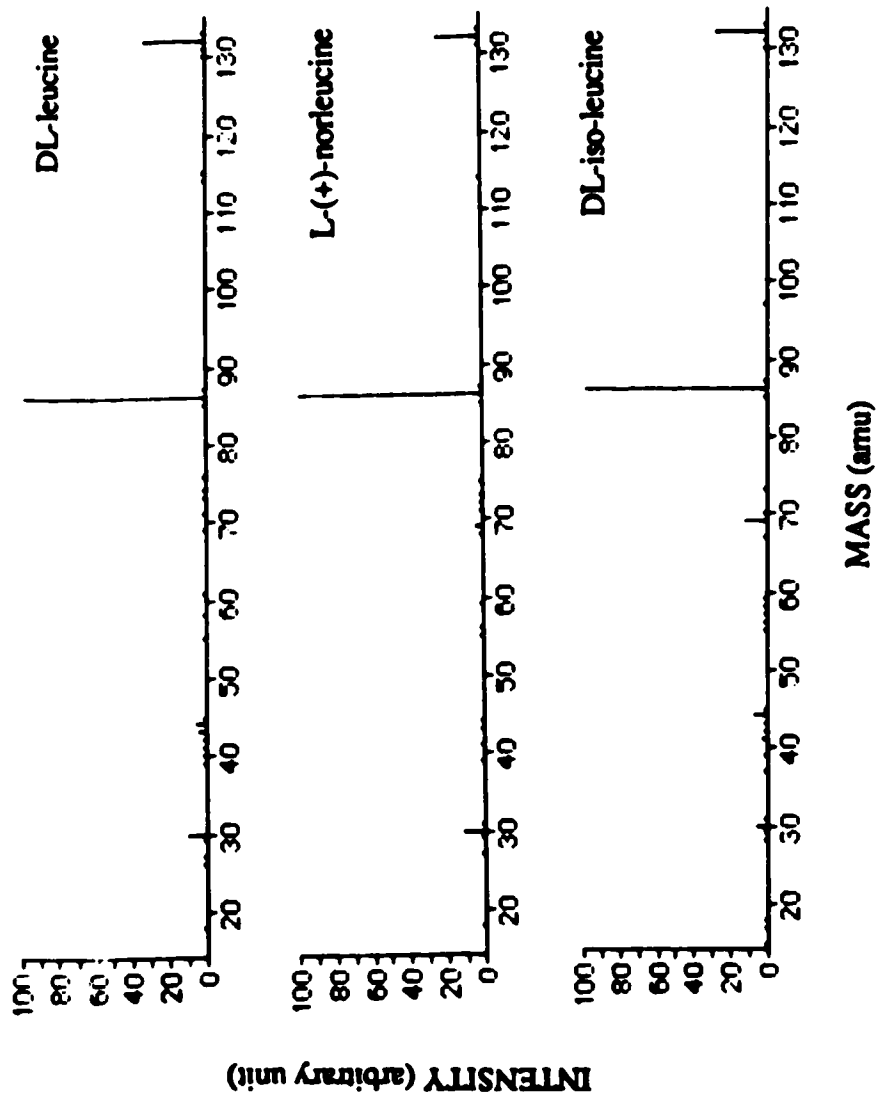
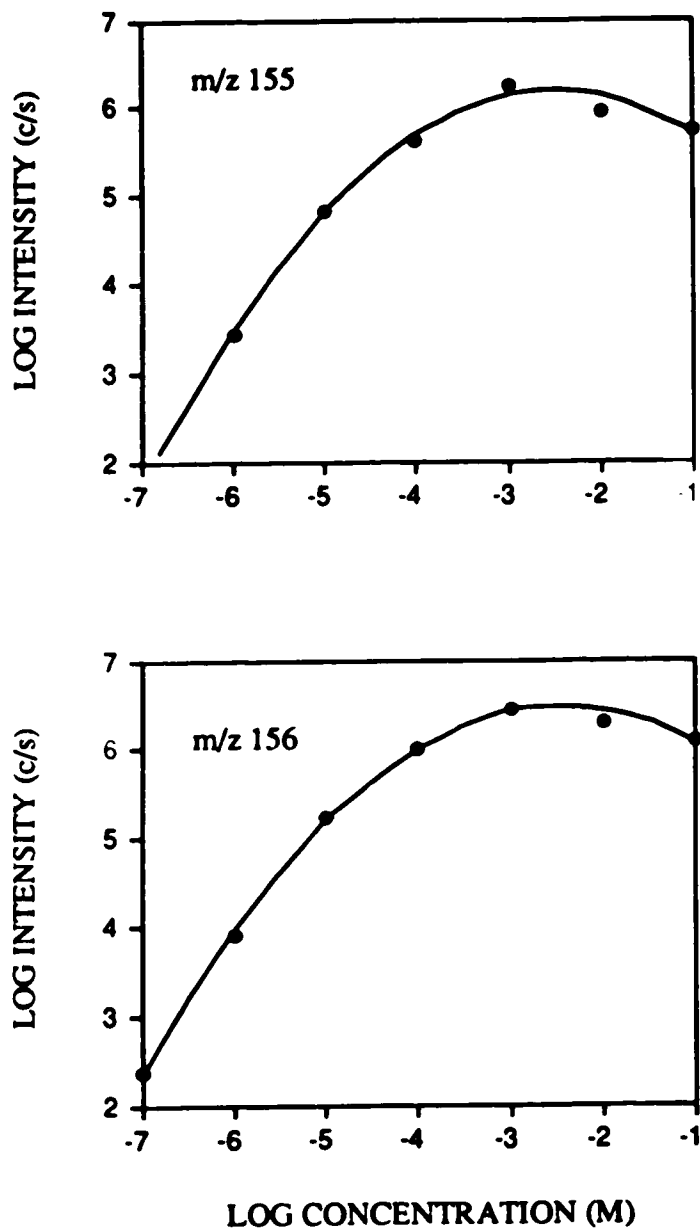


Figure A-15. CAD spectra for leucine, isoleucine, and norleucine.

Calibration curves for these two ions are shown in Figure A-16. Stock standard solution (0.1 M) was prepared by dissolving histidine in distilled water. Other solutions were obtained by successive dilution. Samples were introduced with the pneumatic nebulizer/spray chamber/heated tube system. The signal was obtained by integrating 0.1 second (MTL) alternatively between the signals of the two ions for a total time of 2.0 minutes (TT), under the multiple conventional scan (MI) mode. 552 integrations (or sequences, in TAGA's jargon) are obtained for each ion, at one concentration. The product of MTL  $\times$  number of integrations  $\times$  2 equals 110.4 seconds, which is smaller than 120 sec (2 min.), because of the sequential nature of the scan.

The two curves have similar shape: rise in a monotonic fashion at the beginning, reach maximum at concentration of about 0.001 M, then sensitivities drop at higher concentration. The signal strength of m/z 156 is also higher, with the signal ratio between the two ions ranging from 2.8 to 1.6.

The mechanism for the reduction of sensitivity at high concentration is uncertain. One speculation is that a large amount of the ions saturated the channel electron detector (at 0.001 M, intensity of m/z 156 is  $>2 \times 10^6$  count/s). If this is the case, reducing transmission efficiency ( $T_m$ ) of the ions will extend the working range of the calibration curve to higher concentration.  $T_m$  was reduced by scanning both quadrupole 1 and 3 simultaneously. The resulting calibration curves are shown in Figure A-17. The sensitivity is reduced



**Figure A-16.** Calibration curves of Histidine; top curve for ion of  $m/z=155$ , bottom curve for ion of  $m/z=156$ . Samples are introduced with pneumatic nebulizer.

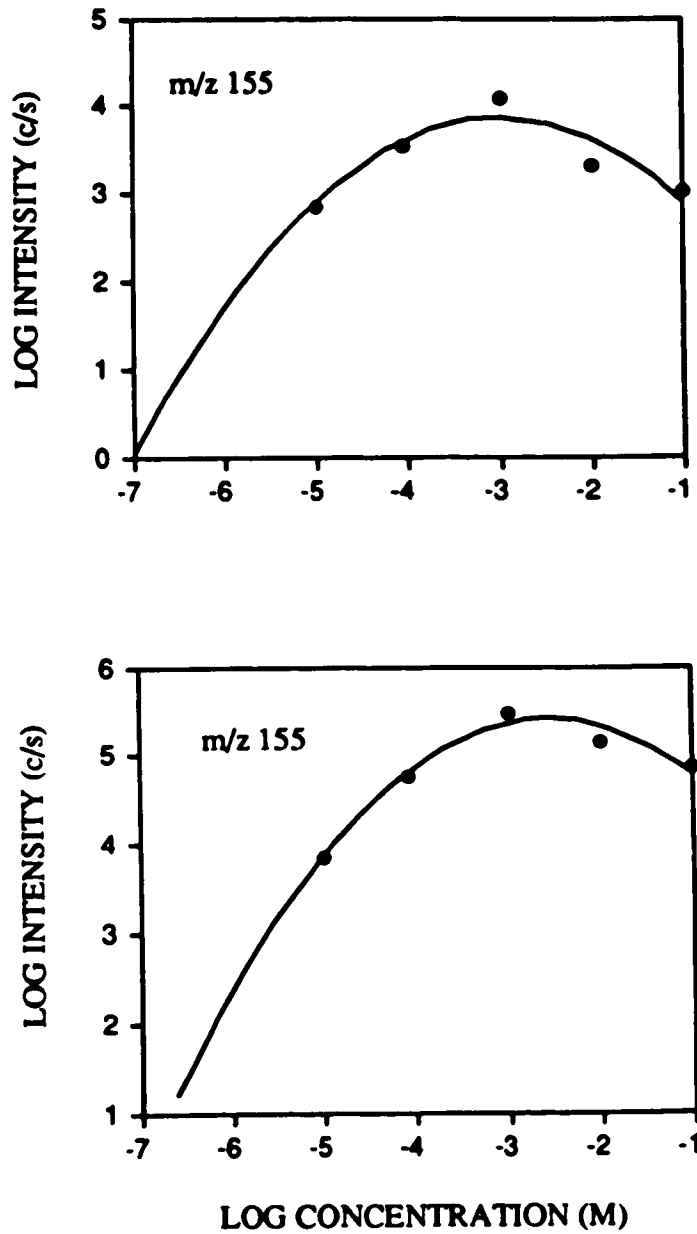


**Figure A-17.** Calibration curves of Histidine with both quadrupoles Q1 and Q3 operating simultaneously. Samples are introduced with pneumatic nebulizer.

by about an order of magnitude, but the trend of the curve remains the same. Therefore, the intensity roll-off is *not* due to the saturation of the detector.

Calibration curves with the intensity of both ions combined are shown in Figure A-18. The curves have higher sensitivity and similar trends compared to those of the individual ions.

The calibration curves demonstrate that correlation between analyte concentration *in solution* to that of ion intensity is possible. However, the relation is not linear and quite complicated.

Calibration curves for histidine introduced into the APCI with the ultrasonic nebulizer/heated tube system are shown in Figure A-19 and A-20. The shape of the curves and ion sensitivity are similar to those of the pneumatic nebulizer system. Therefore, both techniques are equally efficient for sample introduction.

The calibration curves for glucose are more complicated (Figure A-21 and A-22), but the general trend is similar to those of histidine. Major species included ions of  $m/z$  181, 163, and 198, i.e.  $M+1$ ,  $(M+1)-18$ , and  $M+18$ , respectively. The roll-off of intensity at high concentration is comparable to the histidine calibration curves, but the sensitivity is also reduced at low concentration.

For histidine and glucose, it has been demonstrated that fairly low concentration of the analytes in solution ( $10^{-7}$  M) can be measured with the APCI/MS technique. However, it

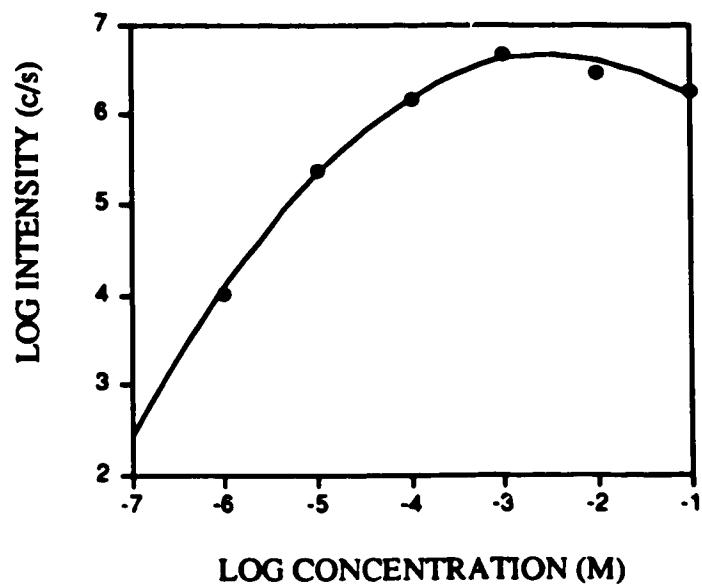


**Figure A-18.** Calibration curves of Histidine; the intensity is the sum of that of ions  $m/z$  155 and 156. Samples are introduced with pneumatic nebulizer.

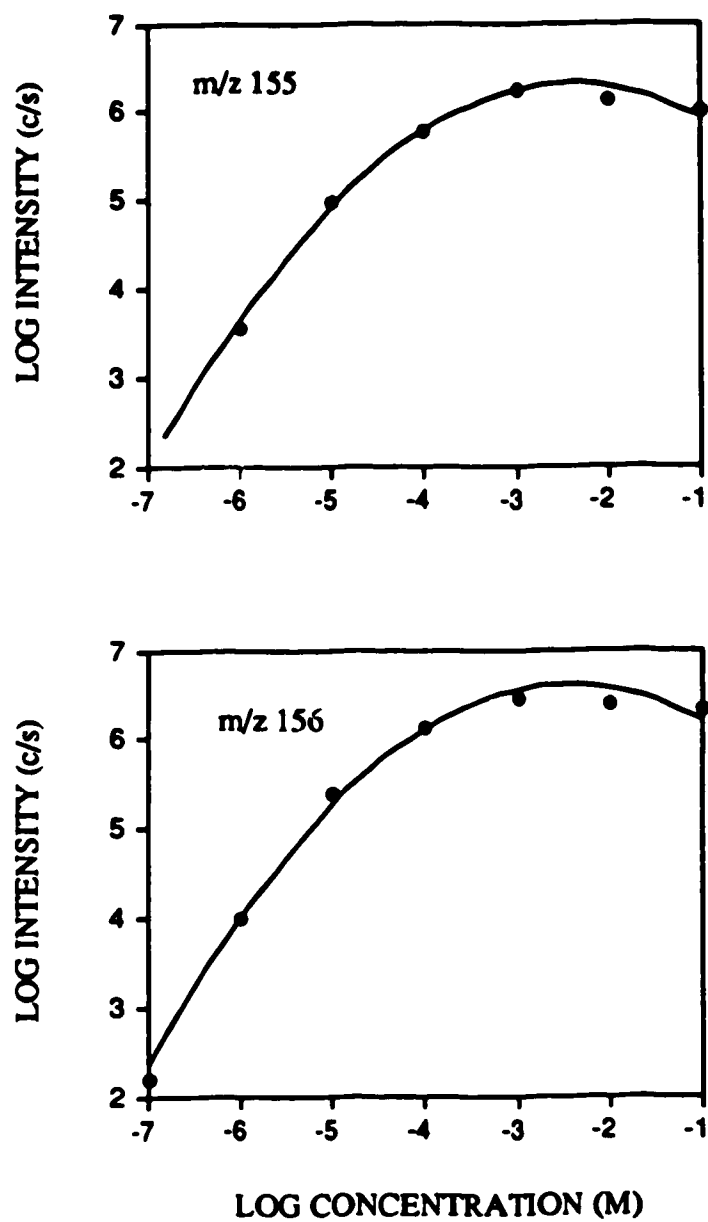


**Figure A-19.** Calibration curves of Histidine; top curve for ion of  $m/z=155$ , bottom curve for ion of  $m/z=156$ . Samples are introduced with ultrasonic nebulizer.



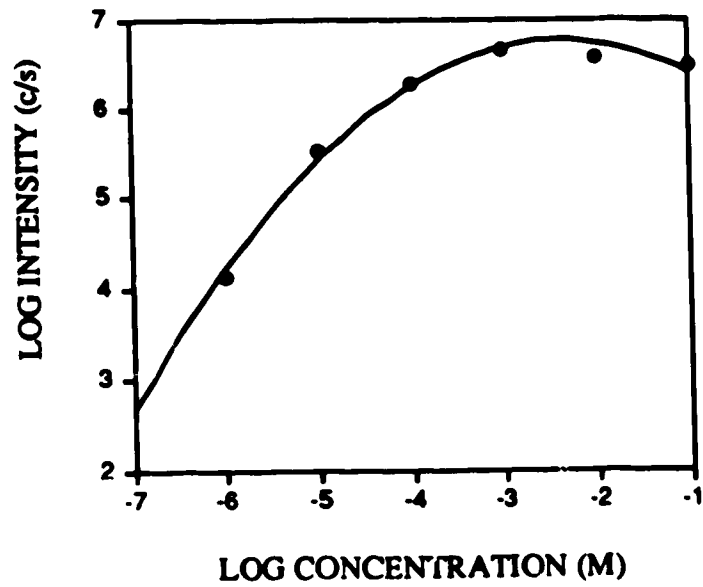


**Figure A-20.** Calibration curves of Histidine; the intensity is the sum of that of ions  $m/z$  155 and 156. Samples are introduced with ultrasonic nebulizer.

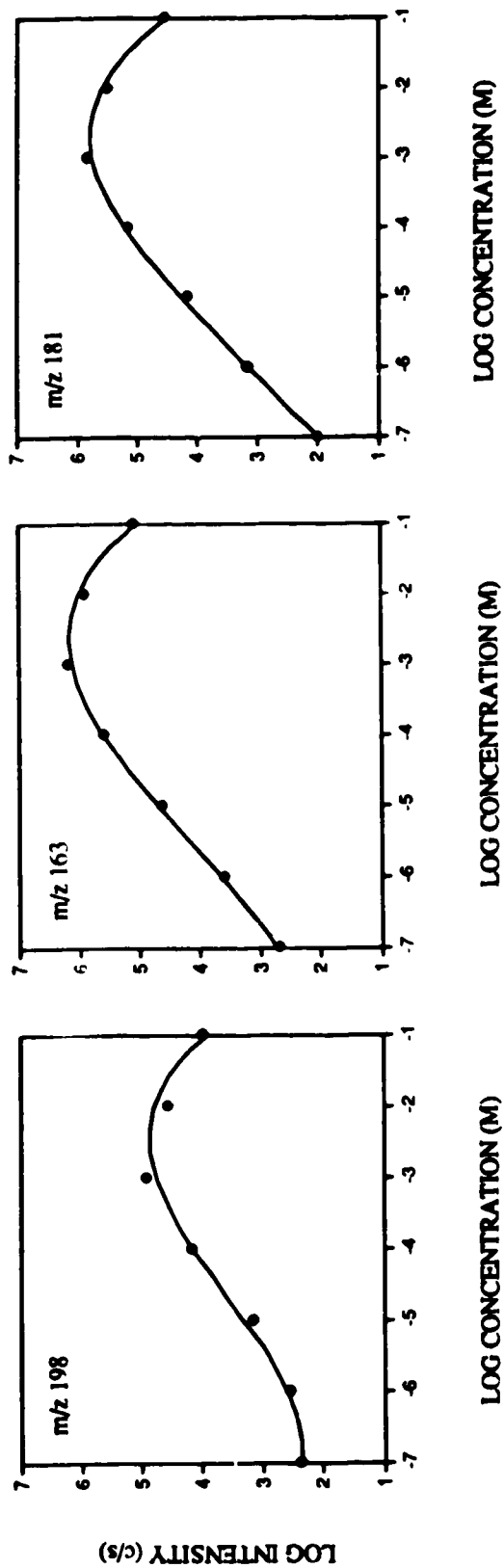


**Figure A-21.** Calibration curves of glucose; from left to right, for ions of  $m/z=181$ , 163, and 198 respectively. Samples are introduced with pneumatic nebulizer.

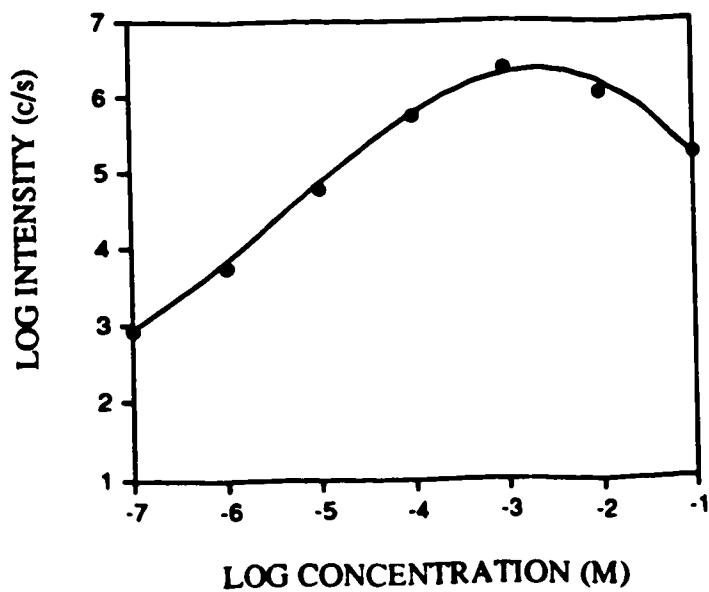


**Figure A-22.** Calibration curves of glucose; the intensity is the sum of that of ions  $m/z$  163, 181 and 198. Samples are introduced with pneumatic nebulizer.

should be emphasized that the standards are simple aqueous solution, with no solute other than the analyte. Drastic change in ion intensity and their ratio may occur in the presence of other components. The change of ion intensity of glucose ( $\sim 10^{-4}$  M) in 0.1 M ammonium acetate buffer at different pH is shown in Figure A-23. The fourfold increase of intensity for m/z 198 is possibly due to the formation of glucose-ammonium cluster. Therefore, interpretation of ion intensity should proceed with caution.

#### **A.5 Conclusion**

Both qualitative and quantitative analyses have been performed with the nebulizer/heated tube sample introduction technique for the APCI. The system has been proved to be simple and effective.

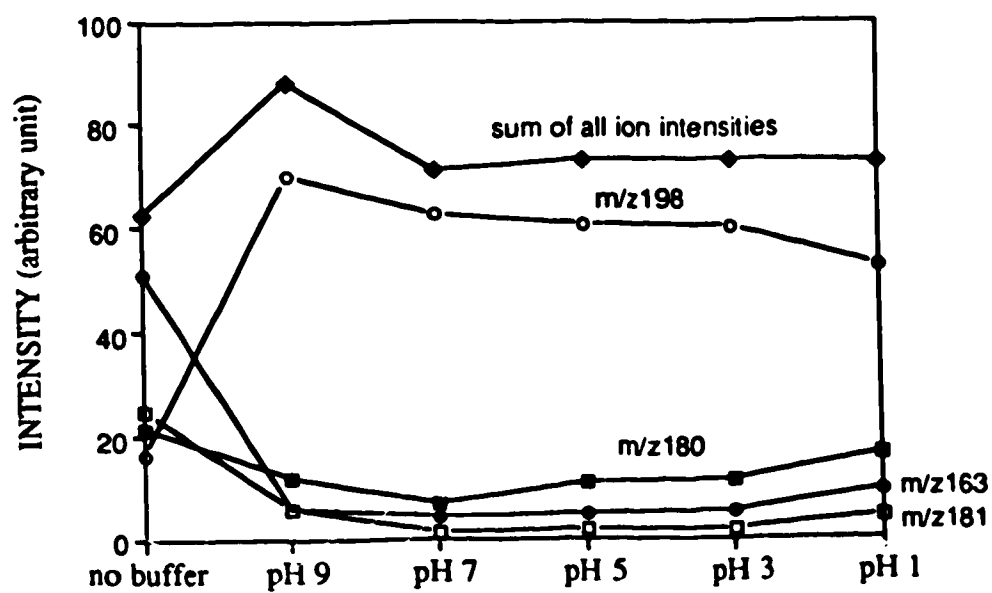


**Figure A-23.** Intensity of ions of glucose in 0.1 M of ammonium acetate buffer at different pH. The pH of aqueous glucose solution without buffer is 6.6.

### References

1. E.C. Horning, M.G. Horning, D.I. Carroll, I. Dzidic, and R.N. Stillwell, *Anal. Chem.* **45**, 936 (1973)
2. N.M. Reid, J.A. Buckley, J.B. French, C.C. Poon, *Adv. Mass Spectrom.* **8b**, 1843 (1979)
3. D.I. Carroll, I. Dzidic, E.C. Horning, and R.N. Stillwell, *Appl. Spectrosc. Rev.* **17**, 337 (1981)
4. C.J. Proctor and J.F.J. Todd, *Org. Mass Spectrom.* **18**, 509 (1983)
5. J.D. Henion, B.A. Thomson, and P.H. Dawson, *Anal. Chem.* **54**, 4<sup>e</sup> (1982)
6. H. Kambara, *Anal. Chem.* **54**, 143 (1982)
7. A.J. Alexander, P. Kebarle, A.F. Fuciarelli, and J.A. Raleigh, *Anal. Chem.* **59**, 2484 (1987)
8. A. Good, D.A. Durden, and P. Kebarle, *J. Chem. Phys.* **52**, 222 (1970)
9. Y.K. Lau, S. Ikuta, and P. Kebarle, *J. Am. Chem. Soc.* **104**, 1462 (1982)
10. J.D. Henion, *Anal. Chem.* **50**, 1687 (1978)
11. P. Arpino and G. Guiochon, *Anal. Chem.* **51**, 682A (1979)
12. F.W. McLafferty, ed., *Tandem Mass Spectrometry*, John Wiley and Sons, New York (1983)
13. J.W.H. Lam, *Characterization of ICP-MS Using Mixed Gas*, Ph.D. Thesis, University of Alberta (1988)

14. R.M. Belchamber, 'Noise Characterization of an ICP for Atomic Emission Analysis', Ph.D. Thesis, University of Alberta (1981)
15. J. Sunner, G. Nicol, and P. Kebarle, Anal. Chem. **60**, 1300 (1988)
16. S.G. Lias, J.F. Liebman, and R.D. Levin, J. Phys. Chem. Ref. Data **13**, 695 (1984)
17. J. Sunner, M.G. Ikonou, and P. Kebarle, Anal. Chem. **60**, 1308 (1988)

## Appendix B. Program Listing

The programs developed for the DSI system are listed in the following pages. The configuration of the Apple II Plus computer is listed in the Table B-1. This configuration should be followed so that the programs would run properly. All programs are stored in a disk called "DSI system disk" which should be placed in Drive 1. A blank disk in Drive 2 is required for data storage.

**Table B-1.** Apple II Plus configuration for the DSI system

---

Slot #	Peripheral Cards	Function
1	Grappler+ parallel printer card	robot interface
2	Super Serial Card	HW 7470A plotter
3	Videoterm 80 Column Card	text display*
4	A6 T/D Card	stepper motor
5	AI13 board	A/D conversion
6	Disk II Controller Card	floppy disk drive
7	Parallel Printer Card	Centronic printer

---

\* a switch is used to switch between the video outputs of the Apple II and the Videoterm card. The Apple video output is always in graphic mode for emission signal time profile display. The Videoterm output is used for 80 column text display.



## PROGRAM DA.MAIN

```

100 REM ***DIRECT SAMPLE INSERTION SYSTEM DATA ACQUISITION***
110 HIMEM: 3604P: REM $8CD0
120 D$ = CHR$ (4)
130 PRINT D$;"PR#3": REM INITIALIZE 80-COLUMN CARD
140 REM ***PARAMETER PREPARATION***
150 DIM A%(3000),C%(6),P(3),W(3),WT(30),CN(30,6),GN(30,6),EL$(30,6)
160 GOSUB 1000: REM CAPTION
170 GOSUB 1040: REM PARAMETER
180 GOSUB 1740: REM LOAD SUBROUTINE
190 REM ***DATA ACQUISITION***
200 F = 1: REM FIRST SAMPLE NUMBER
210 FOR CT = F TO N
220 GOSUB 1000: REM SCREEN CAPTION
230 PRINT "sample #";CT;":      push any key when ready";
240 GET C$: PRINT : PRINT CHR$ (12)
250 IF RB$ < > "N" THEN GOSUB 1830: REM ROBOT
260 M% = 0:D% = 1
270 FOR I = 1 TO N2
280 CALL 36864: & MOTA,P(I),D%,M%: REM STEPPER MOTOR
290 IF I = N2 THEN 320
300 IF PEEK (35392) = 1 THEN 300: REM CHECK MOTOR STATUS
310 IF W(I) > 0 THEN CALL 36768 + (I - 1) * 48: REM DELAY TIMER
320 NEXT
330 CALL 36608: REM INITIALIZE AY13
340 M% = 0:D% = 0
350 CALL 36864: & MOTA,P1,D%,M%: REM STEPPER MOTOR
360 IF PEEK (35392) = 1 THEN 360
370 NE$ = N$ + "/"# + STR$ (CT): REM DATA FILE NAME
380 GOSUB 1000: REM SCREEN CAPTION
390 GOSUB 2500: REM SPACE ON DISK
400 PRINT "name of file=" ;NE$
410 PRINT "data transfering to disk"
420 PRINT D$;"OPEN";NE$;"D2": REM ALL DATA FILES IN DRIVE 2
430 PRINT D$;"DELETE";NE$
440 PRINT D$;"OPEN";NE$
450 PRINT D$;"WRITE";NE$
460 PRINT N1$
470 K1 = (R - 1) * N1
480 FOR I = 1 TO N1
490 K2 = K1 + I
500 FOR J = I TO K2 STEP N1
510 PRINT A%(J)
520 NEXT J
530 NEXT I
540 PRINT D$;"CLOSE";NE$
550 PRINT : PRINT "data transfer finished";
560 CALL 36864: & MOTA,P2,D%,M%: REM STEPPER MOTOR BACK TO BASE
570 IF PEEK (35392) = 1 THEN 570
580 IF RB$ < > "N" THEN PRINT CHR$ (12): GOSUB 1900
590 GOSUB 1000: REM SCREEN CAPTION
600 PRINT "sample #";CT
610 PRINT "<1> plot data on screen,"
620 PRINT "<2> continue, or"
630 PRINT "<3> exit."
640 PRINT : INPUT "enter number of your choice ";C
650 ON C GOTO 1970,660,690

```

```

660 POKE 36352,LO: POKE 36353,HI: REM HI-BYTE AND LO-BYTE OF NUMBER OF
DATA POINTS
670 NEXT CT
680 END
690 REM ***HOME ROBOT***
700 IF RBS = "N" THEN 680
710 IF CT = N THEN 680
720 PRINT D$;"PR#1"
730 PRINT "M89": PRINT "N"
740 PRINT D$;"PR#3"
750 GOTO 680
1000 REM ***CAPTION***
1010 PRINT CHR$(12): HOME
1020 PRINT : PRINT TAB(20)"*** ICP-DSIS DATA ACQUISITION ***": PRINT
1030 RETURN
1040 REM ***PARAMETER OF MOTOR, AI13 AND SAMPLE***
1050 INPUT "name of parameter file=" ;N1$
1060 PRINT D$;"OPEN";N1$;"D2"
1070 PRINT D$;"READ";N1$
1080 INPUT N2
1090 FOR I = 1 TO N2
1100 INPUT P(I): INPUT W(I)
1110 NEXT I
1120 INPUT N1
1130 INPUT R: INPUT HT: INPUT LO
1140 FOR I = 1 TO N1
1150 INPUT C$(I)
1160 NEXT I
1170 INPUT N
1180 FOR I = 1 TO N
1190 INPUT WT(I)
1200 FOR J = 1 TO N1
1210 INPUT ELS(I,J)
1220 NEXT J
1230 FOR J = 1 TO N1
1240 INPUT CN(I,J): INPUT GN(I,J)
1250 NEXT J
1260 NEXT I
1270 PRINT D$;"CLOSE";N1$
1280 GOSUB 1000
1290 PRINT "parameter of stepper motor:-"
1300 PRINT TAB(4)"stage #"; TAB(4)"# of pulse"; TAB(4)"waiting time
(sec)"
1310 PRINT TAB(4)"-----"; TAB(4)"-----"; TAB(4)"-----"
-----"
1320 FOR I = 1 TO N2
1330 C$ = STR$(P(I))
1340 L = LEN(C$):TB = 18 - L
1350 PRINT TAB(6)I; TAB(10)P(I); TAB(TB)W(I)
1360 NEXT
1370 PRINT : PRINT "parameter of AI13:-"
1380 PRINT TAB(4)"scan #"; TAB(4)"channel #"
1390 PRINT TAB(4)"-----"
-----"
1400 FOR I = 1 TO N1
1410 PRINT TAB(5)I; TAB(9)C$(I)
1420 NEXT
1430 PRINT : INPUT "confirm (y/n)? ";C$
1440 IF C$ = "N" THEN 1050

```

```

1450 GOSUB 1000
1460 PRINT "parameter of sample:--"
1470 FOR I = 1 TO N
1480 PRINT "sample #";I; TAB( 6)"weight= ";WT(I);" mg"
1490 PRINT TAB( 4)"channel #"; TAB( 4)"element"; TAB( 4)"conc'n
      (ppm)"; TAB( 4)"preamp gain"
1500 PRINT TAB( 4)"-----"; TAB( 4)"-----"; TAB( 4)"-----"
      "; TAB( 4)"-----"
1510 FOR J = 1 TO N1
1520 L1 = LEN (EL$(I,J)):C$ = STR$ (CN(I,J)):L2 = LEN (C$)
1530 TB(1) = 13 - L1:TB(2) = 16 - L2
1540 PRINT TAB( 8)C$(J); TAB( 10)EL$(I,J);
1550 PRINT TAB( TB(1))CN(I,J); TAB( TB(2))GN(I,J)
1560 NEXT J
1570 PRINT : PRINT
1580 IF I / 2 - INT ( I / 2 ) = 0 THEN PRINT "push any key to
      continue";: GET C$: GOSUB 1000
1590 NEXT I
1600 PRINT : INPUT "confirm (y/n)? ";C$
1610 IF C$ = "N" THEN 1050
1620 POKE 7,N1
1630 POKE 36352,LO: POKE 36353,HI
1640 FOR I = 1 TO N1
1650 POKE (36353 + I),C$(I) + 16: REM GAIN="1"
1660 NEXT I
1670 POKE 206,W(1): POKE 207,W(2)
1680 P = 0
1690 FOR I = 1 TO N2:P = P + P(1): NEXT
1700 P1 = INT ( P / 2 ):P2 = INT ( P / 2 + .5)
1710 INPUT "using robot (y/n)? ";RBS$
1720 PRINT : INPUT "generic name of data file= ";N$
1730 RETURN
1740 REM ***LOADING SUBROUTINE***
1750 PRINT : PRINT "loading subroutines for DSIS..."
1760 PRINT D$;"BLOAD DAI13.OBJ,D1": REM ALL SUBROUTINES IN DRIVE 1
1770 PRINT D$;"BLOAD TIMER1.OBJ"
1780 PRINT D$;"BLOAD TIMER2.OBJ"
1790 PRINT D$;"BLOAD AMPRAMP"
1800 PRINT D$;"BLOAD RMPDATA"
1810 PRINT D$;"BLOAD CTRL.IOB.CHAR"
1820 RETURN
1830 REM ***BRING CUP TO DSID***
1840 PRINT D$;"PR#1"
1850 FG = 1: IF CT = F THEN FG = 0
1860 GOSUB 2190: REM FROM HOLDER
1870 GOSUB 2380: REM TO DSID
1880 PRINT D$;"PR#3"
1890 RETURN
1900 REM ***RETURN CUP***
1910 PRINT D$;"PR#1"
1920 FG = 1: IF CT = N THEN FG = 0
1930 GOSUB 2440: REM FROM DSID
1940 GOSUB 2280: REM TO HOLDER
1950 PRINT D$;"PR#3"
1960 RETURN
1970 REM ***PLOT RESULT***
1980 PRINT : PRINT "full scale of x-axis= ";R
1990 INPUT "ELEMENT= ";EL$

```

```

2000 I = 1: IF EL$ = EL$(CT,I) THEN 2040
2010 I = I + 1: IF I > N1 THEN PRINT "no channel for this element":
      GOTO 1990
2020 IF EL$ = EL$(CT,I) THEN 2040
2030 GOTO 2010
2040 HGR2 : HCOLOR= 3
2050 FOR J = 0 TO 150 STEP 30
2060 HPLOT 0,J TO 250,J
2070 NEXT J
2080 FOR J = 0 TO 250 STEP 50
2090 HPLOT J,0 TO J,150
2100 NEXT J
2110 X = 0:S = R / 250
2112 IF (S - INT (S)) > 0 THEN S = INT (S) + 1
2120 K = (R - 1) * N1 + I
2130 FOR J = I TO K STEP N1 * S
2140 X = X + 1
2150 Y = 150 - A%(J) * 150 / 4095
2160 HPLOT X,Y
2170 NEXT J
2180 GOTO 590
2190 REM ***GET CUP FROM SAMPLE HOLDER***
2200 IF FG = 1 THEN 2220: REM FROM OTHER POSITION
2210 PRINT "M90"
2220 PN = 4 * CT: PRINT "M";PN
2230 PN = (CT - 1) * 4 + 1: PRINT "M";PN
2240 PRINT "C"
2250 PN = (CT - 1) * 4 + 2: PRINT "M";PN
2260 PRINT "M89": PRINT "N"
2270 RETURN
2280 REM ***BRING CUP TO HOLDER***
2290 PRINT "M89"
2300 PN = (CT - 1) * 4 + 2: PRINT "M";PN
2310 FOR I = 1 TO 2
2320 PN = PN + 1
2330 PRINT "M";PN
2340 NEXT I
2350 IF FG = 1 THEN 2370
2360 PRINT "M89": PRINT "N"
2370 RETURN
2380 REM ***BRING CUP TO DSID***
2390 PRINT "M91": PRINT "M92": PRINT "M93": PRINT "M94"
2400 PRINT "M97": PRINT "M98"
2410 PRINT "M95": PRINT "M94": PRINT "M93": PRINT "M92": PRINT "M91"
2420 PRINT "N"
2430 RETURN
2440 REM ***GET CUP FROM DSID***
2450 PRINT "M91": PRINT "M92": PRINT "M93": PRINT "M94": PRINT "M95"
2460 PRINT "M96": PRINT "C": PRINT "M97"
2470 PRINT "M94": PRINT "M93": PRINT "M92": PRINT "M91"
2480 PRINT "N"
2490 RETURN
2500 REM ***SPACE ON DISK***
2510 CALL 36048: REM $8CD0 FOR CTRL SUBROUTINE
2520 SC = 0: REM PESET FREE SECTOR COUNTER
2530 F = 128:T = 192:SP = 4: REM TRACK #18-34
2540 GOSUB 2650
2550 F = 120:T = 68:SP = - 4: REM TRACK #16-3

```

```

60  GOSUB 2650
2570 PRINT "number of sectors used= ";496 - SC
2580 PRINT "number of sectors free= ";SC
2590 IF SC > 50 THEN 2630
2600 PRINT CHR$(7)
2610 PRINT "space on disk may be not enough for data file, new data
      disk please!"
2620 INPUT "push any key when ready ";C$
2630 PRINT
2640 RETURN
2650 REM ***COUNT # OF SECTOR USED***
2660 FOR I = F TO T STEP SP
2670 FOR J = 0 TO 1
2680 X = PEEK (36096 + I + J)
2690 FOR K = 0 TO 7
2700 X = X - 2 ^ K
2710 IF X < 0 THEN K = 7: GOTO 2730
2720 SC = SC + 1
2730 NEXT K
2740 NEXT J
2750 NEXT I
2760 RETURN

```

#### PROGRAM PARATE

```

100 REM ***PARAMETER FILE CREATION***
110 D$ = CHR$(4)
120 PRINT D$;"PR#3": REM INITIALIZE 80-COLUMN CARD
130 TEXT : HOME : PRINT CHR$(12)
140 PRINT TAB(20)"*** DSIS PARAMETER FILE CREATION ***": PRINT
150 DIM A$(150,3),WT(30)
160 REM ***CURRENT PARAMETER FILE***
170 PRINT D$;"OPEN CURPA,D1"
180 PRINT D$;"READ CURPA"
190 INPUT N2
200 FOR I = 1 TO N2
210 FOR J = 1 TO 2
220 INPUT CD:A$(I,J) = STR$(CD)
230 NEXT J
240 NEXT I
250 INPUT N1: INPUT R
260 INPUT HI: INPUT LO
270 FOR I = 1 + N2 TO N1 + N2
280 INPUT CD:A$(I,1) = STR$(CD)
290 NEXT
300 PRINT D$;"CLOSE CURPA"
310 PRINT "current stepper motor parameter:-"
320 GOSUB 1500: REM VARIABLE LABEL
330 FOR I = 1 TO N2
340 L = LEN (A$(I,1)):TB = 18 - L
350 PRINT TAB(6)I; TAB(10)A$(I,1); TAB(TB)A$(I,2)
360 NEXT
370 PRINT : PRINT "current A13 parameter:-"
380 GOSUB 1540: REM VARIABLE LABEL
390 FOR I = 1 + N2 TO N1 + N2
400 PRINT TAB(6)I - N2; TAB(9)A$(I,1)

```

```

410 NEXT
420 PRINT : PRINT "number of data point for each channel=" ;R
430 INPUT "any modification (y/n)? ";C$
440 IF C$ = "N" THEN 780
450 REM ***STEPPER MOTOR AND AI13 PARAMETER***
460 PRINT CHR$(12)
470 PRINT "**** STEPPER MOTOR PARAMETER ****"
480 INPUT " number of stages for stepper motor=" ;N2: IF N2 = 0 THEN
480
490 GOSUB 1500: REM VARIABLE LABEL
500 F2 = 1:T2 = 2
510 RL(1) = 18
520 FOR I = 1 TO N2
530 PRINT TAB(6)I; TAB(10)
540 GOSUB 1580
550 NEXT
560 PRINT : PRINT
570 PRINT "**** AI13 PARAMETER ****"
580 INPUT " number of channel (ie. element)=" ;N1: IF N1 = 0 THEN 530
590 PRINT
600 GOSUB 1540: REM VARIABLE LABEL
610 F1 = 1 + N2:T1 = N1 + N2
620 F2 = 1:T2 = 1
630 FOR I = F1 TO T1
640 PRINT TAB(5)I - N2; TAB(9)
650 GOSUB 1580
660 NEXT
670 PRINT : INPUT " number of data point for each channel=" ;R
680 S = R / 256:HI = INT(S):LO = (S - HI) * 256
690 IF LO = 0 THEN HI = HI - 1
700 FG = 1: REM RENEW CURPA
710 PRINT D$;"OPEN CURPA,D1"
720 PRINT D$;"DELETE CURPA"
730 PRINT D$;"OPEN CURPA"
740 PRINT D$;"WRITE CURPA"
750 GOTO 1050
760 PRINT D$;"CLOSE CURPA"
770 FG = 0: REM RESET FLAG
780 REM ***SAMPLE PARAMETER***
790 PRINT CHR$(12)
800 PRINT "**** SAMPLE PARAMETER ****"
810 INPUT " number of sample=" ;N
820 F2 = 1:T2 = 3
830 RL(1) = 13:RL(2) = 16
840 FOR M = 1 TO N
850 F1 = 1 + N1 + N2 + (M - 1) * N1:T1 = N1 + N2 + M * N1
860 PRINT : PRINT " sample #";M;"-:"
870 INPUT " weight (mg)=" ;WT(M)
880 IF M > 1 THEN GOSUB 1770: IF C$ < > "N" THEN 970
890 PRINT TAB(4)"channel #"; TAB(4)"element"; TAB(4)"conc'n (ppm)";
TAB(4)"preamp gain"
900 PRINT TAB(4)"-----"; TAB(4)"-----"; TAB(4)"-----";
TAB(4)"-----"
910 K = N
920 FOR I = F1 TO T1
930 K = K + 1
940 PRINT TAB(8)A$(K,1); TAB(10)
950 GOSUB 1580

```

```

960 NEXT I
970 NEXT M
980 REM ***PARAMETER CONVERSION AND STORAGE***
990 PRINT CHR$(12)
1000 INPUT "name of parameter file= ";N1$
1010 PRINT D$;"OPEN";N1$;"D2"
1020 PRINT D$;"DELETE";N1$
1030 PRINT D$;"OPEN";N1$
1040 PRINT D$;"WRITE";N1$
1050 REM STEPPER MOTOR
1060 F1 = 1:T1 = N2:F2 = 1:T2 = 2
1070 PRINT N2
1080 GOSUB 1860
1090 REM AI13
1100 F1 = 1 + N2:T1 = N1 + N2:F2 = 1:T2 = 1
1110 PRINT N1: PRINT R
1120 PRINT HI: PRINT LO
1130 GOSUB 1860
1140 IF FG = 1 THEN 760
1150 REM SAMPLE PARAMETER
1160 F2 = 2:T2 = 3
1170 PRINT N
1180 FOR M = 1 TO N
1190 PRINT WT(M)
1200 F1 = 1 + N1 * M + N2:T1 = N1 * (M + 1) + N2
1210 FOR I = F1 TO T1
1220 PRINT A$(I,1)
1230 NEXT I
1240 GOSUB 1860
1250 NEXT M
1260 PRINT D$;"CLOSE";N1$
1270 END
1500 REM ***MOTOR VARIABLE LABEL***
1510 PRINT TAB(4)"stage #"; TAB(4)"# of pulse"; TAB(4)"waiting time
(sec)"
1520 PRINT TAB(4)"-----"; TAB(4)"-----"; TAB(4)"-----"
-----"
1530 RETURN
1540 REM ***AI13 VARIABLE LABEL***
1550 PRINT TAB(4)"scan #"; TAB(4)"channel #"
1560 PRINT TAB(4)"-----"; TAB(4)"-----"
1570 RETURN
1580 REM ***GET PARAMETER ROUTINE***
1590 FOR J = F2 TO T2
1600 GET C$:A$(I,J) = C$
1610 PRINT C$;: GET C$
1620 L = LEN(A$(I,J))
1630 IF C$ = CHR$(13) THEN 1660
1640 IF C$ = CHR$(27) THEN GOSUB 1720: GOTO 1600
1650 A$(I,J) = A$(I,J) + C$: GOTO 1610
1660 TB = RL(J) - L
1670 IF TB < 1 THEN TB = 1
1680 PRINT TAB(TB)
1690 NEXT J
1700 PRINT
1710 RETURN
1720 REM ***ERASER***
1730 FOR ER = 1 TO L

```

```

1740 PRINT CHR$(8);
1750 NEXT
1760 RETURN
1770 REM ***SAME PARAMETER FOR SAMPLE***
1780 INPUT " same parameter as before (y/n)? ";C$
1790 IF C$ = "N" THEN RETURN
1800 FOR I = F1 TO T1
1810 FOR J = F2 TO T2
1820 A$(I,J) = A$(I - N1,J)
1830 NEXT J
1840 NEXT I
1850 RETURN
1860 REM ***CONVERSION AND STORAGE***
1870 FOR I = F1 TO T1
1880 FOR J = F2 TO T2
1890 CD = VAL (A$(I,J)): PRINT CD
1900 NEXT J
1910 NEXT I
1920 RETURN

```

#### PROGRAM TRAINING

```

0 REM REVISED JAN 7,1986
1 REM REVISED SEPT 10,1986
2 REM REVISED OCT 3,1986
3 REM LENGTH= 10161 BYTES
100 REM *** ROBOT RM101 TRAINING WITH APPLE ][ ***
110 DIM A$(100,6),B$(100,6),A$(100)
120 D$ = CHR$(4)
130 S = 5: REM DEFAULT SPEED= 5
140 SC = 0: REM INITIALIZE STEP COUNTER
150 A1 = 1000:A2 = 100:A3 = 100:A6 = 650: REM DEFAULT MOTOR INCREMENT
160 M1 = 0:M2 = 875:M3 = - 938:M4 = - 800:M5 = 800: REM MOTOR PARA.
170 REM ***SET HOME POSITION AND SPEED***
180 PRINT D$;"PR#1"
190 PRINT "H"
200 PRINT "S";S
210 PRINT D$;"PR#3"
220 REM ***GREETING***
230 SPEED= 150
240 PRINT CHR$(12): VTAB (10): HTAB (20)
250 PRINT "**** ROBOT TRAINING WITH APPLE ][ ****"
260 HTAB (32): PRINT "by W.T.Chan"
270 SPEED= 255
280 VTAB (22): PRINT TAB( 55)"welcome!"
290 PRINT TAB( 55): INPUT "push return to continue.";C$
300 REM ***SET-UP***
310 GOSUB 2000: PRINT : REM SET INCREMENT
320 GOSUB 3020: REM SET SPEED
330 PRINT "file name for data storage= TEMP"
340 CV = PEEK (37)
350 VTAB (CV): HTAB (29)
360 INPUT "";N1$
370 IF N1$ < > "" THEN 400
380 N1$ = "TEMP"
390 VTAB (CV): HTAB (29): PRINT N1$

```



```

400 PRINT : PRINT "need menu of movement (y/n)? N"
410 VTAB (CV + 2): HTAB (29)
420 INPUT " ";C$
430 IF C$ = "" THEN C$ = "N"
440 IF C$ < > "Y" THEN 670
450 REM ***MENU***
460 GOSUB 1000: REM CAPTION
470 PRINT "enter the character of your choice:-"
480 PRINT TAB( 6)"U for body clockwise rotation,"
490 PRINT TAB( 6)"J for body anti-clockwise rotation,"
500 PRINT TAB( 6)"I for shoulder upward movement,"
510 PRINT TAB( 6)"K for shoulder downward movement,"
520 PRINT TAB( 6)"O for elbow upward movement,"
530 PRINT TAB( 6)"L for elbow downward movement,"
540 PRINT TAB( 6)"C for finger close,"
550 PRINT TAB( 6)"F for finger open,"
560 PRINT TAB( 6)"R for hand clockwise rotation,"
570 PRINT TAB( 6)"T for hand anti-clockwise rotation,"
580 PRINT TAB( 6)"E for print parameter,"
590 PRINT TAB( 6)"D for store parameter on disk,"
600 PRINT TAB( 6)"M for multi-step movement,"
610 PRINT TAB( 6)"W for change increment,"
620 PRINT TAB( 6)"X for speed change,"
630 PRINT TAB( 6)"S for show menu, and"
640 PRINT TAB( 6)"ctrl-Q for quit."
650 PRINT : INPUT "push return when ready. ";C$
660 REM ***MOVEMENT***
670 PRINT CHR$( 12): PRINT "action? ";
680 GET C$: HOME : PRINT CHR$( 12)
690 IF C$ = "U" THEN INC = A1: GOSUB 1000: GOTO 860
700 IF C$ = "J" THEN INC = - A1: GOSUB 1000: GOTO 860
710 IF C$ = "I" THEN INC = A2: GOSUB 1060: GOTO 860
720 IF C$ = "K" THEN INC = - A2: GOSUB 1060: GOTO 860
730 IF C$ = "O" THEN INC = A3: GOSUB 1160: GOTO 860
740 IF C$ = "L" THEN INC = - A3: GOSUB 1160: GOTO 860
750 IF C$ = "C" THEN INC = A6: GOSUB 1270: GOTO 860
760 IF C$ = "F" THEN INC = - A6: GOSUB 1270: GOTO 860
770 IF C$ = "R" THEN INC = - 1800: GOSUB 1320: GOTO 860
780 IF C$ = "T" THEN INC = 1800: GOSUB 1320: GOTO 860
790 IF C$ = "E" THEN GOSUB 8000: GOTO 670
800 IF C$ = "D" THEN GOSUB 4000: GOTO 670
810 IF C$ = "M" THEN GOSUB 5000: GOTO 670
820 IF C$ = "W" THEN GOSUB 2000: GOTO 670
830 IF C$ = "X" THEN GOSUB 3000: GOTO 670
840 IF C$ = "S" THEN 460
850 IF C$ = CHR$( 17) THEN 10030: REM CTRL-Q
860 PRINT : PRINT D$;"PR#3"
870 FG = 0
880 GOTO 670
999 REM -----
1000 REM ***BODY ROTATION***
1010 M1 = M1 + INC
1020 IF ABS (M1) > 3000 THEN PRINT "body motor M1 exceeds limit by ";
      ABS (M1) - 3000:M1 = M1 - INC: GOSUB 1460: GOTO 1050
1030 B1 = B1 + INC
1040 PRINT D$;"PR#1": PRINT "I";INC;"",0,0,0,0,0"
1050 RETURN
1060 REM ***SHOULDER MOVEMENT***

```

```

1070 M2 = M2 + INC
1080 IF ABS (M2) > 1875 THEN PRINT "shoulder motor M2 exceeds limit
    by "; ABS (M2) - 1875:M2 = M2 - INC: GOSUB 1460: GOTO 1150
1090 DC = INC * .04 / .05
1100 GOSUB 1370
1110 IF FG = 1 THEN M2 = M2 - INC: GOTO 1150
1120 B2 = B2 + INC:B4 = B4 + A4:B5 = B5 + A5
1130 PRINT D$;"PR#1": PRINT "I0,";INC;"0,";A4;" ";A5;"0"
1140 A4 = 0:A5 = 0
1150 RETURN
1160 REM ***ELBOW MOVEMENT***
1170 M3 = M3 + INC
1180 IF M3 > 562 THEN PRINT "elbow motor M3 exceeds upper limit by
    ";M3 - 562:M3 = M3 - INC: GOSUB 1460: GOTO 1260
1190 IF M3 < - 938 THEN PRINT "elbow motor M3 exceeds lower limit by
    ";M3 + 938:M3 = M3 - INC: GOSUB 1460: GOTO 1260
1200 DC = INC * .08 / .05
1210 GOSUB 1370
1220 IF FG = 1 THEN M3 = M3 - INC: GOTO 1260
1230 B3 = B3 + INC:B4 = B4 + A4:B5 = B5 + A5
1240 PRINT D$;"PR#1": PRINT "I0,0,";INC;" ";A4;" ";A5;"0"
1250 A4 = 0:A5 = 0
1260 RETURN
1270 REM ***FINGER MOVEMENT***
1280 B6 = B6 + INC
1290 PRINT D$;"PR#1"
1300 PRINT "I0,0,0,0,0,";INC
1310 RETURN
1320 REM ***HAND ROTATION***
1330 B4 = B4 + INC:B5 = B5 + INC
1340 PRINT D$;"PR#1"
1350 PRINT "I0,0,0,";INC;" ";INC;"0"
1360 RETURN
1370 REM ***CHECK HAND LIMIT***
1380 C4 = C4 \ DC
1390 A4 = INT (C4):A5 = - A4:C4 = C4 - A4
1400 M4 = M4 + A4
1410 IF ABS (M4) < 1800 THEN 1450
1420 PRINT "hand motor M4 & M5 exceed limit by "; ABS (M4) - 1800
1430 M4 = M4 - A4:C4 = C4 + A4 - DC
1440 FG = 1: GOSUB 1460
1450 RETURN
1460 REM ***STOP AND CONTINUE***
1470 INPUT "push return to continue. ";C$
1480 RETURN
1999 REM -----
2000 REM ***SET MOTOR INCREMENT***
2010 T1 = A1:T2 = A2:T3 = A3:T6 = A6: REM MAKE A COPY
2020 GOSUB 10000: REM CAPTION
2030 PRINT "enter increment (in steps) for each motor:-"
2040 CV = PEEK (37) + 1
2050 PRINT TAB (6)"body motor      M1= ";A1
2060 PRINT TAB (6)"shoulder motor M2= ";A2
2070 PRINT TAB (6)"elbow motor    M3= ";A3
2080 PRINT TAB (6)"finger motor   M6= ";A6
2090 VTAB (CV)
2100 HTAB (21): INPUT "M1= ";T1$
2110 IF T1$ < > "" THEN 2130

```

```

2120 T1$ = STR$ (T1): VTAB ( PEEK (37)): HTAB (25): PRINT T1
2130 HTAB (21): INPUT "M2= ";T2$
2140 IF T2$ < > "" THEN 2160
2150 T2$ = STR$ (T2): VTAB ( PEEK (37)): HTAB (25): PRINT T2
2160 HTAB (21): INPUT "M3= ";T3$
2170 IF T3$ < > "" THEN 2190
2180 T3$ = STR$ (T3): VTAB ( PEEK (37)): HTAB (25): PRINT T3
2190 HTAB (21): INPUT "M6= ";T6$
2200 IF T6$ < > "" THEN 2220
2210 T6$ = STR$ (T6): VTAB ( PEEK (37)): HTAB (25): PRINT T6
2220 T1 = VAL (T1$):T2 = VAL (T2$):T3 = VAL (T3$):T6 = VAL (T6$)
2230 PRINT "confirm (y/n)? ";: GET C$: PRINT
2240 IF C$ = CHR$ (27) THEN RETURN : REM DO NOTHING
2250 IF C$ = "N" THEN 2090
2260 A1 = T1:A2 = T2:A3 = T3:A6 = T6: REM CHANGE IT
2270 RETURN
2999 REM -----
3000 REM ***SPEED CHANGE***
3010 GOSUB 10000: REM CAPTION
3020 PRINT "speed of motors (1-5)= ";S
3030 T = S: REM MAKE A COPY
3040 CV = PEEK (37)
3050 VTAB (CV): INPUT "speed of motors (1-5)= ";T$
3060 IF T$ < > "" THEN 3080
3070 T$ = STR$ (T): VTAB (CV): HTAB (24): PRINT T
3080 T = VAL (T$)
3090 IF T < 1 OR T > 5 THEN PRINT CHR$ (7) + CHR$ (7);: GOTO 3050
3100 PRINT "confirm (y/n)? ";: GET C$: PRINT
3110 IF C$ = CHR$ (27) THEN RETURN : REM DO NOTHING
3120 IF C$ = "N" THEN 3050
3130 S = T: REM CHANGE IT
3140 PRINT D$;"PR#1": PRINT "S";S: PRINT D$;"PR#3"
3150 RETURN
3999 REM -----
4000 REM ***STORE PARAMETER***
4010 SC = SC + 1: REM ADVANCE COUNTER
4020 N$ = N1$: REM FILE NAME
4030 GOSUB 10000: REM CAPTION
4040 PRINT "step #";SC;"- ";B1;" ";B2;" ";B3;" ";B4;" ";B5;" ";B6
4050 INPUT "label for storage = ";A$
4060 PRINT "confirm (y/n)? ";: GET C$: PRINT
4070 IF C$ = CHR$ (27) THEN SC = SC - 1: RETURN
4080 IF C$ = "N" THEN VTAB ( PEEK (37) - 1): GOTO 4050
4090 IF SC = 1 THEN GOSUB 9500: REM INIT DATA FILE
4100 PRINT D$;"OPEN";N$
4110 PRINT D$;"WRITE";N$
4120 PRINT SC
4130 PRINT D$;"CLOSE";N$
4140 PRINT D$;"APPEND";N$
4150 PRINT D$;"WRITE";N$
4160 PRINT A$
4170 PRINT B1: PRINT B2: PRINT B3: PRINT B4: PRINT B5: PRINT B6
4180 PRINT D$;"CLOSE";N$
4190 RETURN
4999 REM -----
5000 REM ***MULTI-STEP MOVEMENT***
5010 GOSUB 10000: REM CAPTION
5020 PRINT "<1> parameter from disk,"

```

```

5030 PRINT "<2> direct input of parameter, or"
5040 PRINT "<3> abort."
5050 INPUT "please enter your choice:- ";C$
5060 IF C$ = "1" THEN GOSUB 6000
5070 IF C$ = "2" THEN GOSUB 7000
5080 IF C$ = "3" THEN RETURN
5090 IF NOT (C$ = "1" OR C$ = "2") THEN VTAB ( PEEK (37)): GOTO 5050
5100 IF C1$ = CHR$ (27) OR SP = 0 THEN 5010
5110 PRINT CHR$ (12)
5120 PRINT D$;"PR#1"
5130 FOR I = 1 TO SP
5140 PRINT "P";I;" ";B%(I,1);" ";B%(I,2);" ";B%(I,3);" ";B%(I,4);" ";
    B%(I,5);" ";B%(I,6)
5150 NEXT I
5160 FOR I = 1 TO SP
5170 PRINT "M";I
5180 NEXT I
5190 PRINT D$;"PR#3"
5200 M1 = 0:M2 = 875:M3 = - 938:M4 = - 800:M5 = 800: REM HOME PARA
5210 M1 = M1 + B%(SP,1):M2 = M2 + B%(SP,2):M3 = M3 + B%(SP,3):M4 = M4 +
    B%(SP,4):M5 = M5 + B%(SP,5):M6 = M6 + B%(SP,6)
5220 B1 = B%(SP,1):B2 = B%(SP,2):B3 = B%(SP,3):B4 = B%(SP,4):B5 =
    B%(SP,5):B6 = B%(SP,6)
5230 RETURN
5999 REM -----
6000 REM ***PARAMETER FROM DISK FILE***
6010 PRINT : INPUT "name of parameter file= ";N$
6020 IF N$ = "" THEN VTAB ( PEEK (37) - 1): GOTO 6010
6030 IF NOT (N$ = N1$ AND SC = 0) THEN 6070
6040 PRINT "file ";N1$;" is empty!"
6050 INPUT "push <RETURN> to continue. ";C1$
6060 C1$ = CHR$ (27): RETURN
6070 GOSUB 9000: REM READ DATA
6080 GOSUB 10000: REM CAPTION
6090 PRINT "the following steps are available:--"
6100 J = 1
6110 FOR I = 1 TO ST
6120 PRINT "<";I;">";A$(I);
6130 L = LEN (A$(I))
6140 IF I > 9 AND I < = 99 THEN L = L + 1
6150 IF I > 99 THEN L = L + 2
6160 HTAB (L): PRINT TAB( 10);
6170 J = J + 1
6180 IF J > 6 THEN J = 1: PRINT
6190 NEXT I
6200 PRINT : PRINT
6210 PRINT "enter the sequence of movement by number:--"
6220 PRINT TAB( 6)"-I for initial position"
6230 PRINT TAB( 6)"-N for home position"
6240 PRINT TAB( 6)"-E for end of entry"
6250 SP = 1
6260 PRINT "<";SP;">";: INPUT " ";C1$
6270 IF C1$ = "E" THEN SP = SP - 1: GOTO 6360
6280 IF C1$ = "I" THEN GOSUB 6390: GOTO 6350
6290 IF C1$ = "N" THEN GOSUB 6430: GOTO 6350
6300 C = VAL (C1$)
6310 IF C < = 0 OR C > ST THEN VTAB ( PEEK (37)): GOTO 6260
6320 FOR I = 1 TO 6

```

```

6330 B%(SP,I) = A%(C,I)
6340 NEXT I
6350 SP = SP + 1: GOTO 6260
6360 PRINT : PRINT "confirm (y/n)? ";: GET C1$: PRINT
6370 IF C1$ = "N" THEN 6080
6380 RETURN
6390 REM INITIAL POSITION
6400 B%(SP,1) = B1:B%(SP,2) = B2:B%(SP,3) = B3
6410 B%(SP,4) = B4:B%(SP,5) = B5:B%(SP,6) = B6
6420 RETURN
6430 REM HOME POSITION
6440 FOR I = 1 TO 6
6450 B%(SP,I) = 0
6460 NEXT
6470 RETURN
6999 REM -----
7000 REM ***DIRECT INPUT OF MULTI-STEP PARAMETER***
7010 PRINT : INPUT "number of steps=" ;C1$
7020 SP = VAL (C1$)
7030 IF SP > 0 THEN 7070
7032 PRINT CHR$(29) + CHR$(31)
7040 PRINT "confirm (y/n)? ";: GET C1$: PRINT
7050 IF C1$ < > "N" THEN RETURN
7060 VTAB ( PEEK (37) - 2): GOTO 7010
7070 PRINT "input parameters for M1 to M6:--"
7080 FOR I = 1 TO SP
7090 PRINT TAB(10)"step #";I;: INPUT "- ";B%(I,1),B%(I,2),B%(I,3),
    B%(I,4),B%(I,5),B%(I,6)
7100 GOSUB 7190: REM CHECK PARAMETER CORRECTNESS
7110 NEXT I
7120 PRINT CHR$(29) + CHR$(31): REM CLEAR LINE & REVERSE LINEFEED
7130 PRINT "confirm (y/n)? ";: GET C1$: PRINT
7140 IF C1$ < > "N" THEN RETURN
7150 CV = PEEK (37): REM CURRENT CURSOR VERTICAL POSITION
7160 CV = CV - SP - 3
7170 VTAB (CV): GOTO 7010
7180 RETURN
7190 REM PARAMETER CHECK
7200 CV = PEEK (37)
7210 IF B%(I,4) = - B%(I,5) AND ABS (B%(I,2) * .04 + B%(I,3) * .08 -
    B%(I,4) * .05) < .5 THEN 7260: REM PARA. O.K.
7220 VTAB (23): PRINT TAB(10)"--- parameter error, re-enter please! -
    --" + CHR$(7)
7230 I = I - 1: REM REENTRY FOR THIS STEP
7240 VTAB (CV)
7250 RETURN
7260 VTAB (23): PRINT CHR$(29)
7270 VTAB (CV + 1)
7280 RETURN
7999 REM -----
8000 REM ***PRINT PARAMETER***
8010 GOSUB 1000: REM CAPTION
8020 PRINT "--- printer at on-line mode please! ---"
8030 PRINT TAB(6)"<1> current position,"
8040 PRINT TAB(6)"<2> parameter from current file,"
8050 PRINT TAB(6)"<3> parameter from file on disk, or"
8060 PRINT TAB(6)"<4> abort."
8070 INPUT "please enter your choice:- ";C$

```

```

8080 IF NOT (C$ = "1" OR C$ = "2" OR C$ = "3" OR C$ = "4") THEN VTAB
      ( PEEK (37)): GOTO 8070
8090 PRINT : REM SPACING
8100 IF C$ = "1" THEN GOSUB 8160
8110 IF C$ = "2" THEN GOSUB 8260
8120 IF C$ = "3" THEN GOSUB 8370
8130 IF C$ = "4" THEN RETURN
8140 IF C1$ = CHR$ (27) THEN 8010
8150 RETURN
8160 REM CURRENT POSITION
8170 PRINT "current position= ";B1;"", "B2;"", "B3;"", "B4;"", "B5;"", "B6
8180 INPUT "label for this position = ";A$
8190 PRINT "confirm (y/n)? ";: GET C1$: PRINT
8200 IF C1$ = CHR$ (27) THEN RETURN
8210 IF C1$ = "N" THEN VTAB ( PEEK (37) - 1): GOTO 8180
8220 PRINT D$;"PR#7"
8230 PRINT TAB( 6)A$;"": ";B1;"", "B2;"", "B3;"", "B4;"", "B5;"", "B6
8240 PRINT D$;"PR#3"
8250 RETURN
8260 REM CURRENT FILE
8270 IF SC > 0 THEN 8320
8280 PRINT "current file is empty!"
8290 INPUT "push <RETURN> to continue. ";C1$
8300 C1$ = CHR$ (27)
8310 RETURN : REM EMPTY FILE, BACK TO MENU
8320 N$ = N1$
8330 GOSUB 9000: REM GET CURRENT FILE
8340 PRINT "file ";N1$;" contain:- "
8350 GOSUB 8440: REM PRINT
8360 RETURN
8370 REM OTHER FILE
8380 INPUT "name of parameter file= ";N$
8390 IF N$ = "" THEN VTAB ( PEEK (37)): GOTO 8380
8400 GOSUB 9000: REM GET FILE
8410 PRINT "file ";N$;" contain:-"
8420 GOSUB 8440
8430 RETURN
8440 REM PRINT
8450 GOSUB 8530: REM PRINT FILE ON SCREEN
8460 PRINT : PRINT "push return for print-out. ";: GET C1$: PRINT
8470 IF C1$ = CHR$ (27) THEN RETURN
8480 PRINT D$;"PR#7"
8490 PRINT "80N": REM "ctrl-I 80N" FOR 80 COLUMN OUTPUT
8500 GOSUB 8530: REM PRINT FILE VIA PRINTER
8510 PRINT D$;"PR#3"
8520 RETURN
8530 REM PRINT FILE
8540 FOR I = 1 TO ST
8550 PRINT TAB( 6)A$(I);"": ";
8560 FOR J = 1 TO 5
8570 PRINT A$(I, J);"", ";
8580 NEXT J
8590 PRINT A$(I, J)
8600 NEXT I
8610 RETURN
8999 REM -----
9000 REM ***READ PARAMETER ON DISK***
9010 PRINT D$;"OPEN";N$

```

```

9020 PRINT D$;"READ";N$
9030 INPUT ST
9040 FOR I = 1 TO ST
9050 INPUT A$(I)
9060 FOR J = 1 TO 6
9070 INPUT A%(I,J)
9080 NEXT J
9090 NEXT I
9100 PRINT D$;"CLOSE";N$
9110 RETURN
9500 REM ***INITIALIZE DATA FILE***
9510 PRINT D$;"OPEN";N$
9520 PRINT D$;"DELETE";N$
9530 RETURN
9999 REM -----
10000 REM ***CAPTION***
10010 PRINT CHR$(12): PRINT TAB(20)"*** ROBOT TRAINING ***". PRINT
10020 RETURN
10030 REM ***EXIT***
10040 PRINT
10050 PRINT D$;"PR#1"
10060 PRINT "N"
10070 PRINT D$;"PR#3": PRINT CHR$(12);
10080 END

```

#### PROGRAM FILE BLENDER

```

0 REM CREATED OCT 9,1986
100 REM ***FILE BLENDER***
110 DIM A$(200),B$(200),C$(200),C1$(12)
120 DIM A%(200,6),B%(200,6),C%(200,6)
130 D$ = CHR$(4)
140 GOSUB 11000: REM SCREEN SET-UP
150 FOR I = 0 TO 12: READ C1$(I): NEXT
160 F = 0:T = 8:TB = 10
170 GOSUB 9000: REM REQUEST COMMAND
180 ON C GOSUB 1000,2000,3000,4000,5000,6000,7000,8000,13000
190 GOTO 160: REM LOOP BACK
999 REM -----
1000 REM ***OPEN FILE***
1010 VTAB(22): GOSUB 12000
1020 PRINT "R"- read a file for <1>old or <2>new file window"
1030 VTAB(23): GOSUB 12000
1040 VTAB(23): INPUT "window: ";C$
1050 IF C$ = "" THEN RETURN
1060 C = VAL(C$)
1070 IF C < 1 OR C > 2 THEN 1040
1080 VTAB(23): HTAB(15)
1090 INPUT "file name= ";N$
1100 IF N$ = "" THEN RETURN
1110 GOSUB 1160: REM READ FILE
1120 ON C GOSUB 1280,1410
1130 GOSUB 10000: REM RENEW WINDOW
1140 GOTO 1030
1150 RETURN
1160 REM READ FILE

```

```

1170 PRINT D$;"OPEN";N$
1180 PRINT D$;"READ";N$
1190 INPUT ST
1200 FOR I = 1 TO ST
1210 INPUT C$(I)
1220 FOR J = 1 TO 6
1230 INPUT C%(I,J)
1240 NEXT J
1250 NEXT I
1260 PRINT D$;"CLOSE";N$
1270 RETURN
1280 REM OLD FILE WINDOW
1290 FOR I = 1 TO ST
1300 CA = CA + 1
1310 A$(CA) = C$(I)
1320 FOR J = 1 TO 6
1330 A%(CA,J) = C%(I,J)
1340 NEXT J
1350 NEXT I
1360 EA = CA:SA = CA - 53
1370 IF SA < 1 THEN SA = 1
1380 S = SA:E = EA:CV = 4:T = 9
1390 FOR I = S TO E:C$(I) = A$(I): NEXT
1400 RETURN
1410 REM NEW FILE WINDOW
1420 FOR I = 1 TO ST
1430 CB = CB + 1
1440 B$(CB) = C$(I)
1450 FOR J = 1 TO 6
1460 B%(CB,J) = C%(I,J)
1470 NEXT J
1480 NEXT I
1490 EB = CB:SB = CB - 35
1500 IF SB < 1 THEN SB = 1
1510 S = SB:E = EB:CV = 15:T = 6
1520 FOR I = S TO E:C$(I) = B$(I): NEXT
1530 RETURN
1999 REM -----
2000 REM ***ENTER STEPS TO NEW FILE***
2010 VTAB (22): GOSUB 12000
2020 PRINT "ER: enter steps from old to new file"
2030 VTAB (23): GOSUB 12000
2040 CB = CB + 1
2050 VTAB (23): PRINT "step#";CB;"= ";
2060 INPUT "";C$
2070 IF C$ = "" THEN CB = CB - 1: RETURN
2080 C = VAL (C$)
2090 IF C < 1 OR (C > CA) THEN 2050
2100 VTAB (23): HTAB (15)
2110 INPUT "label= ";C$
2120 IF C$ = "" THEN CB = CB - 1: RETURN
2130 B$(CB) = C$
2140 FOR I = 1 TO 6
2150 B%(CB,I) = A%(C,I)
2160 NEXT
2170 EB = CB:SB = CB - 35
2180 IF SB < 1 THEN SB = 1
2190 S = SB:E = EB:CV = 15:T = 6

```



```

2200 FOR I = S TO E: C$(I) = B$(I): NEXT
2210 GOSUB 10000
2220 GOTO 2030
2230 RETURN
2999 REM -----
3000 REM ***STORE FILE***
3010 VTAB (22): GOSUB 12000
3020 PRINT "ST: store new file"
3030 VTAB (23): GOSUB 12000
3040 IF CB > 0 THEN 3060
3050 INPUT "empty file, <RETURN> to continue. "; C$: RETURN
3060 VTAB (23): INPUT "name= "; N$
3070 IF N$ = "" THEN RETURN
3080 L$ = LEFT$(N$,1)
3090 IF ASC(L$) < 65 OR ASC(L$) > 90 THEN 3060
3100 PRINT D$;"OPEN";N$
3110 PRINT D$;"DELETE";N$
3120 PRINT D$;"OPEN";N$
3130 PRINT D$;"WRITE";N$
3140 PRINT CB
3150 FOR I = 1 TO CB
3160 PRINT B$(I)
3170 FOR J = 1 TO 6
3180 PRINT B$(I,J)
3190 NEXT J
3200 NEXT I
3210 PRINT D$;"CLOSE";N$
3220 RETURN
3999 REM -----
4000 REM ***SHOW DATA OF A STEP***
4010 VTAB (22): GOSUB 12000
4020 PRINT "SH: show parameter from <1>old file or <2>new file"
4030 VTAB (23): GOSUB 12000
4040 INPUT "file= "; C$
4050 C = VAL(C$)
4060 IF C$ = "" THEN RETURN
4070 IF NOT (C = 1 OR C = 2) THEN GOTO 4030
4080 VTAB (23): HTAB (12)
4090 INPUT "step# = "; P$
4100 P = VAL(P$)
4110 IF P$ = "" THEN RETURN
4120 ON C GOSUB 4160,4270
4130 IF C$ = "!" THEN PRINT CHR$(7);: GOTO 4080
4140 GOTO 4030: REM LOOP BACK
4150 RETURN
4160 REM OLD FILE
4170 IF P < 1 OR (P > CA) THEN C$ = "!": RETURN
4180 VTAB (23): GOSUB 12000
4190 PRINT "file<" ; C ; "> step#"; P ; ": ";
4200 FOR I = 1 TO 5
4210 PRINT A$(P,I);", ";
4220 NEXT
4230 PRINT A$(P,I);
4240 PRINT TAB(10);
4250 INPUT "<RETURN> to continue "; C$
4260 RETURN
4270 REM NEW FILE
4280 IF P < 1 OR (P > CB) THEN C$ = "!": RETURN

```

```

4290 VTAB (23): GOSUB 12000
4300 PRINT "file<" ; C ; "> step#"; P ; " : ";
4310 FOR I = 1 TO 5
4320 PRINT B$(P,I); ", ";
4330 NEXT
4340 PRINT B$(P,I);
4350 PRINT TAB( 10);
4360 INPUT "<RETURN> to continue "; C$
4370 RETURN
4999 REM -----
5000 REM ***EDIT***
5010 VTAB (22): GOSUB 12000
5020 PRINT "ED: edit a step in new file"
5030 VTAB (23): GOSUB 12000
5040 VTAB (23): INPUT "step# = "; P$
5050 IF P$ = "" THEN RETURN
5060 P = VAL (P$)
5070 IF P < 1 OR P > CB THEN 5040
5080 VTAB (23): HTAB (12)
5090 PRINT "label = "; B$(P)
5100 GOSUB 5220
5110 VTAB (23): HTAB (19)
5120 INPUT " "; C$
5130 IF C$ < > "" THEN B$(P) = C$
5140 VTAB (23): HTAB (19): PRINT B$(P)
5150 GOSUB 5220
5160 VTAB (23): HTAB (38)
5170 INPUT " "; B$(P,1), B$(P,2), B$(P,3), B$(P,4), B$(P,5), B$(P,6)
5180 S = SB: E = EB: CV = 15: T = 6
5190 FOR I = S TO E: C$(I) = B$(I): NEXT
5200 GOSUB 10000
5210 GOTO 5030: REM LOOP BACK
5212 RETURN
5220 REM PRINT PARA
5230 VTAB (23): HTAB (32)
5240 PRINT "para = ";
5250 FOR I = 1 TO 5
5260 PRINT B$(P,I); ", ";
5270 NEXT
5280 PRINT B$(P,I)
5290 RETURN
5999 REM -----
6000 REM ***ROLL IT***
6010 F = 9: T = 12: TB = 28
6020 GOSUB 9000: REM REQUEST COMMAND
6030 IF C$ = CHR$(13) THEN RETURN
6040 ON C GOSUB 6070, 6180, 6290, 6400
6050 GOTO 6010: REM LOOP BACK
6060 RETURN
6070 REM OLD FILE/ROLL BACKWARD
6080 VTAB (22): GOSUB 12000
6090 PRINT "O<-: roll old file window backward"
6100 IF SA = 1 THEN RETURN : REM REACH UPPER LIMIT
6110 SA = SA - 54
6120 IF SA < 1 THEN SA = 1
6130 EA = SA + 53
6140 IF (EA > CA) THEN EA = CA
6150 GOSUB 6510: REM ASSIGN VARIABLES

```

```

6160 GOSUB 10000: REM ROLL IT
6170 RETURN
6180 REM OLD FILE/ROLL FORWRAD
6190 VTAB (22): GOSUB 12000
6200 PRINT "O->: roll old file window forward"
6210 IF (EA = CA) THEN RETURN
6220 EA = EA + 54
6230 IF (EA > CA) THEN EA = CA
6240 SA = EA - 53
6250 IF SA < 1 THEN SA = 1
6260 GOSUB 6510: REM ASSIGN VARIABLES
6270 GOSUB 10000: REM ROLL IT
6280 RETURN
6290 REM NEW FILE/ROLL BACKWARD
6300 VTAB (22): GOSUB 12000
6310 PRINT "N<-: roll new file window backward"
6320 IF SB = 1 THEN RETURN
6330 SB = SB - 36
6340 IF SB < 1 THEN SB = 1
6350 EB = SB + 35
6360 IF (EB > CB) THEN EB = CB
6370 GOSUB 6570
6380 GOSUB 10000
6390 RETURN
6400 REM NEW FILE/ROLL FORWRAD
6410 VTAB (22): GOSUB 12000
6420 PRINT "N->: roll new file window forward"
6430 IF (EB = CB) THEN RETURN
6440 EB = EB + 36
6450 IF (EB > CB) THEN EB = CB
6460 SB = EB - 35
6470 IF SB < 1 THEN SB = 1
6480 GOSUB 6570
6490 GOSUB 10000
6500 RETURN
6510 REM OLD FILE WINDOW VARIABLE
6520 S = SA:E = EA:CV = 4:T = 9
6530 FOR I = S TO E
6540 C$(I) = A$(I)
6550 NEXT
6560 RETURN
6570 REM NEW FILE WINDOW VARIABLE
6580 S = SB:E = EB:CV = 15:T = 6
6590 FOR I = S TO E
6600 C$(I) = B$(I)
6610 NEXT
6620 RETURN
6999 REM -----
7000 REM ***FLUSH OLD FILE***
7010 CA = 0
7020 S = 0:E = 0:CV = 4:T = 9
7030 GOSUB 10000
7040 RETURN
7999 REM -----
8000 REM ***FLUSH NEW FILE***
8010 CB = 0
8020 S = 0:E = 0:CV = 15:T = 6
8030 GOSUB 10000

```

```

8040 RETURN
9999 REM -----
9000 REM ***COMMAND MODE***
9010 VTAB (22): GOSUB 12000: HTAB (TB)
9020 C1 = 0
9030 FOR I = F TO T
9040 C1 = C1 + 1
9050 PRINT "<";C1;">";C1$(I);" ";
9060 NEXT I
9070 PRINT : GOSUB 12000
9080 VTAB (23): PRINT "command: ";: GET C$: PRINT
9090 C = VAL (C$)
9100 IF (C < = 0 OR C > C1) AND C$ < > CHR$ (13) THEN 9080
9110 RETURN
9999 REM -----
10000 REM ***RENEW FILE WINDOW***
10010 VTAB (CV)
10020 FOR I = 1 TO T
10030 PRINT CHR$ (29)
10040 NEXT
10050 VTAB (CV)
10060 J = 1
10070 IF S = 0 THEN RETURN
10080 FOR I = S TO E
10090 PRINT "<";I;">";C$(I);
10100 L = LEN (C$(I))
10110 IF I > 9 AND I < 99 THEN L = L + 1
10120 IF I > 99 THEN L = L + 2
10130 HTAB (L): PRINT TAB( 10);
10140 J = J + 1
10150 IF J > 6 THEN J = 1: PRINT
10160 NEXT I
10170 RETURN
11000 REM ***SCREEN SET UP***
11010 PRINT CHR$ (12);
11020 VTAB (1): HTAB (36): PRINT "FILE BLENDER"
11030 VTAB (2): GOSUB 11090
11040 VTAB (3): PRINT "old file:--"
11050 VTAB (13): GOSUB 11090
11060 VTAB (14): PRINT "new file:--"
11070 VTAB (21): GOSUB 11090
11080 RETURN
11090 REM PRINT LINE
11100 FOR I = 1 TO 80
11110 PRINT CHR$ (95);
11120 NEXT I
11130 PRINT
11140 RETURN
12000 REM CLEAR LINE AND REVERSE LINE FEED
12010 PRINT : PRINT CHR$ (31) + CHR$ (29) + CHR$ (31)
12020 RETURN
13000 REM ***QUIT***
13010 PRINT CHR$ (12)
13020 END
15000 DATA RF,EN,ST,SH,ED,<->,FO,FN,Q
15010 DATA O<->,O->,N<->,N->

```

## PROGRAM DA.POSITION

```

0 REM CREATED JAN 10,1986
1 REM REVISED FEB 17,1986
2 REM REVISED APRIL 2,1986
100 REM *** POSITION SEQUENCES FOR RM101 ***
110 REM * FOR CUP HOLDER POSITIONS:- *
120 REM * 1st SET FOR HOLDING AND OPEN *
130 REM * 2nd SET FOR UP AND CLOSE *
140 REM * 3rd SET FOR UP AND OPEN *
150 REM * 4th SET FOR UP-UP AND OPEN *
160 REM *****
170 D$ = CHR$ (4)
180 N = 10: REM NUMBER OF CUPS TO BE TRANSFER
190 PRINT CHR$ (12): HOME
200 RESTORE
210 READ X: IF X < > 830446 THEN PRINT "ERROR IN DATA SET": STOP
220 PRINT D$;"PR#1"
230 PRINT "H"
240 PRINT "S5"
250 REM ***SET POSITION FOR HOLDER ORIENTATION AND DSID***
260 I1 = 89:I2 = 98
270 GOSUB 500
280 REM ***SET POSITION FOR CUPS***
290 I1 = 1:I2 = N * 4
300 GOSUB 500
310 PRINT D$;"PR#3"
320 READ X: IF X < > 830446 THEN PRINT "ERROR IN DATA SET": STOP
330 END
500 REM ***READ DATA AND SET POSITION***
510 FOR I = I1 TO I2
520 READ P1,P2,P3,P4,P5,P6
530 PRINT "P";I;" ";P1;" ";P2;" ";P3;" ";P4;" ";P5;" ";P6
540 NEXT
550 RETURN
1000 REM ***DATA CHECKER***
1010 DATA 830446
1020 REM ***HOLDER ORIENTATION***
1030 DATA 1200,0,0,0,0,0
1040 DATA 1200,0,0,0,0,-800
1050 REM ***ROAD TO DSID***
1060 DATA -3,-700,300,-80,80,0
1070 DATA -3,-900,600,240,-240,0
1080 DATA -3,-1050,850,520,-520,0
1090 DATA -3,-1240,1100,768,-768,0
1100 DATA -3,-1240,1100,768,-768,-800
1110 REM ***DSID HOLD AND UP***
1120 DATA -3,-1314,1140,767,-767,-800
1130 DATA -3,-1315,1160,804,-804,0
1140 DATA -3,-1315,1160,804,-804,-800
1150 REM ***CUP#1 POSITION***
1160 DATA 1045,-2235,588,-850,850,-800
1170 DATA 1045,-2217,577,-854,854,0
1180 DATA 1045,-2217,577,-854,854,-800
1190 DATA 1045,-2107,507,-878,878,-900
1200 REM ***CUP#2 POSITION***
1210 DATA 1096,-2227,569,-877,877,-900

```

```

1220 DATA 1096,-2211,559,-881,881,0
1230 DATA 1096,-2211,559,-881,881,-800
1240 DATA 1096,-2100,489,-904,904,-900
1250 REM ***CUP#3 POSITION***
1260 DATA 1149,-2237,566,-890,890,-900
1270 DATA 1149,-2219,555,-894,894,0
1280 DATA 1149,-2219,555,-894,894,-800
1290 DATA 1149,-2109,485,-918,918,-900
1300 REM ***CUP#4 POSITION***
1310 DATA 1201,-2249,568,-898,898,-900
1320 DATA 1201,-2231,557,-902,902,0
1330 DATA 1201,-2231,557,-902,902,-800
1340 DATA 1201,-2121,487,-926,926,-900
1350 REM ***CUP#5 POSITION***
1360 DATA 1253,-2244,562,-906,906,-900
1370 DATA 1253,-2224,550,-910,910,0
1380 DATA 1253,-2224,550,-910,910,-800
1390 DATA 1253,-2114,480,-934,934,-900
1400 REM ***CUP#6 POSITION***
1410 DATA 1304,-2247,560,-911,911,-900
1420 DATA 1304,-2229,549,-914,914,0
1430 DATA 1304,-2229,549,-914,914,-800
1440 DATA 1304,-2119,479,-938,938,-900
1450 REM ***CUP#7 POSITION***
1460 DATA 1356,-2241,559,-908,908,-900
1470 DATA 1356,-2222,547,-912,912,0
1480 DATA 1356,-2222,547,-912,912,-800
1490 DATA 1356,-2112,477,-936,936,-900
1500 REM ***CUP#8 POSITION***
1510 DATA 1409,-2247,566,-902,902,-900
1520 DATA 1409,-2228,554,-905,905,0
1530 DATA 1409,-2228,554,-905,905,-800
1540 DATA 1409,-2118,484,-929,929,-900
1550 REM ***CUP#9 POSITION***
1560 DATA 1464,-2249,576,-887,887,-900
1570 DATA 1464,-2231,565,-891,891,0
1580 DATA 1464,-2231,565,-891,891,-800
1590 DATA 1464,-2121,495,-915,915,-900
1600 REM ***CUP#10 POSITION***
1610 DATA 1514,-2254,585,-873,873,-900
1620 DATA 1514,-2235,574,-876,876,0
1630 DATA 1514,-2235,574,-876,876,-800
1640 DATA 1514,-2125,504,-900,900,-900
10000 REM ***DATA CHECKER***
10010 DATA 830446

```

**PROGRAM DP2.0**

```

100 REM ***DIRECT SAMPLE INSERTION SYSTEM DATA PROCESSING***
110 REM CREATED ON JUNE 15,1985
120 REM REVISED ON JUNE 16,1988
130 REM REVISED ON SEPT 11,1988
140 ONERR GOTO 7000: REM DISK ERROR HANDLING
150 REM ! INTEGER I,J,K,N,N1,N2,F1,T1,F2,T2,PN,PT,R,RT,S,X,Y
160 HIMEM: 38400
170 DS = CHR$ (4)

```

```

180 NO$ = "***: REM INITIALIZE CURRENT DATA FILE NAME
190 N2$ = "***: REM INITIALIZE CURRENT PARAMETER FILE NAME
200 DIM A$(3000),CN(6),GN(6),EL$(6): REM DATA POINT ARRAY,
    CONCENTRATION, GAIN AND ELEMENT ARRAYS
210 DIM B$(1000),R$(10): REM DATA AVERAGING BUFFER, DATA POINTS
    REGISTER
220 PRINT DS;"PR# 3": REM USE 80-COLUMN CARD
230 GOSUB 8000: GOTO 310
240 GOSUB 8000: REM CAPTION
250 PRINT " current data file= ";NO$
260 PRINT " sample weight= ";WT
270 PRINT " element= ";EL$(PT)
280 PRINT "concentration (ppm)= ";CN(PT)
290 PRINT " gain= ";GN(PT)
300 PRINT
310 PRINT "<1> plot on screen,"
320 PRINT "<2> plot on paper,"
330 PRINT "<3> integration,"
340 PRINT "<4> new set of data,"
350 PRINT "<5> data sets summation,"
360 PRINT "<6> boxcar averaging, or"
370 PRINT "<7> exit."
380 PRINT
390 INPUT "enter the number of your selection ";C$
400 C = VAL (C$)
410 IF C < 1 OR C > 7 THEN VTAB ( PEEK (37)): PRINT CHR$ (7);: GOTO
    390
420 PRINT CHR$ (12)
430 IF C = 7 THEN 460
440 ON C GOSUB 1000,2000,3000,4000,5000,6000
450 GOTO 240
460 END
1000 REM ***PLOT ON SCREEN***
1010 PRINT : PRINT "full scale of X-axis= ";R
1020 INPUT "plot with the previous graph (y/n)?" ;C$
1030 IF C$ < > "N" THEN 1110
1040 HGR2 : HCOLOR= 3
1050 FOR I = 0 TO 150 STEP 30
1060 HPLOT 0,I TO 250,I
1070 NEXT I
1080 FOR I = 0 TO 250 STEP 50
1090 HPLOT I,0 TO I,150
1100 NEXT I
1110 X = 0:S = R / 250
1120 FOR I = 1 TO R1 STEP S
1130 X = X + 1
1140 Y = 150 - A$(I) / 4095 * 150
1150 HPLOT X,Y
1160 NEXT I
1170 RETURN
2000 REM ***PLOT ON PAPER***
2010 C$ = CHR$ (3): RESTORE
2020 INPUT "plot on the previous paper? ";C1$
2030 IF C1$ < > "N" THEN GOSUB 2470: GOTO 2390
2040 OFFSET = 0
2050 INPUT "full scale of Y-axis= ";Y
2060 INPUT " X-axis= ";X
2070 INPUT "no. of division on X-axis= ";S: PRINT

```

```

2080 S = X / S
2090 INPUT "title= ";A$
2100 PRINT CHR$(12)
2110 PRINT D$;"PR#2"
2120 PRINT "IN;IP1250,750,9250,6250;"
2130 PRINT "SC0,";X;"0,";Y;";"
2140 PRINT "SP1;PA0,0,PD,";X;"0,";X;",";Y;"0,";Y;"0,0,PU;"
2150 PRINT "SR1.2,2.4;"
2160 PRINT "PA";X / 2;",";Y;";"
2170 L = LEN (A$)
2180 PRINT "CP"; - L / 2,"2;LB";A$;C$
2190 PRINT "PA";X / 2;",";Y;"CP"; - L / 2,"1.8;"
2200 FOR I = 1 TO L: PRINT "LB"; CHR$(95);C$: NEXT I
2210 PRINT "SR;"
2220 PRINT "TL1,0;"
2230 FOR I = 0 TO X STEP S
2240 PRINT "PA";I,"0;XT;"
2250 A$ = STR$(I / 10):L = LEN (A$)
2260 PRINT "CP"; - L / 2,"-1;LB";A$;C$
2270 NEXT I
2280 READ A$:L = LEN (A$)
2290 PRINT "PA";X / 2,"0;CP"; - L / 2,"-3;LB";A$;C$
2300 Y1 = Y / 5:Y2 = Y / 2
2310 FOR I = Y1 TO Y STEP Y1
2320 PRINT "PA0,";I;"YT;"
2330 A$ = STR$(I):L = LEN (A$)
2340 PRINT "CP"; - 1 - L,"0;LB";A$;C$
2350 NEXT I
2360 READ A$:L = LEN (A$)
2370 PRINT "DI0,1;PA0,";Y2;"CP"; - L / 2,"4;LB";A$;C$
2380 PRINT "DI1,0;"
2390 PRINT "PA1,";A$(1) + OFFSET,"PD;"
2400 FOR I = 1 TO R1
2410 PRINT "PA";I,A$(I) + OFFSET;";"
2420 NEXT I
2430 PRINT "PU;"
2440 PRINT "SP;": PRINT D$;"PR#3"
2450 DATA TIME (SEC),INTENSITY
2460 RETURN
2470 INPUT "offset on Y-axis= ";OFFSET
2480 PRINT CHR$(12): PRINT D$;"PR#2": PRINT "SP1;"
2490 RETURN
3000 REM ***INTEGRATION***
3010 INPUT "use old integration ranges? ";C$
3020 IF C$ < > "N" THEN GOTO 3060
3030 INPUT "1st integration range= ";F1,T1
3040 INPUT "2nd integration range= ";F2,T2
3050 GOTO 3080
3060 PRINT "1st integration range= ";F1;"",";T1
3070 PRINT "2nd integration range= ";F2;"",";T2
3080 S1 = 0:S2 = 0
3090 FOR I = F1 TO T1
3100 S1 = S1 + A$(I)
3110 NEXT I
3120 FOR I = F2 TO T2
3130 S2 = S2 + A$(I)
3140 NEXT I
3150 PRINT : PRINT " area for 1st integration= ";S1

```



```

3160 PRINT "                2nd integration= ";S2
3170 IF T2 < > F2 THEN PRINT "                difference= ";S1 - S2
      * (T1 - F1 + 1) / (T2 - F2 + 1)
3180 PRINT : PRINT " concentration= ";CN(PT);", gain= ";GN(PT);",
      weight= ";WT
3190 GOSUB 8050
3200 RETURN
4000 REM ***DATA FILE***
4010 GOSUB 8000: REM CAPTION
4020 INPUT "name of data file= ";NE$
4030 IF NE$ = NO$ THEN 4080: REM SAME DATA FILE
4040 GOSUB 4300: REM GET PRARMETER FILE NAME
4050 IF N1$ < > N2$ THEN GOSUB 4400: REM GET PRARMETER
4060 NO$ = NE$: REM CURRENT DATA FILE NAME
4070 N2$ = N1$: REM CURRENT PARAMETER FILE NAME
4080 GOSUB 8000
4090 PRINT "current data file= ";NO$
4100 PRINT " sample weight= ";WT
4110 PRINT " element= ";
4120 FOR I = 1 TO N1
4130 PRINT EL$(I);
4140 IF I < N1 THEN PRINT ", ";
4150 NEXT
4160 PRINT : PRINT " data pt./channel= ";R: PRINT
4170 GOSUB 4700: REM SELECT ELEMENT AND LOCATE DATA SECTOR
4180 PRINT "no. of data points to be loaded= ";R
4190 VTAB ( PEEK (37)): INPUT "no. of data points to be loaded= ";R1$
4200 R1 = VAL (R1$)
4210 IF R1$ = "" THEN R1 = R: VTAB ( PEEK (37)): HTAB (34): PRINT R1
4220 IF (R1 < = 0) OR (R1 > R) THEN PRINT CHR$(7);: GOTO 4190
4230 GOSUB 4800: REM GET DATA
4240 RETURN
4300 REM GET PRARMETER FILE NAME
4302 N$ = NE$: REM TEMPORARY FILE NAME FOR ERROR HANDLING
4310 PRINT D$;"OPEN";NE$;","D2"
4320 PRINT D$;"READ";NE$
4330 INPUT N1$
4340 PRINT D$;"CLOSE";NE$
4350 RETURN
4400 REM GET PARAMETER
4402 N$ = N1$: REM TEMPORARY FILE NAME FOR ERROR HANDLING
4410 FL$ = RIGHT$(NE$,2)
4420 IF LEFT$(FL$,1) = "#" THEN FL$ = RIGHT$(FL$,1)
4430 PRINT D$;"OPEN";N1$
4440 PRINT D$;"READ";N1$
4450 INPUT N2
4460 PN = N2 * 2
4470 GOSUB 4600: REM POSITION OF PARAMETER
4480 INPUT N1: INPUT R
4490 PN = ( VAL (FL$) - 1) * (N1 * 3 + 1) + N1 + 3
4500 GOSUB 4600: REM POSITION
4510 INPUT WT
4520 FOR I = 1 TO N1
4530 INPUT EL$(I)
4540 NEXT
4550 FOR I = 1 TO N1
4560 INPUT CN(I): INPUT GN(I)
4570 NEXT

```

```

4580 PRINT D$;"CLOSE";N1$
4590 RETURN
4600 REM POSITION IN PARAMETER FILE
4610 PRINT D$;"POSITION";N1$;",R";PN
4620 PRINT D$;"READ";N1$
4630 RETURN
4700 REM SELECT ELEMENT AND LOCATE DATA SECTOR
4710 INPUT "please select an element:- ";EL$
4720 PT = 0
4730 FOR I = 1 TO N1
4740 IF EL$ = EL$(I) THEN PT = I
4750 NEXT
4760 IF PT = 0 THEN VTA$ ( PEEK (37)): PRINT CHR$ (7);: GOTO 4710
4770 PN = R * (PT - 1) + 1
4780 RETURN
4800 REM GET DATA
4802 N$ = NE$: REM TEMPORARY FILE NAME FOR ERROR HANDLING
4810 PRINT D$;"OPEN";NE$
4820 PRINT D$;"POSITION";NE$;",R";PN
4830 PRINT D$;"READ";NE$
4840 FOR I = 1 TO R1
4850 INPUT A$(I)
4860 NEXT
4870 PRINT D$;"CLOSE";NE$
4880 RETURN
5000 REM ***AVERAGE DATA SETS***
5010 GOSUB 8000
5020 PRINT "max. no. of data pt./profile= 1000": PRINT
5030 INPUT "number of files= ";C$
5040 N = VAL (C$)
5050 IF N = 0 THEN VTA$ ( PEEK (37)): PRINT CHR$ (7);: GOTO 5030
5060 PRINT
5070 J = 1
5080 GOSUB 5590: REM GET 1ST DATA FILE NAME
5090 NO$ = N$(1): REM RECORD OF PARAMETER NAME
5100 GOSUB 4300: REM GET PARAMETER FILE NAME
5110 N$ = N1$: REM TEMPORARY FILE NAME FOR ERROR HANDLING
5120 N2$ = N1$: REM TEMPORARY FILE NAME FOR COMPARISON
5130 GOSUB 4400: REM GET PARAMETER
5140 RT = R: REM KEEP TRACK OF NO. OF DATA PT.S
5150 GOSUB 5630: REM CHECK IF NO. OF DATA PT.>1000
5160 R$(J) = R: REM DATA POINTS TO BE PROCESSED
5170 PRINT "          element=";
5180 FOR I = 1 TO N1
5190 PRINT EL$(I);
5200 IF I < N1 THEN PRINT ", ";
5210 NEXT
5220 PRINT
5230 GOSUB 4700: REM SELECT AN ELEMENT
5240 PRINT
5250 FOR J = 2 TO N
5260 GOSUB 5590: REM GET DATA FILE NAMES
5270 NO$ = NO$ + ", " + N$(J)
5280 GOSUB 4300
5290 IF N2$ = N1$ THEN R$(J) = R: GOTO 5380
5300 GOSUB 4400
5310 IF R < > RT THEN PRINT CHR$ (7);"data sets not compatible!":
      GOSUB 8050: RETURN

```

```

5320 GOSUB 5630: REM CHECK IF NO. OF DATA PT.>1000
5330 R%(J) = R
5340 FOR I = 1 TO N1
5350 IF EL$ = EL$(I) THEN N2$ = N2$ + "," + N1$: GOTO 5380
5360 NEXT
5370 PRINT "element ";EL$;" not in file ";N$(J): GOSUB 8050: RETURN
5380 NEXT J
5390 PRINT : PRINT "now clearing buffer...";
5400 FOR I = 1 TO R%(1):B%(I) = 0: NEXT
5410 PRINT : PRINT
5420 FOR J = 1 TO N
5430 PRINT "now processing data file ";N$(J)
5440 NE$ = N$(J)
5450 GOSUB 4300: GOSUB 4400: GOSUB 4720
5460 R1 = R%(J)
5470 GOSUB 4800
5480 FOR K = 1 TO R1
5490 B%(K) = B%(K) + A%(K)
5500 NEXT K
5510 NEXT J
5520 FOR K = 1 TO R1
5530 B%(K) = INT (B%(K) / N + 0.5)
5540 NEXT K
5550 FOR I = 1 TO R1
5560 A%(I) = B%(I)
5570 NEXT I
5580 RETURN
5590 REM GET DATA FILE NAME
5600 PRINT "name of data file #";J;: INPUT "= ";N$(J)
5610 NE$ = N$(J)
5620 RETURN
5630 REM CHECK NO. OF DATA PT.
5640 IF R < 1000 THEN 5670
5650 PRINT CHR$( 7): PRINT "no. of data points is truncated to 1000."
5660 R = 1000
5670 RETURN
6000 REM ***BOXCAR AVERAGING***
6010 GOSUB 8000
6020 INPUT "please enter no of pt.s in the boxcar=" ;N
6030 FOR I = 1 TO R1 - N + 1
6040 B%(I) = 0
6050 FOR J = 1 TO N
6060 B%(I) = B%(I) + A%(I + J - 1)
6070 NEXT J
6080 B%(I) = INT (B%(I) / N + 0.5)
6090 NEXT I
6100 FOR I = 1 TO R1
6110 A%(I) = B%(I)
6120 NEXT
6130 R1 = R1 - N + 1
6140 RETURN
7000 REM ***DISK ERROR HANDLING***
7010 REM CAN HANDLE ONLY ONE ERROR AT A TIME
7020 ER = PEEK (222)
7030 IF ER < > 4 AND ER < > 5 AND ER < > 8 THEN PRINT CHR$( 7):
PRINT "disk error ";ER;" , can't continue!": STOP
7040 IF ER = 5 THEN PRINT D$;"OPEN";N$: PRINT D$;"DELETE";N$

```

```

7050 PRINT : PRINT "please insert the disk with the file ";N$;" in
      drive 2,"
7060 INPUT "then hit <RETURN> to continue.";C$
7070 PRINT D$;"OPEN";N$
7080 PRINT D$;"READ";N$
7090 RESUME
8000 REM ***CAPTION***
8010 PRINT CHR$(12)
8020 PRINT : PRINT TAB(20)**** DSIS DATA PROCESSING ****
8030 PRINT
8040 RETURN
8050 REM ***PAUSE***
8060 PRINT : PRINT "push any key to continue ";; GET C$
8070 RETURN

```

#### PROGRAM ADP

```

100 REM ***AUTOMATIC DATA PROCESSING FOR DSID***
110 REM !INTEGERI, I1, I2, J, K, CT, ET, GL, N, N1, R
120 HIMEM: 38400
130 D$ = CHR$(4)
140 DIM A%(1000), B(20), C%(6), P(3), W(3), WT(30), CN(30,6), GN(30,6),
      IN(10), FG(30), LC(30)
150 DIM BG(30), IT(30), SL(30), CR(30), CD(30,2), AS(10,3), EL$(30,6), E$(10)
160 REM ***PREPARATION***
170 GOSUB 1000: REM CAPTION
180 GOSUB 1040: REM PARAMETERS
190 GOSUB 1690: REM ELEMENT NAME
200 REM ***CALCULATION***
210 GOSUB 1000
220 FOR GL = 1 TO ET
230 GOSUB 1780: REM PRINT-OUT CAPTION
240 FOR CT = 1 TO N
250 NE$ = N$ + "/"# + STR$(CT)
260 LC(CT) = 0:FG(CT) = 0
270 FOR I = 1 TO N1
280 IF EL$(CT,I) = E$(GL) THEN LC(CT) = I
290 NEXT I
300 IF LC(CT) = 0 THEN 520
310 PN = (LC(CT) - 1) * R + 1: REM POSITION OF DATA IN DATA FILE
320 PRINT D$;"OPEN";NE$
330 PRINT D$;"POSITION";NE$;" ,R";PN
340 PRINT D$;"READ";NE$
350 FOR I = 1 TO R
360 INPUT A%(I)
370 NEXT I
380 PRINT D$;"CLOSE";NE$
390 GOSUB 1870: REM DETERMINE INTEGRATION RANGE
400 IF FG(CT) < > 0 THEN 510
410 BG(CT) = 0:IT(CT) = 0
420 FOR I = F1 TO T1
430 IT(CT) = IT(CT) + A%(I)
440 NEXT I
450 FOR I = F2 TO T2
460 BG(CT) = BG(CT) + A%(I)
470 NEXT I

```

```

480 CR(CT) = (T1 - F1 + 1) / (T2 - F2 + 1)
490 BG(CT) = BG(CT) * CR(CT)
500 SL(CT) = IT(CT) - BG(CT)
510 GOSUB 2350: REM PRINT INTEGRATION RANGE
520 NEXT CT
530 GOSUB 2430: REM PRINT-OUT
540 IF C$ < > "N" THEN GOSUB 2640: REM LEAST SQUARE ANALYSIS
550 NEXT GL
560 PRINT D$;"PR#3"
570 END
1000 REM ***CAPTION***
1010 PRINT CHR$(12)
1020 PRINT TAB(16)"*** AUTO DATA PROCESSING FOR DSID ***": PRINT
1030 RETURN
1040 REM ***MOTOR, AI13 AND SAMPLE PARAMETER***
1050 INPUT "generic name of data file= ";N$
1060 NE$ = N$ + "/" + STR$(1)
1070 PRINT D$;"OPEN";NE$;"D2"
1080 PRINT D$;"READ";NE$
1090 INPUT N1$
1100 PRINT D$;"CLOSE";NE$
1110 PRINT "name of parameter file= ";N1$
1120 PRINT D$;"OPEN";N1$;"D2"
1130 PRINT D$;"READ";N1$
1140 INPUT N2
1150 FOR I = 1 TO N2
1160 INPUT P(I): INPUT W(I)
1170 NEXT I
1180 INPUT N1
1190 INPUT R: INPUT HI: INPUT LO
1200 FOR I = 1 TO N1
1210 INPUT C$(I)
1220 NEXT I
1230 INPUT N
1240 FOR I = 1 TO N
1250 INPUT WT(I)
1260 FOR J = 1 TO N1
1270 INPUT EL$(I,J)
1280 NEXT J
1290 FOR J = 1 TO N1
1300 INPUT CN(I,J): INPUT GN(I,J)
1310 NEXT J
1320 NEXT I
1330 PRINT D$;"CLOSE";N1$
1340 PRINT : INPUT "print parameter? ";C$
1350 IF C$ = "N" THEN RETURN
1360 PRINT D$;"PR#7": PRINT "      80N": REM PRINTER
1370 PRINT "parameter of stepper motor:-"
1380 PRINT TAB(4)"stage #"; TAB(4)"# of pulse"; TAB(4)"waiting time
(sec)"
1390 PRINT TAB(4)"-----"; TAB(4)"-----"; TAB(4)"-----"
-----"
1400 FOR I = 1 TO N2
1410 C$ = STR$(P(I))
1420 L = LEN(C$):TB = 18 - L
1430 PRINT TAB(6)I; TAB(10)P(I); TAB(TB)W(I)
1440 NEXT
1450 PRINT : PRINT : PRINT "parameter of AI13:-"

```

```

1460 PRINT TAB( 4)"scan #"; TAB( 4)"channel #"
1470 PRINT TAB( 4)"-----"
1480 FOR I = 1 TO N1
1490 PRINT TAB( 5)I; TAB( 9)C%(I)
1500 NEXT
1510 PRINT " number of data point for each channel= ";R
1520 PRINT : PRINT : PRINT "parameter of sample:-"
1530 FOR I = 1 TO N
1540 PRINT "sample #";I; TAB( 6)"weight= ";WT(I);" mg"
1550 PRINT TAB( 4)"channel #"; TAB( 4)"element"; TAB( 4)"conc'n
(ppm)"; TAB( 4)"preamp gain"
1560 PRINT TAB( 4)"-----"; TAB( 4)"-----"; TAB( 4)"-----"
"; TAB( 4)"-----"
1570 FOR J = 1 TO N1
1580 L1 = LEN (EL$(I,J)):C$ = STR$(CN(I,J)):L2 = LEN (C$)
1590 TB(1) = 13 - L1:TB(2) = 16 - L2
1600 PRINT TAB( 8)C%(J); TAB( 10)EL$(I,J);
1610 PRINT TAB( TB(1))CN(I,J); TAB( TB(2))GN(I,J)
1620 NEXT J
1630 PRINT
1640 IF (I - 3) / 4 - INT ((I - 3) / 4) = 0 THEN PRINT CHR$( 12)
1650 NEXT I
1660 PRINT CHR$( 12): REM FORM FEED
1670 PRINT D$;"PR#3"
1680 RETURN
1690 REM ***ELEMENT NAME***
1700 PRINT : PRINT "enter name of element which data sets are to be
analysed:-"
1710 ET = 0
1720 PRINT TAB( 4)"element #";ET + 1;: INPUT "= ";C$
1730 IF C$ = "" THEN 1750
1740 ET = ET + 1:ES(ET) = C$: GOTO 1720
1750 PRINT : INPUT "least square analysis? ";C$
1760 IF C$ < > "N" THEN INPUT "nominal weight of sample= ";NW
1770 RETURN
1780 REM ***PRINT-OUT CAPTION***
1790 PRINT D$;"PR#3"
1800 PRINT "analysing data set of element ";ES(GL)
1810 PRINT D$;"PR#7"
1820 PRINT " 80N"
1830 PRINT : PRINT "element= ";ES(GL): PRINT
1840 PRINT "sample #"; SPC( 2);"integration range"
1850 PRINT "-----"; SPC( 2);"-----"
1860 RETURN
1870 REM ***INTEGRATION RANGE***
1880 S = 0:V = 0
1890 FOR I = R * 0.9 TO R
1900 S = S + A%(I)
1910 NEXT I
1920 AV = S / (R * 0.1 + 1)
1930 FOR I = R * 0.9 TO R
1940 V = V + (AV - A%(I)) ^ 2
1950 NEXT I
1960 SD = SQR (V * 10 / R)
1970 FOR I = 1 TO R / 50
1980 B(I) = 0
1990 PRINT D$;"PR#3"
2000 FOR J = 1 + (I - 1) * 50 TO I * 50

```

```

2010 B(I) = B(I) + A%(J)
2020 NEXT J
2030 NEXT I
2040 I = R / 50
2050 IF B(I - 1) + 6 * 50 * SD < B(I) AND B(I - 1) < B(I) * .99 THEN
  2080
2060 I = I - 1: IF I > 1 THEN 2050
2070 IF I = 1 AND B(1) - B(R / 50) < 6 * 50 * SD THEN FG(CT) = 1:
  RETURN
2080 FOR J = 1 TO 10
2090 B(J) = 0
2100 FOR K = 1 + (I - 1) * 50 + (J - 1) * 5 TO (I - 1) * 50 + J * 5
2110 B(J) = B(J) + A%(K)
2120 NEXT K
2130 NEXT J
2140 FOR J = 1 TO 10
2150 IF B(J) > B(J - 1) THEN K = J
2160 NEXT J
2170 F1 = 1 + (I - 1) * 50 + (K - 1) * 5: F2 = F1 + 20
2180 IF F2 > 0.8 * R THEN FG(CT) = 2: RETURN
2190 S1 = 0: S2 = 0
2200 FOR I = F1 TO F1 + 19
2210 S1 = S1 + A%(I)
2220 NEXT I
2230 FOR I = F2 TO F2 + 19
2240 S2 = S2 + A%(I)
2250 NEXT I
2260 IF S1 - S2 < = 2 * 20 * SD THEN 2300
2270 S1 = S2: S2 = 0: F2 = F2 + 20
2280 IF F2 > 0.8 * R THEN FG(CT) = 2: RETURN
2290 GOTO 2230
2300 T1 = F2 - 1 + R / 10
2310 F1 = 1: T2 = R
2320 F2 = R - (T1 - F1)
2330 IF F2 < T1 THEN F2 = T1 + 1
2340 RETURN
2350 REM ***PRINT INTEGRATION RANGE***
2360 PRINT D$;"PR#7": PRINT "      80N";
2370 PRINT TAB( 4)CT;
2380 HTAB (10)
2390 IF FG(CT) < > 0 THEN PRINT "  not available": RETURN
2400 PRINT F1; SPC( 2)"TO ";T1;" and ";
2410 HTAB (25): PRINT F2; SPC( 1)"TO ";T2
2420 RETURN
2430 REM ***PRINT-OUT***
2440 PRINT : PRINT : PRINT
2450 PRINT "wt"; TAB( 3)"conc"; TAB( 3)"gain"; TAB( 3)"peak int"; TAB(
  3)"bkg int"; TAB( 3)"net int"; TAB( 3)"corr factor"
2460 PRINT "---"; TAB( 3)"-----"; TAB( 3)"-----"; TAB( 3)"-----"; TAB(
  3)"-----"; TAB( 3)"-----"; TAB( 3)"-----"
2470 FOR I = 1 TO N
2480 IF LC(I) = 0 THEN 2610
2490 PRINT WT(I);
2500 HTAB (5): PRINT CN(I,LC(I));
2510 HTAB (12): PRINT GN(I,LC(I));
2520 IF FG(I) = 1 THEN HTAB (24): PRINT "no peak observed": GOTO 2610
2530 IF FG(I) = 2 THEN HTAB (20): PRINT "vaporization not completed":
  GOTO 2610

```

```

2540 HTAB (17): PRINT IT(I);
2550 A$ = STR$ (BG(I)):SP = 7 - LEN (A$)
2560 IF SP < 0 THEN BG(I) = INT (BG(I) + .5): GOTO 2550
2570 HTAB (27): PRINT BG(I);: PRINT SPC( SP)
2580 A$ = STR$ (SL(I)):SP = 7 - LEN (A$)
2590 IF SP < 0 THEN SL(I) = INT (SL(I) + .5): GOTO 2580
2600 PRINT TAB( 3)SL(I);: PRINT SPC( SP): PRINT TAB( 4)CR(I)
2610 NEXT I
2620 PRINT CHR$ (12)
2630 RETURN
2640 REM ***LEAST SQUARE ANALYSIS***
2650 GF = 0: REM SET GAIN NORMALIZATION FACTOR
2660 FOR I = 1 TO N
2670 IF LC(I) = 0 THEN 2690
2680 IF GF < GN(I,LC(I)) THEN GF = GN(I,LC(I))
2690 NEXT I
2700 FOR I = 1 TO N
2710 IF LC(I) = 0 THEN 2730
2720 SL(I) = SL(I) * 10 ^ (GF - GN(I,LC(I)))
2730 NEXT I
2740 FOR I = 1 TO N
2750 FG(I) = 0
2760 FOR J = 1 TO 3
2770 AS(I,J) = 0
2780 NEXT J
2790 NEXT I
2800 K = 0
2810 FOR I1 = 1 TO N
2820 IF LC(I1) = 0 OR FG(I1) = 1 THEN 2900
2830 J = 0:K = K + 1
2840 AS(K,2) = CN(I1,LC(I1))
2850 FOR I2 = I1 TO N
2860 IF LC(I2) = 0 THEN 2880
2870 IF AS(K,2) = CN(I2,LC(I2)) THEN AS(K,1) = AS(K,1) + SL(I2):AS(K,3)
      = AS(K,3) + WT(I2):FG(I2) = 1:J = J + 1
2880 NEXT I2
2890 AS(K,1) = AS(K,1) / J:AS(K,3) = AS(K,3) / J
2900 NEXT I1
2910 FOR I = 1 TO K
2920 IN(I) = AS(I,1)
2930 NEXT I
2940 FOR J = 1 TO 10
2950 GOSUB 3010: REM AVERAGE OF ALL CONC N
2960 IF J > 1 THEN GOSUB 3080: REM CORRECTION
2970 GOSUB 3130: REM SLOPE AND INTERCEPT
2980 NEXT J
2990 GOSUB 3220: REM PRINT LSA RESULT
3000 RETURN
3010 REM ***AVERAGE OF ALL***
3020 AX = 0:AY = 0
3030 FOR I = 1 TO K
3040 AX = AX + AS(I,2):AY = AY + AS(I,1)
3050 NEXT I
3060 AX = AX / K:AY = AY / K
3070 RETURN
3080 REM ***CORRECTION***
3090 FOR I = 1 TO K
3100 AS(I,1) = IN(I) + (1 - AS(I,3) / NW) * A

```



```
3110 NEXT I
3120 RETURN
3130 REM ***SLOPE AND INTERCEPT***
3140 B = 0:QT = 0
3150 FOR I = 1 TO K
3160 B = B + (AS(I,2) - AX) * (AS(I,1) - AY)
3170 QT = QT + (AS(I,2) - AX) ^ 2
3180 NEXT I
3190 B = B / QT
3200 A = AY - B * AX
3210 RETURN
3220 REM ***LSA RESULT PRINT-OUT***
3230 PRINT
3240 PRINT TAB( 5)"conc"; TAB( 5)"weight"; TAB( 5)"meas. int."; TAB(
5)"calc. int."
3250 PRINT TAB( 5)"-----"; TAB( 5)"-----"; TAB( 5)"-----"; TAB(
5)"-----"
3260 FOR I = 1 TO K
3270 HTAB (5): PRINT AS(I,2);
3280 HTAB (14): PRINT AS(I,3);
3290 HTAB (23): PRINT IN(I);
3300 HTAB (38): PRINT AS(I,1)
3310 NEXT I
3320 PRINT : PRINT "intercept=" ;A
3330 PRINT "      slope=" ;B
3340 PRINT "  content=" ;(A / B) * (10 / NW);"ppm"
3350 PRINT CHR$( 12)
3360 RETURN
```

## SUBROUTINE DAI13

```

1   PTR      EQU      $6
2   NUMBER   EQU      $7
3   ARYPTR   EQU      $8
4   AARY     EQU      $6B
5   RCOND    EQU      $$E00
6   INOUT    EQU      $C0C0
7           ORG      $$F00
8           LDA      AARY
9           CLC
10          ADC      #8           ;POINT TO THE 1ST ELEMENT
11          STA      ARYPTR
12          LDA      AARY+1
13          ADC      #0
14          STA      ARYPTR+1
15   BIGLOOP  LDA      NUMBER
16          STA      PTR
17          LDY      #0
18          LDX      #0
19   GETLOOP  INX
20          LDA      RCOND+1,X
21          STA      INOUT       ;INITIALIZE ADC WITH RCOND
22          PHA
23          PLA
24          PHA
25          PLA
26          INY
27          LDA      INOUT+1     ;LOAD HI-BYTE OF RESULT
28          AND      #$F        ;STRIPE OUT FLAGS
29          STA      (ARYPTR),Y
30          INY
31          LDA      INOUT
32          STA      (ARYPTR),Y
33          DEC      PTR
34          BNE     GETLOOP
35          CLC
36          TYA
37          ADC      ARYPTR     ;RENEW ARRAY ADDRESS
38          STA      ARYPTR
39          LDA      ARYPTR+1
40          ADC      #0
41          STA      ARYPTR+1
42   CLOCK    LDA      #100     ;0.1 SEC CLOCK
43   DSEC     LDX      #200
44   WAIT     DEX
45          BNE     WAIT
46          SEC
47          SBC      #01
48          BNE
49          DEC      RCOND     ;DATA POINT COUNTER
50          BNE     BIGLOOP
51          DEC      RCOND+1
52          BPL     BIGLOOP
53          RTS

```

## SUBROUTINE TIMER1

1	TIME	EQU	\$CE
2	COUNT1	EQU	\$8F9D
3	COUNT2	EQU	\$8F9E
4		ORG	\$8FA0
5		LDA	TIME
6		TAX	
7		LDA	#0
8		STA	COUNT1
9	LOOP1	LDA	#133
10		STA	COUNT2
11	LOOP2	PHA	
12		PLA	
13		PHA	
14		PLA	
15		PHA	
16		PLA	
17		DEC	COUNT1
18		BNE	LOOP2
19		DEC	COUNT2
20		BNE	LOOP2
21		DEX	
22		BNE	LOOP1
23		RTS	

## SUBROUTINE TIMER2

1	TIME	EQU	\$CF
2	COUNT1	EQU	\$8F9D
3	COUNT2	EQU	\$8F9F
4		ORG	\$8FD0
5		LDA	TIME
6		TAX	
7		LDA	#0
8		STA	COUNT1
9	LOOP1	LDA	#133
10		STA	COUNT2
11	LOOP2	PHA	
12		PLA	
13		PHA	
14		PLA	
15		PHA	
16		PLA	
17		DEC	COUNT1
18		BNE	LOOP2
19		DEC	COUNT2
20		BNE	LOOP2
21		DEX	
22		BNE	LOOP1
23		RTS	

## SUBROUTINE CTL.IOB.CHAR

8CD0-	A9 8C	LDA	#\$8C
8CD2-	A0 DA	LDY	#\$DA
8CD4-	20 D9 03	JSR	\$03D9
8CD7-	60	RTS	
8CD8-	00	BRK	
8CD9-	00	BRK	
8CDA-	01 60	ORA	(\$60,X)
8CDC-	02	???	
8CDD-	00	BRK	
8CDE-	11 00	ORA	(\$00),Y
8CE0-	F0 8C	BEQ	\$8C6E
8CE2-	00	BRK	
8CE3-	8D 00 00	STA	\$0000
8CE6-	01 00	ORA	(\$00,X)
8CE8-	00	BRK	
8CE9-	60	RTS	